EFFECT OF GRAVITY ON LAMINAR PREMIXED GAS COMBUSTION

by

Paul David Ronney

B.S., University of California, Berkeley
(1978)

M.S., California Institute of Technology
(1979)

Submitted to the
Department of Aeronautics and Astronautics
in Partial Fulfillment of the
Requirements for the Degree of

DOCTOR OF SCIENCE

at the

MASSACHUSETTS INSTITUTE OF TECHNOLOGY

June 1983

Signature of Author _____
Department of Aeronautics and Astronautics, March 4, 1983

Certified by _____
Harold Y. Wachman
Thesis Supervisor

Certified by _____
I. Miller
Thesis Supervisor

Certified by _____
Glenn C. Williams
Thesis Supervisor

Accepted by _____
Harold Y. Wachman
Chairman, Department Doctoral Committee

EFFECT OF GRAVITY ON LAMINAR PREMIXED GAS COMBUSTION

by

Paul David Ronney

Submitted to the Department of Aeronautics and Astronautics
on March 4, 1983 in partial fulfillment of the
requirements for the Degree of Doctor of Science
in the field of Physics of Fluids

ABSTRACT

For the first time, a comprehensive study of the gravitational effects on laminar premixed gas combustion has been undertaken. Flammability limits, burning velocities, and minimum ignition energies for stoichiometric and lean methane-air mixtures at pressures of 50 to 1500 Torr were measured in normal earth gravity (one-g) and zero-gravity (zero-g). This information is of value for the assessment of flammability hazards of materials used in spacecraft construction, evaluating the effectiveness of spacecraft fire suppression systems, and improving our knowledge of some inadequately understood combustion phenomena.

The zero-g flammability limit was always between the one-g upward and downward limits at the same pressure. Burning velocities were identical in one-g and zero-g for fast-burning mixtures. For slow-burning mixtures only the zero-g observations could be interpreted to obtain burning velocity information because of the severe flame front distortion in one-g caused by natural convection. Down to the zero-g flammability limit, burning velocities for these slow-burning mixtures were just as expected based on existing models and extrapolation of current and previous one-g results. Minimum ignition energies were identical in one-g and zero-g except extremely near the zero-g flammability limit, where the zero-g minimum ignition suddenly increased drastically. In zero-g, for sub-limit mixtures and near-limit mixtures with a subcritical spark energy input, a new type of unstable combustion phenomena which could only be observed in zero-g, termed Sudden Infant Flame Death, or SIFD, was discovered. The phenomena appeared to be independent of the geometry of the system. SIFD was characterized by an observed flame front radius r_b increasing with time t as given by the relation $r_b \sim t^{1/2}$, a chemical energy release often orders of magnitude greater than the spark energy input, and sudden extinction. All zero-g flame propagation was spherically symmetric except for a few very unusual SIFDs at 1500 Torr.

The conclusions were that gravitional effects on combustion were less significant at reduced pressure; that the observed one-g upward flammability limit was caused by a very low burning velocity and a very high minimum ignition energy which made flame propagation impractical below a certain fairly well-defined concentration; that the one-g downward flammability limit was caused by the inability of the flame to propagate downward against the buoyancy of its own burned gases; that the zero-g flammability limit and SIFD behavior were caused by a flame-front instability that was probably thermodynamic in nature although it could not be attributed to heat losses;

and that gravitational forces added a certain stability to near-limit flame propagation. The exact cause of the instability could not be determined but future experiments which might rectify this situation were suggested.

Thesis Supervisor: Harold Y. Wachman
Professor of Aeronautics and Astronautics

Thesis Supervisor: Rene H. Miller
Slater Professor of Flight Transportation

Thesis Supervisor: Glenn C. Williams
Professor of Chemical Engineering

Acknowledgements

This investigation was supported largely by Grant #NAG3-173 from the NASA Lewis Research Center, Space Directorate, Space Propulsion Divison, Electric Propulsion and Space Experiments Branch, In-space Research and Technology Section.

I would like to express my gratitude to the members of my Thesis Committee, Professors Harold Y. Wachman and Rene H. Miller of the Department of Aeronautics and Astronautics, and Professor Glenn C. Williams of the Department of Chemical Engineering, for their guidance and support, their (apparent) confidence in me, for the freedom they allowed me in conducting this investigation, and for basically leaving me alone when I wanted to be left alone. I would like to thank all the people at NASA-Lewis for their support throughout the investigation, namely branch chief Tom Cochran, section head Tom Labus, grant monitors Dan Vento and Lee Sarsfield, photographic technicians Ernie Walker and Dave Clinton, and miscellaneous Kurt Sacksteder. I would like to give very special thanks to NASA mechanic Jim Tresler, whose professional skill and tireless efforts made the drop testing infinitely easier and more productive, and to Jim and his family for treating me as family. At MIT, I would like to express my indebtedness to technical instructors Al Shaw, Don Weiner, and Earle Wassmouth for their help and advice in the design, construction, and testing of the experimental apparatus; to Phyllis Collymore for the typing and word processing of this thesis despite my ignorance of the CMS SCRIPT/VS word processing system; and to undergraduate students Bill Longabaugh, Steve Adkins, and Karl Gemperli, who worked with me in the Gravity's Role on Ignition Energy and Flammability (GRIEF) group in the Space Systems Laboratory (SSL), for their help in all phases of this investigation. I would also like to thank Ralph, my 1969 Toyota Land Cruiser, for getting me from home to MIT and back for 3 years, rain, shine, or snow*, and all those who contributed to the R2D2 cookie jar. Finally, I would like to thank en masse all others who may have helped or hindered me along the way but were accidentally or intentionally left off of this page.

This thesis is dedicated to my parents, Milton and Elizabeth Ronney, for without their enduring love, support, and understanding, none of this would have been possible.

* Eleven days before the defense of this thesis, Ralph broke his #6 piston, thus diminishing the thanks due him. May his old engine rest in pieces.

CONTENTS

Chapter 1. Motivation

1.1 Why study gravitational effects on combustion?

The study of combustion under conditions of reduced gravity has a number of important applications. Because gravity-induced effects are prevalent in many forms of combustion, studying combustion in the absence of gravity allows additional insight into the more fundamental processes involved. Understanding the effects of gravity on combustion is of particular importance in the design of spacecraft and in the assessment of the flammability hazards associated with the materials used in their construction. An example of this is electrical wiring insulation. Electrical malfunctions are considered to be the most likely source of ignition of a fire on a spacecraft and the most difficult to eliminate [1]. While most spacecraft undergo extensive testing of flammability hazards on earth, it is understood that these hazards will be different in a zero-gravity (zero-g) environment in ways which cannot be assessed a priori. Furthermore, spacecraft fire suppression systems tested on earth cannot be expected to perform the same way in zero-g. Thus, information on the flammability characteristics of materials and fire suppressant effectiveness in zero-g is of value to the spacecraft designer.

1.2 Previous investigations

The experimental investigations undertaken to date on combustion under conditions of zero-gravity (more correctly, reduced gravity) can be categorized as follows: 1) laminar gas jet diffusion flames [2-4], 2) single

droplet liquid fuel combustion [5-8], 3) solid fuel combustion [9-12], 4) porous particle cloud combustion [13], and 5) laminar premixed gas combustion [14-17]. Some analytical work has also been done [18-22]. Reviews of these experimental and analytical investigations appear in references [23-25].

These investigations show that gravity affects the properties of combustion processes primarily through the phenomenon of natural convection. In a gravitational field, hot, burned, less dense gases rise relative to the cooler, unburned, denser surrounding gases, causing a convective gas flow. This process is called free, natural, or buoyant convection. The results indicate that gravitational effects can be expected in steady combustion processes when burning velocities are comparable to or less than the gas velocities due to natural convection (typically a few centimeters per second at atmospheric pressure) and in transient processes when the characteristic time scales are comparable to or greater than the time for development of significant flow due to natural convection (typically a few tenths of a second at atmospheric pressure).

The investigations on combustion under conditions of reduced gravity have also indicated that natural convection affects combustion in at least three ways. First, it induces convective mixing of fuel and oxidant for systems in which the fuel and oxidant are not initially mixed, broadly called diffusion flames, which generally tends to aid burning. In the absence of convection, molecular diffusion is the only available mechanism for mass transport. Second, natural convection produces convective heat transfer from the hot, burned gases to the cold, unburned gases and solid bodies around the burned gases, which may accelerate or retard burning depending on whether heat transferred to the unburned gas causes subsequent burning or is merely lost in heating the cold gases and solid bodies. This of course will depend on the

rate of chemical reaction and geometrical considerations. Third, natural convection produces fluid mechanical effects which may have a variety of effects on combustion, again depending on geometry, however, in most instances these effects aid upward flame propagation and retard downward flame propagation in a gravitational environment.

Some investigators [26-29] have studied the effects of gravity forces greater than normal earth gravity (one-g) on combustion, using a centrifuge to obtain high g-loadings. This approach is beyond the scope of the current investigation, but the results merit inspection. In general if combustion is enhanced by the presence of earth gravity, it will be further enhanced by higher g-loadings, and if earth gravity retards burning, it will be further inhibited by higher g-loadings, as would be intuitively expected.

It appears that the lack of mixing due to natural convection is the predominant factor in the effects of gravity on diffusion flames (which include categories 1) through 4) previously mentioned), thus, diffusion flames generally do not burn as well in the absence of gravity. One might therefore expect laminar premixed gas combustion (category 5) previously mentioned), where the fuel and oxidant are intimately mixed on the molecular level before combustion, to be unaffected by gravity forces. On the contrary, it has been found in some instances that gravitational effects are still important in this form of combustion, apparently due to the effects of gravity on heat transfer and fluid mechanics. Thus, investigating the effects of gravity on laminar premixed gas combustion allows the study of the effects of natural convection on heat transfer and fluid mechanics in combustion processes while effectively eliminating the complicating process of mixing and the gravitational effects on the mixing process. Such studies may provide greater insight into the

effects of gravity on the actual combustion processes occurring in these flames.

In addition to the utility of studying laminar premixed gas combustion in zero-g as a means of improving our understanding of other combustion processes, there is a lack of understanding of several important properties of this seemingly simple process itself. Based on the one-g experiments performed on laminar premixed gas combustion, it is evident that gravitational effects are significant in determining some of these properties. Additional zero-g studies are required to further our understanding of these properties, as is discussed in the following chapter.

1.3 Conclusion

Investigating the effects of gravity on laminar premixed gas combustion allows the study of the effect of natural convection on combustion processes without the influence of mixing processes inherent in diffusion flames. This information may be useful for the assessment of flammability hazards associated with materials used in spacecraft construction. There are also unanswered questions concerning certain fundamental properties of laminar premixed gas combustion and it is suspected that gravitation effects may be responsible for some of these properties. For these reasons, this study will investigate the effect of gravity on the properties of laminar premixed gas combustion.

Chapter 2. Laminar premixed gas combustion

2.1 Fundamentals of laminar premixed gas combustion

2.1.1 Definition and idealization

Laminar premixed gas combustion (LPGC) in its broadest sense is a self-propagating chemical reaction in a gas or mixture of gases with laminar flow characteristics which results in the liberation of heat and visible radiation. LPGC is normally idealized as a plane wave propagating into an initially quiescent mixture in an adiabatic, constant pressure system of infinite extent. The general mechanism for propagation is as follows [30-32]: The cold, "unburned" gas is not strictly in chemical equilibrium but has a sufficiently slow reaction rate at its initial temperature that chemical reactions can be neglected. The unburned gas is heated by conduction and possibly radiation by the burned gas behind the flame zone. Occurring simultaneously is the diffusion of combustion products and chemically active species in and behind the flame zone to the unburned gas ahead of the flame zone and vice versa. When the unburned gas temperature is high enough to cause chemical reaction to proceed at a sufficiently high rate, the reaction becomes self-accelerating as further reaction increases the gas temperature due to the heat liberated by reaction and thus the reaction rate increases still further. Eventually consumption of the reactants allows chemical equilibrium to be obtained at some high temperature relative to the unburned gases. These high-temperature gases heat the next layer of unburned gases and the reaction is self-propagating. Typical profiles of temperature, reaction rate, and reactant concentration for an idealized one-dimensional system are

shown schematically in Fig. 2-1. Often the flame is further approximated as having two distinct zones, a preheat zone for temperatures below the point of inflection of the flame temperature profile where thermal conduction occurs with relatively little chemical reaction, and a reaction zone for temperatures above the point of inflection of the flame temperature profile where reaction occurs with relatively little heat conduction. For hydrocarbon flames, the main luminous region is usually near the point of inflection of the temperature profile, at a temperature of 800-1000°K [33].

Thus, in general, even in the idealized case LPGC is a complex interaction of thermal conduction, molecular diffusion and chemical reaction, almost always with numerous molecular species and intermediate chemical reactions.

The pressure drop across the flame front due to the momentum flux change is practically always negligible compared to the initial pressure because flow velocities are small compared to the speed of sound [31]. Also, the kinetic energy flux of the flowing gases is usually small compared to the rate of heat production in LPGC [31]. These facts provide some welcome simplification of the physical model.

A complicating factor in LPGC is the spontaneous formation of a cellular flame structure in fuel-oxidizer mixtures where the less diffusive component is present in excess [30]. This of course means that one dimensionality is lost in these flames. It is believed [30] that this effect is due to preferential diffusion of the more diffusive component ahead of the flame front, thus creating "pockets" of more rapidly burning mixture which protrude ahead of the "planar" flame front.

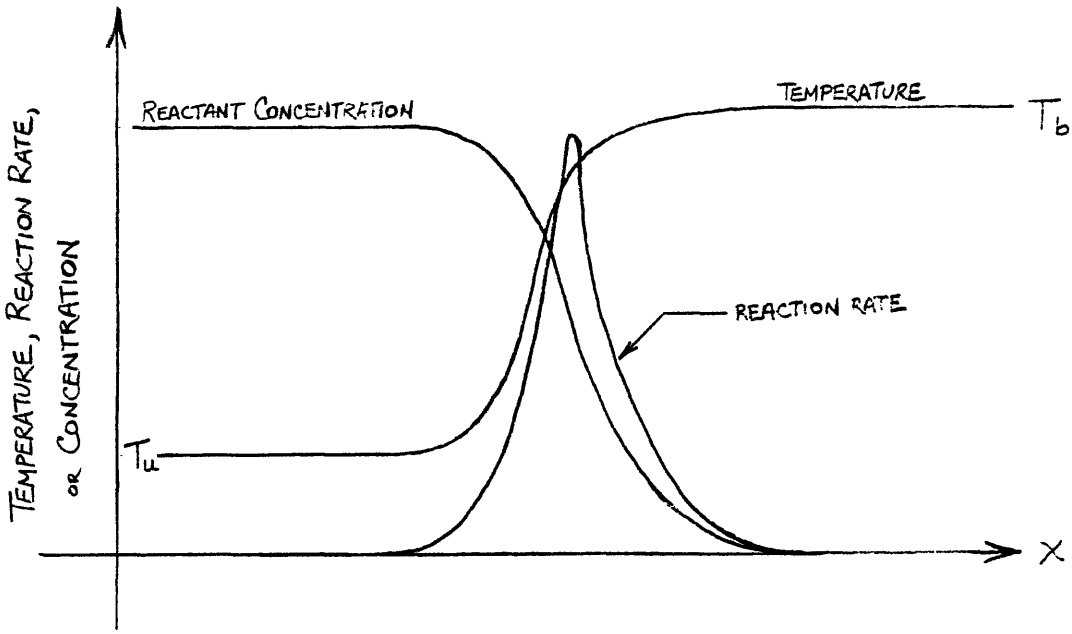

Figure 2-1. Typical temperature, reaction rate, and reactant concentration profiles for idealized one-dimensional laminar premixed gas flame

---

2.1.2 Importance of laminar premixed gas combustion

LPGC is of great interest to the combustion researcher for a number of reasons. Perhaps the most persuasive reason for studying LPGC is that it probably represents the simplest possible flame (despite the complexities previously noted) in that any other conceivable combustion system would have more variables. Aiding this simplification is the fact that LPGC does not require mixing of reactants, it has simple geometric properties and a minimal role of fluid mechanics, and the gases involved have simple equations of state. In principle one could predict all combustion properties of a laminar premixed gas flame propagating into an initially quiescent mixture by specifying only the state of the unburned gas, i.e. temperature, pressure, and concentrations of reactants.

Another utility of the study of LPGC is that it is one of the few combustion systems for which detailed analytical solutions exist [34-37]. Thus, comparisons of observed versus predicted behavior can be made in order to confirm our understanding of the physical processes occurring in a flame.

The simplicity of LPGC makes it a valuable research tool, however, also important is its applicability to many other combustion systems. For example, the study of a laminar premixed gas flame in a laboratory environment can be used to provide information on rates of reaction [31] and molecular diffusion velocities [33], which can then be used to model combustion in a system of practical importance, such as an internal combustion engine. The study of LPGC is also of great interest in mine safety research because dangerous concentrations of flammable gases may accumulate in mine shafts, sometimes with tragic consequences, and the combustion of these gases can often be considered to be LPGC. It may also be possible to apply information on LPGC to other forms of combustion, e.g. diffusion flames, where mixing of fuel and oxidant occurs first, then perhaps the actual combustion process can be modeled using information gathered from studies on LPGC.

2.1.3 Experimental realization of laminar premixed gas combustion

In experimental practice, the idealized one-dimensional, steady, adiabatic, constant pressure laminar premixed gas flame of infinite extent cannot be realized and various techniques have been devised to approximate this idealization. In this section some of the more common experimental techniques will be described and their respective limitations discussed, particularly with regard to their utility for studying gravitational effects on LPGC. The five techniques to be discussed in this section include the Bunsen burner, flat flame burner, tube, closed bomb, and soap bubble methods.

These methods are shown schematically in Fig. 2-2. In the first two methods, the position of the flame front is fixed in the laboratory frame, and in the last three the flame front is moving in the laboratory frame but the burned or unburned gases are fixed.

In the bunsen burner (Fig. 2-2a) fuel and air are mixed at the base of a tube oriented vertically with the outlet at the top. A cone-shaped flame is produced at the outlet and is stabilized on the lip of the tube in the boundary layer region. In the flat-flame burner (Fig. 2-2b) an attempt is made to produce a close approximation to the idealized one-dimensional flame through the judicious use of screens, tube arrays, porous metal matrices, etc. to produce a uniform outlet velocity profile and then balancing the gas flow velocity against the burning velocity (defined in section 2.2.4) of the combustible mixture. If the flame thickness (defined in section 2.2.2) is small compared to the burner diameter, edge effects such as heat loss to the burner rim can be neglected and a one-dimensional flame is approximated. These two burner methods are at a distinct disadvantage for studying gravitational effects on LPGC for at least two reasons. First, both the unburned and burned gases are moving in the laboratory frame, thus aerodynamic effects are always present to some extent. Disturbances due to boundary layer formation, edge effects, and natural convection may become significant at lower flow velocities, where flame thicknesses are largest and gravitational effects are expected to be most significant. Second, because of the short duration of zero-g available in ground-based tests, these flames must first be ignited and stabilized in one-g, thus creating thermal gradients and flow patterns which may affect the behavior of the flame when zero-g is initiated.

In the tube method of observing LPGC (Fig. 2-2c) a cylindrical tube is filled with a combustible mixture, ignited at one end, and a flame propagates

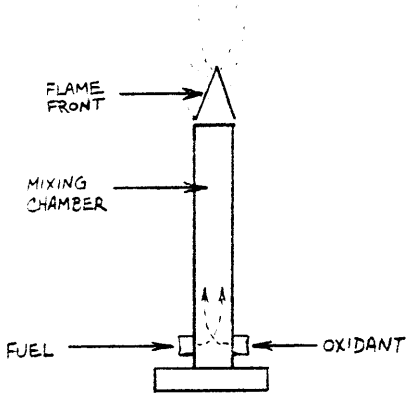

a) Bunsen burner

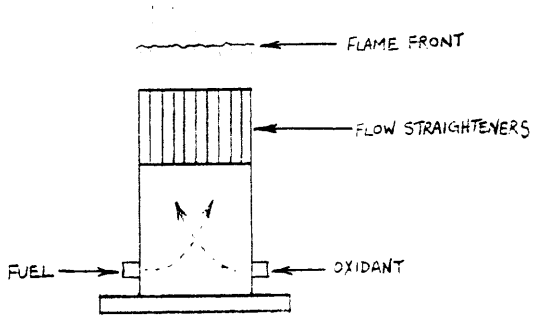

b) flat-flame burner

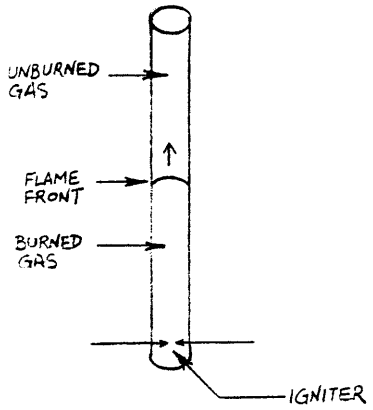

c) tube

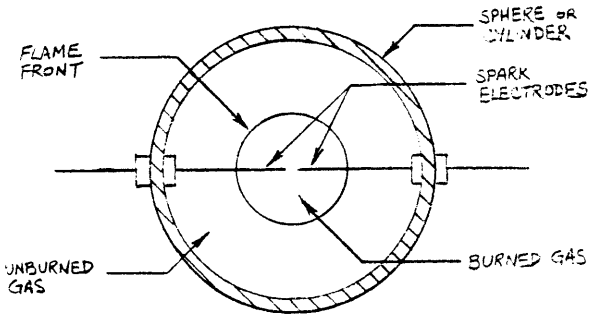

d) closed bomb

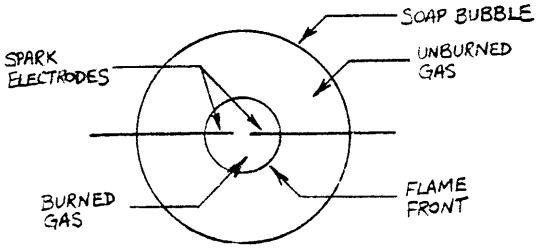

e) soap bubble

Figure 2-2. Experimental apparatus for observing laminar premixed gas combustion

throughout the tube. The tube is usually open to the atmosphere at one end and closed at the opposite end. Ignition at the open end or closed end causes the unburned or burned gases, respectively, to be stationary in the laboratory frame. The tube may be oriented either horizontally or vertically. In the latter case flame propagation may be from top to bottom or vice versa. The tube method allows the flame to "choose" its own propagation characteristics, not subject to the aerodynamic constraints of the Bunsen or flat flame burners, but does not generally yield a flat, one dimensional flame front. Allowances can be made for this in interpreting results [38]. A disadvantage of the tube method as well as other methods of examining flame propagation in which the flame front is not fixed in the laboratory frame is that it is difficult to measure flame structure. Either temperature and/or concentration probes would have to move along with the flame front or a large array of probes would have to be used. As this study will concentrate on macroscopic properties and not the fine structure of flames, this is not a serious disadvantage. The most serious drawback to the tube method is that for studying combustion at reduced or elevated pressures, as is important in this investigation, the tube must be enclosed in a pressure vessel, adding to the size and weight of the experimental package. Also, at reduced pressures, the laminar flame thickness increases (section 2.2.2), thus the wall effects such as conduction heat loss become increasingly significant. This problem can be avoided by using a larger diameter tube, but this necessitates a still larger pressure vessel.

In the soap bubble technique (Fig. 2-2e) a soap bubble is carefully blown full of combustible mixture and ignited at the center. Combustion takes place inside a vessel with large dimensions relative to the soap bubble. The method allows spherically symmetric flame propagation at essentially constant

pressure. As with the tube method, the flame is free to "choose" its own propagation velocity. While a spherical flame front is not the same as a planar flame front, if the flame thickness is small in relation to the observed radius of the flame, the flame can be considered locally steady and one-dimensional in flame-front fixed coordinates. There are two principal disadvantages of this method for the current investigation. The first disadvantage is the complexity of blowing bubbles of combustible mixture, particularly in an apparatus to be used in zero-g. The second disadvantage is the difficulty of using the method at reduced pressures because of the evaporation of the bubble and increased flame thickness which necessitates the use of larger bubbles.

The closed bomb method (Fig. 2-2d) is similar to the soap bubble method except that the entire vessel, usually a sphere or a cylinder of equal height and diameter, is filled with combustible mixture and ignited at the center. The closed bomb method lends itself well to the investigation of combustion at reduced and elevated pressures simply by making the bomb itself a pressure vessel. As with the soap bubble method, the spherical flame can be approximated as locally steady and one-dimensional if the flame thickness is small in relation to the observed radius of the flame front.

The only particular disadvantage of the closed bomb method is that, unlike the other methods described here, the combustion takes place at continuously increasing pressure and temperature over time due to expansion of the burned gas bubble. At any given time the pressure can be considered constant throughout the vessel, since burning velocities are small compared to the speed of sound [30]. Thus, for reliable results, it is necessary to have a vessel large enough that the flame radius at which the effects of finite flame thickness becomes negligible is still small enough relative to the

dimensions of the vessel that expansion of the burned gas bubble has not caused significant pressure and temperature changes in the unburned gas. In order to discern at what point the effects of rising pressure and temperature become important, expressions are needed relating to pressure and temperature of the unburned gases to the observed flame front radius. Such an analysis is given in appendix C.

2.2 Characteristics of laminar premixed gas combustion

Probably the most important global characteristics of laminar premixed gas flames are the flammability limits, minimum ignition energies, and burning velocities, as these parameters signify, respectively, whether a flame can be made to propagate in the "combustible" mixture, what is required to initiate the flame, and how rapidly the flame propagates once steady state conditions have been achieved. All three of these characteristics have been identified as potentially being affected by gravity and will form the primary emphasis of this study. Two other characteristics will also be discussed here. Information on flame temperature is necessary to calculate burning velocities in the present work and estimate heat loss effects. Estimates of flame thickness are required to assess the effects of finite flame radius on the observed phenomena.

These five characteristics, flame temperatures, flame thicknesses, flammability limits, minimum ignition energies, and burning velocities, probably comprise all of the significant global characteristics of LPGC. This section will discuss the definition and estimation of the first two and the definition, measurement, models, and possible gravitational effects of the latter three. Other characteristics that describe the fine structure of a

flame such as flame temperature profiles, concentrations of intermediate chemical species, radiation spectra, etc. are of less interest to the present work and will not be discussed here.

2.2.1 Flame temperature

The adiabatic flame temperature is defined as the temperature which the unburned gases will reach after chemical equilibrium is attained, assuming no heat losses. By definition, it can be calculated from equilibrium considerations only, i.e. the specific heats of the gases involved, the heats of formation of the products, and equilibrium constants. Information on reaction rates, thermal conductivity, and molecular diffusivities, which is required for calculation of dynamic characteristics of flames, such as burning velocities, is not required for calculation of adiabatic flame temperatures.

In practice flames rarely achieve the adiabatic flame temperature because of heat losses and the finite times required for completion of flame reactions. Heat losses during combustion processes are difficult to calculate precisely but the experimental evidence summarized in Chapter 5 shows that these losses were probably small in the current investigation. The effect of finite reaction times on flame temperature is even more difficult to calculate because of the scarcity of accurate kinetic data and the complexity of the many competing reactions. These effects are discussed in section 4.3.2. In this study the adiabatic flame temperature is used when values of flame temperature are required with the understanding that errors may result as outlined in section 4.3.2. Details of the adiabatic flame temperature calculations are presented in appendix B.

2.2.2 Flame thickness

Even in a one dimensional laminar premixed gas flame of infinite extent a characteristic dimension of the flame itself exists. This dimension is related to the distance over which the significant portion of the flame phenomena occur. It is usually expressed in terms of the shape of the temperature or reactant concentration profile. Any measure of flame thickness is somewhat arbitrary, as the flame temperature and concentration profiles approach their respective limits asymtotically, at least in the ideal case. Two of the commonly used definitions of flame thickness are presented graphically in Fig. 2-3.

One of the commonly used definitions [30-32] of flame thickness is the preheat zone thickness δ (Fig. 2-3a):

$$\delta = (T_i - T_u)/(dT/dx)_i$$

where T_i and $(dT/dx)_i$ refer to the temperature and slope, respectively, at the point of inflection of the temperature profile, and T_u is the unburned gas temperature. It is easily shown [30] that if one assumes no reaction from $T = T_u$ to $T = T_i$ then this definition of the flame thickness can be expressed as

$$\delta = k/\rho_u C_p S_u$$

where k is the thermal conductivity of the gas, ρ_u is the unburned gas density, S_u is the burning velocity, and C_p the gas specific heat at constant pressure. This equation is merely a statement that the heat conducted from the burned gas raises the unburned gas temperature to $T = T_i$, where chemical reactions can occur. The utility of this equation for the preheat zone thickness is that it gives an estimate of flame thickness based on easily measurable quantities. Since k and C_p are mostly independent of pressure P and ρ_u is directly proportional to pressure, generally $\delta \sim (PS_u)^{-1}$.

Estimating the reaction zone thickness, where reaction occurs with relatively little conduction, with measurable quantities is much more difficult because of the many competing reactions and chemical species.

Another common definition of flame thickness (Fig. 2-3b) [36, 37] is the distance between the points where the reactant concentration is 99% and 1% of its initial value. This definition gives a measure of the dimension over which the flame exerts 98% of its influence, similar to the concept of a 99% boundary layer influence thickness [39] in boundary layer theory. Unless very detailed information on reaction rates, thermal conductivity, and molecular diffusivity is available, this flame thickness cannot be computed accurately and must be measured experimentally. The effects of pressure and burning

---

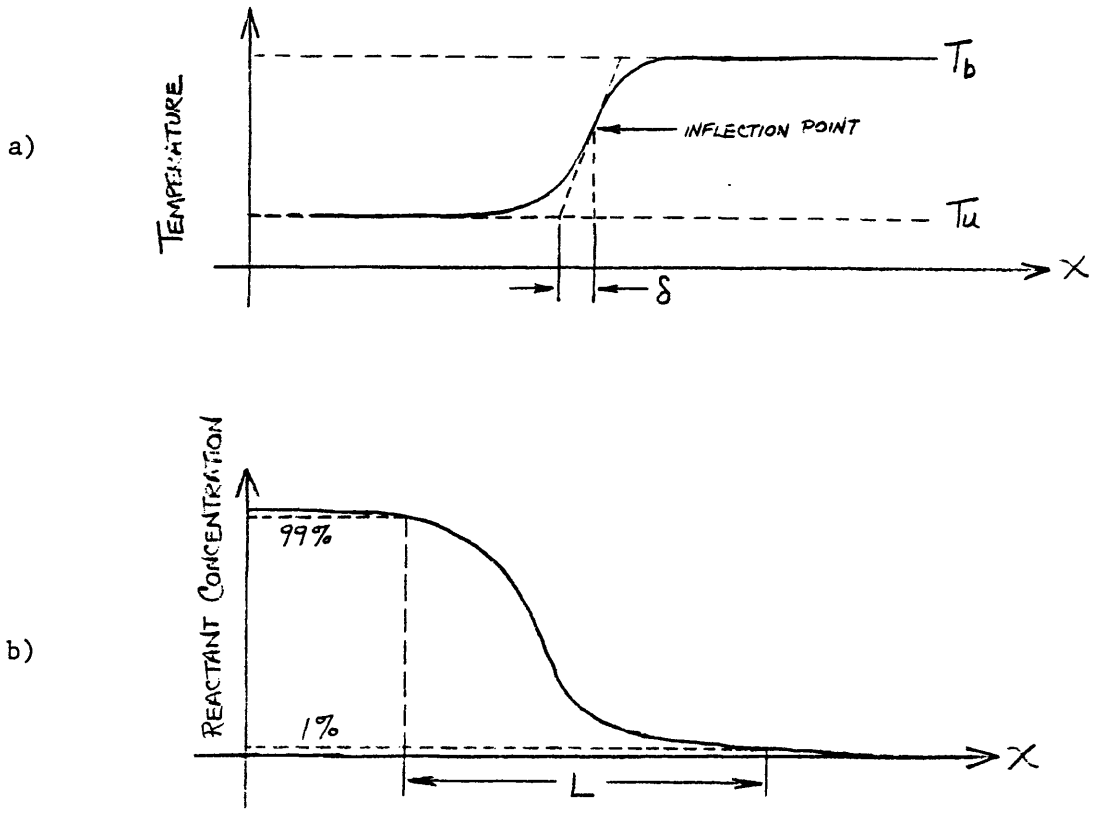

Figure 2-3. Definitions of flame thickness

velocity on flame thickness determined by this definition appear to be essentially the same as for the previous definition [37].

Because of the difficulty in estimating any flame thickness other than the preheat zone thickness, this estimate will be used in this study when a value is necessary. One could of course make accurate measurements of temperature profiles to determine flame thickness, but this is tedious and difficult to implement, particularly in an experimental apparatus to be used in a zero-g experiment, and so is beyond the scope of the current investigation.

2.2.3 Flammability limits

2.2.3.1 Description of flammability limits

It has been observed experimentally that increasing the concentration of a diluent gas in a flammable mixture beyond a limiting value will render the mixture incapable of producing a steadily propagating flame. Such concentration limits are termed flammability limits. The diluent may be the fuel, oxidizer, or an inert gas. Observed flammability limits are of course dependent on the state of the unburned gas mixture, but in addition have been found to be dependent on the experimental apparatus and procedures, probably due to their differing influences on heat losses, aerodynamics, natural convection, and perhaps other unknown factors. Despite extensive research over the past 50 years or so, there is still little agreement among researchers as to the causes of flammability limits, and it is still not clear whether flammability limits can exist in an idealized one-dimensional, steady, adiabatic, constant pressure laminar premixed gas flame of infinite extent. A crucial fact that has practically always been observed experimentally is that

the burning velocity is small but finite at the flammability limit. Even the most complete adiabatic models [34-37] of burning velocity predict that the burning velocity approaches zero asymtotically with increasing dilution of the combustible mixture, and thus no well-defined flammability limit is predicted. Reviews of the literature on flammability limits appear in references [16,40-43] so no attempt to summarize all the available data will be made here.

2.2.3.2 Methods of determining flammability limits.

All of the methods of realizing a laminar premixed gas flame presented in section 2.1.3 have been used at some time to determine flammability limits, with the possible exception of the soap bubble method. In this section these methods and their respective limitations will be discussed.

In the Bunsen or flat-flame burner method, a combustible mixture is stabilized on the burner and progressively diluted with excess fuel, oxidant, or inert gas until extinction of the flame occurs. The concentration at the point of extinction is deemed the flammability limit. As mentioned in section 2.1.3, aerodynamic effects may be significant, particularly for slow burning mixtures near the flammability limit. In fact, Andrews and Bradley [41] have concluded that,

> "...as a result of free convection, the experimentally observed limits on burners are those of [aerodynamic] stability."

Apparently all investigations on flat flame burners have been with upward gas flow, which corresponds to downward propagation of the flame front relative to the unburned gases. Undoubtedly this is because of the complicated flow patterns that would arise with downward gas flow in a burner, as the buoyant

burned gases would attempt to rise back into the flame zone, creating instabilities. Performing flammability limit experiments on burners in zero-g would eliminate the aerodynamic instabilities due to natural convection for either flow geometry, but the other problems previously mentioned concerning the use of burners would still exist. Thus, burner experiments are not attractive for measuring flammability limits in zero-g.

While many sizes and shapes of tubes are used in flammability limit experiments, probably the most common apparatus of any kind for determining flammability limits is a cylindrical tube, 5 cm in diameter, 1.5 m long, open at the ignition end and closed at the opposite end, termed a Standard Flammability Limit Tube (SFLT). The ignition source is a high energy spark or a small auxilliary flame. Propagation may be either from top to bottom or vice versa. A mixture is termed "flammable" if it will support combustion over the entire length of the tube. Extensive investigations on flammability limits in this apparatus have been reported by Coward and Jones [44] and others.

The 5 cm tube diameter was found by these investigators to be the smallest for which wall effects were insignificant at atmospheric pressure in the sense that enlarging the tube did not change the flammability limit significantly. Since flame thickness is inversely proportional to pressure (section 2.2.2), one would expect a 50 cm tube to be required at 0.1 atmosphere, a very large tube indeed. The large body of information available on flammability limits in tubes along with experimental simplicity make the SFLT an attractive candidate for studying flammability limits in zero-g at atmospheric pressure, but lower pressures necessitate the use of a much larger tube and thus diminish the utility of the SFLT.

In the closed bomb method of measuring flammability limits, the bomb is filled with a "combustible" mixture and ignited by a spark of sufficient energy. The criteria for defining the flammability limit may be the limiting mixture for flame propagation throughout the bomb [45], for horizontal propagation in the bomb [45], for upward propagation only [41], or for a given pressure rise in the vessel due to combustion [41].

Any closed bomb flammability limit criterion is inevitably arbitrary because the propagation of near-limit mixtures in a bomb is unsteady and asymmetrical due to complex fluid motion generated by natural convection. This is a distinct disadvantage of the bomb method for measuring flammability limits compared to the burner or tube methods, where a steadily propagating flame does occur even for near-limit mixtures, hence the flammability limit can be defined less arbitrarily as the limiting mixture for steady propagation. The unsteady, asymmetrical nature of near-limit flame propagation in a closed bomb in one-g also makes the determination of a limit burning velocity extremely difficult. In zero-g one would expect all flame propagation to be spherically symmetric because the flame "sees" all directions as equivalent. Because of this spherical symmetry, the flame could be considered locally steady and one-dimensional in zero-g if the flame thickness were small in comparison to the observed flame radius. This would make it possible to specify a closed bomb flammability limit criterion that is both well-defined and non-arbitrary, i.e. by specifying that the flammability limit be the limit of locally steady flame propagation, as well as measure a well-defined limit burning velocity.

Another problem concerning the measurement of flammability limits in a closed bomb is the effect of rising pressure and temperature during combustion. If extinguishment of a "nonflammable" mixture occurs before the

temperature and pressure rise become significant, then the mixture can truly be considered nonflammable. However, if extinguishment occurs only after the pressure and temperature rise become significant, the experiment is inconclusive. These effects on the results of the present investigation will be discussed in detail in section 4.2.3.

2.2.3.3 Results of flammability limit experiments

In the first part of this section, the effect of apparatus type and gravitational conditions on flammability limits will be presented. For comparison, the numerical results for lean (i.e. fuel-deficient) methane-air mixtures at atmospheric pressure and room temperature will be given. More complete listings in the reviews [16, 41] show limits varying from 4.5% to 6.6% methane, depending on the apparatus, procedure, and author(s). In the second part of this section the effects of the state of the unburned gases and heat losses on flammability limits will be considered.

Badami and Egerton [47] measured flammability limits and limit burning velocities for a wide variety of fuels and combinations of fuels on a flat-flame burner at atmospheric pressure. The mean limit burning velocity for single fuel mixtures was 3.6 ± 0.2 cm/s. The range was from 3.1 to 4.2 cm/s. The range of limit burning velocities for all mixtures tested was 3 to 5 cm/s. For methane in air the lean flammability limit was 5.31% with a burning velocity of 3.40 cm/s. The fact that the limit burning velocities were so similar for such a wide variety of fuels is strong evidence that these limits are due primarily to aerodynamic effects and are not fundamental properties of the combustible mixtures, as suggested in section 2.2.3.2.

For flammability limits measured in tubes and closed bombs, where both upward and downward propagation limits are commonly observed, there appears to

be no exception to the rule that for a given fuel/oxidizer/diluent system and experimental apparatus, a wider range of mixtures will sustain upward flame propagation than downward propagation, with an intermediate range for horizontal propagation. This fact clearly illustrates the presence of gravitational effects on flammability limits. In fact, Levy [46] concluded that the observed limits for upward flame propagation in a SFLT were caused by the inability of the flame to propagate at a rate greater than or equal to the rate of rise of a hot gas bubble in the tube, given by $S_b = 0.328(gD)^{1/2}$, where S_b is the rate of propagation of the flame or bubble, g is the gravitational acceleration, and D is the tube diameter. The flame front is quite convex with respect to the unburned gases, similar to the observed shape of a bubble interface moving up a long tube. This formula suggests that for smaller tube diameters or reduced gravity the flammability range would become wider because a slower burning mixture could be made to propagate, and indeed Levy found that the lean limit for methane-air mixtures was leaner in a 5 cm tube (5.3%) than in a 9.5 cm tube (5.6%) and in both cases the rate of flame propagation at the limit was that given by his equation. The same phenomenon was observed for lean propane-air mixtures. It should be noted that the rate of propagation is not the same as the burning velocity (section 2.2.4.2). Of course, for smaller D other effects such as conductive heat loss to the tube wall become important [30] and at some point the above formula no long applies.

For downward propagation in a tube the phenomena are even more complex. Some flames at the flammability limit tip from side to side as they propagate down the tube, in a "walking" motion [16,46]. For lean methane-air mixtures this occurs at about 5.9% methane. For near-limit mixtures where the less diffusive component is present in excess, cellular flame effects described in

section 2.1.1 often become important. Bregeon et al. [47] found that lean mixtures of methane and oxygen could support downward propagation with more diluent nitrogen in a 2.5 cm diameter tube than a 5 cm tube, despite the fact that conductive heat loss to the tube wall would have been more significant in the 2.5 cm tube. They concluded that this result was due to heat loss to the unburned gas between flame cells, as cells were observed in the 5 cm tube and not the 2.5 cm tube, which was apparently too small for cell formation. It is interesting that Bregeon et al. predict flammability limit behavior of methane, oxygen and nitrogen mixtures, some of which had oxygen to nitrogen ratios similar to air, based on this flame cell structure, whereas Levy [46] and Reuss [16] observed that while cell structure is observed for near-limit downward propagating mixtures of methane and air, at the flammability limit the "walking" phenomenon is observed and no cell structure exists.

It appears that the burning velocity at the downward flammability limit in a tube is a constant, at least for a given pressure, regardless of the tube diameter or fuel. A downward limit burning velocity at atmospheric pressure of 8-9 cm/s was found be Bregeon et al. [47] for hydrogen-air mixtures in 2.5 cm and 5.1 cm tubes, Reuss [16] for methane-air mixtures in a 5 cm tube, and Krivulin et al. [29] for hydrogen-, propane-, methane-, and ammonia-air mixtures in a 3.6 cm tube. Bregeon et al. found that for fuel-rich hydrogen/oxygen/nitrogen mixtures, the limit burning velocity for downward propagation was somewhat higher than this value, but these hydrogen/oxygen/nitrogen mixtures are less dense than the other combustible mixtures studied, which all had densities quite close to that of air alone because of the low fuel concentrations. Probably a more reasonable limit criteria than a constant limit burning velocity would be a relationship dependent on the burned and unburned gas densities as well as the limit

burning velocity. In any case, the criterion of a constant burning velocity at the downward flammability limit seems to apply to a wide variety of gas mixtures, which is strong evidence that these limits, like those observed on burners or for upward propagation in tubes, are due to aerodynamic effects and natural convection, and so are not fundamental properties of combustible mixtures.

The case of horizontal propagation in tubes is more difficult to analyze because the flame front is very asymmetric with respect to the tube axis, with the leading edge of the flame front at the top of the tube [44]. Obviously this asymmetry is caused by gravity, so gravitation effects are significant for horizontal as well as upward and downward propagation in tubes.

The difficulties in measuring flammability limits in a closed bomb due to the arbitrariness of any definition have been discussed. It appears that a wider range of mixtures will sustain propagation in a large closed bomb or open channel than in a burner or tube, but such near-limit propagation in the bomb or channel is upward only, unsteady, and dies out after rising some distance owing to self-destructive natural convection currents and the ensuing turbulence generated by the burned gases [30, 44]. For lean mixtures of methane in air this limit is about 5.2% methane [30]. For slightly faster burning mixtures (i.e. slightly richer mixtures in this example), a ball of flame begins to rise, deforms into a mushroom-shaped cloud due to the interaction of shearing forces at the flame boundary with the unburned gas velocity normal to the flame front due to flame propagation, and extinguishes upon reaching the top of the bomb or channel [42, 43]. For lean mixtures of methane and air this occurs up to about 5.5% [41]. For still faster burning mixtures, the same phenomena occur but the flame front spreads downward after reaching the top of the vessel if there is any unburned gas remaining [43].

For still faster burning mixtures the flame can propagate downward from its origin as well as upward and the mushroom-shaped cloud is not observed. For lean mixtures of methane in air this limit is about 5.8% [41]. A discussion of these phenomena is given by Andrews and Bradley [41]. It is clear that a flammability limit defined by any of these phenomena is influenced by gravitational effects.

Thus, it appears that all of the techniques commonly used to determine flammability limits are influenced by gravitational effects, and it is not clear what the net result of these effects is. It appears that gravity-induced natural convection causes a minimum flame propagation velocity which is dependent on the experimental apparatus to be required for stable flame propagation. Therefore, one might expect that in the absence of gravity, very slow-burning mixtures could exhibit steady propagation. As a result, one would expect flammability limits to be wider in zero-g, and perhaps abolished altogether. In practice other factors such as heat losses to the surroundings must become important at some point and so some flammability limit will probably always be observed. It is clear from this discussion that investigation of flammability limits under varying gravitational conditions would add insight to the questions raised about the fundamental nature (or lack thereof) of flammability limits.

Krivulin and collaborators [28, 29] have investigated the effect of gravity forces g greater than normal earth gravity ($g = g_o$) on flammability limits using a centrifuge to obtain high g-forces. "Upward" and "downward" flammability limits were measured for methane-, propane-, and ammonia-air mixtures in a tube 3.6 cm diameter and 15.5 cm long, and for hydrogen-air mixtures in a tube 0.8 cm in diameter and 7 cm long. For both upward and downward propagation the flammable range narrowed with increasing g and the

difference between the upward and downward limits became greater as g increased. For upward propagation no simple formula for the limiting burning velocity could be found. The limit burning velocity was not measured directly but inferred from the measured concentration of fuel at the flammability limit and data on the dependence of burning velocity on concentration determined by other investigators. While the burning velocity S_u is not the same as the observed propagation velocity S_b, it still appears based on the above results that Levy's formula for the propagation velocity at the upward flammability limit, $S_b = 0.328(gD)^{1/2}$, would not fit Krivulin's results. For downward propagation all the data for the burning velocity at the flammability limit $S_{u,lim}$ closely fit an equation of the form $S_{u,lim} = K(g/g_o)^{1/3}$, with $K \simeq 8$-9 cm/sec, independent of the fuel type or tube diameter. Again this information suggests that the observed flammability limits are caused by the inability of the flame to propagate at a certain minimum velocity required by the particular experimental apparatus, and that gravitational effects are instrumental in determining this minimum burning velocity.

Only two investigations have been performed to date on flammability limits in zero-g. Krivulin et al. [15] investigated the flammability limits for rich (i.e. oxygen deficient) propane-air mixtures and lean hydrogen-air mixtures in a closed bomb at atmospheric pressure and found that in both cases a wider range of mixtures would support upward propagation in one-g than would support propagation in zero-g. Because of their spherical symmetry, the zero-g flames consumed all of the available fuel in the bomb. This of course was not the case for the one-g upward-only propagation. For complete propagation in one-g, i.e. complete consumption of the available fuel, the flammable range was narrower than for either zero-g propagation or one-g upward-only propagation. These authors also found the zero-g burning velocity

at the zero-g flammability limit to be about 1.2 cm/s for hydrogen and 2.0 cm/s for propane. Reuss [16] investigated the flammability limits of lean methane-air mixtures in a SFLT at atmospheric pressure and found that the zero-g flammability limit was leaner than either the 1-g upward or downward propagation limit. The present author estimates (section 4.3.3) the burning velocity at the zero-g flammability limit in this experiment to be 1.7 cm/s. It did not appear that the flame propagation rate approached zero as Levy's [48] formula, $S_b = 0.328(gD)^{1/2}$, would predict.

These results suggest that in conditions of near-zero gravity, flammability limits still exist, and a finite burning velocity is observed at the limit. The results at $g = g_o$ and higher strongly suggested that at zero-g, flame propagation could be possible down to extremely low burning velocities. In both of the zero-g experiments mentioned, sub-limit mixtures exhibited some propagation before extinguishment occurred. The observed propagation speed was continuously decreasing until extinguishment occurred. It is significant that both of these experiments observed this behavior despite the differences in geometry and fuels. It does not appear that a continuously decreasing propagation speed before extinguishment has been observed in any of the commonly used experimental apparatus in one-g. It is reasonable to conclude that in zero-g another mechanism for extinguishment exists which is not significant when gravitational effects are present.

Ambient pressure has a variety of effects on flammability limits. The concentration of reactants at the flammability limits do not show consistent trends with pressure. In the case of methane-air mixtures the lean limit concentration shifts toward the stoichiometric value up to about 20 atmospheres and shifts away above this pressure, whereas the rich limit shifts toward stoichiometric up to 30 atmospheres and away above this pressure [45].

The same type of phenomena are observed for hydrogen and carbon monoxide. For horizontal or upward propagation of rich hydrocarbon-air mixtures, the flammable range is continually widening with increasing pressure, and the narrowing effect up to a certain pressure is not observed [42, 46].

In general, the difference between upward and downward flammability limits is greater at higher pressures [42], apparently due to the increased effect of natural convection. Thus, one is led to believe that ambient pressure is a significant factor in determining gravitational effects on combustion, and any proper study of these effects should cover a wide range of ambient pressures.

There is no evidence for either an absolute upper or lower pressure limit of combustion. Fristrom and Westenberg [33] conclude:

> "The practical upper limit appears to be set by the courage (or foolhardiness) of the investigator, while the lower limit is set by the size of the reaction vessel and the available pumping speed."

These complicated pressure effects on flammability limits are probably due to opposing pressure effects on the processes occuring in near-limit flames. For example, burning velocities for slow-burning hydrocarbon-air mixtures decrease [50] and natural convection effects increase [42] with increasing pressure, which tends to decrease the flammable range with increasing pressure, but contrary to this, increasing pressure decreases conductive and radiative heat losses [31], which tends to expand the flammable range with increasing pressure.

Diffusivity of reactants apparently plays an important role in determining flammability limits. The effects of cellular flames caused by preferential diffusion on flammability limits have already been discussed.

Clusius et al. [51] found that the lean flammability limits for hydrogen and deuterium in oxygen were 3.8% and 5.3%, respectively, for upward propagation in a SFLT. The ratio of these concentrations, 1.39, is close to the ratio of the diffusion coefficients for hydrogen and deuterium in oxygen, 1.38. Since hydrogen and deuterium have virtually identical chemical properties, the conclusion was that the difference in flammability limits was due to the difference in diffusion coefficients. Other evidence for the effects of diffusion can be found in the data compiled by Coward and Jones [44]. These authors found that most fuel/oxygen/nitrogen mixtures which had less than the stoichiometric (chemically properly proportioned) concentration of the more diffusive reactant (fuel or oxygen) could support combustion with larger concentrations of diluent nitrogen than could stoichiometric fuel-oxygen mixtures. This indicates that mixtures which have less than the stoichiometric amount of the more diffusive component are "stronger" in some sense than stoichiometric mixtures.

It is possible that these diffusion related effects on flammability limits are merely burning velocity related effects in disguise. While Bregeon et al. [49] found that cellular flame structure was important in determining downward flammability limits for hydrogen/oxygen/nitrogen and methane/oxygen/nitrogen mixtures in tubes, the limit burning velocity was about 10 cm/s for a wide range of hydrogen/oxygen/nitrogen mixtures. Therefore, it is possible that the cellular flame structure alters the burning velocity and thus the flammability limit. Clusius et al. and Coward and Jones did not report limit burning velocities so no specific conclusions can be drawn from their data. One would expect, however, that the same factors which widen the flammability limits of a mixture would also increase its burning velocity for a given concentration. It is clear that diffusion plays an

important role in determining flame behavior such as burning velocity (section 2.1.1), so this suggestion is at least plausible.

An increase in unburned gas temperature apparently always results in a widening of flammability limits [30, 40, 42]. The net effect is that, with good approximation, the adiabatic flame temperature is constant at the flammability limit for a given fuel/oxidant combination [30]. Different experimental apparatus of course yield different flammability limits and therefore different flame temperatures, but self-consistent data from a given apparatus seem to show a constant temperature. For most hydrocarbons this limiting flame temperature is about 1600-1650°K for upward propagation in a SFLT [30]. The results are more consistent for lean mixtures in the case of hydrocarbons, as complications arise with rich mixtures of hydrocarbons due to the formation of soot, "cool flames" [30], and more complicated reaction schemes.

It is quite likely that this constancy of adiabatic flame temperature at the flammability limit is a ramification of the apparent constancy of burning velocity at the flammability limit. The burning velocities for mixtures of a given fuel/oxidant/diluent combination are, with good approximation, a function of adiabatic flame temperature only (section 2.2.4.3). The result is that a constant burning velocity at the flammability limit will also imply an approximately constant adiabatic flame temperature at the flammability limit.

It is also possible that the roles are reversed, that is, the "fundamental" parameter is a constant adiabatic flame temperature at the flammability limit and as a result the burning velocity is constant at the flammability limit. In light of all the previously mentioned experimental results, this prospect seems less likely than a constant burning velocity at the flammability limit. Further evidence for constant burning velocity at the

flammability limit can be found in the data of Badami and Egerton [47]. It is well known that small concentrations of water vapor have a strong catalytic effect on carbon monoxide-air flames, and so mixtures of carbon monoxide, air, and water vapor do not obey the rule that a constant adiabatic flame temperature implies a constant burning velocity. Badami and Egerton found that limit burning velocities for carbon monoxide-air mixtures with varying water vapor content on a flat flame burner were in the 3-4 cm/s range, the same as observed for many other fuels, although the concentration of carbon monoxide (and therefore the adiabatic flame temperature) at the flammability limit varied considerably.

A novel means of examining flammability limits, or more accurately the lack of flammability limits, is the "Swiss roll" burner (Fig. 2-4) of Lloyd and Weinberg [52] and Jones et al. [53]. In this burner the incoming unburned gas is preheated by the burned gas in a counterflow heat exchanger that has been rolled into a spiral to reduce heat losses to the surroundings. This allows heat transfer to the unburned gas without dilution by the combustion products. These authors concluded that by increasing the heat transferred to the unburned gas (by increasing the number of turns, reducing heat losses, etc.), the range of flammable mixtures could be extended at will and the maximum attainable flow velocities were at least an order of magnitude higher than the maximum laminar burning velocity for normal combustion of stoichiometric mixtures. The outstanding experimental observation was that the temperature in the reaction zone was a constant, independent of mixture ratio, flow velocity, or heat losses. This temperature was 1403 ± 39°K for methane-air mixtures. The adiabatic flame temperature program in Appendix C yields a methane concentration of 4.62 ± 0.20% corresponding to this temperature. This concentration is about as low as any of the values for the

lean flammability limit of methane-air mixtures reported in the literature. The authors took this constant temperature in the reaction zone to imply a minimum reaction rate was required using an activation energy argument similar to the one presented in section 2.2.4.3. Thus, there is some evidence that a minimum reaction rate is required for combustion, or at least the reaction rate becomes practically zero and combustion cannot be maintained below some minimum flame temperature.

Kaskan [54], Yumlu [55], and Pritchard et al. [56] have shown that extraction of heat from the burned gases above a flat flame burner results in a reduction in burning velocity, and if enough heat is extracted, extinction of the flame. Some of the results from Pritchard et al. are shown in Fig. 2-5. These results are not surprising considering the effects of unburned gas temperature on flammability limits. These authors also found limit burning velocities in the range of 3-5 cm/s for a wide variety of mixtures, which is identical to the range found by Badami and Egerton [47] for a flat-flame burner without heat extraction. Minimum flame temperatures measured by Kaskan, Yumlu, and Pritchard et al. for hydrocarbon-air mixtures ranged from 1550-1750°K. For methane-air mixtures, the range was 1600-1700°K. This flame temperature corresponds to an adiabatic methane-air mixture of 5.60 - 6.10% methane. This is close to but somewhat richer than the lean flammability limit of 5.31% measured by Badami and Egerton for methane-air mixtures.

Dixon Lewis and Isles [57] and Kydd and Foss [58] were able to reduce the limit burning velocity on flat-flame burners down to 1.5 - 2 cm/s by artificial heating of the burned gases, in the former case electrically and in the later case by a small auxilliary flame. Also, flammability limits could be widened to almost zero fuel concentration in this way. Both found unsteady flame behavior at these very low burning velocities, with "holes" developing

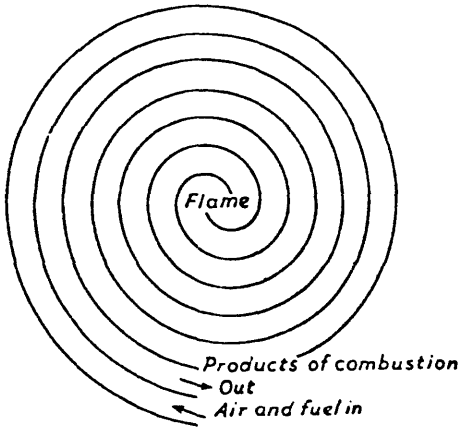

Figure 2-4. "Swiss roll" burner [52]

---

in the flame. Both investigators concluded that the observed limits were not fundamental, but due instead to aerodynamic instabilities caused by natural convection.

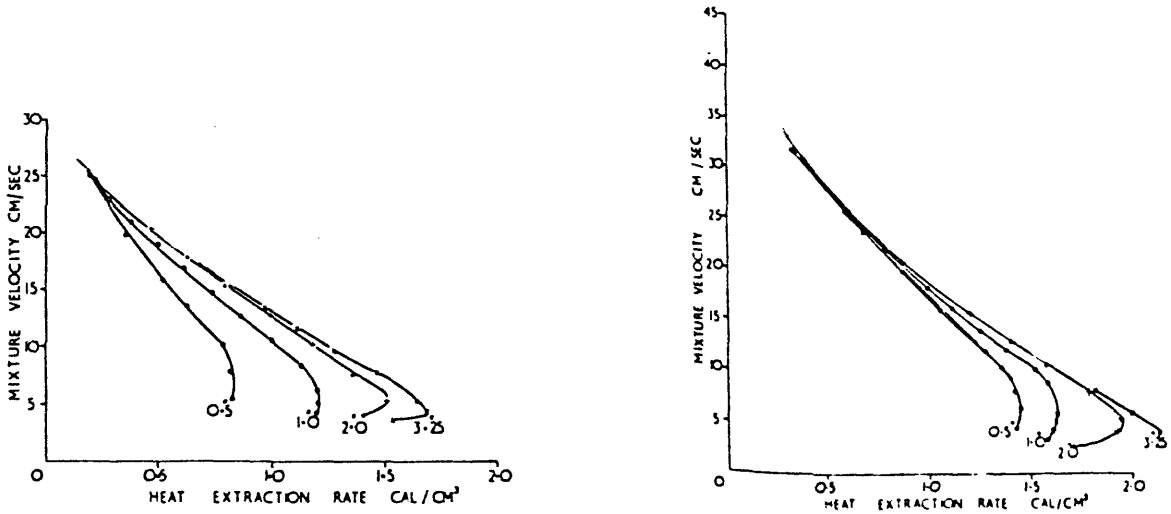

a) b)

Figure 2-5. Effect of heat loss on burning velocity [56]
a) 8% methane in air, b) 10% methane in air.
The numbers refer to burner diameter in inches.

These results are further evidence that observed flammability limits on burners are caused by aerodynamic effects, probably due to natural convection, and are not fundamental properties of combustible mixtures. These results also show that under the proper circumstances mixtures well outside the normal limits of flammability can be forced to propagate and mixtures well within the normally flammable range can be extinguished, making the concept of fundamental flammability limits less and less viable.

2.2.3.4 Models for prediction of flammability limits

A few simple ideas for predicting flammability limits have already been mentioned. It is suggested here, based on a large body of experimental data, that the limit burning velocity for flat-flame burner experiments is about 3-5 cm/s, regardless of fuel type or heat losses, at least for a given pressure. A possible exception occurs when combustion is accompanied by auxilliary heat input. There does not appear to be any data in the literature on flammability limits measured on flat-flame burners for pressures other than atmospheric. It is quite likely that different limit burning velocities would be found at other pressures since natural convection effects are found to be more significant at higher pressures, at least for flammability limits measured in tubes and closed bombs (section 2.2.3.3). The limit burning velocity would probably be a function of the gravitational conditions because it appears to be due to aerodynamic stability limits caused by natural convection, and would probably be less at reduced gravity. For upward propagation in tubes, there is substantial evidence (and some conflicting evidence) that the limit propagation velocity (not the burning velocity) is given by the equation $S_b = 0.328(gD)^{1/2}$. This is equal to the rate of rise of a bubble in the tube, and, according to Levy [48], is not dependent on the fluid densities as long

as the difference is adequate to give the bubble buoyancy and sufficient stability. This implies that S_b is independent of fuel type or pressure. For downard propagation in tubes, the limit burning velocity appears to be $S_{u,lim} \simeq K(g/g_o)^{1/3}$, with K $\simeq$ 8-9 cm/s, independent of fuel type or tube diameter. As with flat-flame burners, this formula may be dependent on ambient pressure, but there does not appear to be any data in the literature to test this notion. It is possible that the inconsistent effects of pressure on flammability limits for upward vs. downward propagation in tubes is due to the difference in pressure effects on limit propagation velocities, but again there appears to be no data in the literature to support or discredit this idea. No specific ideas for predicting flammability limits in closed bombs have been advanced thus far because of the many possible definitions for flammability limits in closed bombs and the complicated role of natural convection and the resulting fluid mechanics.

A number of theories have been presented in the literature which model flammability limits based on heat losses to the surroundings. Some theories consider limits based in whole or in part on losses to solid boundaries such as tube walls or flat parallel plates. These theories actually predict flame quenching limits (section 2.2.5.2), not flammability limits, and so, strictly speaking, lie beyond the scope of the current investigation. Nevertheless, it will be important to assess quenching effects on the experimental results in the current investigation and so the effects of conductive heat loss will be considered here briefly. Other theories attempt to predict limits based upon radiative heat losses without requiring heat sinks near the flame zone. Such theories could be independent of experimental apparatus and gravitational conditions, and so are of more interest to this work.

The most widely cited theory of flammability limits based on radiant heat loss is that presented by Spalding [59]. He assumed a one-dimensional system with two flame zones, an upstream zone in which a first-order reaction (a reaction in which the reaction rate is linearly related to the reactant concentration) takes place without heat loss, and a downstream zone in which heat loss takes place without reaction. He also assumed that the system was large enough that conduction heat losses were negligible and that the system was small enough that no reabsorption of radiation emitted by the gas occurred, i.e. that the surroundings absorbed all of the emitted radiation. In an infinitely large system, all emitted radiation would be reabsorbed by some part of the gas and no net heat loss would occur. Spalding concluded that if the dependence of the reaction rate on temperature were stronger than the dependence of the heat loss rate on temperature, a flammability limit was predicted at a finite fuel concentration with a finite burning velocity. For non-limit mixtures, two burning velocities were predicted but Spalding showed that the lower value was probably unstable. The results of Spalding's theory are shown in Fig. 2-6. In Fig. 2-6a the original figure from Spalding's paper is reproduced. λ is a dimensionless parameter which is proportional to S_u^{-2}. K is a dimensionless heat loss parameter. For the example shown, the reaction rate is proportional to T^{11}, where T is the gas temperature at any point, and the heat loss is proportional to T^4, which is representative of radiative heat transfer. The value of K at the nose of the curve corresponds to the maximum heat loss allowed or the minimum fuel concentration required. For greater values of K, no real values of λ exist. λ_c corresponds to the burning velocity at the flammability limit. Values of $\lambda < \lambda_c$ are stable and values of $\lambda > \lambda_c$ are unstable. Some calculations have been made here in order to translate these results into physically meaningful terms, in this case burning

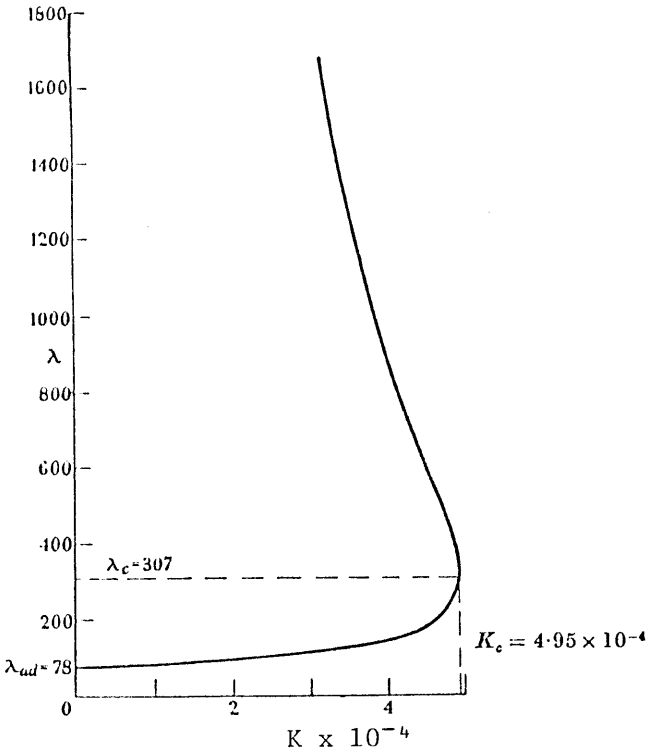

a)

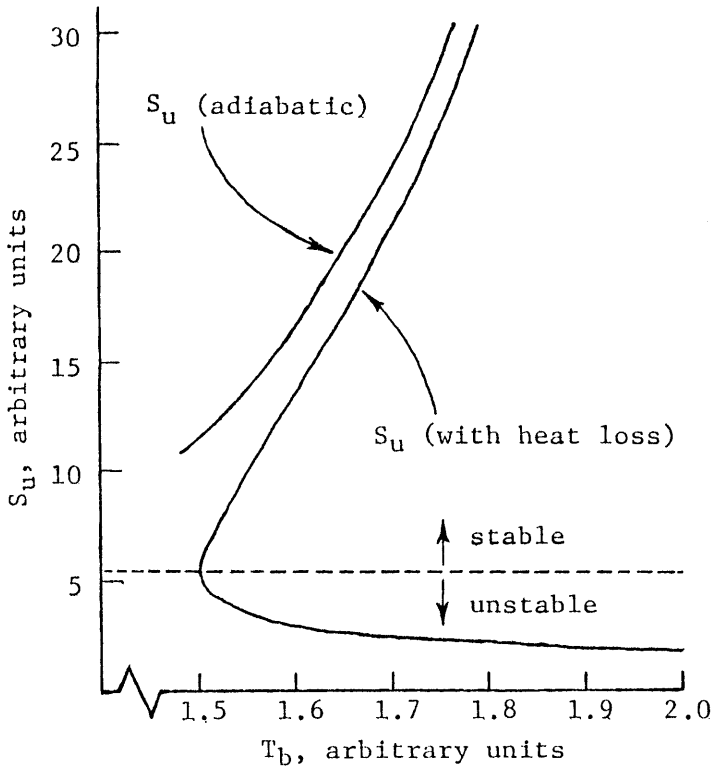

b)

Figure 2-6. Predictions of Spalding's [59] flammability limit theory, a) from Spalding's paper, b) calculated from Spalding's theory

velocity S_u and adiabatic flame temperature T_b. The details of the calculations are presented in appendix D and the results are shown in Fig. 2-6b. If dissociation of the combustion products can be neglected, which is usually reasonable below about 2000°K, then T_b is linearly related to the fuel concentration. A crucial prediction of Spalding's theory is that as T_b decreases or as the fuel concentration approaches the flammability limit, S_u drops further and further below its adiabatic value and at the flammability limit dS_u/dT_b approaches infinity. For conductive heat loss (i.e. quenching effects) rather than radiant heat loss the results are very similar. Other models of flammability limits based on heat losses [31,60] also appear to show similar results. This information will be very important in interpreting the experimental results of this study. Another prediction of Spalding's theory is that the limit burning velocity should be inversely proportional to the square root of ambient pressure, i.e. $S_{u,lim} \sim P^{-1/2}$, and at atmospheric pressure this burning velocity is 1.2 cm/s for lean hydrocarbon-air mixtures.

While it is not likely that the simplified theories of Spalding or other authors are completely accurate, one would expect them to show the proper trends with changing parameters (heat loss, ambient pressure, adiabatic flame temperature , etc.) if observed flammability limits could be attributed to radiative heat losses. There is certainly evidence, as Spalding presents, that such theories can give reasonable results when properly applied to flame quenching due to conductive heat losses in tubes. Also, a comparison of Figs. 2-5 and 2-6b shows substantial similarities between heat extraction from the burned gases in a flat-flame burner experiment and the theoretical effect of heat loss due to radiation, in particular the rapidly increasing slope of the burning velocity vs. heat loss curve near the point of extinction. Spalding warns against making too close a comparison, however, as radiant heat loss is

not the same as heat extraction by a cooled plate. On the cooled flat-flame burner, some of the supposedly "unstable" burning velocities can apparently be stabilized, as Fig. 2-5 shows. The conclusion is that such simplified theories can probably predict the general behavior, although not the exact results, of flame extinction due to heat loss.

On the other hand, Egerton and Powling [61] found no significant difference in the upward flammability limit of hydrogen-air mixtures measured in clear, silvered, and blackened standard flammability limit tubes, as so concluded that radiant heat losses were negligible. Bregeon et al. [49] came to the same conclusion by estimating radiant heat losses based on engineering data.

Thus, it is certainly not clear whether radiant heat losses can explain observed flammability limits. Evidence has already been presented suggesting that many or all observed limits are due to gravitational effects. Since flammability limits are observed even in zero-g, and observed limit burning velocities in zero-g are close to those predicted by Spalding [59], it is possible that such limits are indeed caused by radiative heat losses. This could explain the apparently unique mode of flame extinction in observed zero-g. The next crucial task to confirm or discredit this notion is to determine the shape of the S_u vs. T_b or fuel concentration curve near the zero-g flammability limit. Apparently such an investigation has not been performed to date.

Rosen [62] tried to predict flammability limits based on stability criteria. He showed that under certain conditions, a small disturbance in the heat production rate at a point in the flame front could grow without bounds, somewhat similar to a transition from laminar to turbulent flow in a non-reacting fluid. The flammability limit was defined as the limit of

stability and a finite burning velocity existed at the flammability limit. However, Rosen linearized the equations of mass and energy conservation and assumed steady state conditions existed. Since chemical reactions do not behave linearly with temperature, and any stability problem is inherently unsteady, it is not clear that such an analysis is valid. Furthermore, using a typical overall activation energy of 30 kcal/mole [47,63], Rosen's analysis appears to show that practically all hydrocarbon-air flames are unstable, clearly contrary to fact. Strehlow [32] suggested that if the temperature at the point of inflection of the flame temperature profile were greater than $(T_b - T_u)/2$, or somewhat equivalently, a short reaction zone was supporting a long preheat zone, the flame could be unstable. He did not provide any details to substantiate this idea. Contrary to Rosen, Layzer [64] and Richardson [65] concluded that all laminar steady-state flames are stable and small disturbances die away without leading to extinction. Spalding [59] also deduced such a result using qualitative arguments. It would intuitively appear that a flame front backed by an infinitely large burned gas volume without heat losses is resistant to temperature or heat production rate disturbances. There is no apparent mechanism for stopping the flame reactions totally because of the infinite burned gas volume behind the flame zone. Conversely, there is no apparent mechanism for accelerating the flame reactions indefinitely because of the infinite unburned gas volume ahead of the flame front. It seems that the flame, on the whole, must propagate at a speed balanced by the rate of chemical reaction, thermal conduction, and molecular diffusion. In essence this is the argument presented by Spalding.

Karlovitz et al. [66] developed the concept of "flame stretch" to model flame extinction. If a flame is propagating into a region where the flow streamlines are diverging, the heat conducted from the reaction zone to the

preheat zone is being distributed, or "stretched", into an increasing volume, thus the temperature gradient in the preheat zone is decreasing and therefore the burning velocity must decrease. If the burning velocity decreases to the point where it cannot propagate against the stream velocity or gas velocity due to natural convection, the flame is extinguished, or "blown off". Obviously significant flame stretch can occur only when the flame thickness is roughly comparable to the radius of curvature of the flame front. Significant flame stretch would not be expected on the flat-flame burners if the flame produced were truly flat, in closed bombs of adequate size, or in large tubes. Strehlow and Savage [67] predicted that if the upward flammability limit in a SFLT were due to flame stretch and the flame front were hemispherical, δ/r_t should be a constant at the limit, where δ is the preheat zone thickness previously defined and r_t is the tube radius. Since $\delta = k/\rho_u S_u C_p$, for a given fuel $\delta \sim 1/S_u$, and the theory of Strehlow and Savage would predict $S_u \sim (1/r_t)$ at the flammability limit. Levy's [48] theory predicts $S_b \sim (gD)^{1/2}$ or $S_b \sim r_t^{1/2}$. While the relationship between S_u and S_b for upward propagation in tubes is not clear, it is clear that an increase in S_u will always lead to an increase in S_b, so it is not possible for both criteria to hold at the flammability limit. Levy presented data which seemed to validate his theory, so it appears that the "flame stretch" concept does not predict flammability limits, at least for upward propagation in tubes, which is the most logical application of the concept.

Some investigators have attempted to predict flammability limits based on natural convection and buoyancy effects. The simple theory advanced by Levy [48] for upward propagation in tubes has already been mentioned. Lovachev [20] equated the Archemedian force acting on a rising spherical bubble, or "kernel", of burned gas to the drag force acting on the bubble to determine

the limiting rate of rise of the bubble and assumed that at the flammability limit the rate of rise of the bubble was equal to the rate of expansion of the bubble due to normal flame propagation. In this way he derived an expression for the limit burning velocity of

$$S_{u,lim} = 2\left[\frac{2}{3}\frac{k}{\rho_u C_p P_m}\left(1 - \frac{\rho_b}{\rho_u}\right)\left(\frac{\rho_b}{\rho_u}\right)^2 \frac{g}{C_w}\right]^{1/3},$$

where P_m is a coefficient dependent on the shape of the reaction rate vs. temperature curve (usually 0.25-0.5), ρ_b is the burned gas density, g is the gravitational acceleration, and c_w is the drag coefficient for a sphere of radius $r_b = 2k/\rho_u C_p S_{u,lim} P_m$, and the other parameters are as previously defined. The crucial predictions of this theory are that $S_{u,lim} \sim g^{1/3}$ and $S_{u,lim} \sim P^{-1/3}$, where P is the ambient pressure. Lovachev calculated that $S_{u,lim} \simeq$ 5-7 cm/s for lean hydrocarbon-air flames at atmospheric pressure and earth gravity. It appears that Lovachev's analysis is intended to predict downward propagation limits, although, incredibly, he does not state so explicitly. If this is so, the prediction of the model that $S_{u,lim} \sim g^{1/3}$ is in good agreement with the findings of Krivulin et al. [29] (section 2.2.3.3). The prediction that $S_{u,lim} \simeq$ 5-7 cm/s is in fair agreement with the value of 8-9 cm/s found by a number of investigators (section 2.2.3.3). Still, there are several unrealistic assumptions in this model, notably that the rising bubble of gas can be treated as a sphere in all respects, that r_b is equal to the flame thickness at the point of extinction, that the drag force acting on the bubble is the only factor which accounts for failure of the flame to propagate, and that at the limit, the bubble fails to accelerate but may continue to propagate at a steady rate. The shortcomings of Lovachev's theory are discussed in the reviews [16, 41].

Hertzberg [21] invented the questionable concept of a "combustion force", defined as the gradient of kinetic energy across the flame front, and proposed flammability limits by relating this force in differing and sometimes improper ways to the buoyancy force acting on the burned gases. The limit burning velocities calculated this way were

$$S_{u,lim} = \left[\frac{3}{8}\ \frac{\rho_u - \rho_b}{\rho_u + \rho_b}\ \alpha g\ \frac{\rho_b}{\rho_u}\right]^{1/3} \qquad \text{for upward propagation,}$$

$$S_{u,lim} = \left[2\alpha g\ \frac{\rho_b}{\rho_u}\right]^{1/3} \qquad \text{for horizontal propagation, and}$$

$$S_{u.lim} = \frac{1}{2}\ \frac{\rho_b}{\rho_u}\left[\frac{(\rho_u - \rho_b)}{(\rho_u + \rho_b)}\ gr\right]^{1/2} \qquad \text{for downward propagation,}$$

where α is a diffusivity related to both thermal and molecular diffusivities but is not clearly defined by the author and r_t is the tube radius, or flame kernel radius if the flame is unconfined. This analysis predicts limit burning velocities with gravitational dependencies of $g^{1/3}$, $g^{1/3}$, and $g^{1/2}$ for upward, horizontal, and downward propagation, respectively. Also, the theory predicts that $S_{u,lim} \sim P^{-1/3}$ for upward and horizontal propagation and that $S_{u,lim}$ is independent of pressure for downward propagation. Finally, $S_{u,lim}$ is independent of tube radius for upward and horizontal propagation, but $S_{u,lim} \sim {r_t}^{1/2}$ for downward propagation. The effects of g and r on $S_{u,lim}$ predicted by this analysis are contrary to the results cited in the previous section. While the pressure dependence on $S_{u,lim}$ has not been established experimentally, Hertzberg's analysis is in conflict with the previously cited theories which seem to show better agreement with the experimental data on the effects of g and r_t on $S_{u,lim}$. For methane-air mixtures, Hertzberg

calculated that $S_{u,lim}$ = 3 cm/s, 6 cm/s and 9 cm/s for upward, horizontal, and downward propagation, respectively, the last for a 30 cm diameter tube. According to Hertzberg's theory, for a 5 cm diameter tube, $S_{u,lim}$ would be 3.7 cm/s. Experiment shows that $S_{u,lim} \simeq$ 8-9 cm/s, independent of tube radius. A very critical analysis of Hertzberg's work is given in one of the reviews [16].

It is interesting to note that all of these convective theories of flammability limits predict that as $g \rightarrow 0$, $S_{u,lim} \rightarrow 0$. This implies that at g = 0, no flammability limit would exist. Again, this is contrary to fact.

Rather than attempting to predict convective flammability limits based on the notion of a rising spherical hot gas bubble or "combustion force", it would seem more logical to predict upward flammability limits by modeling the motion of a rising vortex ring or mushroom cloud with simultaneous flame propagation, as this is what is observed experimentally. If the ring or cloud broke up or became unstable instead of propagating smoothly, the mixture could be considered nonflammable. Such an analysis would require proper modeling of the fluid mechanics and hydrodynamic stability aspects as well as chemical reaction. It is very likely that the results would be sensitive to the initial (i.e. ignition) conditions. Apparently this type of analysis has not been performed to date. For downward propagation, it would seem reasonable to model the flammability limit as a stagnation in a one-dimensional system of arbitrary size where the flame front cannot propagate downward against the convective rise of the burned gases. Again this type of analysis does not appear in the literature. For horizontal propagation the situation is less clear, as simple intuition does not yield a reasonable model for predicting extinction of a flame propagating normal to the gravity vector. Undoubtedly two- or three-dimensional effects would be

important, and probably stability considerations similar to the upward propagating flame as well.

2.2.4 Burning velocity

2.2.4.1 Definition and measurement techniques

Burning velocity is defined as the rate of propagation of the flame front of an idealized laminar premixed gas flame (section 2.1.1) with respect to the unburned gases. Unlike flammability limits, it is clear that burning velocities are fundamental properties of combustible mixtures. All of the methods for realizing laminar premixed gas flames described in section 2.1.3 have been used to measure burning velocities, and agreement between these methods for a given mixture is fair, usually within a factor of two. Critical reviews of burning velocity measurements are given by Andrews and Bradley [38] and Gaydon and Wolfhard [68], so no attempt at a complete review will be made here.

Because burning velocities are fundamental properties of combustible mixtures and exist for idealized flames, they do not, by definition, depend on gravitational forces. For combustible mixtures with burning velocities much greater than natural convective gas velocities, measurements of burning velocities in one-g present no special difficulties. For slow burning mixtures, below about 10 cm/s, gravitational effects become significant and different experimental methods yield very different values of burning velocity. Measuring burning velocities in zero-g would eliminate these problems and allow more accurate measurements down to very low values. This is of great value in assessing the importance of heat losses in determining zero-g flammability limits (section 2.2.3.4). It is also of value in

verifying analytical predictions of burning velocity, as it is of interest to know if models which may accurately predict flame behavior for fast burning mixtures can also predict flame behavior for slow burning mixtures.

The basic methods of measuring burning velocities are derived from the equation of mass conservation, $\dot{m}$ = constant, where $\dot{m}$ is the mass flow rate. Along with the definition of burning velocity, this becomes $\dot{m} = \rho_u S_u A_f$ = constant, where A_f is the flame area for a one-dimensional or quasi-one-dimensional system. ρ_u is easily calculated from the ideal gas law, and A_f can be measured for a given experiment, so if $\dot{m}$ can be found, S_u is then determined. Measuring A_f does present some problems, because it will vary somewhat depending on what technique is used to visualize the flame, i.e. visual observation, schlieren photography, or shadow photography. This is particularly true for flames of significant thickness relative to the dimensions of the experimental apparatus.

For a Bunsen or flat-flame burner, $\dot{m}$ is easily measured from the flow rates of fuel and oxidizer into the burner. The only difficulties are in determining the "correct" value of A_f to use and compensation for edge effects. Such techniques are critiqued in the previously cited reviews.

In the tube method, the mass conservation equation yields [38]

$$S_u = (A_t/A_f)(S_b - S_g),$$

where A_t is the tube cross-sectional area, S_b is the observed flame propagation speed, and S_g is the average unburned gas velocity. If the tube is closed at the non-ignition end then $S_g = 0$. Viscous drag, finite flame thickness, and heat sink effects at the tube wall change the equation somewhat, as indicated in the reviews.

In the soap bubble method, the mass conservation equation yields [38]

$$S_u = (r_u/r_b)^3 S_b,$$

where r_u and r_b are the initial and final (burned) radius of the soap bubble, respectively. Again, finite flame thickness alters the equation somewhat, as discussed in the reviews.

In the closed bomb method, unlike the previously mentioned methods, combustion takes place at continually increasing pressure and temperature. This is an asset if it is desired to determine burning velocities as a function of pressure and temperature but a detriment if only an accurate value at the initial conditions is desired. Methods of calculation exist for both cases, and as the latter case is of the most interest in this study, only methods for calculation of a value of burning velocity at the initial temperature and pressuue in a closed bomb will be considered here. In a closed bomb both the effects of finite flame thickness at small flame radii and rising pressure and temperature during combustion at large flame radii may be significant. If accurate measurements of burning velocity at the initial conditions are desired, it is necessary to use a vessel large enough that the flame radius at which the effects of finite flame thickness become negligible is still small relative to the vessel dimensions. An estimate of the significance of rising pressure and temperature during combustion on burning velocities measured in this investigation is given in section 4.3.3.

If the effects of finite flame thickness and rising pressure and temperature can be neglected, then the mass conservation equation $\dot{m} = \rho_u S_u A_f = \rho_b S_b A_f$ yields [38]

$$S_u = (\rho_b/\rho_u) S_b = n(T_u/T_b) S_b,$$

where n is the ratio of total moles per unit mass in the burned gas to total moles per unit mass in the unburned gas. The second equality assumes a constant pressure across the flame, which is a reasonable assumption (section 2.1.1). Calculations of n along with T_b are presented in Appendix B. If the

effect of finite flame thickness cannot be neglected, but the pressure rise in the vessel due to combustion is still small, Andrews and Bradley [38] proposed the following modification:

$$S_u = (\bar{\rho}_b/\rho_u)S_b = n(T_u/T_b)IS_b,$$

where $\bar{\rho}_b$ is the average burned gas density and

$$I = \left[\frac{3T_b}{r_b^3}\int_0^{r_b}\frac{r^2dr}{T(r)}\right],$$

a correction to account for the fact that not all of the "burned" gas in the flame front is completely burned, but a temperature (and therefore a density) profile exists, as shown in Fig. 2-7. Here r_b must be taken at the position in the flame front for which S_b is actually determined. This could be the position of the luminous zone, schlieren zone, or shadow zone, depending on how the flame is visualized. Andrews and Bradley did not make this distinction, as they took r_b as the radius where $T \simeq T_u$, which is not well defined and is certainly beyond the point visualized by any of the aforementioned methods. This would lead to an overestimate of I and therefore S_u. The method requires knowledge of the flame temperature profile and the position in the profile that is visualized to determine S_b. This information is seldom known accurately. In order to calculate I for different mixtures, Andrews and Bradley measured overall flame thicknesses for these mixtures and assumed that all had temperature profiles geometrically similar to the measured profile in a stoichiometric mixture. This may be reasonable for near-stoichiometric mixtures, but for slower burning mixtures, more of the overall flame thickness is in the preheat zone and less is in the reaction zone [32], so the profiles are not similar. Because it was not intended to measure flame temperatures directly in the current investigation, and flame

temperature profiles are difficult to calculate accurately, the method of Andrews and Bradley will not be used here. This will lead to an underestimation of S_u. Steps will be taken to minimize these errors and an estimation of their magnitude will be presented in section 4.3.2.

Andrews and Bradley [69] have also determined burning velocities in a closed bomb by measuring S_b using the normal methods and measuring S_g, the unburned gas velocity in the laboratory reference frame, with a hot-wire anemometer. By definition $S_u = S_b - S_g$. It is very difficult to use a hot-wire anemometer in an experiment to be performed in zero-g, so this method will not be considered here.

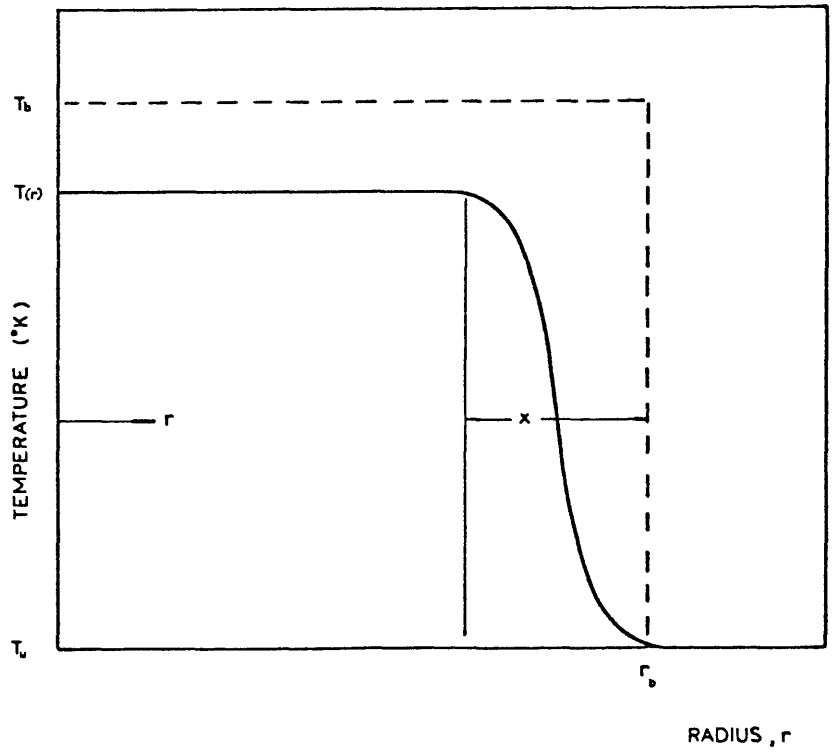

Figure 2-7. Correction in burning velocity calculation to account for finite flame thickness in spherical flame front [38]

2.2.4.2 Results of burning velocity measurements

As would be expected, the burning velocity for a given fuel and oxidizer is a maximum for a near-stoichiometric mixture and tapers off on either side of this maximum. Addition of diluent gases reduces burning velocity as well. A typical result [70] for methane-air mixtures at atmospheric pressure and room temperature is shown in Fig. 2-8. It should be noted that, at least for lean mixtures, the plot of S_u vs. concentration is practically a straight line, as some models (section 2.2.4.3) predict. Extrapolation of this line predicts zero burning velocity at about 4.8% methane. Of course, the theory predicts that S_u approaches zero asymtotically with decreasing concentration, but S_u would be extremely small below this value. It is interesting that this value is about the same as the methane concentration of 4.62% corresponding to the minimum reaction temperature for methane of 1403°K found by Weinberg and collaborators [52, 53] for a "Swiss roll" burner with heat recirculation (section 2.2.3.3). Badami and Egerton [47] found straight-line plots of S_u vs. concentration for a wide variety of lean fuel-air mixtures below 8 cm/s, although for some fuels there was a "kink" in the line at about 5 cm/s. Extrapolation to $S_u \simeq 0$ for methane yielded a concentration of about 4.75%. Thus, it appears quite likely that for many fuel-air mixtures, below a certain point the burning velocity drops almost linearly with reactant concentration toward zero, and so below a certain fairly well-defined concentration the burning velocity is so close to zero that combustion cannot be maintained under normal conditions.

As with flammability limits, burning velocities exhibit a wide variety of behavior with changing pressure. The effects of pressure on burning velocity has been reviewed by Gaydon and Wolfhard [48]. They have shown that the effect can often be expressed in the form $S_u = KP^n$, where K and n are

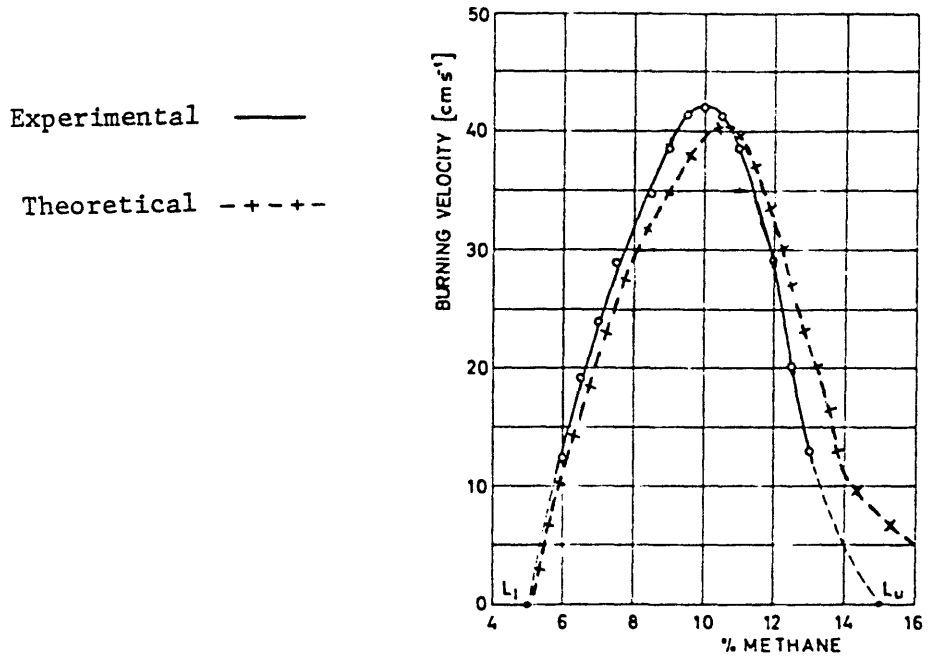

Figure 2-8. Experimental results [70] and theoretical predictions [37] of burning velocities of methane-air mixtures at standard conditions

---

constants for a particular fuel and mixture ratio. Andrews and Bradley [69] have shown that for stoichiometric methane-air mixtures with P > 5 atmospheres, n ≃ -0.5. For lower pressures n decreases, leveling off at about 0.12 for P < 0.6 atmospheres [37]. Lewis [71] found that for a wide variety of hydrocarbon-air and hydrocarbon-oxygen mixtures, n is positive for S_u > 100 cm/s and negative for S_u < 100 cm/s. His results are shown in Fig. 2-9. Other fuels may show different effects, or no effect at all with changing pressure.

Fristrom and Westenberg [33] point out that pressures below 0.1 atmosphere, practically all molecular collsions are bimolecular. At higher pressures, trimolecular and higher order collisions become more important, so

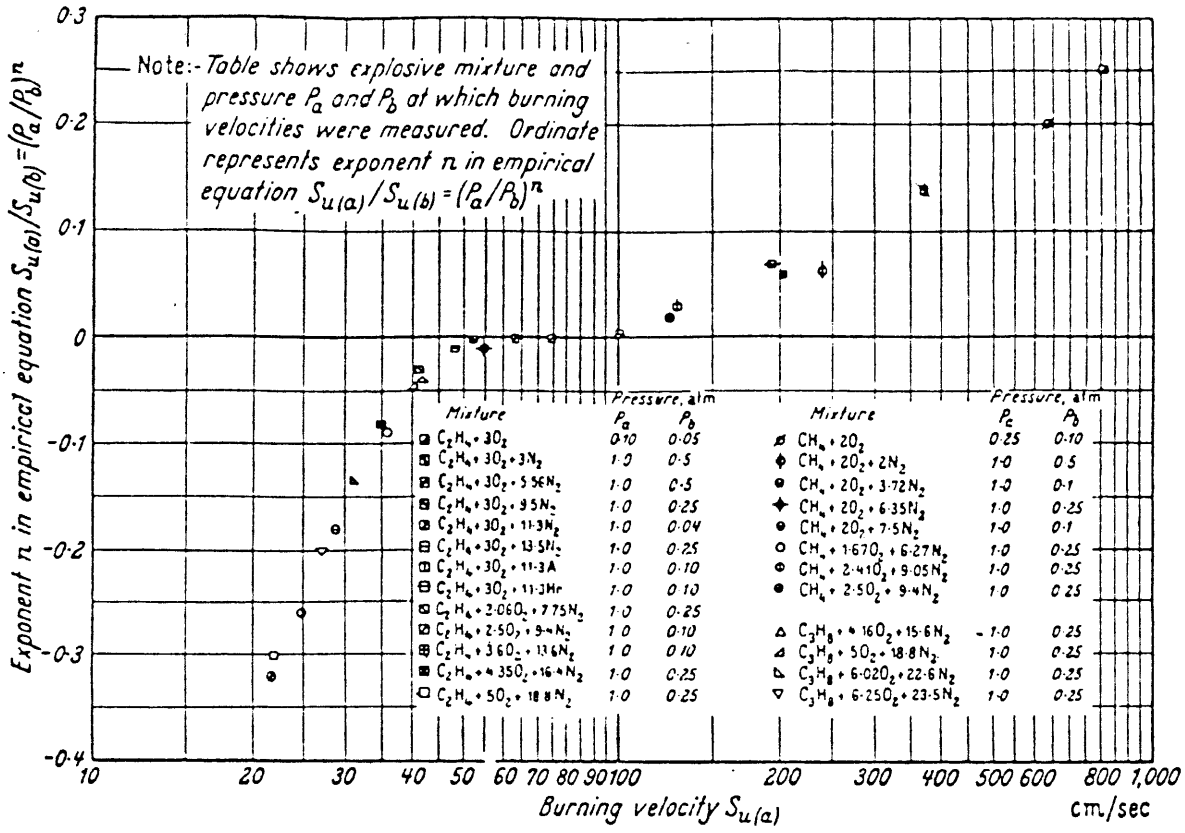

Figure 2-9. Effect of pressure on burning velocities in hydrocarbon-oxygen-nitrogen mixtures [71]

---

one would expect different reactions to be significant in higher pressure flames. Since different reactions are important to different flames, this may provide a partial explanation of the wide variety of pressure effects on burning velocities. These authors also believe that since trimolecular collisions are required to achieve equilibrium in flames that contain radicals, as most flames do, at low pressures it is more reasonable to consider the flame as consisting of only bimolecular reactions without attainment of chemical equilibrium because trimolecular collisions become increasingly rarer at reduced pressures. This reduces the apparent flame

temperature and will increase the underestimate of S_u at low pressures as calculated by the equation $S_u = n(T_u/T_b)S_b$.

An increase in unburned gas temperature apparently always increases burning velocity. This is in harmony with the effects of temperature on flammability limits. Some authors [37, 69] show this effect in an equation of the form $S_u = a + bT_u^n$, where a, b, and n are constants, typically with n = 2. Probably a more instructive approach is to examine the effect of adiabatic flame temperature on burning velocity. Gaydon and Wolfhard [68] have shown that a single curve of S_u vs. T_b fits practically all the burning velocity data for hydrocarbons, alcohols, ethers, and carbon disulfide burning in air or oxygen. Data for different fuels, such as hydrogen, or different oxidizers, such as nitrous oxide, will lie on other self-consistent curves. Data from Kaskan [54] shows that plotting log S_u vs. $1/T_b$ yields a straight line with negative slope, hence the equation is of the form $S_u = a \exp(-b/T)$.

An explanation for these observations can be found in the effect of temperature on reaction rate. Simple flame theory [31] predicts an equation of the form

$$S_u \sim (1/\rho_u)[(k/C_p)\dot{w}]^{1/2},$$

where $\dot{w}$ is the chemical reaction rate per unit volume. If the flame can be considered to have only a single overall reaction, then the reaction rate is given by

$$\dot{w} \sim P^n \exp[-E_a/RT_b],$$

where n is the order of reaction [not to be confused with the burning velocity exponent cited earlier in this section] (typically 1-2), E_a is the overall activation energy, and R is the universal gas constant. Since $\rho_u \sim P$, $k \sim T_b$ (approximately), and C_p is mostly independent of P and T_b, the equation for burning velocity becomes

$$S_u \sim p^{(n-2)/2} T_b^{1/2} \exp[-E_a/2RT_b].$$

For a typical activation energy for hydrocarbon-air flames of 30 kcal/mole [47, 63], a change in T_b from 2000°K to 1000°K will lower S_u by a factor of 62. Reaction rate depends on concentration of reactants as well as temperature, but the dependence is given by $\dot{w} \sim c^n$, where c is the reactant concentration, so $S_u \sim c^{n/2}$. This effect is usually overwhelmed by the effect of concentration on T_b and thus S_u. The same argument applies to the effect of concentration on thermal conductivity or molecular diffusivity. Thus, burning velocity is usually more dependent on E_a/T_b than any other single factor. Different fuels will have different activation energies, but families of fuels such as hydrocarbons have similar activation energies [47], probably because of similar reaction mechanisms. The conclusion is that for a given fuel or family of fuels, burning velocity can often be considered, with reasonable approximation, to be a function only of adiabatic flame temperature.

The experimentally observed effects of heat loss on burning velocity were presented in section 2.2.3.3 and analytical predictions were presented in section 2.2.3.4. The conclusion was that heat loss effects on burning velocity should only be important fairly near a flammability limit caused by heat loss, with little effect for significantly faster burning mixtures.

Two investigations have been made on the effect of gravity on flame propagation velocity. While burning velocities are fundamental properties of combustible mixtures defined for an idealized one-dimensional laminar flame and do not depend on external effects such as heat losses or gravity, in practice such effects may alter the measured burning velocities. Parfenov [14] investigated the effect of gravity on flame propagation velocities for lean hydrogen-oxygen mixtures in a tube of unspecified diameter closed at both

ends. He found that the flame propagation velocity was greater in one-g than zero-g although, incredibly, he did not state whether the one-g flame propagation velocities were measured for upward or downward propagation. His results would suggest that the one-g propagation was upward. At 100 Torr (0.13 atmosphere) ambient pressure, the effect of gravity on flame propagation velocity was negligible above $S_u \simeq 15$ cm/s. Reuss [16] investigated the effect of gravity on flame propagation velocities for lean methane-air mixtures at atmospheric pressure in a SFLT. He found that one-g downward and zero-g flame propagation velocities were about equal and one-g upward propagation velocities were considerably higher, particularly for near-limit mixtures. He also computed burning velocities for a 5.87% methane-air mixture using the method outlined in section 2.2.4.1 and found values of 13.2, 8.6, and 6.8 cm/s for upward, downward, and zero-g propagation, respectively. He attributed these differences to different amounts of heat loss. It will be shown in section 4.3.3 that heat loss was probably not significant in his experiment, so the variation in burning velocities is somewhat puzzling. Obviously gravitational effects are involved, but the manifestation of these effects is not clear.

2.2.4.3 Models for prediction of burning velocity

Prediction of burning velocities, even for an idealized one-dimensional flame, is a challenging task due to the complex interactions of chemical reaction, thermal conduction, and molecular diffusion for a multicomponent gas mixture. Early theories circumvented the problem by assuming a single overall reaction rate expression such as the one presented in the previous section, a single averaged thermal conduction coefficient, and a diffusion coefficient D estimated by assuming a Lewis number $Le = \rho C_p D/k$ of unity or zero. Obviously

such simple models can hope to accurately predict the behavior of only the simplest of flames. A review of these early theories is given by Williams [31].

More recent models of flame propagation [34-37] attack the problem more completely, employing large reaction mechanisms and more realistic conduction and diffusion models. Even in these models, however, some empiricism is often employed. For example, values of various reaction rates taken from the literature are sometimes "modified" slightly in order to obtain better agreement between the model and experimental data. In the case of methane-air and methane-oxygen combustion, probably the most complete model is that presented by Tsatsaronis [37]. His results are shown in Fig. 2-8. He found that only two of the 29 elementary reactions in his postulated reaction mechanism were negligible, illustrating the necessity of a complex model to properly describe flame behavior. While the details of these flame models will not be presented here, some comparisons will be made between the predictions of Tsatsaronis' model and the findings of this investigation in chapter 4, and the implication of these comparisons will be discussed.

2.2.5 Minimum ignition energy

2.2.5.1 Definition and measurement techniques

It has been found that small sparks or other sources of ignition energy can be passed through a combustible gas mixture without producing ignition. If the ignition energy is increased sufficiently, a flame is initiated and propagates throughout the mixture. This minimum ignition energy (MIE) is a fundamental property of the combustible mixture but is even more dependent on the experimental apparatus than flammability limits or burning velocities are.

It is not obvious that a minimum total energy should be a criterion, i.e. it could be assumed that if the gas were raised to an adequately high temperature, even in only an extremely small volume, a self-propagating flame would result. This is not borne out by experiment; the actual requirement is a minimum total energy requirement in a sufficiently small volume, or equivalently a minimum energy density (i.e. temperature) in a sufficiently large volume. At the flammability limit, the MIE is essentially infinite, that is, no matter how much energy is imparted to the mixture, it will not produce a flame which can propagate throughout an indefinitely large volume of the mixture. Lewis and von Elbe [30] and others believe the existence of a minimum total energy requirement for ignition can usually be explained by a purely thermal theory (Fig. 2-10): A small amount of energy at a high temperature is introduced into the gas mixture. When the resulting heat conduction and chemical reaction wave reaches a distance from the origin roughly comparable to the flame thickness, if the temperature at the origin has dropped below the steady-state flame temperature (Fig. 2-10a), then the reaction rate at the spark origin is too low, the temperature gradient in the flame front is too shallow, and will continue to grow flatter, leading to extinction of the flame, although a small quantity of fuel will be consumed. Thus, the initial energy introduced into the gas mixture was insufficient for ignition. If the initial energy is increased slightly (Fig. 2-10b), when the thermal wave has extended to the flame thickness, the temperature at the origin is above the steady-state flame temperature, the reaction rate at the spark origin is sufficiently high, the temperature gradient is sufficiently steep and the profile sufficiently wide, and a steady flame develops which propagates throughout the mixture.

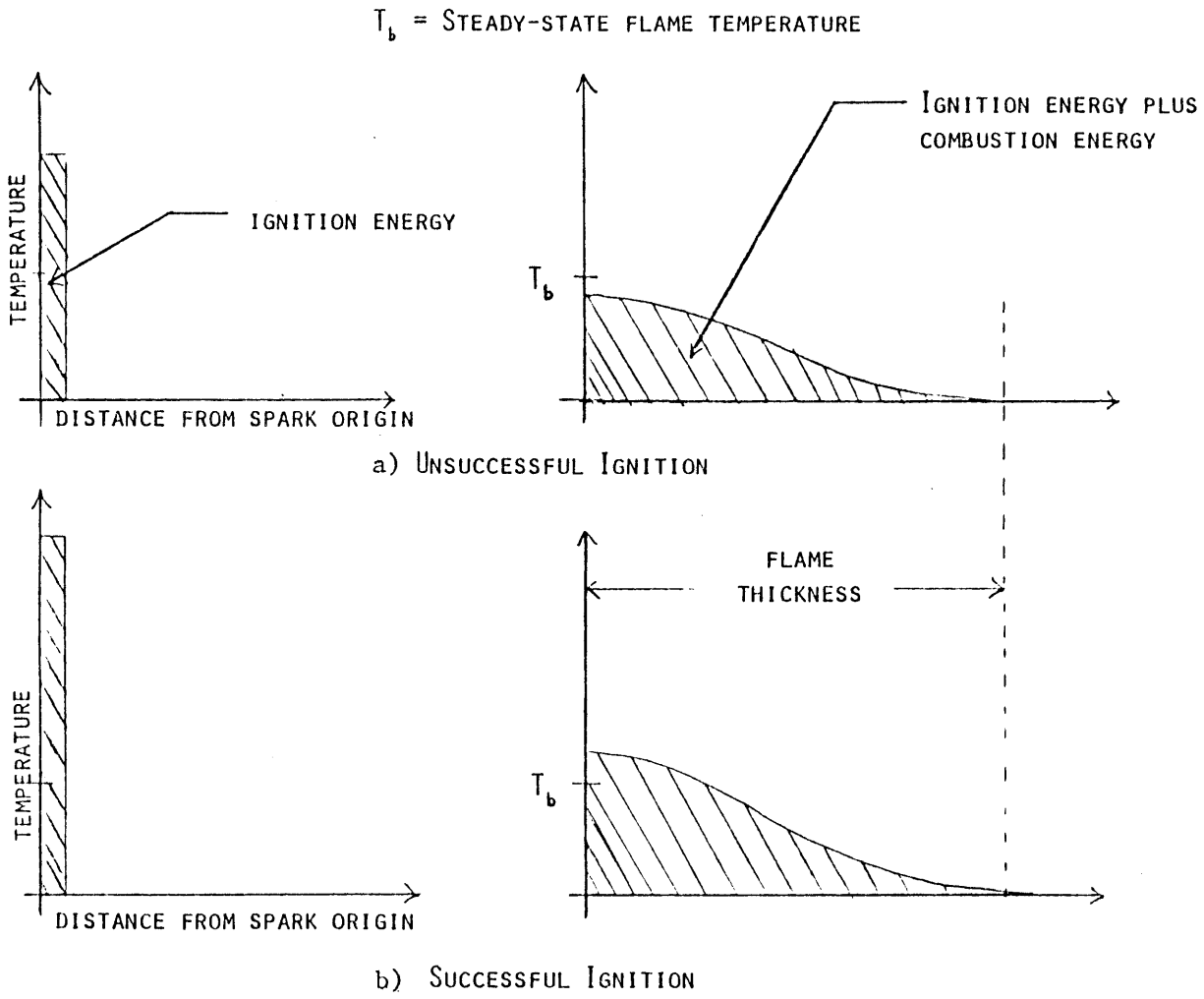

Figure 2-10. Postulated ignition mechanism

Based on this explanation for the existence of a minimum energy for ignition, the criterion for ignition can be stated as follows: ignition will occur if enough energy has been added to the gas to raise a sphere of gas with a radius roughly equal to the flame thickness to the adiabatic flame temperature. This criteria can be shown [31] to be about the same as the statement that enough energy must be added to the combustible mixture to balance the rate of heat generation in the flame with the conductive heat loss to the unburned gases.

The most common energy source for determining minimum ignition energies in premixed gases is electric spark discharges. Other sources sometimes employed include impact (friction) sparks, electrically heated wires, and more recently, lasers. Electric spark dicharges have numerous advantages for studying minimum ignition energies: simplicity of implementation, high energy density, short energy release duration, and relative ease of control and measurement of both total energy release and energy release rate. Also, most of the available data on minimum ignition energies for premixed gases have been determined using electric spark discharges. The electric spark ignition problem also has importance in practical considerations, such as the investigation of flammability hazards associated with materials subject to electrical malfunctions. The importance of these investigations to the problems under study here was discussed in the introduction. For these reasons, this investigation will utilize electric spark discharges for the determination of minimum ignition energies, and other sources of ignition energy will not be considered here.

A number of investigators have reported results for spark ignition in flowing gases. While such an approach may have some practical applications, it introduces at least two new variables, flow velocity and turbulence

intensity (if any). Because of this complication, spark ignition in flowing gases will not be considered here.

Investigations of minimum ignition energies in nonflowing gases virtually always employ closed bombs. The most commonly used apparatus is that of the U.S. Bureau of Mines [72] or the Bureau of Mines apparatus modified by Blanc et al. [73]. A 5 inch diameter spherical bomb is used. The bomb is filled with combustible mixture and a bank of high-voltage capacitors, in series with a spark gap located at the geometric center of the vessel, is slowly charged until the voltage exceeds a critical value and breakdown occurs across the spark gap. The energy E dissipated in the spark is assumed to be the energy stored in the capacitors just prior to breakdown, so $E = 1/2\ CV^2$, where C is the total capacitance of the circuit and V is the voltage across the capacitors just prior to breakdown. If the spark did not produce ignition, C is increased and the process is repeated until ignition occurs. The energy stored in the capacitors in the test which just produced ignition is deemed the MIE. Other authors [74-77] use alternate methods of producing sparks in order to obtain better control of spark duration and spark power. In this case the energy dissipated in the spark is usually determined by measuring spark voltage and current waveforms on an oscilloscope and computing the spark energy from the expression

$$E = \int_0^{t_s} P(t)dt = \int_0^{t_s} I(t)V(t)dt$$

where t_s is the spark duration and P(t), I(t), and V(t) are the instantaneous spark power, current, and voltage, respectively. The effect of these various types of sparks will be discussed in the following section.

It should be noted that as ambient pressure or burning velocity decreases, the characteristic dimension of the flame increases, so a larger vessel is needed to insure that ignition or extinction of the spark kernel

will occur before wall effects become significant. This implies that a vessel larger than the 5 inch diameter sphere used by the Bureau of Mines may be required for low pressure, slow-burning mixtures.

2.2.5.2 Results of minimum ignition energy investigations

Numerous investigations [77-80] have shown that in the early stages of flame development from a spark or other short duration, high intensity source, expanding flame kernels from sparks of insufficient energy for ignition are indistinguishable from sparks of adequate energy for ignition. In fact, these are indistinguishable from sparks in inert gas alone. These observations show that the early stages of spark kernel development are not affected by chemical reaction, but only by the spark parameters and the thermodynamic properties of the gas. Extinguishment for sparks of insufficient energy for ignition in combustible mixtures occurs at a radius of propagation somewhat larger than for spark kernels in inert gas alone. The radius at which distinction between ignition and non-ignition spark kernels in a combustible mixture becomes possible is only slightly less than the extinction radius for non-ignition spark kernels. This critical radius seems to be at the point where the expanding bubble of gas has slowed down to about the expansion rate of a normal flame in that gaseous mixture. Beyond this radius, flame kernels resulting from sparks of subcritical energy soon extinguish, while flame kernels resulting from sparks with greater than this critical energy develop into a steadily propagating flame. The observed flame kernel radius shows a logarithmic time dependence in the initial stages of propagation, that is, below the critical radius. Above the critical radius, if a steadily propagating flame develops, the time dependence of course becomes linear. These results seem to apply to a wide variety of fuels, concentration ratios,

and minimum ignition energies, suggesting similar mechanisms of propagation and extinguishment for these varying conditions. A typical result [80] for 8.5% methane in air at 0.1 atmosphere and 40 millijoules spark energy is shown in Fig. 2-11.

It appears that the amount of energy liberated by chemical reaction before extinction in subcritical flame kernels is about an order of magnitude higher than the spark energy input. This indicates that some self-propagation occurs even under conditions that will not lead to indefinite steady-state propagation. The energy liberated by chemical reaction can be estimated from the sensible energy E_s residing in the flame kernel, which is given by

$$E_s = m_b C_p (T_b - T_u) = \rho_b V_b C_p (T_b - T_u),$$

where m_b, ρ_b, and V_b are the mass, density, and volume, respectively, of the burned gas bubble. For an ideal gas and spherical bubble, this equation becomes

$$E_s = [4\Pi\gamma/3(\gamma-1)](1 - T_u/T_b)Pr_b^3,$$

where γ is the specific heat ratio of the gas, P is the ambient pressure, and r_b is the observed flame kernel radius. For typical lean hydrocarbon-air mixtures $\gamma \simeq 1.4$, $T_u = 300^\circ K$, and $T_b = 1500 - 2200^\circ K$. Using an average T_b of $1800^\circ K$ (the variance in T_b will cause only a small change in the $1 - T_u/T_b$ term), the equation becomes

$$E_s \simeq 12\ Pr_b^3.$$

This equation overestimates the sensible heat residing in the bubble because not all of the gas in the bubble will be at T_b due to incomplete combustion, heat losses, and the effect of finite flame thickness. On the other hand, there will probably be some sensible heat due to combustion residing outside the observed radius of the flame kernel because the visualized radius of the flame kernel will be at a temperature $T_{vr} > T_u$, and finite flame thickness

dictates that some gas outside this visualized radius will be at a temperature above T_u but below T_{vr}. The value of T_{vr} will depend on the method of flame visualization, i.e. optical, schlieren, or shadowgraph photography. The effects of incomplete combustion inside the visualized radius of the flame kernel and hot gas outside the flame kernel will tend to cancel each other out to some extent, so the above equation is probably a reasonable estimate of E_s. Table 2-1 shows the ratio of the estimated sensible energy residing in the burned gas kernel just before extinction to the initial spark energy for investigations reported in the literature where enough information was given to calculate such a ratio. It is seen that this ratio varies from about 5 to 20 for a wide range of conditions. These results again suggest that the mechanism for extinction of subcritical flame kernels is similar for these varying conditions. This information will be useful in interpreting the results of the present investigation.

It should be noted that some authors [75,78] do not report minimum ignition energies, but rather the probability of ignition for a given spark

---

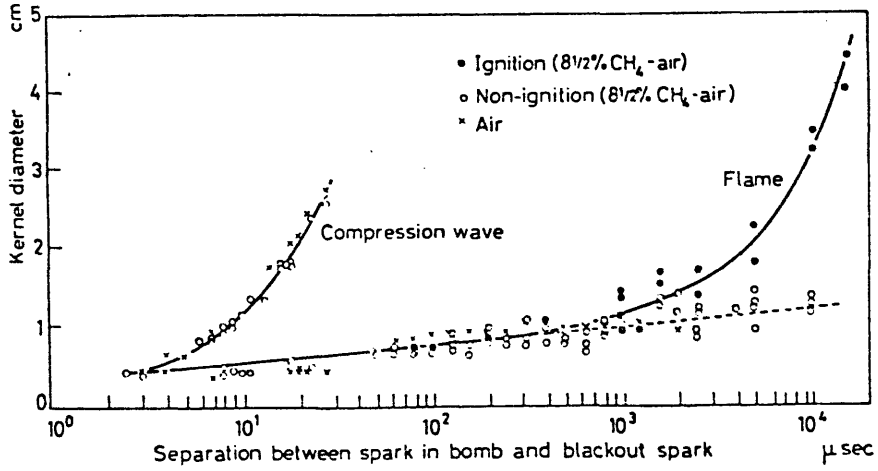

Figure 2-11. Spark or flame kernel development at 0.1 atmosphere for a 40 millijoule spark [80]

Reference	Conditions	Spark Energy (E)	Extinction Radius	Calculated Energy Released (E_s)	E/E_s
[77]	3.0% propane DC spark	6.50 mj	4.0 mm	77 mj	12
[77]	3.0% propane AC spark	8.34 mj	3.5 mm	51 mj	6.2
[79]	8.5% methane	~ 1 mj	2.0 mm	10 mj	10
[78]	2.7% propane	4.08 mj	2.4 mm	17 mj	4.2
[83]	4.0% propane	1.14 mj	~2 mm	10 mj	8.8
[29]	8.8% propane zero-g	17 J	65 mm	384 J	23

Table 2-1. Ratio of energy release to spark energy input in subcritical flame kernels for various fuel-air mixtures at atmospheric pressure

energy. It seems that spark ignition in gases is somewhat of a stochastic process, and reporting ignition probabilities "smooths out" the data. A statistical averaging procedure may be acceptable if it is possible to perform a large number of tests, but with the fairly limited number of tests available in a zero-g experiment, such a procedure is clearly not feasible. The degree of randomness appears to be fairly low, however, as Lintin and Wooding [79] reported that for an 8.5% methane-air mixture at atmospheric pressure, increasing or decreasing the spark energy by 5% from the value required for 50% probability of ignition resulted in 100% or 0% probability of ignition, respectively. If the stochastic nature of spark ignition for other mixtures is also confined to a region whose width is about 10% of the minimum ignition energy, then these random effects can probably be neglected in the current investigation.

The MIE of a combustible mixture depends somewhat on the type of spark employed. Kono et al. [77] found that for short duration sparks, minimum ignition energies were equivalent for AC and DC discharges, but for longer spark durations, the MIE was lower for DC discharges. These authors also found that the MIE was lower for a steady DC spark than for one with a high initial energy pulse. Swett [74] found that minimum ignition energies were slightly lower for arc discharges than glow discharges. Of course, these effects cannot be explained by the simple thermal hypothesis advanced in the previous section, but the minimum ignition energies found using these different types of sparks seem to agree to withn a factor of 2 or 3, which is probably about as good as can be expected. Nevertheless, caution should be exercised when comparing results obtained with differing types of spark discharges.

The minimum spark ignition energy has been shown [30,72,74,77,81] to be dependent on the spark electrode configuration. In virtually every case it is found that the MIE is less with smaller electrodes. The prevailing opinion of these authors is that this is due to greater conductive heat loss from the hot, burning gases to larger electrodes as the flame kernel is developing, thus increasing the energy input required for ignition. Indeed, it is found [30] that for large flat parallel plate electrodes, if the gap between the electrodes is less than a critical distance, no self-propagating flame is observed regardless of the ignition energy. This critical distance is called the quenching distance. The quenching distance d is related to the flame preheat zone thickness δ by an expression of the form [31]

$$d = a\delta$$

where $a \simeq 40$ and is not strongly dependent on the properties of the combustible mixture. The quenching distance also seems to be about equal to the critical flame diameter previously discussed [30,80].

Some authors [74,81] have found that the electrode material has an effect on the MIE, perhaps due to a slight evaporation of electrode materials caused by the spark, which would absorb some of the energy that would otherwise heat the gas. Other authors [82] have found no effect of electrode material. In any event the effect seems to be fairly small, but it indicates that comparisons of minimum ignition energies should be made only for similar electrode materials.

The MIE has also been found [30,74,77,81] to be dependent on the spark electrode gap. A typical plot [30] of MIE vs. spark gap is shown in Fig. 2-12. It is seen that the energy is lowest when the spark gap is equal to the quenching distance. For flat parallel plate electrodes the energy rises very abruptly for smaller gaps, whereas for small diameter electrodes the rise is

much more gradual. For gaps larger that the quenching distance, the MIE is practically constant out to about twice the quenching distance, then (not shown in the figure) rises slowly for still larger spark gaps. The accepted explanation [30] for this behavior is that below the quenching distance, even small diameter electrodes cause significant conductive heat loss which increases the minimum energy required for ignition. For spark gaps significantly larger than the quenching distance, the spark energy is dissipated over a volume larger than the minimal flame kernel, hence the energy required for ignition is increased. So, in some sense, the most "fundamental" MIE, that is, the one obtained with the least amount of complicating effects, is that obtained with the spark gap at the quenching distance. Data on quenching distances for a wide variety of conditions are given by Lewis and von Elbe [30]. In cases where data are not available, the quenching distance can be determined experimentally if necessary. In any case, the MIE is not a strong function of spark gap when the gap is reasonably close to the quenching distance, so a MIE close to the "fundamental" value can be obtained over a fairly wide range of spark gaps.

The MIE has also been found [75-77,81] to be a function of the spark duration. A reasonably well defined optimum spark duration exists which minimizes the total energy requirement for ignition. This duration depends primarily on the properties of the combustible mixture, although such factors as the type of discharge and the quenching effect of the electrodes have some effect as well [77]. Only a few values of optimum spark duration have been reported in the literature, and some of these are shown in table 2-2.

Kravchenko et al. [75] point out that the optimum spark duration they found for a stoichiometric methane-air mixture is about the same as the critical flame kernel development time found by Lintin and Wooding [79] under

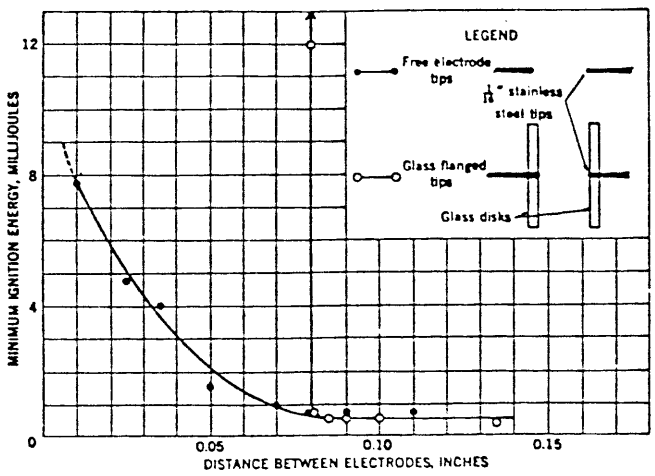

Figure 2-12. Effect of spark gap on minimum ignition energy for stoichiometric natural gas (about 83% CH_4 + 17% C_2H_6) and air mixture at atmospheric pressure [30]

---

the same conditions. Kono et al. [77] found similar agreement for a 3.0% propane-air mixture. Kono et al. also found that for progressively leaner mixtures of propane, in which the burning velocity was decreasing, and presumably the ignition development time was increasing, the optimum spark duration was increasing. Thus, one is led to believe that the optimum spark duration is about the same as the critical flame kernel development time. This time would be on the order of δ/S_u, and since, roughly, $\delta \sim 1/S_u$, this time would be proportional to $1/S_u^2$.

The reason for the existence of a lower bound on optimum spark duration is not clearly understood. It cannot be explained by the simple thermal hypothesis. Kravchenko et al. [75] believe short-duration sparks cause greater turbulence and therefore greater conductive heat loss from the hot burned gas to the cold unburned gas. Kono et al. [77] believe short-duration sparks cause greater turbulence and therefore greater conductive heat loss to

Reference	Conditions	Optimum spark duration	Minimum ignition energy
[75]	8.5% methane atm. press.	110 μs	0.6 mj
[75]	20% hydrogen atm. press.	10 μs	-- *
[81]	50% hydrogen atm. press.	1 μs	0.05 mj
[77]	2.2% propane ** atm. press.	5000 μs	200 mj
[77]	3.5% propane atm. press.	50 μs	0.3 mj
[76]	4.2% propane 0.17 atm.	75 μs	5 mj

* Not given by the author; 0.03 mj according to [30]
** Lean flammability limit

Table 2-2. Optimum spark durations for various fuel-air mixtures

---

the spark electrodes. Lewis and von Elbe [30] feel that shock waves produced by short-duration, high intensity sparks dissipate energy and cause minimum ignition energies to be higher for these short-duration sparks. Rose and Priede [81] suggest that effects associated with ionization of the spark gap for a longer period of time with longer duration sparks on some way reduce the total energy requirement. Swett [74] believes that the difference in the way the energy is distributed along the discharge length for different spark durations causes longer duration sparks to be more effective for ignition. Thus, there is a wide variety of opinions as to the cause of a lower bound on optimum spark duration.

The reason for an upper bound on optimum spark duration is well understood [75,77] and fits the simple thermal theory of ignition. If the

spark duration is too long, the flame will have spread out beyond the region of influence of the spark electrodes before the spark ceases, and the energy imparted to the gas by the latter part of the spark does not affect the ignition process but only increases the total energy imparted to the gas.

Based on these results, it appears that the spark duration which yields the most "fundamental" MIE is equal to the time of development of a minimal flame kernel, which is also the spark duration which yields the minimum value of MIE. This is similar to the previously described observation that the spark gap which yields the most "fundamental" MIE energy is equal to the quenching distance, which is also the diameter of the minimal flame kernel. Unfortunately, there is very little data available on optimum spark durations. Because of this, it may be necessary to determine optimum spark durations in the current investigation, although it is not necessary to have exact values because minimum ignition energies are only weakly dependent on spark duration, particularly for spark durations below the optimal value [77].

Minimum ignition energies are of course dependent on the state of the unburned gas as well as the parameters of the spark itself. Lewis and von Elbe [30] have shown that for most fuels the minimum value of MIE does not occur for a stoichiometric mixture, but rather for one in which the less diffusive component of the mixture is present in excess. This is the same result as for the effect of diluent gases on flammability limits (section 2.2.3.3). Again this suggests that mixtures with more than the stoichiometric concentration of the less diffusive component are "stronger" in some sense than stoichiometric mixtures. For most hydrocarbon-air mixtures at atmospheric pressure, the minimum value of MIE is about 0.25 millijoule. This is in keeping with the observations that the adiabatic flame temperatures at the flammability limits and the maximum burning velocities of hydrocarbon-air

mixtures are all very similar. For mixtures either richer or leaner than optimum the MIE is of course greater, only slightly for near-optimal mixtures, but considerably for mixtures near the flammability limit. In the case of lean methane-air mixtures at atmospheric pressure the MIE varies from a minimum of 0.3 millijoule at 8.5% methane, to 2.0 millijoule at 5.7%, to a practically infinite value at the lean flammability limit for upward propagation in a closed bomb (about 4.5-5.0%) [30].

The effects of pressure on minimum ignition energies are considerably simpler than the effects of pressure on burning velocities or flammability limits. For a given combustible mixture, the MIE is usually inversely proportional to the square of the absolute pressure [33]. The explanation for such an effect is quite simple and understandable, as will be explained in the following section. The situation may change radically, however, as the flammability limit is approached. If the flammability limit widens with decreasing pressure, then obviously for a mixture sufficiently close to the flammability limit, the MIE would be higher at a high pressure than at a lower pressure for the same mixture.

As one would expect, increasing the unburned gas temperature decreases the minimum ignition energy requirement [74]. This is not at all surprising considering the effects of temperature on flammability limits and burning velocities. There does not appear to be adequate data in the literature, however, to draw firm conclusions as to the exact dependence of minimum ignition energy on temperature.

There have been no investigations to date on the effect of gravity on minimum ignition energies. Unlike flammability limits or burning velocities, it is not clear that such an effect would exist. For gravitational effects to be significant, the time for development of a minimal flame kernel would

probably have to be of the same order as or greater than the time for development of significant natural convection. An estimate of the conditions necessary for this to happen is presented in the next section. It is also not clear what effect gravity would have on minimum ignition energies. Natural convection could aid heat and mass transfer in the flame zone, which would probably reduce minimum ignition energies, or it could cause heat loss to the unburned gases, which would increase the MIE requirement. In light of the effects of gravity on burning velocities and flammability limits in large closed vessels, in which gravity usually aids the combustion process (sections 2.2.3.3 and 2.2.4.2), it might be expected that minimum ignition energies would be higher in a low-g environment.

2.2.5.3 Models for prediction of minimum ignition energy

Early predictions [30,31] of MIE were based on the concept outlined in section 2.2.5.1 of heating a minimal flame kernel to the adiabatic flame temperature. This yields a MIE estimate of

$$E_{min} = 4\Pi r_{min}^3 \rho_b C_p (T_b - T_u),$$

where r_{min} is the radius of the minimal flame kernel. By relating r_{min} to the flame thickness δ or quenching distance d ($\simeq 40\delta$), along with the ideal gas relations and neglecting T_u/T_b in comparison to 1, this equation becomes

$$E_{min} \sim (kT_u/S_u)^3/P^2,$$

with the proportionality constant depending on whether the flame thickness, quenching distance, or some combination of these is taken to represent r_{min}. Since k and S_u are mostly independent of pressure, this equation shows that $E_{min} \sim P^{-2}$, as mentioned in the previous section.

Other predictions of minimum ignition energies for point sources of ignition [84,85] are not dependent on empirically determined flame parameters

such as burning velocity or quenching distance but instead use simplified reaction rate laws similar to those used in early models of burning velocity (section 2.2.4.3). Yang [84] assumed a point mass sink at the origin in his model with gas flow toward this origin, a physically unrealistic situation. In addition, the model requires solution of a set of equations for a "critical mass flow rate" which is, in essence, the burning velocity. Finally, both of these models yield equations for minimum ignition energy which are dimensionally inconsistent, and so even if their shortcomings can be ignored no meaningful results can be obtained.

To properly model ignition phenomena would require, at the very least, a spherically symmetric model that included a complete reaction mechanism, multispecies thermal conduction and molecular diffusion, nonsteady behavior, and initial conditions, including the temporally and spatially dependent ignition energy input. Such models have only recently become available [86,87]. While these models have only been applied to hydrogen/oxygen/nitrogen and hydrazine mixtures so far, there is no apparent reason they could not be extended to other combustible mixtures if the reaction mechanism and reaction rates were sufficiently well known.

It is proposed here to estimate the conditions required for significant gravitational effects on ignition by equating the time for development of a minimal flame kernel to the time required for the minimal flame kernel to rise a distance due to natural convection equal to its radius. Obviously this is a very crude model, but it should indicate the effect of various parameters (pressure, gravitational acceleration, etc.) on the conditions required for significant gravitational effects. Andrews and Bradley [41] give the rate of convective rise S_c of a burning gas bubble as a function of time t by the equation

$$S_c = (\rho_u/\rho_b - 1)gt/4.$$

By integrating S_c to obtain the position y as a function of t subject to the initial condition y = 0 at t = 0 and solving for t, the result is

$$t = [8y/g(\rho_u/\rho_b - 1)]^{1/2}.$$

The time of development for a minimal flame kernel can be estimated as $t = r_{min}/S_b$. Taking $r_{min} \simeq \delta$ and $S_b = S_u(\rho_u/\rho_b)$ (section 2.2.4.1), the result is $t = (\rho_b/\rho_u)/(\delta/S_u)$. By the assumption of this model $y = \delta$ when these two times are equal. With the additional relation $\delta = k/\rho_u C_p S_u$ (section 2.2.2), the final result is

$$S_{u,crit} = \frac{1}{2}\left[\frac{k}{\rho_u C_p}\left(\frac{\rho_b}{\rho_u}\right)^2\left(\frac{\rho_u}{\rho_b} - 1\right) g\right]^{1/3}.$$

Below this value of S_u, the effects of gravity on the ignition process may be significant. The form of this equation is remarkably similar to the limit burning velocity based on natural convection predicted by Lovachev [20] (section 2.2.3.4), despite the differences in what the two models attempt to predict. On closer inspection, the models are quite similar. Both models assume the critical flame size is that of a minimal flame kernel, but this is much more reasonable for an ignition condition than an extinction condition. The only substantial difference in the two analyses is the manner in which the rate of rise of the flame kernel is determined. Lovachev assumed that the flame kernel was rising at a constant rate determined by balancing the drag and buoyancy forces, but Andrews and Bradley [41] showed that drag forces are not significant when $r = \delta$. In the current model, the kernel is still accelerating at a rate determined by equating the buoyancy force with the rate of change of momentum of the flame kernel, which is certainly more reasonable, at least for small flame radii. The current model probably underestimates the

maximum burning velocity for which gravitational effects on ignition may be significant, as it was assumed that $r_{min} = \delta$ even though δ is only a measure of the preheat zone thickness, which is less than the radius of the minimal flame kernel, although even if $r_{min} = 10\delta$, $S_{u,crit}$ would increase only by a factor of $(10)^{1/3} = 2.2$.

This analysis does not predict what the effect of gravity on ignition might be, but predicts the critical burning velocity $S_{u,crit} \sim g^{1/3} P^{-1/3}$, just as Lovachev's model does. For near-limit hydrocarbon-air flames at atmospheric pressure and room temperature, typically $T_b = 1500^oK$, $T_u = 300^oK$, $k = 0.063$ W/m^oK (at the mean temperature of 900^oK), $\rho_u = 1.18$ kg/m^3, $C_p = 1.12 \times 10^3$J/kg^oK, $\rho_b/\rho_u \simeq T_u/T_b = 0.20$, and $g = 9.80$ m/s^2, thus $S_{u,crit} \simeq 2.1$ cm/s, lower than any limit burning velocity measured by any of the conventional means.

Jones [88] attempted to predict the effect of gravity on minimum ignition energies. He used a radially symmetric nonsteady model which included buoyancy forces, multicomponent thermal conduction and molecular diffusion, and a complex reaction scheme. The model was tested for a carbon monoxide-oxygen ($CO + 2O_2$) mixture at atmospheric pressure and room temperature. His results show that the MIE was about 4% higher at $g = g_o$ than at $g = 0$, and about 6.5% higher at $g = 10g_o$ than at $g = 0$. It is by no means clear that this model provides an adequate simulation of the problem. The calculated MIE at $g = g_o$ was 486 millijoules. No information on minimum ignition energies for carbon monoxide-oxygen mixtures could be found in the literature, but the burning velocity for this mixture is about 40 cm/s [89], so the MIE expected at atmospheric pressure based on the simple model presented in this section is about 0.5 millijoule, a factor of 1000 less than Jones calculated. This experimental value of burning velocity is for a water

vapor content of 1.35%. Since hydrogen and water vapor have a very strong catalytic effect on carbon monoxide combustion, it is amazing that Jones did not state the hydrogen or water vapor content, if any, that he assumed for his mixture. He also did not state the reaction scheme used or what his reaction rate constants were. Jones calculated only a very small gravitational effect on the MIE for this fast-burning mixture, just as the simple model proposed here would suggest. Jones did not attempt to extend his model to other, slower burning mixtures, or different fuels, where gravitational effects on ignition would probably be more significant.

2.3 Conclusions and recommendations for study of gravitational effects on laminar premixed gas combustion

The study of the effect of gravity on laminar premixed gas combustion has several important applications. It allows the investigation of gravitational effects on heat transfer and fluid mechanics while eliminating the complicating process of mixing. Such information is useful in assessing the flammability hazards of materials used in spacecraft construction and the effectiveness of spacecraft fire suppression systems. Also, gravitational effects are present in some inadequately understood combustion phenomena and the study of such phenomena in the absence of gravity would add to the present understanding of the underlying processes.

It is apparent that most if not all observed flammability limits are affected by gravitational forces. Theories of flammability limits due to natural convection predict that no limits would exist in zero-g. Observations have shown that limits do exist even in zero-g, but extinguishment mechanisms appear to be different than in one-g. More observations on flammability limits in zero-g are required, particularly with respect to the investigation

of extinguishment mechanisms. In fact, the National Academy of Sciences [24] concluded that

> "...A few well-designed tests to examine flammability limits for freely propagating near-limit systems under conditions of low gravity appear warranted."

Data should be taken in as large a combustion vessel as possible over a wide range of ambient pressure. Investigations for varying fuels is of secondary interest but still important.

Information on burning velocities of near-limit mixtures is important for understanding the mechanisms causing flammability limits and is also useful in verifying the adequacy of flame propagation models. Unlike fast-burning mixtures, burning velocities for near-limit mixtures are difficult to measure in one-g because of gravitational effects. Performing burning velocity measurements in zero-g should eliminate these difficulties. Photographic observation of the flame front should allow reasonably accurate measurements of burning velocity. Again, as large a vessel as possible should be used and data should be taken over a wide range of ambient pressure.

It is not clear whether gravitational forces can have a significant effect on minimum ignition energy. No such investigations have been performed to date. Order-of-magnitude calculations suggest that such effects could occur for mixtures with burning velocities on the order of a few centimeters per second or less. Electric spark discharges are the most practical energy source for a study of gravitational effects on ignition energy. In order to obtain the most "fundamental" values of minimum ignition energy possible, very small diameter electrodes should be used, the spark gap should be set at the quenching distance or slightly wider for each combustible mixture, and the

spark duration should be set to the optimum value or slightly less for each combustible mixture.

The only commonly used experimental apparatus which could allow reasonably accurate measurements of flammability limits, burning velocities, and minimum ignition energies over a wide range of ambient pressure is a closed bomb, and for this reason will be used in the current investigation. The closed bomb has several additional advantages for this type of study. The closed bomb allows spherically symmetric flame propagation into an initially quiescent mixture, at least for fast burning mixtures or in zero-g, which simplifies interpretation of the results. Also, there is no "flame stretch" and the effects of solid boundaries are as minimal as they could be in any combustion apparatus. Finally, the expansion of the burned gases allows flame propagation to proceed at a rate several times faster than the burning velocity, which allows more observed flame propagation per unit time than other methods, which is a distinct advantage when the duration of zero-g is limited, as in drop tower experiments. The only serious disadvantage of the closed bomb is the rising pressure and temperature during combustion, and in most cases this effect can be neglected or accounted for in interpreting results.

Methane appears to be the proper fuel choice for this investigation because a large body of experimental data and analytical models are available. Also, methane is non-toxic, non-corrosive, and has a low explosion hazard. Stoichiometric and lean mixtures of methane in air or oxygen are the most practical because of the problem of soot formation in rich mixtures and the accompanying complicated reaction mechanism. Since many combustible solid materials found on spacecraft (e.g. plastics) contain long-chain hydrocarbons which break into smaller molecules upon vaporization and burning, a

hydrocarbon fuel such as methane is desirable for representing the burning of such materials. Other fuels tested should include fuels with similar chemical properties but varying diffusion properties in oxygen, such as ethane and propane, and fuels with different reaction mechanisms, such as hydrogen and carbon monoxide.

Chapter 3. Experimental apparatus and procedures

3.1 General

Given the objective of studying the effect of gravity on the properties of laminar premixed gas combustion, choices for the various components of the experimental apparatus must be made and justified. The following five components were identified as necessary for this experiment: zero-gravity mechanism, combustion vessel, gas measuring and mixing system, electronics, and photographic system. Justifications for the selections of these components and their respective limitations are presented here. A discussion of the experimental procedures is included at the end of this chapter.

The purpose of this investigation was not to determine the effect of the experimental apparatus and procedures on laminar premixed gas combustion properties, only the effect of gravity on these properties. Nevertheless, it was necessary to determine with what apparatus and procedures the investigation would yield the most "fundamental" values of these properties, i.e. with complicating effects held to a minimum. It is not claimed that any or all of these effects were eliminated, only that the intention was to minimize them whenever possible.

3.2 Zero-gravity mechanism

One of the fixed conditions of the experimental phase of this investigation was the method of obtaining zero-gravity. All of the zero-gravity tests were to be performed in the 2.2 Second Zero-Gravity

Facility at the NASA Lewis Research Center in Cleveland, Ohio. All other components of the experimental apparatus to be used in the zero-g tests had to conform to the constraints imposed by this system. The facility (Fig. 3-1) provides 2.2 seconds of reduced gravity for an experiment package during a 78 foot free-fall in an 8-story tower. The experiment package is about 95 cm wide, 45 cm deep, and 60 to 120 cm high. An experiment package 80 cm high was used in this project. Air drag forces on the experiment package are effectively eliminated by allowing the package to free-fall within a drag shield which is free-falling itself. Of course, this means that the experiment package must have its own onboard power, sequencing, and data recording. There is a small relative velocity between the drag shield and the experiment package because the drag shield is exposed to atmospheric air drag during free-fall but the experiment package is not. The only air drag force the experiment package "feels" is due to this small relative velocity. The maximum force on the experiment package during free-fall is $10^{-5}g_o$, negligible for the purposes of this investigation. Because of the relative velocity between the drag shield and experiment package, it is necessary to have a 20 cm space between the bottom of the package and the bottom of the inside of the drag shield (Fig. 3-2). The 20 cm gap is chosen so that the experiment package hits the bottom of the inside of the drag shield at the same time as the free-fall ends. At the end of the free-fall, three aluminum spikes bolted to the bottom of the outside of the drag shield penetrate into a deceleration container (a bin of sand) at the bottom of the tower allowing the drag shield and experiment package to decelerate gradually. The spikes have interchangable tips to achieve correct sand penetration depending on package weight. The maximum deceleration is about $30g_o$.

The drop test begins by preparing the experiment package on the fifth floor of the drop tower and installing the package in the drag shield. This entire drop assembly is hoisted to the eighth floor and hung from a 0.075 inch diameter music wire. Umbilical cords, which allow communication between the experiment package and the outside world until free-fall begins, are attached to the experiment package through holes in the drag shield. These umbilicals are brass rods with banana plugs soldered on one end which fit into jacks on the experiment package and bare rod on the other end which is connected to external alligator-type clips. In the present work, two sets of umbilicals were used, one set to activate the camera through a switch a few seconds before the drop and the other set to activate the onboard sequencing through a jumper wire when the drop began. After all onboard systems are set to their drop test configuration, free-fall is initiated by activating a pneumatic cutter which severs the music wire supporting the drop assembly. The assembly falls away, breaking electrical contact with the umbilicals, allowing onboard sequencing to begin. After the drop, the data from the drop is recorded while the experiment package and drag shield are still resting in the sand bin on the first floor. The onboard systems are then shut down, the assembly is hoisted back to the fifth floor, and the experiment package is removed from the drag shield and refurbished for the following test.

The experiment package consisted of the combustion vessel, camera, camera timing light generator, 3 boxes of custom-built electronics, batteries, and circuit breakers. A functional block diagram of this equipment is shown in Fig. 3-3. All of this equipment was mounted to an aluminum frame provided by NASA. Total weight of the experiment package was about 95 kg. Total weight of the entire drop assembly was about 460 kg. A photograph of the completed experiment package is shown in Fig. 3-4.

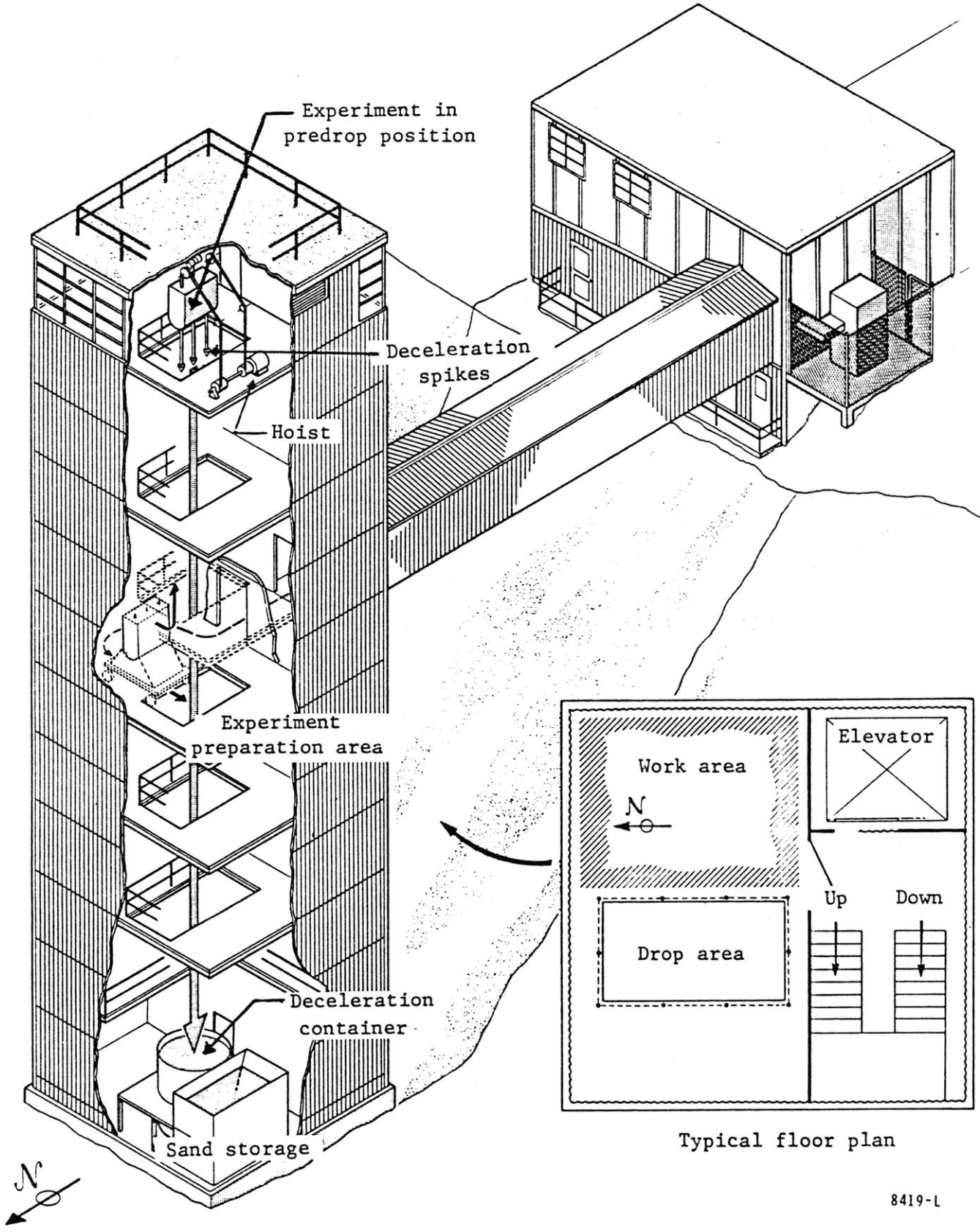

Figure 3-1. 2.2 Second Zero-gravity Facility at NASA Lewis Research Center

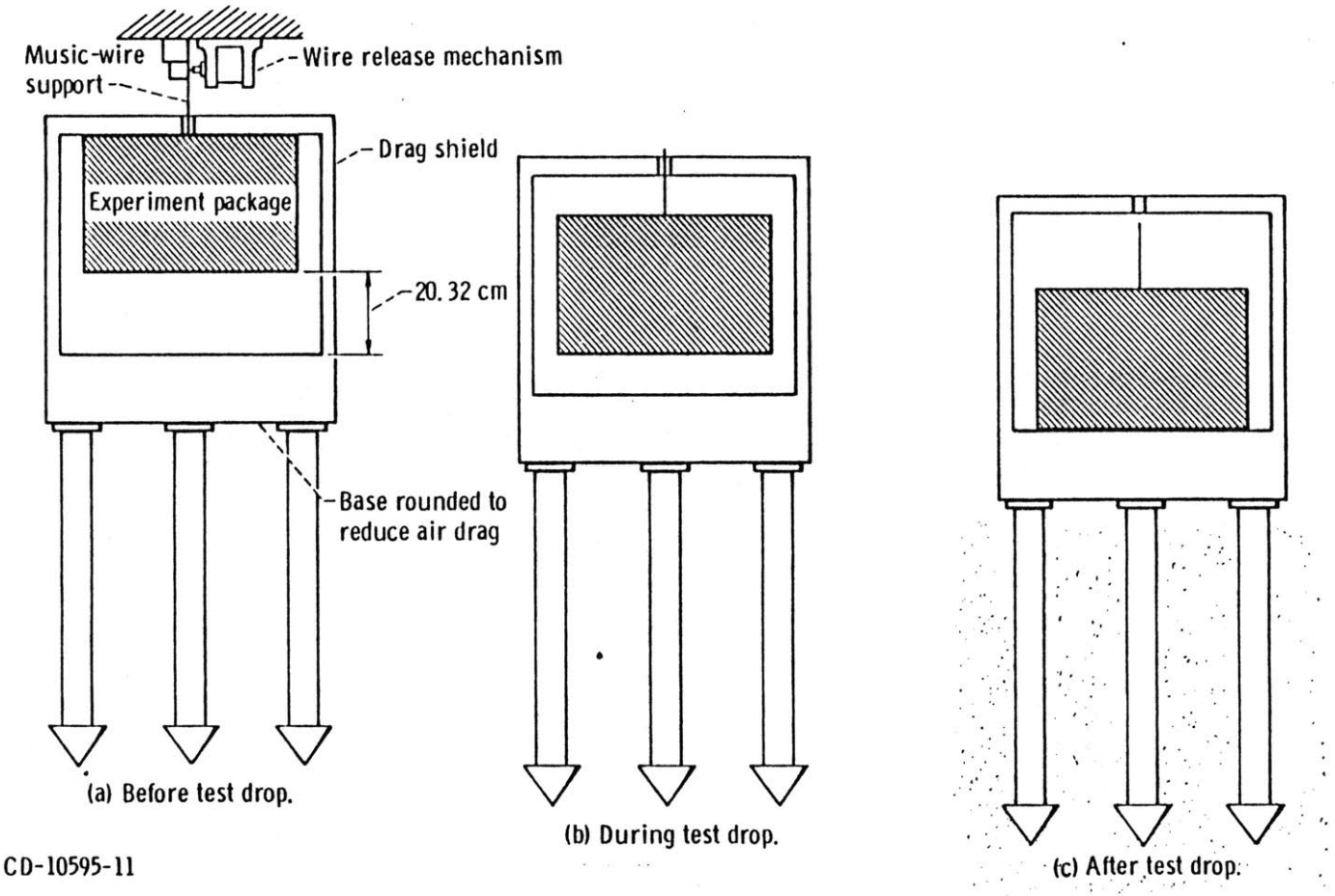

Figure 3-2. Schmatic drawing showing position of experiment package before, during, and after test drop

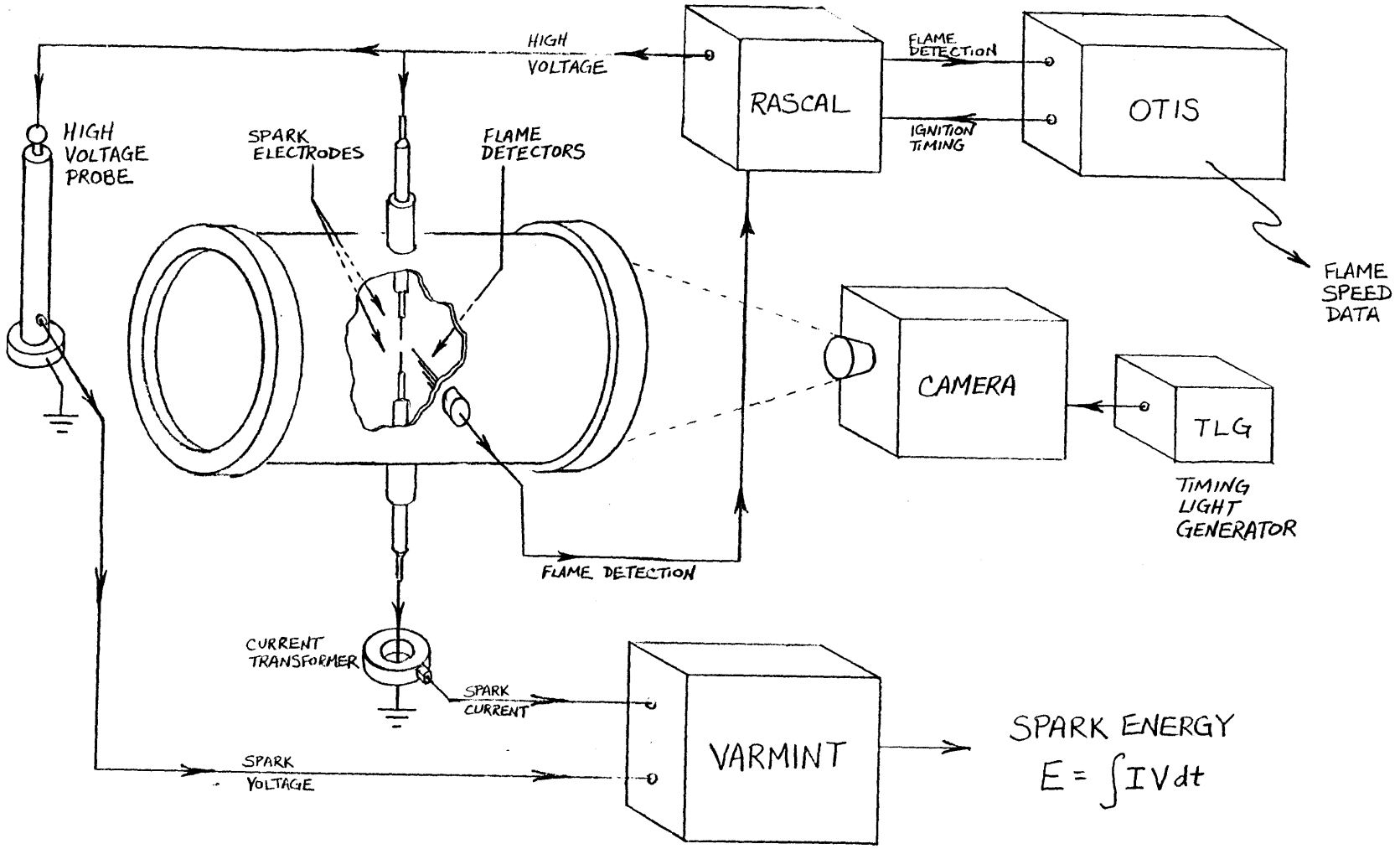

Figure 3-3. Experimental apparatus block diagram

NASA
C-81-5936

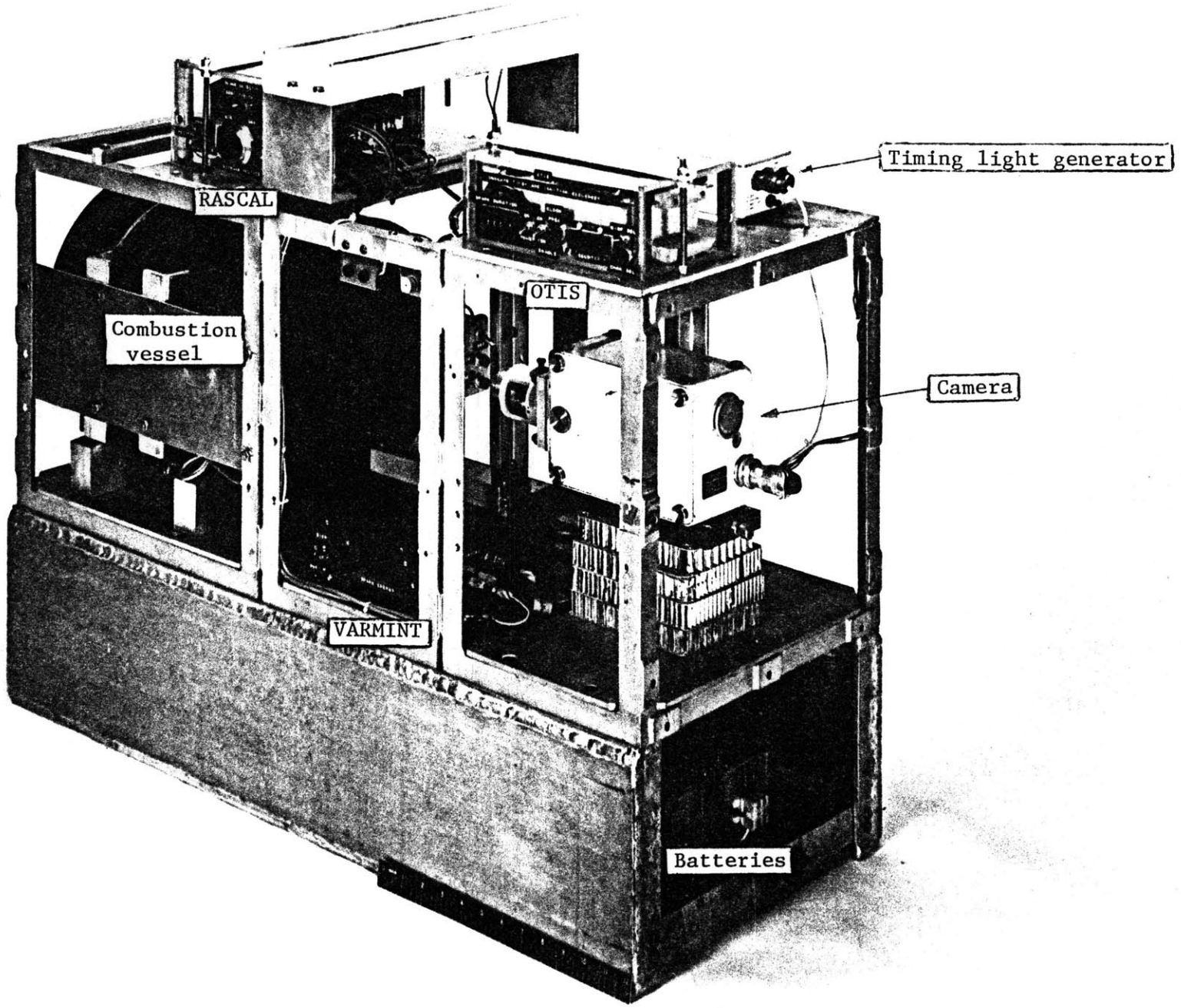

Figure 3-4. Experiment package

3.3 Combustion vessel

3.3.1 Design parameters

While as large a combustion vessel as possible was desired, a vessel with an inside dimension of about 25 cm was the largest that would fit in the drop package. It was obvious that a cylindrical vessel would be much easier to construct than a spherical vessel, so it was decided that a cylindrical vessel 25 cm inside diameter and 25 cm inside length would be used. It was essential to have at least one large transparent window to allow observation and photography of the combustion process. Ports for the gas inlet and flame detectors (section 3.4.1) were also necessary. The maximum expected combustion pressure was about 10 atmospheres, this for a stoichiometric methane-air mixture initially at atmospheric pressure (appendix C), and it was decided that a safety factor of 10 would be employed, hence the vessel had to be designed for a burst pressure of 100 atmospheres. It was not necessary to use materials with good high-temperature properties, because although the combustion temperatures could be as high as 2250°K for stoichiometric methane-air mixtures (appendix B), gases have heat capacities orders of magnitude less than solid materials, so the heat of combustion in a transient process is absorbed by the vessel walls without leading to a significant increase in wall temperature.

It was anticipated that the lowest pressure for which combustion tests would be performed was 50 Torr, that the longest time between the filling of the vessel and the actual combustion test would be 15 minutes (in the drop tower tests), and that the maximum acceptable change in mixture ratio due to

vessel leakage would be 0.5%, so the maximum allowable leakage was about 1 Torr/hour.

The electrode assemblies were required to provide an adjustable spark gap, a gas-tight seal, and because of the metallic combustion vessel, a dielectric strength greater than the maximum anticipated spark gap breakdown voltage. Based on the available data on quenching distances, it appeared that a spark gap continuously variable from zero to at least 2.5 cm was required. Based on the spark gaps and pressures involved, the maximum anticipated spark gap breakdown voltage was about 30,000 volts.

3.3.2 Construction

The combustion vessel was a 10" schedule 40 pipe made from 6061-T6 aluminum. Each end of the pipe was threaded on the outside surface and faced for an O-ring seal on the inside surface. Spark electrode holders were made from cylindrical bars of 6061-T6 aluminum that were cut, drilled, and welded in carefully aligned, diametrically opposed locations on the vessel. These holders were then threaded and faced to receive the spark electrode sleeve threads and O-ring seals. Ports for the gas inlet and flame detector assembly were standard 1/4" pipe fittings sealed with Teflon tape. A quick disconnect fitting was used on the gas inlet part to facilitate removal of the tubing from the gas measuring and mixing system. Two 1/4 inch thick aluminum plates were welded to one side of the combustion vessel and the vessel was bolted to the experiment package framework through these plates. Also holding the vessel in place were two wooden "saddles" with steel straps looped over the top of the vessel and again bolted to the framework. End rings were cut from solid 2-1/2 inch thick blocks of 2024-T4 aluminum, milled and threaded on a lathe. Both the vessel and these end rings were anodized for corrosion

protection. The end rings held transparent 1-1/4 inch thick plexiglas windows in place. The windows were held from collapsing inward by a shoulder machined into the window itself. An O-ring groove was also machined into each window. Standard BUNA-N O-rings were used. The stress formulas and material properties required to size the components were taken from reference [90]. The vessel was hydrostatically proof tested to 20 atmospheres, twice the maximum operating pressure. The detail drawings of the combustion vessel are shown in appendix E.

The electrode assemblies consisted of an inner conducting core, insulator, and outer sleeve, all concentric. The inner conducting core was a 1/8 inch diameter stainless steel rod. The electrode tip was a 0.35 mm diameter tungsten wire crimped into a small stainless steel tube and force fit into a hole in the end of the conducting core. The 0.35 mm wire diameter was chosen as the best compromise between low quenching effect and longevity. The insulators were initially made from plexiglas but these cracked and were replaced with Delrin. The insulators were long enough that the spark could not jump from the conducting core to either the inside or outside of the vessel, and thick enough that the spark could not jump through the insulator to the outer sleeve of the electrode assembly. The outer sleeve was a brass bar, drilled on the inside for the insulator, threaded on the outside to screw into the spark electrode/holder welded to the vessel, and grooved for an O-ring seal. The assembly was made gas-tight on the ends by sealing with epoxy resin. A plastic knob was attached to the end of the assembly to facilitate rotating the assembly for spark gap adjustment. The detail drawings of the spark electrode assemblies are shown in appendix E.

3.3.3 Operational considerations

The spark gap could be set by screwing the electrodes in until the two tungsten wire electrode tips were just touching, and unsrewing each electrode a measured number of turns. Since the thread cut on the electrode sleeves was 16 threads per inch, each turn of the electrode increased the spark gap by 1/16 inch (1.59 mm).

The measured rate of leakage from the vessel was less than 0.3 Torr/hour under all conditions, well below the maximum allowable. As expected, the vessel was not affected by the high temperatures of combustion except for the electrode tips and the sharp edges of the insulators, which became slightly scorched after repeated combustion tests. The optical quality of the plexiglas windows was not diminished at all, even after nearly 750 combustion tests.

It was found that if the electrode tips were dirty (e.g. from skin oil), a very unsteady spark discharge would occur, and so the electrode tips had to be cleaned if handled. Also, at low pressures (100 Torr and below), after several high energy sparks had been fired, the following sparks would not jump from the end of the tungsten wire on the negative electrode, but rather from the base of the wire where it joined the stainless steel rod. The only solution that could be found was to polish the negative electrode tip frequently with fine sandpaper.

3.4 Gas measuring and mixing system

3.4.1 Design

Since the gas measuring and mixing system was not part of the drop

package, the only requirements for the system were accuracy and ease of use. It was not known a priori how accurate the gas concentration measurements had to be, as it was not known how sharply the combustion phenomena would change as a critical concentration, i.e. the flammability limit, was approached. Based on previous results (chapter 2), it appeared that a concentration accuracy better than ± 1% (e.g. 5.00 ± .05% methane) would be required over a wide range of ambient pressures. What was more important than absolute accuracy, however, was repeatability. Hindsight showed that a concentration repeatability of ± 0.05% or better was required for repeatable results near the zero-g flammability limit.

The most reasonable method for accurate measurement of gas concentrations in a closed vessel over a wide range of total pressures is the method of partial pressures. For ideal gases, the ratio of the partial pressures of gases in a mixture is the same as the ratio of molecules of each gas. As methane and air at room temperature and near-atmospheric pressures behave essentially as ideal gases, the accuracy of this method is limited only by the accuracy of the pressure measurements. The only drawback of this method is that there is no guarantee that mixing of the gases is complete. The mixing question will be addressed in the following section.

The gas measuring and mixing system consisted of MAMMAL (Methane-Air Measuring, Mixing And Loading system), cylinders of methane and air, a vacuum pump, and appropriate valving and tubing. The system layout is shown in Fig. 3-5. MAMMAL consisted of a Datametrics 590A-1000T-2P1-V1X-4D electronic pressure transducer, a Datel-Intersil DM-4100L Digital Panel Meter, power supplies for these two units, and suitable switches, valves, and tubing. An electrical schematic of MAMMAL is shown in appendix F, Fig. F-3.

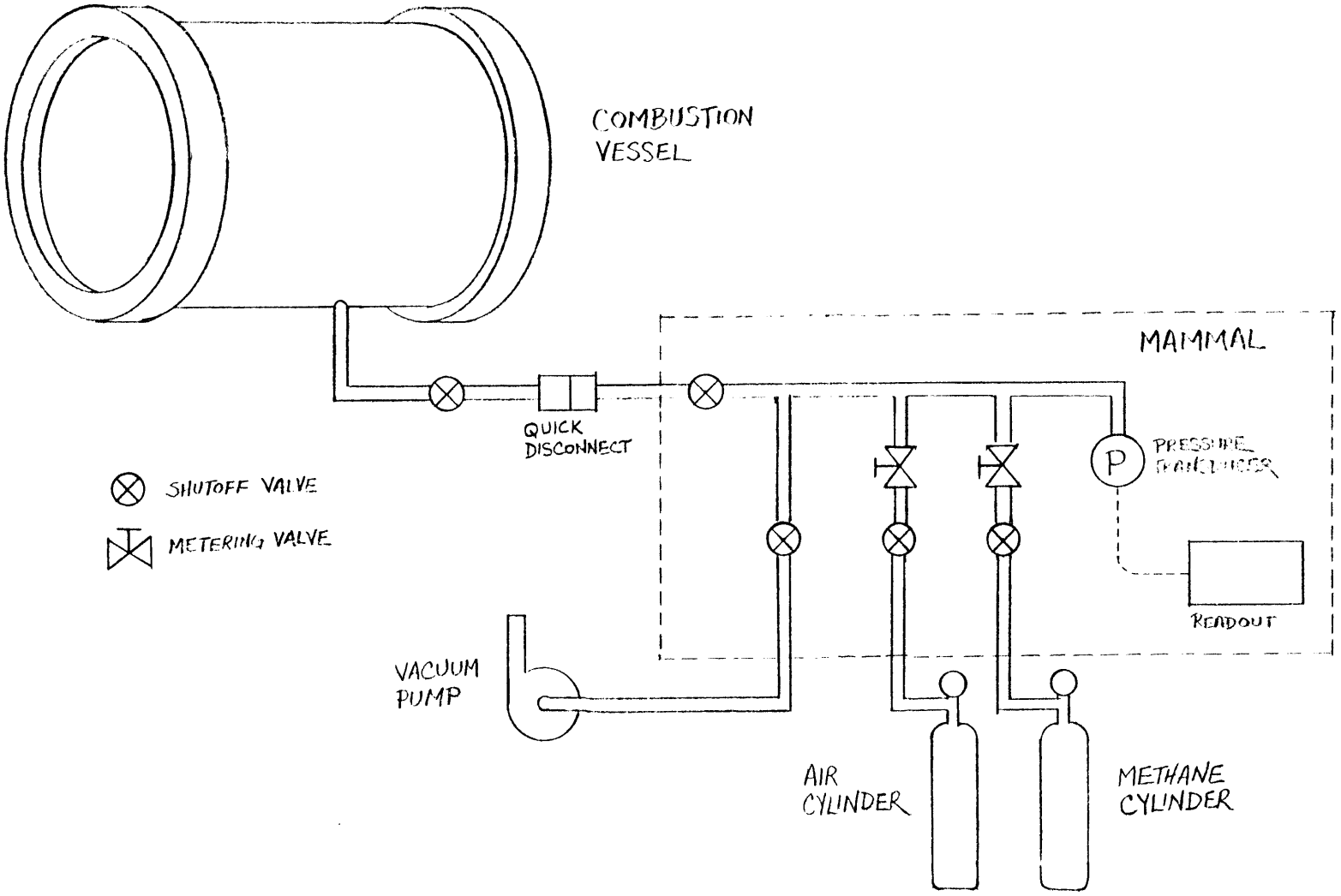

Figure 3-5. Gas measuring and mixing system block diagram

The Datametrics pressure transducer measures absolute pressure by measuring the deflection of a metal diaphragm, one side of which is exposed to a permanent high vacuum and the other side of which is exposed to the pressure to be determined. The diaphragm is positioned between two parallel capacitor plates and the deflection is measured by the change in relative capacitance between the diaphragm and the two plates. The output of the transducer is a voltage proportional to the absolute pressure. This type of pressure transducer has a great advantage over manometers, mechanical pressure gauges, and electronic gauges with resistive or optical deflection sensors in that the zero setting is very stable and the resolution is very high even at the low pressure end of the scale. This allows accurate measurement of concentrations even at very low total pressures. For example, a mixture of 5.0% methane in air at 760 Torr (1 atmosphere) total pressure has a methane partial pressure of 38.0 Torr, whereas the same mixture at 50 Torr total pressure has a methane partial pressure of only 2.5 Torr, so obviously a much higher resolution and zero stability is required in the latter case. The only type of pressure gauge considered that could measure the maximum total pressure studied (1500 Torr) and still have sufficient resolution and zero stability at the lowest total pressure studied (50 Torr) with a single gauge was the capacitance bridge type transducer used in this investigation.

The voltage output of the Datametrics transducer was read by the Datel-Intersil digital panel meter, which is merely a 4 1/2 digit digital voltmeter. This voltmeter was calibrated periodically with the high stability internal voltage reference from the Datametrics transducer.

The methane and air used in the combustion tests came from commercially purchased high pressure gas cylinders. The methane used was 99.97% pure "UHP grade" methane from Matheson Gas Products Co. The air used was standard

compressed dry air with a dew point of -60°C or less. Bottled dry air rather than room air was used to insure consistent gas mixtures and obtain repeatable spark discharges, as spark discharges are sensitive to the moisture content of the gas mixture. Standard single stage pressure regulators were used to reduce the cylinder pressures to the appropriate operating pressures.

Two types of valves were used in the gas system. Shutoff valves were of the spring-loaded toggle valve variety. The advantage of this type of valve is that the seal cannot be ruined by overtightening. For the final stages of mixing, metering valves on the methane and air lines were used to provide fine adjustment of the respective partial pressures. The lines from MAMMAL to the methane cylinder, air cylinder, vacuum pump, and combustion vessel were 1/4" polyethylene tubing. All other lines were 1/4" copper tubing. Swagelok tubing fittings were used throughout. The vacuum pump was a positive displacement type which could evacuate the vessel down to about 0.5 Torr absolute pressure. The vacuum pump oil had a vapor pressure at room temperature of about 10^{-4} Torr, negligible for this experiment.

3.4.2 Operational considerations

The mixing process began by evacuating the combustion vessel down to a low pressure, typically a few Torr, filling the vessel with dry air, and evacuating again. This flushing process removed virtually all traces of gas remaining from the previous test and insured that only dry air at a low pressure remained in the vessel. The partial pressure of methane required for the test was then added and finally air was added to bring the vessel pressure up to the total pressure required for the test. For example, if 5.00% methane in air at 760 Torr total pressure was required, and the vessel pressure after the flushing process was 6.00 Torr, 38.00 Torr of methane would be added to

bring the vessel pressure up to 38.00 + 6.00 = 44.00 Torr, then air would be added to bring the total pressure up to 760 Torr.

The question of accuracy and repeatability has not been addressed precisely until now because it depends on the mixing procedure used. The mixing procedure described here was used to maximize accuracy and repeatability as well as the degree of uniformity of the final mixture.

The absolute accuracy of the pressure measurements can be estimated from the accuracies of the pressure transducer and digital panel meter. The stated accuracy of the pressure transducer was ± 0.15% of reading ± 0.001% of full scale (1000 Torr in this case). The stated accuracy of the digital panel meter was ± 0.02% ± 2 counts. The worst case absolute accuracies for selected values of pressure based on this information is shown in table 3-1. The actual accuracy was probably significantly better for a number of reasons. A calibration chart supplied by Datametrics along with the transducer showed a maximum linearity deviation of 0.025%. Also, the pressure transducer measures absolute pressure, hence it can be used as a barometer. Agreement between atmospheric pressure readings from this system and a standard mercury barometer was within 0.1%. The zero pressure setting was checked by comparing low pressure readings from this system and a MacLeod type vacuum gauge. The agreement at 1.5 Torr was within 0.15 Torr, indicating an accurate and stable zero setting, especially considering that 0.15 Torr is 0.01% of the full range of the pressure transducer.

It should be noted that the system was used to measure pressures up to 1500 Torr although the transducer was only rated for pressures up to 1000 Torr. The accuracy of the transducer at 1500 Torr was checked with a mechanical gauge and agreement between the two was within 0.2%, so it was assumed that pressure measurements at 1500 Torr were also reasonably accurate.

In any case it is the repeatability of this measurement which is most important, not the absolute accuracy, as will be discussed later.

While the absolute accuracy of the pressure measurements appeared to be quite high, the accuracy of the concentration ratios was probably significantly better, as the accuracy of the measured concentration ratios is only dependent on the linearity of the system and not the absolute accuracy. The linearity deviation of the transducer according to the calibration chart was less than 0.025% across the entire pressure range and the zero shift was only 0.15 Torr, so the resulting concentration accuracy varied from about the same as the absolute pressure accuracy at 50 Torr to as high as ± 0.03% at 1500 Torr. The linearity deviation (0.01%) and zero shift (less than one count) of the digital panel meter was negligible.

Still more significant than the absolute accuracy of the measurements of total pressure or concentration ratio was the repeatability of these measurements, as the repeatability ultimately determines the true resolution available. For example, it was not important to know whether a measured concentration of 5.00% methane was truly 5.00% methane or actually 5.05% methane, but it was very critical that a measured concentration of 5.01% methane be reliably about 0.01% higher than a measured concentration of 5.00%

Pressure, Torr	Maximum error, %	Minimum repeatability, %
1500	0.18	0.02
760	0.20	0.02
250	0.25	0.03
199	0.19	0.04
100	0.20	0.06
50	0.23	0.11
25	0.29	0.21

Table 3-1. Worst case absolute accuracy and repeatability of pressure measurements

methane. The observed combustion phenomena (chapter 4) were actually this sensitive to concentration ratio in some cases. It was not as important to have such a high repeatability for the absolute pressure measurements, as the observed combustion phenomena were not as sensitive to small changes in absolute pressure. The Datametrics transducer specifications stated that the measurements were repeatable to within 0.01% of the reading plus 0.005% of the maximum applied pressure between measurements. The non-repeatability of the digital panel meter was negligible. The calculated repeatability of the absolute pressure measurements for a typical maximum applied pressure between measurements of 1000 Torr is shown in table 3-1. It is seen that this repeatability is as high as ± 0.02% at high pressures, which should have been adequate to observe the very sharply changing phenomena. The repeatability of the concentration measurements is similar to this. The satisfying consistency of the experimental results suggests that this very high repeatability was indeed realized.

An important question arises as to the degree of mixedness of the gases in the vessel. While the method of partial pressures accurately predicts the overall mixture ratio of gases, it cannot predict the distribution of the individual gases within the enclosure. The time required for complete mixing by laminar molecular diffusion alond in a system of this size would be rather long (about 20 minutes) but turbulent mixing during the introduction of the gases into the vessel shortens the mixing time considerably. This was precisely the reason for adding the low partial pressure methane gas to the vessel first; when the large volume of air was added, the resulting turbulence and mixing was much greater than if the large volume of air had been introduced first and the small amount of methane gas had been added last. Since the richest mixtures studied in the current investigation contained 9.5%

methane (stoichiometric mixtures), it was always advantageous to add the methane first.

While measuring the degree of mixedness directly would have been a formidable task, there was a simple method for estimating this. Since the thermal, molecular, and viscous diffusivities for ideal gases are all of the same order of magnitude (because the mechanisms for heat, mass, and momentum transport are similar for ideal gases), it can be assumed that when thermal equilibrium is reached, or equivalently when the temperature gradients have decayed to zero, concentration and velocity gradients will have decayed to zero as well. When the high-pressure bottled gases are released into the low-pressure vessel, thermodynamic considerations dictate that the gas temperature must rise. This temperature rise appears as a pressure rise in the constant-volume combustion vessel. Therefore, when the pressure in the vessel has reached equilibrium, thermal equilibrium has been attained, and so concentration and velocity equilibrium have been attained as well. The conclusion is that when the vessel pressure has reached its final value, the temperature is constant throughout the vessel, the methane concentration is uniform, and the gas velocity is zero everywhere. In the present system, the time required to reach equilibrium varied from a few seconds at 50 Torr to a few minutes at 1500 Torr.

There was also experimental evidence that complete mixing had been obtained. The experimental results were consistent and did not depend on the elapsed time between the mixing process and the actual combustion test. If mixing was not complete, the results would have been dependent on the mixing time allowed. More significantly, spontaneous formation and disappearance of protrusions and indentations in the flame front were not observed, as would be expected if the flame was propagating into pockets of overly rich or lean

mixture. While "wrinkled" flame fronts were observed, this was expected (section 2.1.1), and these wrinkles were usually formed in the early stages of flame front growth and propagated smoothly along with the remainder of the flame front. This behavior would not be expected if the wrinkles were due to a spatial nonuniformity in the initial mixture.

3.5 Electronics

3.5.1 Requirements

The most time consuming task of this investigation proved to be the design, building, and testing of the onboard electronics. This was not surprising considering their complexity and the lack of previous electronics experience on the part of the investigator. A general requirement for all of the onboard electronics was that they be relatively small, lightweight, and battery powered, otherwise they could not be used in the drop tests. Also, the equipment had to survive the deceleration loads at the end of the drop. These requirements ruled out the use of any items that were large, bulky, fragile, or had a high power consumption. An especially significant implication was that vacuum tubes could not be used. The basic functional requirements of the electronics could be grouped into four categories: event sequencing, flame detection, spark production, and spark energy measurement.

Several events which occured during the drop had to be properly sequenced. The camera had to be started several seconds before the drop in order to allow it to reach a steady speed by the time the drop began. It was necessary to delay the start of the combustion a tenth of a second or so after the drop began to insure the experiment package was stabilized in zero-g. After this short delay, the spark had to be fired and simultaneously spark

energy computation begun. After a specified time the spark had to be terminated and the spark energy computation ended. In order to conserve film, it was necessary to turn off the camera automatically a few seconds after the drop ended, as the experiment package was not accessible until several minutes after the drop.

It was decided early in the investigation to employ an electronic system to measure the progress of the flame front as a complement/alternative/backup to the photography. Thus, it was necessary to have several flame detector probes inside the combustion vessel, discriminator circuitry for the detectors, and a multichannel timer to record the time interval between the firing of the spark and the arrival of the flame at each detector.

The spark generator had to satisfy several different and sometimes conflicting requirements. Based on known results (section 2.2.5.2), the minimum spark energy required appeared to be about 0.1 millijoule. It was not known a priori what the maximum energy requirement would be because the effect of gravity on ignition energy had not been previously investigated and theories were inadequate to predict these energies. It appeared, however, that at least several hundred millijoules would be required, and early zero-g results showed that still more energy was required under certain circumstances, on the order of several joules at low pressures. Information on quenching distances led to the conclusion that spark gaps from zero to at least 2.5 cm would be required, and from the dependence of quenching distance on pressure, spark gap breakdown voltages of up to 30,000 volts could be expected. There was very little data available on optimum spark duration, but the minimum spark duration required (for a stoichiometric mixture at atmospheric pressure) was about 100 microseconds and the maximum duration required was at least several milliseconds and probably more. It was very

important that the spark discharges be fairly repeatable, as otherwise many of the limited number of drop tests available would be wasted by introducing an improper spark energy into the mixture. It was crucial that the spark could be fired at an exact point in time, i.e. just after the drop began. This ruled out the possibility of using an apparatus similar to that used by the U.S. Bureau of Mines (section 2.2.5.1) because the time at which spark breakdown occurs is unpredictable. Also, spark duration is not controllable in this type of apparatus, an important although not crucial consideration.

The Bureau of Mines apparatus is convenient in that the spark energy is merely the energy stored in the capacitors just before spark breakdown, which is easily calculated. Since this type of system could not be employed in the current investigation, another method of spark generation was required that would undoubtedly require a more elaborate method of determining spark energy. For one-g tests, it is simple enough to measure the spark current and voltage on an oscilloscope and calculate the spark energy from this information (section 2.2.5.1). Still, this is a laborious task if many combustion tests are performed, hence it is useful to have some sort of automatic system for calculating spark energies. Far more important for the current investigation was that it was not possible to use an oscilloscope in the drop tests because of the deceleration loads. It was realized early in the investigation that the spark discharges would not be repeatabale enough to assume that the spark energy for a given set of initial conditions would always be constant. Hence, it was essential to have an onboard spark energy computer to calculate the energy of every individual igniting spark in zero-g. The requirements for such a device were simply that it be usable and reasonably accurate over the entire range of spark energies and durations to be employed in the investigation.

The electronics developed to meet the requirements of this investigation consisted of three boxes of electronics, namely the Onboard Timer and Ignition Sequencer (OTIS), the Remote Automatic Spark Controller And Limiter (RASCAL), and the Voltage-Amperage Resolver, Multiplier and INTegrator (VARMINT), along with the power distribution system, which consisted of the appropriate batteries, relays, circuit breakers, and wiring. An overall electrical system diagram is shown in appendix F, Fig. F-1. In retrospect, these three boxes of electronics could have been combined into a single unit, but they were conceived, designed, and built at different times and it was not considered worthwhile to tamper with a working system in order to consolidate it. Basically, OTIS sequenced all of the onboard events and contained the timers for the flame detectors. RASCAL produced sparks based on the commands from OTIS and had the discriminator circuitry for the flame detectors, the output of which was sent to the timers in OTIS. VARMINT was an analog computer which calculated the energy dissipated in the igniting sparks. These components, OTIS, RASCAL, VARMINT, and the power distribution system, will be discussed separately in the next four sections. The details of these components will not be presented here, but the complete schematics are shown in appendix F.

3.5.2 OTIS

The Onboard Timer and Ignition Sequencer (OTIS) sequenced all onboard events except for the events controlled by the camera stop circuit and recorded the data from the flame detectors. A block diagram of OTIS is shown in Fig. 3-6.

The onboard sequencing began just after free-fall began, when electrical continuity in the experiment package release wire was broken. In one-g tests, the release wire was replaced by a switch. After contact was broken, an

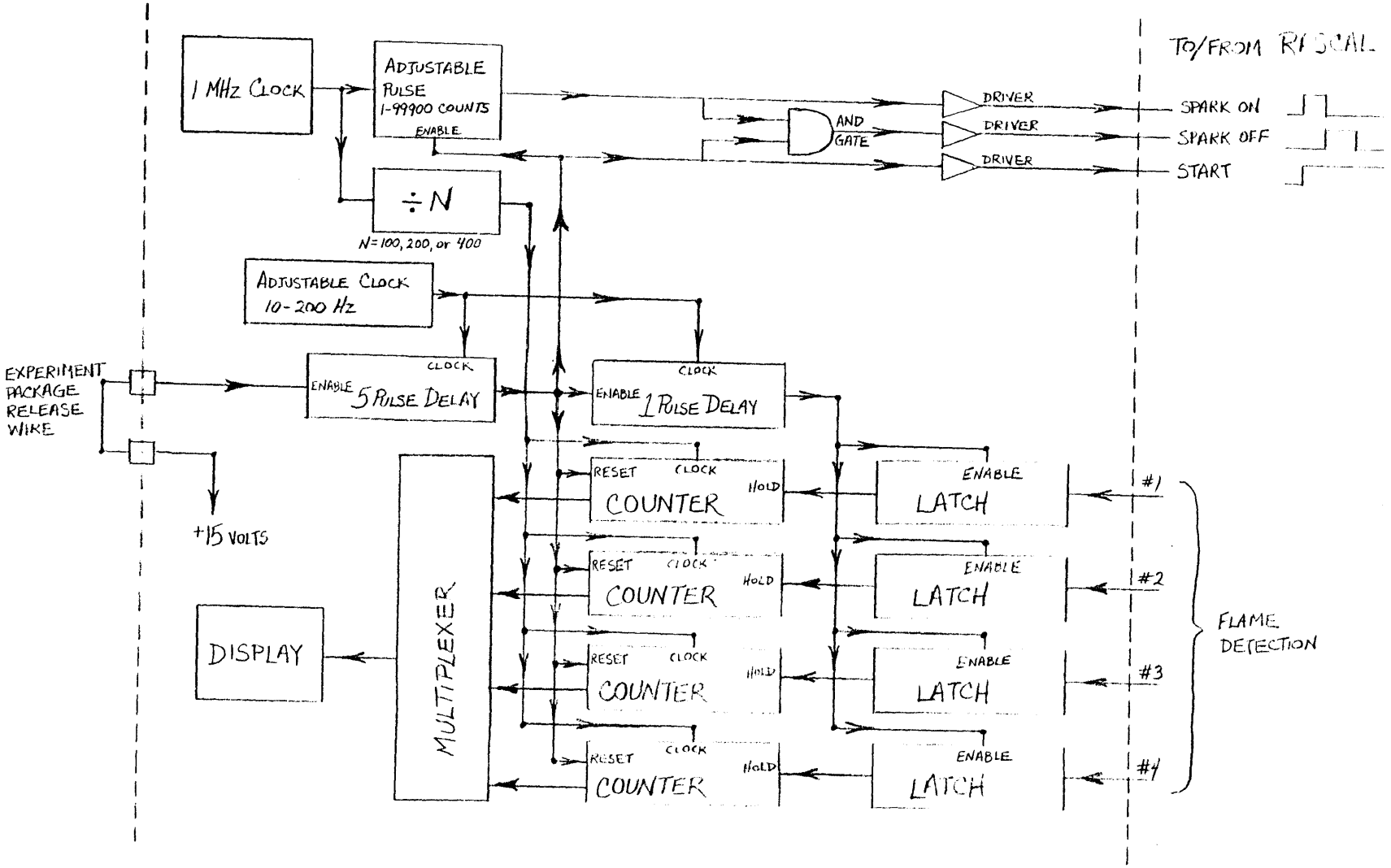

Figure 3-6. OTIS block diagram

adjustable delay of about 0.1 second occurred before the spark was fired. This insured that the experiment package had stabilized in zero-g before the spark fired and combustion began. The spark duration was set by a series of thumbwheel switches on OTIS which commanded a pulse generator. The SPARK ON pulse duration could be varied from 1 to 99900 microseconds. A 1.000 MHz crystal controlled oscillator provided an accurate, stable frequency standard for timing this pulse. The frequency was checked with a frequency counter and found to be accurate to five significant figures. The SPARK ON pulse enabled the DC spark generator circuit in RASCAL. An inversion of this pulse, the SPARK OFF pulse, disabled the DC spark generator at the proper time, allowing sparks of controllable duration to be produced. Occuring simultaneously with the beginning of the SPARK ON pulse was the START command. This enabled the trigger spark circuit in RASCAL, the ignition energy computation in VARMINT, and the flame timers in OTIS.

The four channel flame counter/timer began counting at the same time as the spark firing. Each channel would stop counting when the passing of the flame front was sensed by the corresponding flame detector. By knowing the elapsed time between the spark firing and the arrival of the flame front at each flame detector and the distance from the spark origin to each detector, the flame propagation velocity and therefore the burning velocity could be inferred (section 2.2.4.1). The clock frequency for the counter/timer came from the 1 MHz crystal oscillator through an appropriate frequency divider. The necessary divider ratio depended on the expected time for the completion of combustion. The available clock frequencies were 2.5 KHz, 5.0 KHz, and 10.0 KHz, and could be selected by a rotary switch. Each of the four flame detection signals from RASCAL was sent to a separate latch which would cause the appropriate channel to stop counting when the signal was received.

Because the spark would cause false triggering of the flame detectors in RASCAL, it was necessary to have a delay between the START command and the enabling of the flame detection latches. Of course this delay time had to be less than the time for the flame to reach the first flame detector, otherwise the passage of the flame front by the first detector would not be recorded. The output of the counter/timer went to a multiplexer and then to a 4-digit, 7-segment LED display where the number of counts and therefore the elapsed time between the spark firing and the arrival of the flame front at each detector could be read one channel at a time.

Because OTIS consisted mostly of CMOS integrated circuits which are susceptible to damage from stray high voltage transients, it was considered necessary to electrically isolate OTIS from the spark circuitry even though proper grounding paths for the spark circuit existed. Optical isolators in RASCAL were used which allowed complete electrical separation of OTIS from the spark circuitry. Of course this meant that OTIS required separate batteries, but CMOS circuity consumes very little power, so this was not a major disadvantage. Three standard 9 volt transistor radio batteries were used. Total power consumption by OTIS was about 2.5 watts with the display on and 1.5 watts with the display off.

3.5.3 RASCAL

The Remote Automatic Spark Controller And Limiter (RASCAL) produced sparks of carefully controllable duration and energy content for ignition of the methane-air mixtures and contained the discriminator circuitry for the flame detectors. A block diagram of RASCAL is shown in Fig. 3-7.

The spark system was similar to that used by Kono et al. [77] for their minimum ignition energy experiments in that a short duration, high voltage,

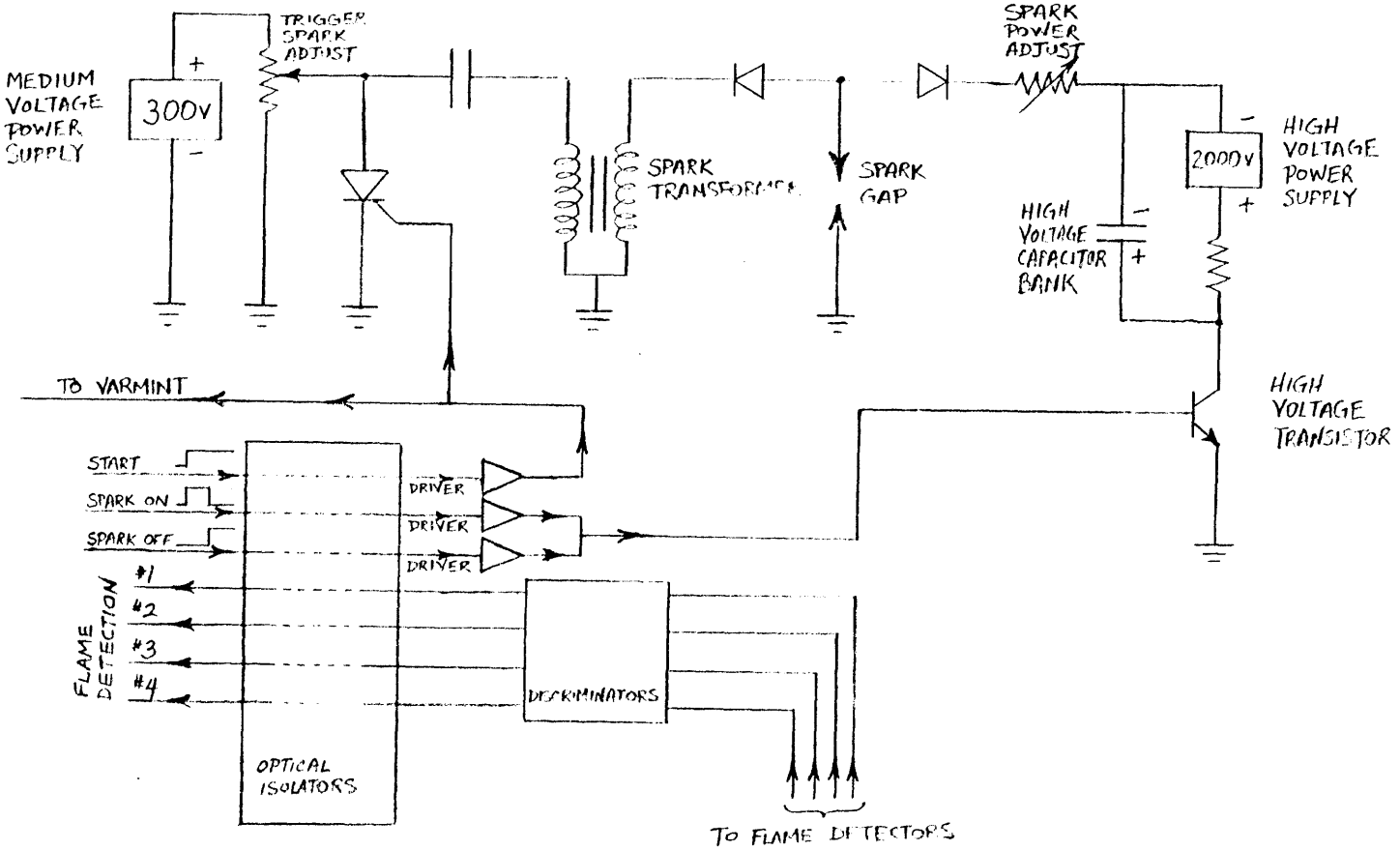

Figure 3-7. RASCAL block diagram

low energy trigger spark was used to cause breakdown of the spark gap and a separate lower voltage source was used to maintain a steady DC spark of controllable power and duration. This was possible because the voltage required to maintain a spark gap in a conducting state is much less than the voltage required to cause the initial breakdown and conduction of electrons.

The trigger spark system utilized a conventional capacitor discharge arrangement. The trigger spark fired when the START command from OTIS was received. The trigger spark intensity could be varied by adjusting the capacitor storage voltage. The maximum trigger spark voltage available was about 40,000 volts. The trigger spark energy varied from 0.1 to 2.0 millijoule. The trigger spark duration was about 20 microseconds. In all combustion tests, the trigger spark intensity was adjusted to the lowest setting that would still insure a consistent and reliable spark. This was done in order to minimize the transient component of the spark in relation to the DC component.

The DC spark generator consisted of a 2000 volt power supply and capacitor bank, a high voltage transistor, and a variable resistor. 2000 volts was determined to be the lowest voltage for which a steady DC spark could be maintained for all combinations of current, spark gap, and total pressure employed in this investigation. Simultaneous with the trigger spark firing, the SPARK ON pulse forward biased the transistor, allowing current to flow from the negative side of the capacitor bank through the variable resistor, through the spark gap to ground, from ground through the transistor, and back to the positive side of the capacitor bank. Also simultaneous with the trigger spark firing, the START pulse disabled the power supplies to the trigger spark and DC spark systems. This was done to reduce the possibility of accidental multiple spark firings and eliminate electromagnetic noise from

these power supplies during and after the spark firing, which was observed to affect the flame detectors and the precision circuitry in VARMINT. At the end of the SPARK ON pulse, the SPARK OFF pulse from OTIS reversed biased the transistor, causing rapid shutoff of the transistor. The spark current could be adjusted by the variable resistor. The current range was from about 0.05 to 5 amps. The DC spark power available ranged from about 30 to 450 watts. The narrow range of spark power compared to the range of spark current was due to an unusual characteristic of spark gaps. Unlike most electronic elements, the voltage drop across a spark gap decreases with increasing current throughout. Thus, an increase in spark current leads to a less than proportional increase in spark power and so limits the available spark power range.

The DC spark generator system was somewhat unusual in that a transistor with a maximum voltage rating of 1500 volts was used to switch a 2000 volt source on and off. This was only possible because of the aforementioned characteristic of spark gaps. When the gap was not conducting, most of the voltage drop was across the spark gap and not the transistor. When the transistor was in a conducting state, there was of course very little voltage drop across it. The only potential problem occurred when the transistor was turning off the spark current. The voltage drop across the variable resistor was decreasing because the current was decreasing and the voltage drop across the transistor was increasing, but fortunately because of the unusual property of the spark gap, the voltage across the gap was increasing as well, and prevented the drop across the transistor from going above a safe level. In essence, the properties of the spark gap allowed the maximum voltage rating of the transistor to be exceeded without damage. Of course high voltage vacuum

tubes could withstand higher voltages, but would have consumed too much power and would have been too fragile for use in drop tests.

The spark system could produce sparks with energies from about 0.1 millijoule to 6 joules depending on spark gap, duration, and total pressure. Current and voltage traces for three typical sparks are shown in Fig. 3-8. The initial current spikes are from the trigger sparks. The more or less rectangular portions of current waveforms are produced by the DC spark generator. For very high energy sparks (Fig. 3-8c) the effect of finite high voltage capacitance becomes significant and the current decreases with time. There was little if any difference in the characteristics of spark discharges in combustible mixtures vs. air alone, or in one-g vs. zero-g. This was expected because in the early stages of the ignition process, combustion reactions are insignificant compared to thermal conduction (section 2.2.5.2) and the time scale for the development of significant convective effects (section 2.2.5.3) was significantly longer than the longest duration sparks utilized (about 25 milliseconds).

While it was desirable to set the spark duration the optimal value for each combustible mixture (section 2.3), this was not always possible because of spark system limitations. For some mixtures with small minimum ignition energies the spark duration could not be made long enough without the spark energy exceeding the value required for ignition. This would happen for two reasons. The first reason was that the trigger spark alone contributed all or nearly all of the energy required for ignition. If the trigger spark intensity were reduced, the voltage across the spark gap would be insufficient to cause breakdown and no spark would occur. A number of different trigger spark systems were tried in order to minimize the trigger spark energy for a given breakdown voltage but none of the systems tried could reduce the energy

a) Pressure: 100 Torr
Spark gap: 1.0 cm
Voltage scale: 500 V/division
Current scale: 100 ma/division
Horizontal scale: 10 μs/division
VARMINT energy: 10.80 mj
Hand-calculated energy: 10.49 mj

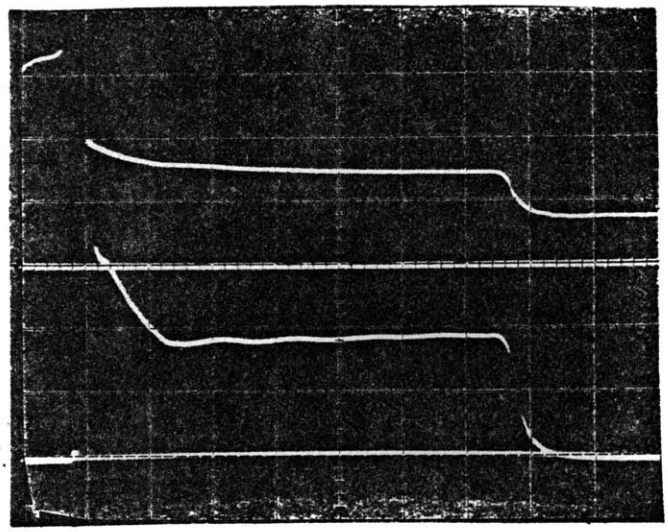

b) Pressure: 1500 Torr
Spark gap: 0.5 cm
Voltage scale: 100 V/division
Current scale: 500 ma/division
Horizontal scale: 50 μs/division
VARMINT energy: 63.9 mj
Hand-calculated energy: 70.62 mj

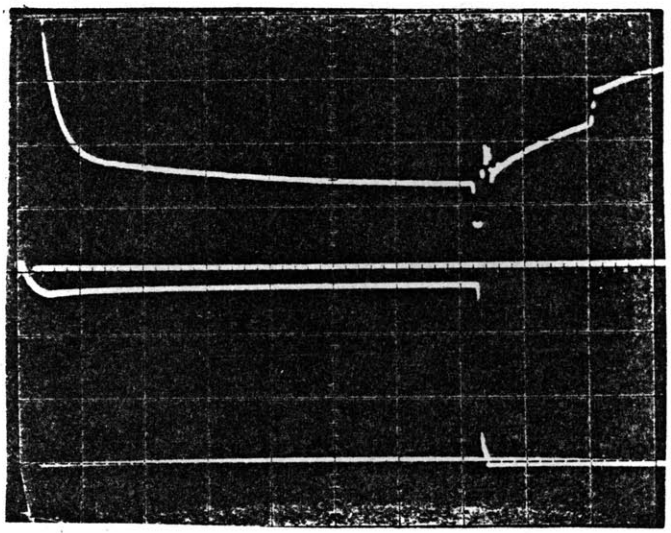

c) Pressure: 250 Torr
Spark gap: 2.0 cm
Voltage scale: 50 V/division
Current scale: 1 A/division
Horizontal scale: 2 ms/division
VARMINT energy: 3.88J
Hand-calculated energy: 3.85 J

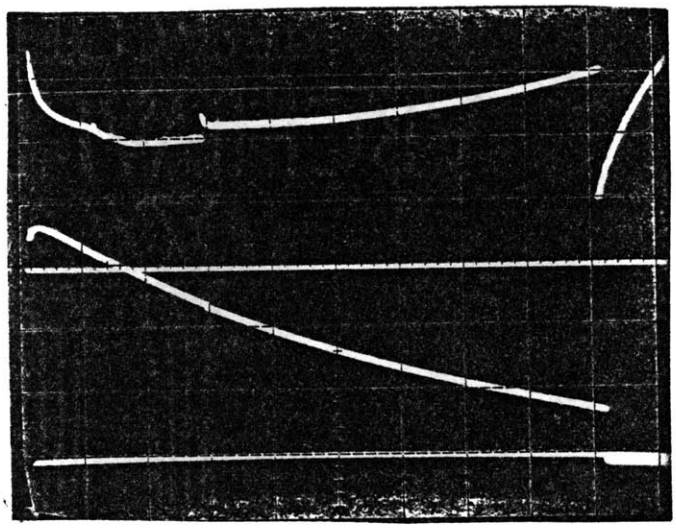

Figure 3-8. Typical spark voltage (upper) and current (lower) vs. time waveforms for spark ignition system used in this investigation

sufficiently for all combustible mixtures studied. The second problem was that the minimum DC spark power attainable was about 30 watts, which in some cases was too high to allow a spark duration as long as the optimum and not exceed the MIE. For some mixtures with a very high MIE, the spark duration could not be made short enough because the maximum DC spark power attainable was about 450 watts. The problems associated with this limitation of the spark system will be discussed in section 4.4.1.

The flame detectors sensed the passing of the flame front by the change in resistance of a small gap between two conductors. Since flame fronts contain ionized gases which conduct electricity, whereas the burned and unburned gases do not, the gap resistance decreases as the flame front passes the gap. This change in resistance is easily detected electronically. In this investigation, the gap was between a 1/16" outside diameter stainless steel tube and a nickel wire, with Teflon insulation tubing separating the tube and wire. Only the extreme tip of the wire at the end of the tube was exposed, hence this was the only point where flame detection could occur. An assembly of four almost colinear detectors spaced at roughly equal intervals between the spark electrodes and the vessel wall was used. The four stainless steel tubes were soldered into a standard 1/4" pipe plug. This plug screwed into a pipe-threaded port in the vessel, and since the vessel was grounded, the tubes were grounded as well. Four holes were drilled in the pipe plug to allow the nickel wires to feed through to the outside of the vessel. The outside of the plug was coated with epoxy resin in order to make a gas-tight seal. The nickel wires went to the discriminator circuitry, where the change in resistance between the wire and ground was detected. The distance from the spark electrodes to each flame detector was measured with precision vernier calipers.

The active element in the discriminator circuitry was a standard integrated circuit voltage comparator. The output of the discriminators was sent to the flame detection latches in OTIS (section 3.5.2). The discriminator circuitry is shown in appendix F, Fig. F-5. This arrangement was found to provide the most consistent flame detection. It was found necessary to have a sensitivity control on the detectors, because a very high sensitivity was required to detect flame front passage in slow-burning lean mixtures, but fast burning mixtures were "noisy" and would cause premature triggering of the detectors at high sensitivities. The best sensitivity setting was found in one-g by trial and error for each combustible mixture and this setting was used in all subsequent one-g and zero-g tests. For some mixtures it was not possible to find a sensitivity setting that would always allow proper triggering. This was especially so for lean mixtures and at low pressures, particularly in the zero-g tests. Ultimately, the film record was relied upon as the primary source of flame propagation velocity data for these mixtures.

3.5.4 VARMINT

The Voltage-Amperage Resolver, Multiplier, and INTegrator (VARMINT) was an analog computer for calculating the energy dissipated in the sparks for ignition. A block diagram of VARMINT is shown in Fig. 3-9. The voltage across the spark gap was measured by an ITT Jennings model R100 high voltage divider probe. The spark current was measured by a Pearson Electric model 411 current transformer. These signals were amplified by appropriate gains by operational amplifiers and multiplied together by an integrated circuit analog multiplier. The result of these operations was a voltage proportional to the instantaneous spark power, since the spark power is the product of the

instantaneous spark voltage and current. The output voltage from the analog multiplier was integrated by an operational amplifier in the resistor-capacitor integrating configuration. The result was an output voltage proportional to the spark energy, which is the time integral of power. Because of integrator drift with time, it was necessary to initialize the integrator so that at the instant the START signal from RASCAL was received, which was also the instant the spark was commanded to fire, the integrator output would be zero, and the integration could begin with the proper initial value. Also due to this integrator drift, it was necessary to feed the integrator output voltage into a unity gain sample-hold amplifier. An adjustable hold delay was included so that the delay could always be set to a value slightly greater than the spark duration. The output of the sample-hold amplifier was fed into an Analog Devices DM-31 digital panel meter so that the output voltage could be displayed in digital form.

Because of the wide range of spark currents, in order to maintain a high signal-to-noise ratio it was necessary to employ two selectable spark current amplifier gains. The lower range was 0 to 1 amp and the higher range 0 to 10 amps. A current overflow detector was added to indicate if the usable amplification range had been exceeded. Because of the wide range of spark energies to be measured, four selectable integrator RC time constants were used, ranging from 2×10^{-6}s to 2×10^{-3}s. All active components were chosen to have a frequency response of 1 MHz or better under operating conditions, thus, the frequency response of the overall system was about 1 MHz. The current transformer did not have a DC response, but the low frequency limit of its response was about 1 Hz, and so was perfectly adequate for measuring the current waveforms in this investigation of 25 milliseconds duration or less.

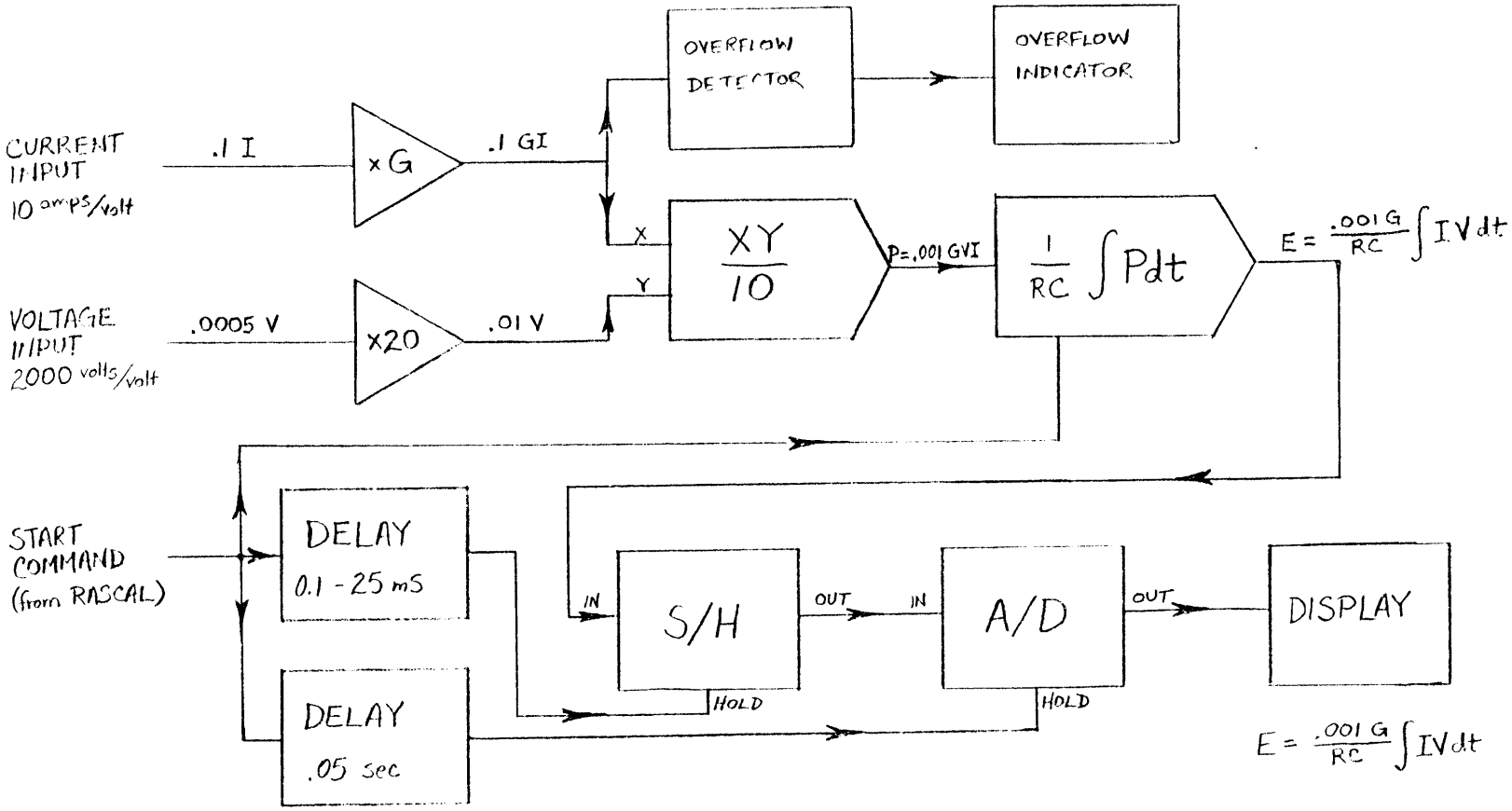

Figure 3-9. VARMINT block diagram

Where precision components were required, components with tolerances of ±0.2% or closer were used.

A problem which was never completely overcome was the trigger spark noise picked up by VARMINT which affected the spark energy computation. High voltage trigger sparks would cause noise in the current preamplifier which was carried through the computation and resulted in errors. The net effect was that VARMINT did not yield accurate and reliable measurements for sparks with energies of less than 2 millijoules at pressures of 760 Torr and above. Since these spark energies at these pressures correspond to the minimum ignition energies of only near-stoichiometric mixtures, where gravitational effects were not observed, this noise problem did not cause serious difficulty under the conditions where it was important for VARMINT to work properly.

In order to verify the accuracy of VARMINT, comparisons were made of spark energies calculated manually from spark voltage and current waveforms measured by an oscilloscope with the spark energies calculated by VARMINT for the same sparks. Three typical examples are shown in Fig. 3-8. Altogether, 29 such comparisons were made and the average discrepancy between the two methods was about 5%, with a maximum of about 15%, except for the problem area noted above. Of course it is not known which method was more accurate, but there was some evidence that the voltage waveforms as measured by VARMINT were more accurate than those measured by the oscilloscope, so it is possible that VARMINT was actually more accurate overall than the oscilloscope. Because of this, VARMINT's accuracy was estimated as ±10%, except for the problem area previously noted, and values of spark energy as calculated by VARMINT are used exclusively in the reported results, except for near-stoichiometric mixtures at 760 Torr where the oscilloscope measurements were used. Since the ignition phenomena in this investigation were no more repeatable than ±5% anyway, the

uncertainty of VARMINT's measurements did not lead to serious problems in interpreting the results.

3.5.5 Power distribution system

The power distribution system consisted of batteries, camera timer and relay, circuit breakers, and wiring. The overall power system layout is shown in appendix F, Fig. F-1. The camera timer is shown in appendix F, Fig. F-2. Two sets of batteries (other than the small 9 volt batteries in OTIS) were used, one set for RASCAL and VARMINT and the other set for the camera, timing light generator, and camera timer and relay. This was done because the camera motor was "noisy" and would put severe voltage "spikes" in the power line. These spikes caused false triggering of the flame detectors in RASCAL and interfered with the precision circuitry in VARMINT when all were connected to the same power source. Thus, it was necessary to isolate the camera power source by using separate batteries. Quiescent power consumption by RASCAL was about 7 watts, mostly by the 2000 volt power supply. VARMINT consumed 3.7 watts with the display on and 1.7 watts with the display off. The camera and timing light generator consumed between 50 and 300 watts depending on the camera framing rate.

The camera and timing light generator were enabled by closing a switch in series with two umbilicals from the drop package (see appendix F, Fig. F-1). When the drop began, contact between these umbilicals was broken. After an adjustable delay, the camera timer removed power from the camera relay and the camera and timing light generator were shut off. This delay was set to about 5 seconds, a few seconds longer than the free-fall time.

3.6 Photography

3.6.1 Camera and timing light generator

The camera used in this investigation was a Teledyne Model DBM-45 16 mm motion picture camera. The framing rate was adjustable from near zero to 400 frames per second. The framing rate used in the current investigation was the maximum rate that would still allow a clear flame image to appear on each frame of film. If the framing rate were too high, the exposure time for each frame would be too low and the flame image would be dim or nonexistent. The maximum usable framing rate for each combustible mixture was found by trial and error. This rate varied from about 400 frames/second for stoichiometric mixtures at high pressures to about 20 frames/second for very lean mixtures at low pressures.

The camera and film merely recorded the light emitted by the flame itself. Direct visual photography was used rather than shadowgraph or schlieren photography. While shadowgraph or schlieren methods have the advantage of greater sensitivity than direct visual photography, these methods had several disadvantages for the current investigation. The most severe problem was that there was simply not enough space in the experiment package for the equipment and unobstructed optical paths required for shadowgraph or schlieren photography. Other problems included the accurate optical alignments required which could have been disturbed by repeated impact loads in drop tests, the delicacy of the optics, and the electrical power requirement of the auxilliary light sources required.

The lens used was an Elgeet 13 mm f1.5 lens attached to the camera by a special ruggedized mount. The maximum available aperture of f1.5 was used in

all tests. The camera and lens were mounted to the experiment package, aligned, and focused by NASA photographic technicians.

The camera framing rate was determined by timing pulses exposed on the edge of the film by a small neon light within the camera. The source of the high voltage pulses required to trigger this neon light was a Photosonics model 78-1005 timing light generator. Two pulse rates were used in this investigation, 10 pulses/second and 100 pulses/second. The pulse rates were checked with a frequency counter and found to be 10.73 and 102.5 pulses/second, respectively. These pulse rates were assumed constant and used throughout the film analysis.

3.6.2 Film and processing

The film used in this study was Kodak 7250 Color Video News Film with a 400 ASA rating. The Kodak catalog number for this film is 121-8700. This was the most sensitive color film of its type available. Color film was used because black and white film is not very sensitive to the deep blue light emitted by methane-air flames. Also, using color film yields some qualitative information on flame temperature (section 4.1). Infrared sensing film could have been used to obtain better temperature information but available infrared films are difficult to work with and generally only provide information on which parts of the flame are above or below a certain fixed temperature, that is, there is very little "gray area".

The film was processed by film laboratories in the Cleveland and Boston areas. Most of the film was force processed to ASA 1600. This allowed a higher framing rate to be used for a given flame. The penalty for forced processing is lower resolution, but for the purposes of this investigation, it

was not necessary to see a very sharp image of the flame front, so this was not a major disadvantage.

3.6.3 Analysis of film data

The only quantitative data obtained from the film records was the flame front radius as a function of time for spherical or nearly spherical flames. This involved determining the framing rate of the camera and the actual flame front radii from the film records. Of course, the electronic flame detectors (section 3.5.3) also performed the same task but yielded only four data points, one for each detector, and no information on the shape or structure of the flame. Also, the flame detectors were not always reliable (section 3.5.3).

The film records were analyzed on a Vanguard 16 mm motion analyzer. This device projected the film images frame by frame onto a glass screen. Movable X-Y crosshairs with position indicators allowed distances between locations on the screen to be determined precisely. A frame counter was also included.

The framing rate for each combustion test was determined from the timing marks on each film record and the known timing pulse rate. For each film record, the timing marks on the film were counted beginning a few frames before ignition and ending a few frames after the completion of combustion. The number of frames for this length of film was determined from the frame counter. The framing rate was the ratio of the number of frames to the number of timing marks multiplied by the timing pulse rate. The framing rate determined this way was assumed to be constant throughout each combustion test, and spot checks of the film records showed this to be substantially correct. The calculated framing rate was usually slightly slower than the value indicated by the framing rate control on the camera. For some unknown

reason, the timing light generator did not work in some zero-g tests, and in these cases the framing rate was estimated from the calculated framing rate for other tests on the same day with the same framing rate setting on the camera.

The flame front radii were measured on the left side of the flame kernel as viewed by the camera, as the flame detector assembly was on the right side and the spark electrodes were on the top and bottom. These solid obstacles caused some distortion of the flame front, particularly at low pressures, so the flame front was most nearly spherical on the left side and therefore it was most reasonable to measure flame radii on this side. The magnification factor of the camera and projector was calibrated by measuring the distance on the projected image from the spark gap to the #1, #2, and #4 flame detectors with the X-Y crosshairs and comparing these to the physically measured distances between these points. Because the flame front is spherical, there will be a small parallax error in measuring flame front radii (Fig. 3-10). The actual flame front radius r_b can be related through geometrical considerations to the measured radius r_m by the equation

$$r_b = r_m L / [r_m^2 + L^2]^{1/2},$$

where L is the distance from the focal point of the lens to the center of the flame kernel. This correction was included in the calculations of the true flame front radii, although the correction was never more than 4%.

Qualitative as well as quantitative information was derived from the film record. It was useful to view near-limit one-g combustion phenomena frame by frame to observe the development of convection and its effects on flame propagation. The zero-g flames could only be observed from the film record, and the ability to observe the shape and propagation characteristics of these flames turned out to be an important asset. From the thickness, intensity,

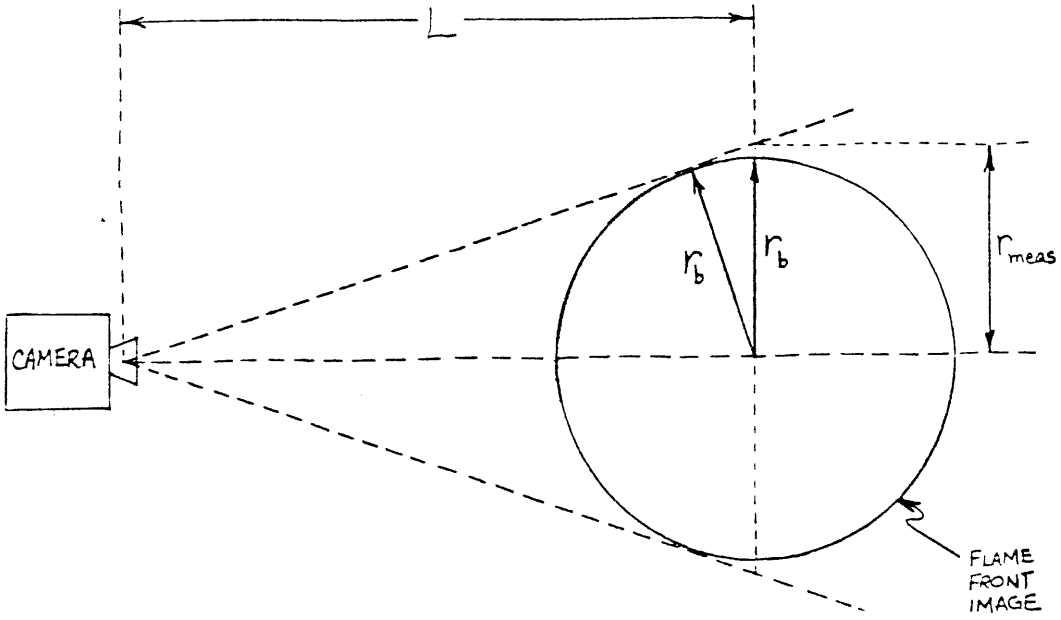

Figure 3-10. Measured and actual flame front radii

---

and color of the luminous zone, some characteristics of the flame structure and flame reactions can be deduced (section 4.5). Since the main luminous zone in hydrocarbon flames occurs at a temperature of about 800-1000°K (section 2.1.1), the boundaries of the volume of gas with this temperature or higher in extinguishing flames could be deduced (section 4.5.2).

3.7 Experimental procedures

3.7.1 Pre-test procedures

All of the experimental apparatus was mounted to the experiment package frame supplied by NASA and all one-g and zero-g combustion tests were performed with the apparatus in this configuration. This insured that

practically all experimental conditions other than gravity were the same for one-g and zero-g tests.

For each combustion test, three experimental parameters had to be selected: total pressure, mixture ratio, and spark energy. These are the primary variables of this investigation and their selection depended on the motivation for the current combustion test.

Once these parameters were chosen, the spark gap and spark duration had to be selected. The spark gap was set to the quenching distance in almost all cases. For most values of total pressure and mixture ratio information on quenching distance was available from the literature (section 2.2.5.2). When such information was not available, quenching distance was estimated from the scaling relations presented in the same section or determined experimentally. A restriction was that the maximum allowable spark gap was 2.5 cm, because for longer gaps the spark would jump from the negative electrode to the No. 1 flame detector and not to the positive electrode. In order to assess the effect of spark gap on MIE in this investigation, a few tests were performed in which the minimum ignition energies for different spark gaps were determined for fixed values of total pressure and mixture ratio. The results and their significance are presented in section 4.4.1. The spark duration was set to the optimum value whenever possible. While information on optimum spark duration was only available in a few cases, in other cases the optimum spark duration could be estimated from the scaling relations presented in section 2.2.5.2 or determined experimentally. In some cases it was not possible to set the spark duration to the optimum value, as explained in section 3.5.2. In order to assess the effect of spark duration on MIE in this experiment, a few tests were performed in which the minimum ignition energies for different spark durations were determined for fixed values of total

pressure and mixture ratio. The results and their significance are presented in section 4.4.1.

Once the spark gap and spark duration were selected and set, the vessel was filled with dry air to the total pressure to be investigated and the trigger spark intensity was adjusted as described in section 3.5.3. Next, the total spark energy was set to the desired value with the spark power adjustment on RASCAL. If the desired spark duration could not be used, the spark duration and spark power were adjusted to obtain the best compromise settings that would still yield the proper spark energy. Other minor adjustments required included the flame timer clock frequency (section 3.5.2), the VARMINT flame detector sensitivity (section 3.5.3), and the VARMINT current and energy scales (section 3.5.4). Finally the combustion vessel was filled with combustible mixture as outlined in section 3.4.2.

Some authors [16, 89] have found it necessary to "condition" the combustion vessel each day by producing several flames in the vessel before repeatable results could be obtained. This was not found to be necessary in the current investigation and so was not done as a matter of course.

3.6.2 Ground tests

In the ground tests the camera (if used) was started a few seconds before firing the spark. When the spark was fired, the propagation of the flame, if any, was observed visually in a darkened room. More quantitative observations were made later from the film record. For each spark, the spark energy calculated by VARMINT was recorded. If no ignition occurred, the spark energy was increased and the process repeated until ignition occurred, if it was possible to produce ignition at all. If ignition occurred and the flame reached the flame detectors, the flame timers in OTIS were read. Ambient air

temperature was maintained at 23 ± 1°C. Each combustion test, including the selection of experimental parameters, gas mixing, testing, and data recording, took 20-30 minutes.

Since each spark burned some quantity of fuel, however small, if enough sparks were passed through the mixture the concentration of reactants would decrease significantly and thus the combustion properties would change. In order to nullify this problem, each test was repeated with fresh mixtures until the value of spark energy was found that was barely adequate to cause ignition with the first spark, and this energy was deemed the minimum ignition energy.

It was possible to obtain a semiquantitative estimate of the fraction of fuel consumed by combustion from the pressure in the vessel after combustion. Once the temperature in the vessel reequilibrated to room temperature after combustion, some of the water vapor formed by the combustion reactions had condensed on the vessel walls, leading to a decrease in the total pressure inside the vessel, since there is no net change in the total moles of gas due to the combustion reaction of methane

$$CH_4 + 2O_2 \rightarrow CO_2 + 2H_2O.$$

Of course it was possible that some of the carbon did not react completely during combustion to form CO_2, but instead reacted only partially to form CO. This would have led to a lower pressure drop than would have otherwise occurred. At room temperature the dissociation of CO, CO_2, and H_2O, which would have led to a further increase in the total moles of gas, was negligible. The time required for temperature equilibration after combustion was of the same order as the time required for temperature equilibration in the gas mixing process (section 3.4.2). The pressure drop was easily measured by the pressure gauge used in the gas mixing system. The pressure drop due to

combustion was greatest for near-stoichiometric mixtures, as these mixtures produced the greatest mole percentage of water vapor, and tapered off smoothly for decreasing fuel concentration until near the flammability limit, where the pressure drop decreased rapidly to near zero (Fig. 4-6), indicating that the possibility of incomplete carbon combustion did not affect the basic qualitative trends expected from simple thermodynamics. Had the incomplete reaction of carbon been a significant effect, the equilibrium pressure in the vessel could have increased in some cases, but this was never observed. It was not possible to obtain strictly quantitative measurements of the degree of completion of reaction, because it was not known a priori what portion of the water vapor had condensed, and calculations of the amount of water expected to stay in the vapor phase from equilibrium considerations did not agree with the measured results. The amount of condensed water was always higher than expected, especially at low pressures, probably due to surface effects. This further suggests that the possibility of incomplete reaction of carbon was not an important factor. Thus, the pressure drop due to combustion was almost certainly a reasonable semiquantative measure of the degree of completion of reaction, which was quite useful information for both one-g and zero-g tests.

These one-g MIE tests were performed for stoichiometric and leaner mixture ratios for total pressures of 1500, 760, 250, 100, and 50 Torr. These tests yielded information on flammability limits, where the minimum ignition energy was essentially infinite, and burning velocities as well as minimum ignition energies. The results are presented in the following chapter.

3.7.3 Drop tests

The procedure for the zero-g (drop) tests was identical to the procedure

for the one-g tests up to the conclusion of the gas mixing process. At this point the experiment package was prepared for the zero-g test and dropped according to the procedures outlined in section 3.1. Since the drop tower was not air conditioned, the ambient air temperature could vary considerably during the day. Under some conditions, this variation had a substantial effect on the results (sections 4.2.2, 4.3.2, and 4.4.1). Ultimately it was necessary to disregard comparisons of one-g and zero-g results under the conditions where the results were sensitive to temperature except where the ambient air temperature in the drop tower was comparable to the ambient air temperature in the one-g tests ($23 \pm 1^{\circ}C$). This $2^{\circ}C$ variation in ambient temperature was small enough to have a negligible effect on the results.

About 10 minutes elapsed from the conclusion of the gas mixing process to the actual drop. A typical drop test event sequence is shown in table 3-2. The events from T + 0.2 sec to T + 0.22 sec are identical to those in the one-g tests. After the drop, the information from OTIS and VARMINT was read, and after the drop assembly was hoisted back to the fifth floor of the drop tower and the experiment package was removed, the pressure in the vessel was read. The elapsed time from the drop itself to the reading of the vessel pressure was about 10 minutes. The total cycle time, including the experiment package preparation, was at least 40 minutes. Nine drops was the most performed in one day, but six to eight drops per day was more common.

As with the one-g tests, the information obtained from each drop test included the flame timer readings, the spark energy as calculated by VARMINT, the vessel pressure after combustion, and the film record. In practice, it was necessary to know immediately after the drop if ignition had occurred in order to set the experimental parameters for the following drop. This could be determined from the flame timer readings when the flame detectors worked

T - 5 sec	Camera ON (manual operation)
T + 0 sec	Cutter activated (manual operation) Free-fall begins
T + 0.1 sec	Umbilical contact broken Onboard sequencing begins
T + 0.2 sec	Trigger spark fires DC spark ON VARMINT spark energy computation begins Flame timers enabled Medium and high voltage power supplies OFF
T + 0.2 sec + t_s	DC spark OFF
T + 0.22 sec	Flame detector latches enabled
T + 2.2 sec	Drop ends
T + 5 sec	Camera OFF

Table 3-2. Typical drop test event sequence

---

properly, since no flame detection would occur if ignition had not occurred, but the flame detectors were not always reliable, as previously mentioned. The foolproof evidence of combustion was the combustion vessel pressure after the drop. If ignition had occurred, a predictable and unmistakable pressure drop would occur. Of course, the film record would also determine whether or not ignition had occurred, but was not available until 2 or 3 days after the test.

The experimental apparatus as a whole performed quite reliably in both the one-g and zero-g tests, but a couple of problems persisted in the zero-g tests. The deceleration loads caused numerous broken wires at solder joints. In retrospect this could have been avoided by using stranded rather than solid core wire. The deceleration loads also caused circuit boards to pop out of their sockets, but this problem was eliminated by the judicious use of foam padding.

Chapter 4. Results and Discussion

4.1 General observations

A total of 735 combustion tests were performed, including 334 drop tests. The drop tests were conducted in the NASA-Lewis 2.2 Second Zero-Gravity Facility during two six-week periods, the first in the fall of 1981 and the second in the summer of 1982. All one-g and zero-g tests were conducted by the author. All procedures concerning the tower operation were conducted by NASA technicians. All data analysis was performed by the author or by undergraduate students under his direct supervision.

As anticipated, there was no detectable difference between one-g and zero-g flame propagation for fast-burning near-stoichiometric mixtures (Fig. 4-1a). In both cases flame propagation was spherically symmetric. For somewhat slower burning leaner mixtures (Fig. 4-1b) the effect of buoyancy in one-g became noticeable, as the flame front reached the top of the vessel slightly before the bottom of the vessel, even though ignition was at the center of the vessel. The zero-g flame propagation for the same mixture was still spherically symmetric. For still slower burning mixtures (Fig. 4-1c), in one-g the flame could not propagate fast enough to burn downward against the buoyancy of its own burned gases. Because of this, the flame kernel rose upward while propagating outward, and owing to shear forces at the flame kernel boundary, deformed into a mushroom-shaped cloud. Upon reaching the top of the vessel, the flame front spread outward and downward, and extinguished at some point on its downward propagation. Again, the zero-g propagation for the same mixture was spherically symmetric. For still slower burning, still

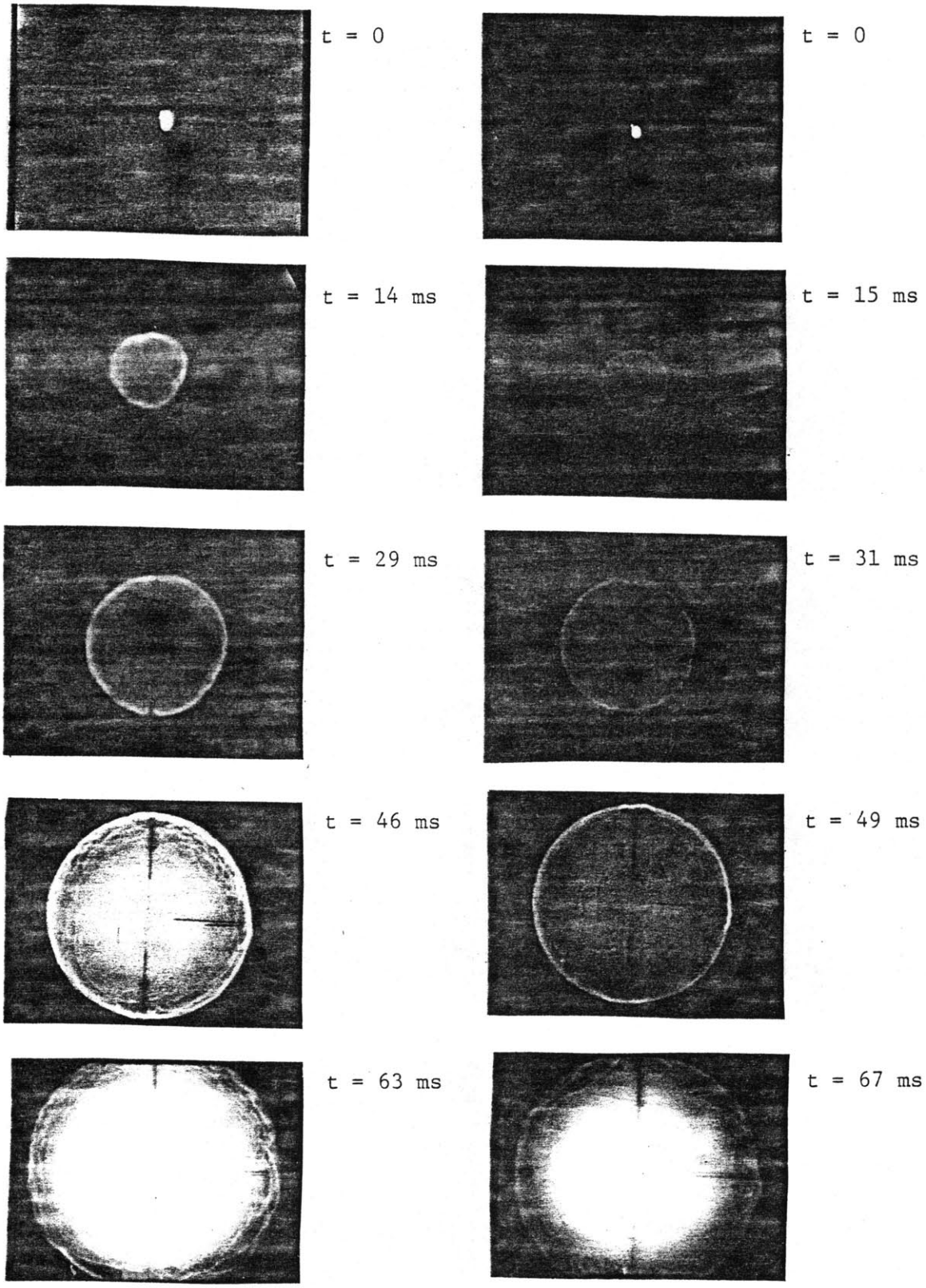

Figure 4-1a. Sequential photographs of combustion of 9.5% methane in air at atmospheric pressure in one-g and zero-g

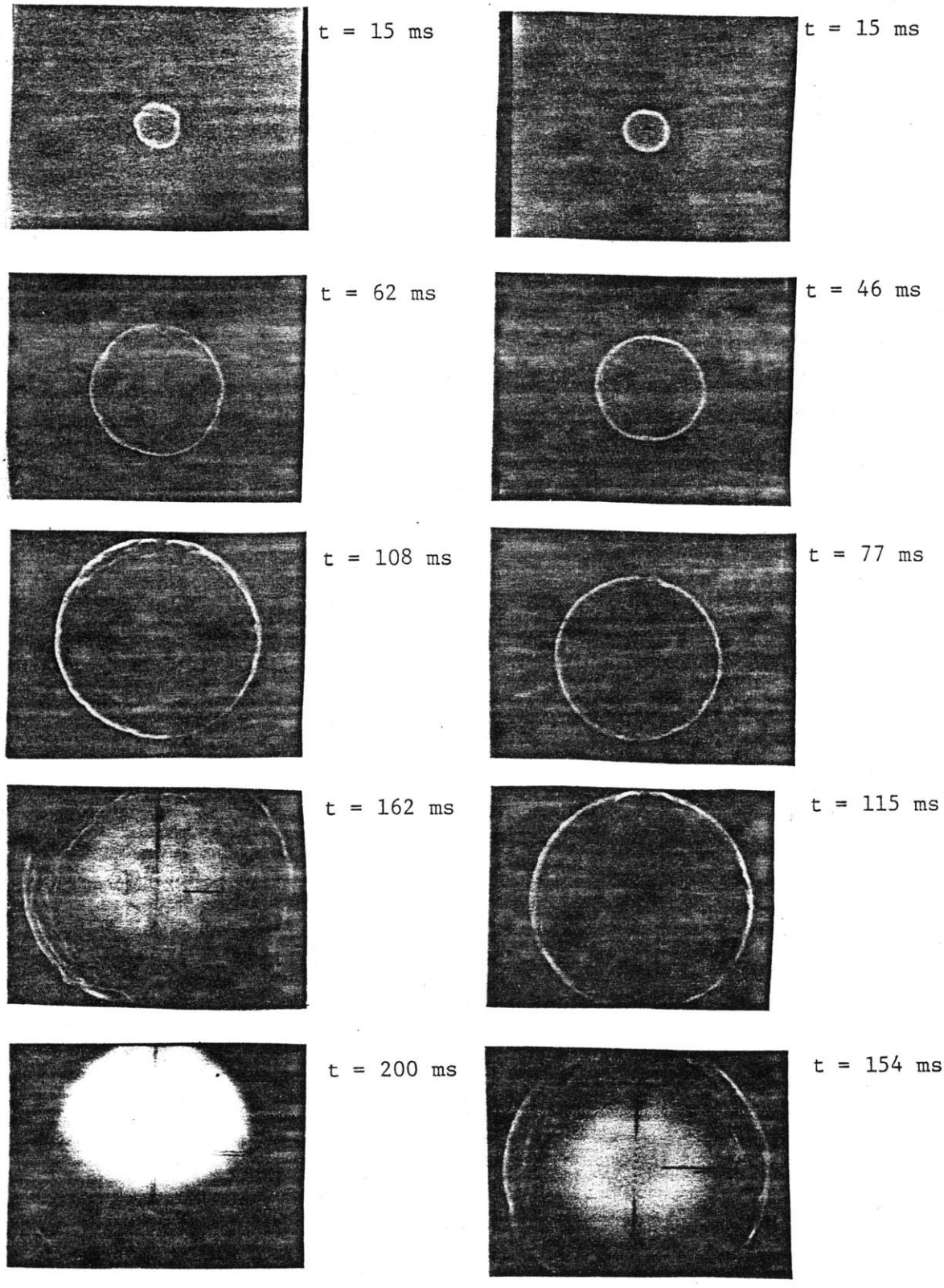

Figure 4-1b. Sequential photographs of combustion of 7.0% methane in air at atmospheric pressure in one-g and zero-g

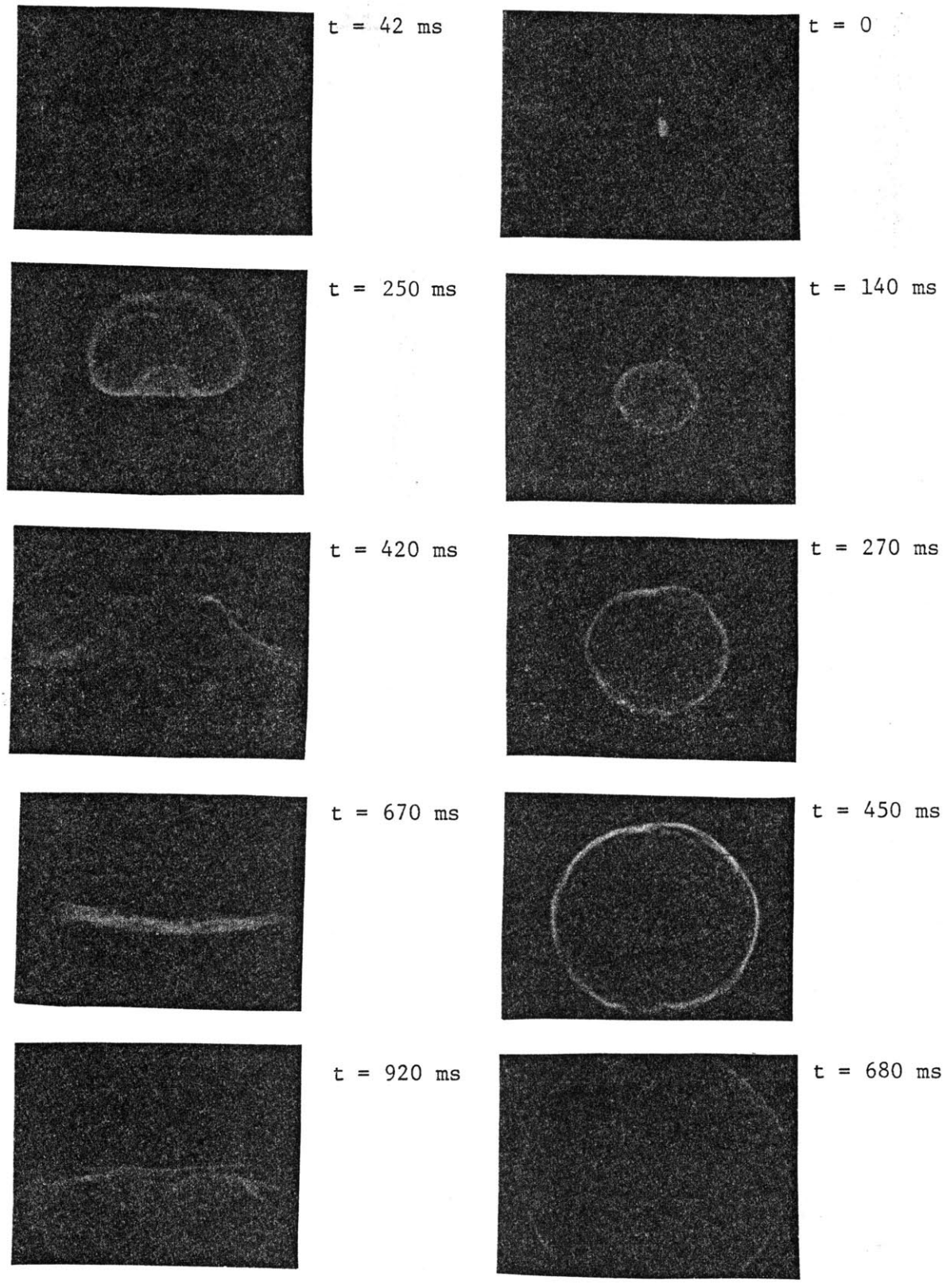

Figure 4-1c. Sequential photographs of combustion of 5.5% methane in air at atmospheric pressure in one-g and zero-g

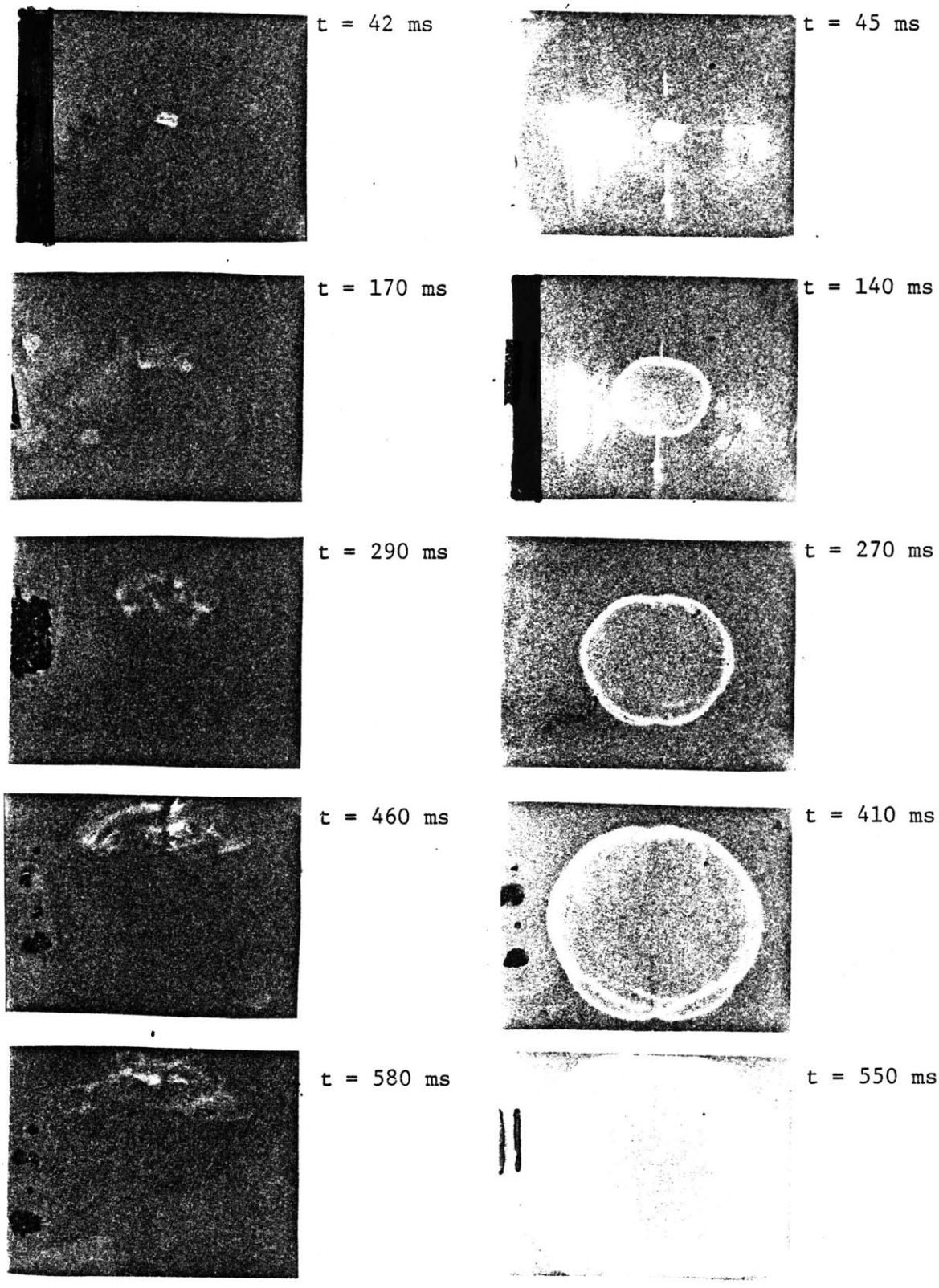

Figure 4-1d. Sequential photographs of combustion of 5.10% methane in air at atmospheric pressure in one-g and zero-g

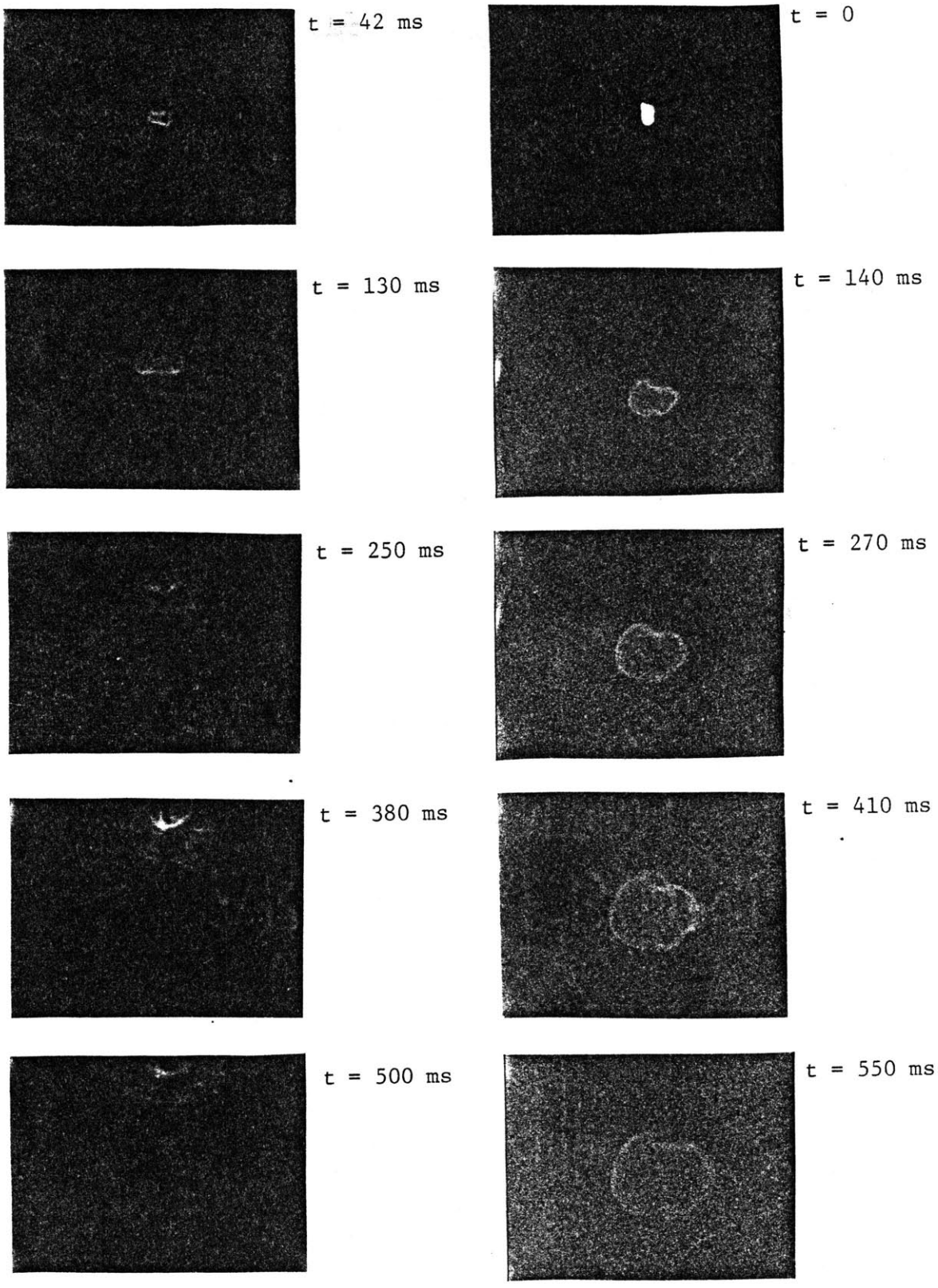

Figure 4-1e. Sequential photographs of combustion of 5.05% methane in air at atmospheric pressure in one-g and zero-g

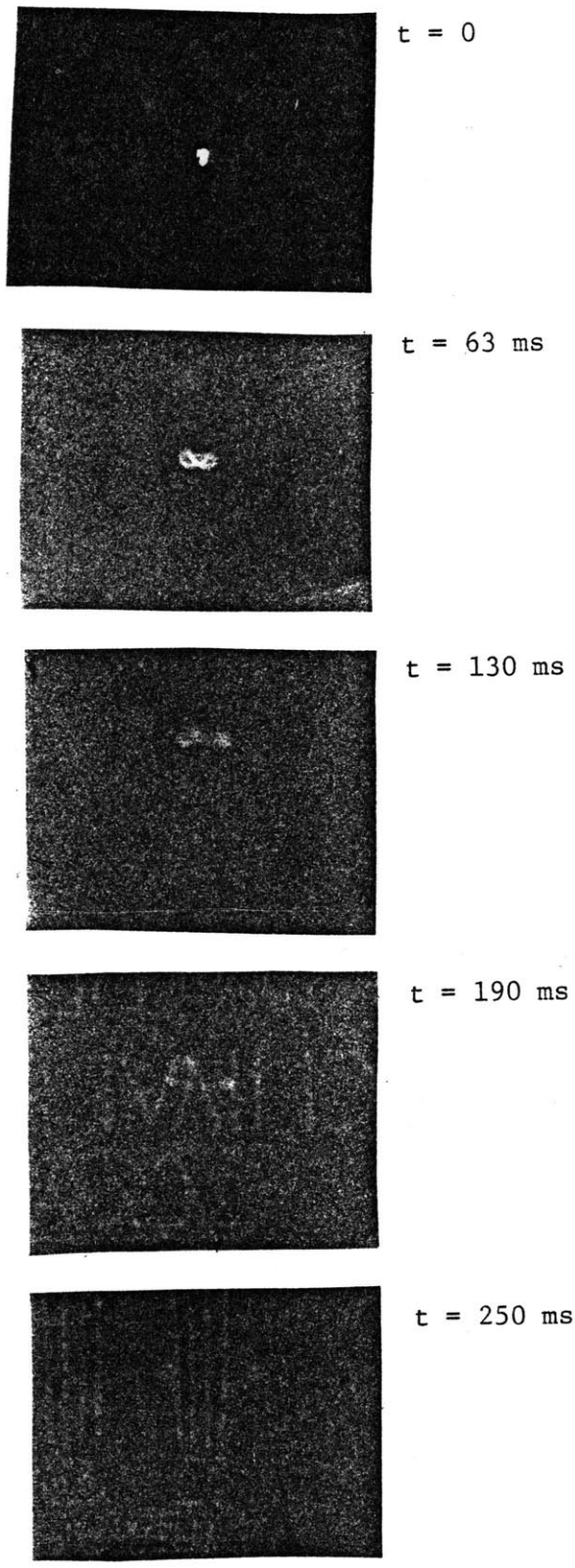

Figure 4-1f. Sequential photographs of combustion of 4.7% methane in air at atmospheric pressure in one-g

leaner mixtures (Fig. 4-1d), in one-g the flame propagated upward in a bubble which flattened out and became more irregular as it rose, without forming the mushroom-shaped cloud, and extinguished upon reaching the top of the vessel. The volume of gas swept out by the flame front was roughly cone-shaped, with the half-angle of this cone narrowing as the fuel concentration decreased. Again in zero-g the flame propagation was spherically symmetric. When the zero-g flammability limit was reached (Fig. 4-1e), zero-g flame propagation suddenly changed radically, but one-g flame propagation did not change noticeably. In zero-g, instead of having flame propagation throughout the vessel, as had occurred for all faster burning mixtures, the flame would propagate outward at a continually decreasing rate until a certain radius was reached and then would suddenly extinguish. This phenomenon was termed "Sudden Infant Flame Death", or SIFD. Flame propagation was still spherically symmetric until extinguishment except for a few very unusual cases at 1500 Torr. The phenomenon of SIFD constitutes the major discovery of this investigation, and so is discussed in nauseating detail in section 4.5. For still slower burning, still leaner mixtures (Fig. 4-1f), in one-g only a very thin wisp of flame was observed which rose toward the top of the vessel, sometimes breaking up into several "flamelets", and extinguished, whereas in zero-g no flame propagation beyond the ignition process was observed. Finally, for even slower burning, even leaner mixtures, no flame propagation beyond the ignition process was observed in either one-g or zero-g.

The phenomena described above and shown in Fig. 4-1 are for a total pressure of 760 Torr, but the results are qualitatively the same at all other total pressures investigated. For a given mixture ratio, gravitational effects are less significant at low pressures, as is apparent from a comparison of Fig. 4-2 and Figs. 4-1 a-c.

These one-g observations are consistent with previously reported results (section 2.2.3.3). The zero-g observations other than SIFD are not entirely new either, having been reported by Krivulin et al. [15] for lean hydrogen-air and rich propane-air mixtures at atmospheric pressure and Reuss [16] for lean methane-air mixtures, although these authors did not investigate pressure effects on these processes.

It should be noted that the significant changes in flame behavior occurred over a narrow range of mixture ratios. The width of the region between the onset of significant gravitational effects (about 6.0% methane) and the total absence of flame propagation (about 4.6% methane) corresponds to a change in methane concentration of only 1.4%. This is fairly small in relation to the 4.2% change in concentration between the midpoint of this region (5.3%) and the stoichiometric concentration (9.5%).

The color of all the methane-air flames investigated was dark blue, as is typical of hydrocarbon-air flames [30,33]. This suggests, but does not prove, that the chemical reaction mechanism is basically the same for all of these flames, or at least that the flame reactions which produce chemiluminescence (the emission of visible light due to chemical reaction) occur regardless of total pressure, mixture ratio, spark energy, or gravitational conditions. If the reactions which produce chemiluminescence were strongly affected by these parameters, some flames would have probably shown a different color or been colorless.

While it was difficult to tell from a two-dimensional projection of a three-dimensional flame front, it appeared that the luminous zone was very thin except for lean mixtures at 50 and 100 Torr, where a relatively broad, diffuse luminous zone was observed. The intensity of the luminous zone was definitely much higher at higher pressures and for mixtures with faster

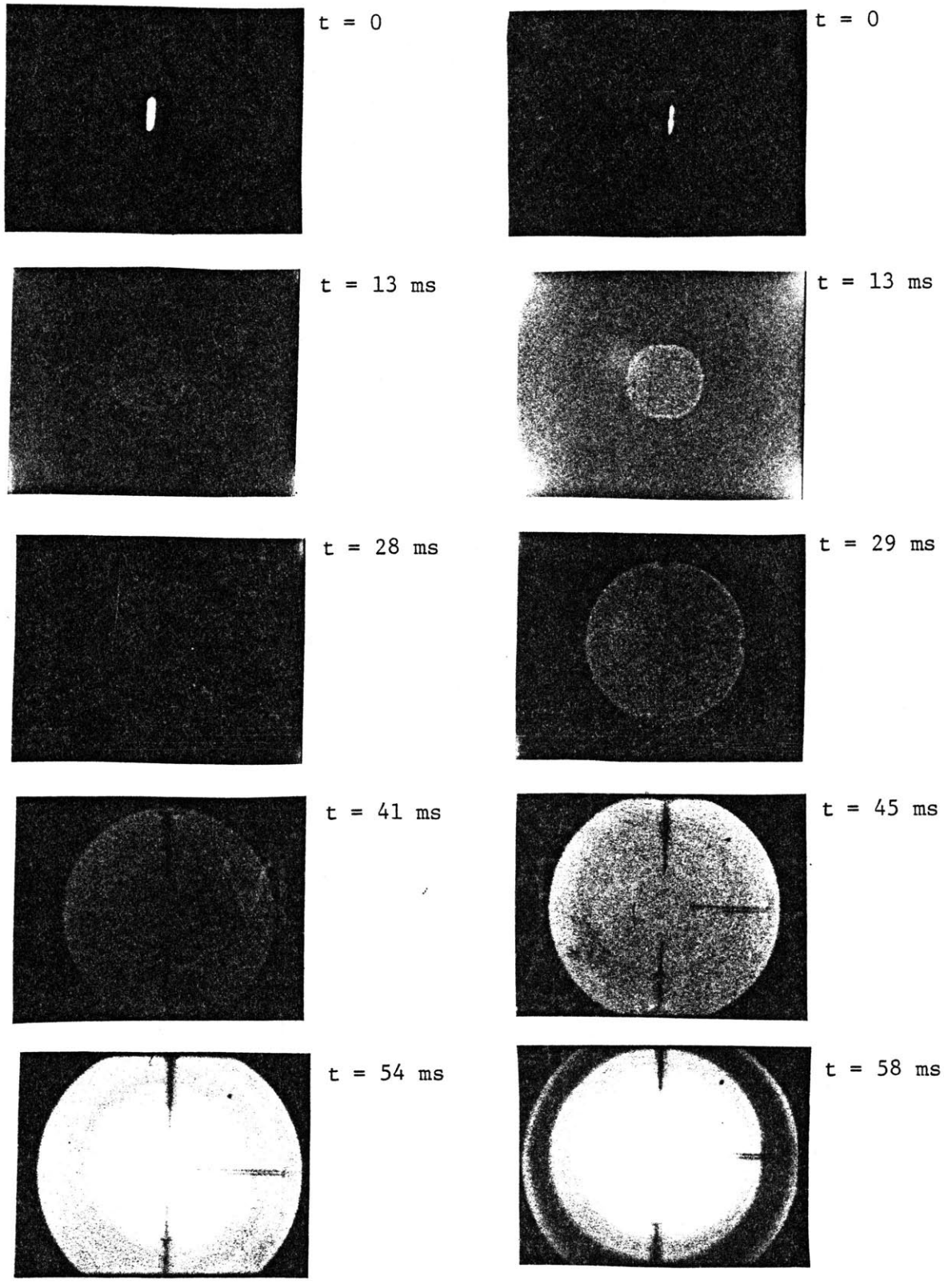

Figure 4-2a. Sequential photographs of combustion of 9.5% methane in air at 100 Torr total pressure in one-g and zero-g

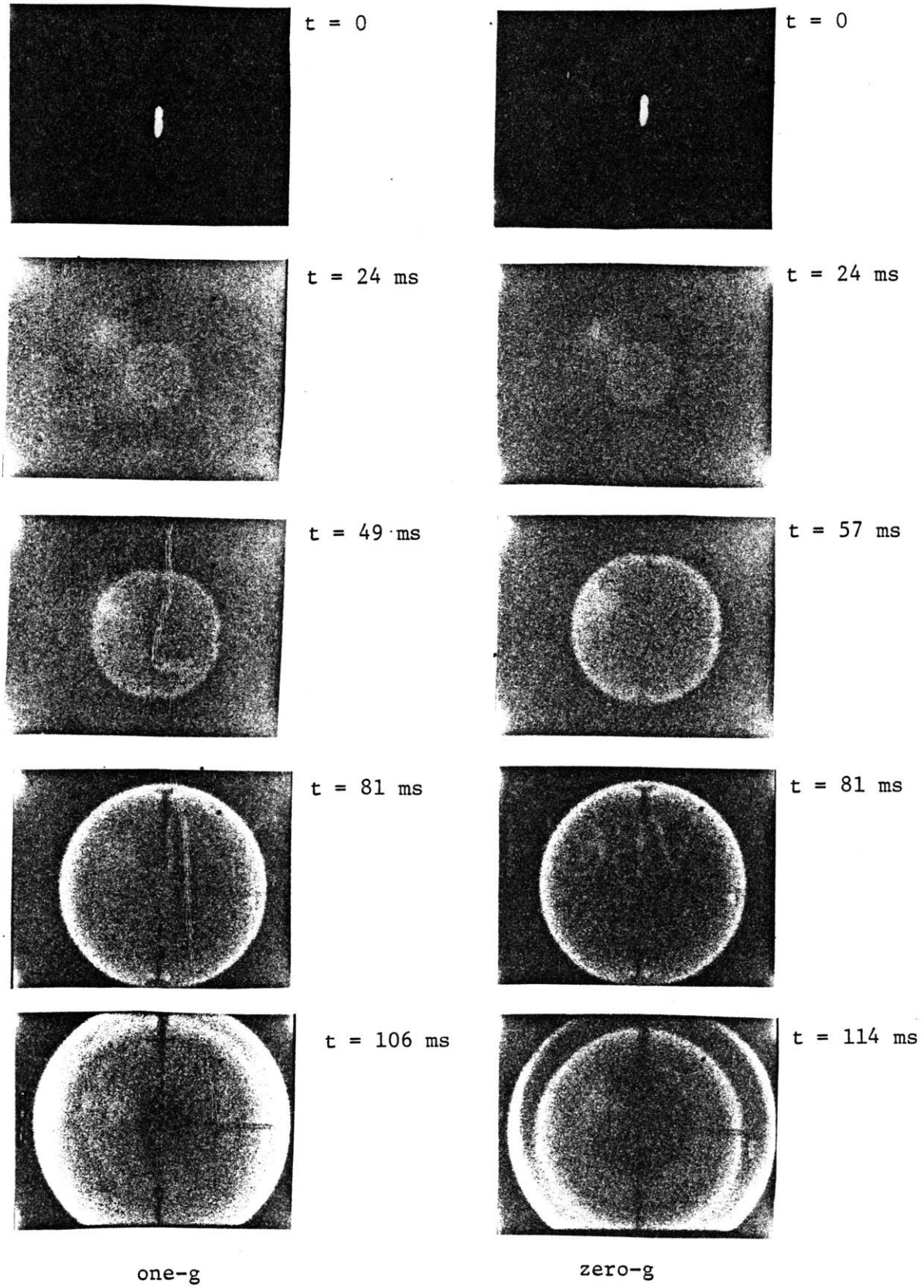

Figure 4-2b. Sequential photographs of combustion of 7.0% methane in air at 100 Torr total pressure in one-g and zero-g

burning velocities. This behavior is to be expected, since flame thicknesses are expected to be smaller at higher pressures and for faster burning mixtures (section 2.2.2), and these conditions also imply faster reaction rates which lead to greater photon fluxes emitted by chemical reaction, thus leading to greater observed light intensities.

As expected, some flames exhibited a cellular, or "wrinkled" flame front, as described in section 2.1.1. The wrinkles were more pronounced at higher pressures, as is apparent from a comparison of Fig. 4-2 and Figs. 4-1 a-c. It is interesting that wrinkles which formed in the early stages of flame development usually propagated throughout the mixture without changing shape or structure. This suggests that such disturbances are caused by the ignition process or shortly thereafter, and are quite stable and self-propagating. Whether or not such phenomena can be caused by preferential diffusion of methane, as conventional wisdom (section 2.1.1) would dictate, is not clear, and to clarify this matter would require measurement of methane concentrations in the flame front, which is beyond the scope of the current investigation. In any case, such disturbances did not appear to affect the overall properties of the combustible mixture, and so are not of particular interest to this work.

In some mixtures at 1500 Torr (Fig. 4-3), in addition to the fine wrinkles, gross deformities in the flame front were observed in zero-g, although the overall flame propagation was still more or less spherically symmetric. Again, these deformities were first observed in the early stages of flame development and propagated throughout the mixture without changing shape or structure. Since preferential diffusion would only account for small, even disturbances in the flame front (section 2.1.1), it appears that

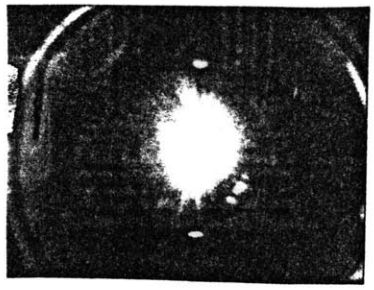
t = 0

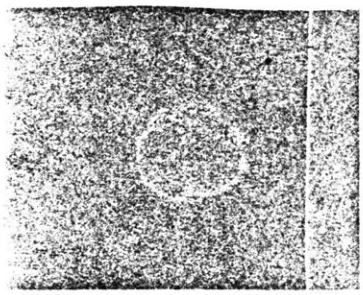
t = 0.48 sec

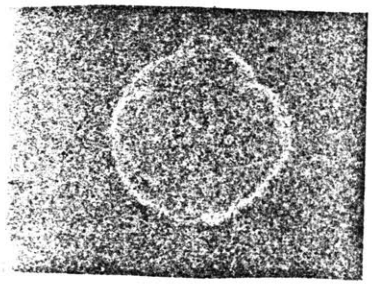
t = 1.00 sec

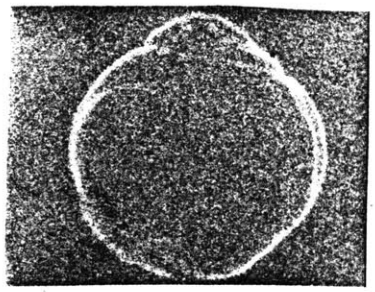
t = 1.55 sec

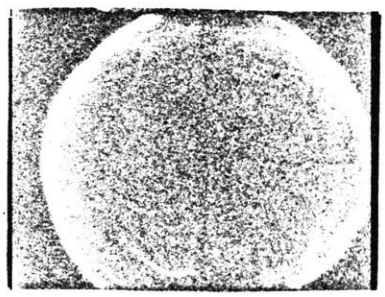
t = 2.03 sec

Figure 4-3. Sequential photographs of combustion of 5.30% methane in air at 1500 Torr total pressure in zero-g

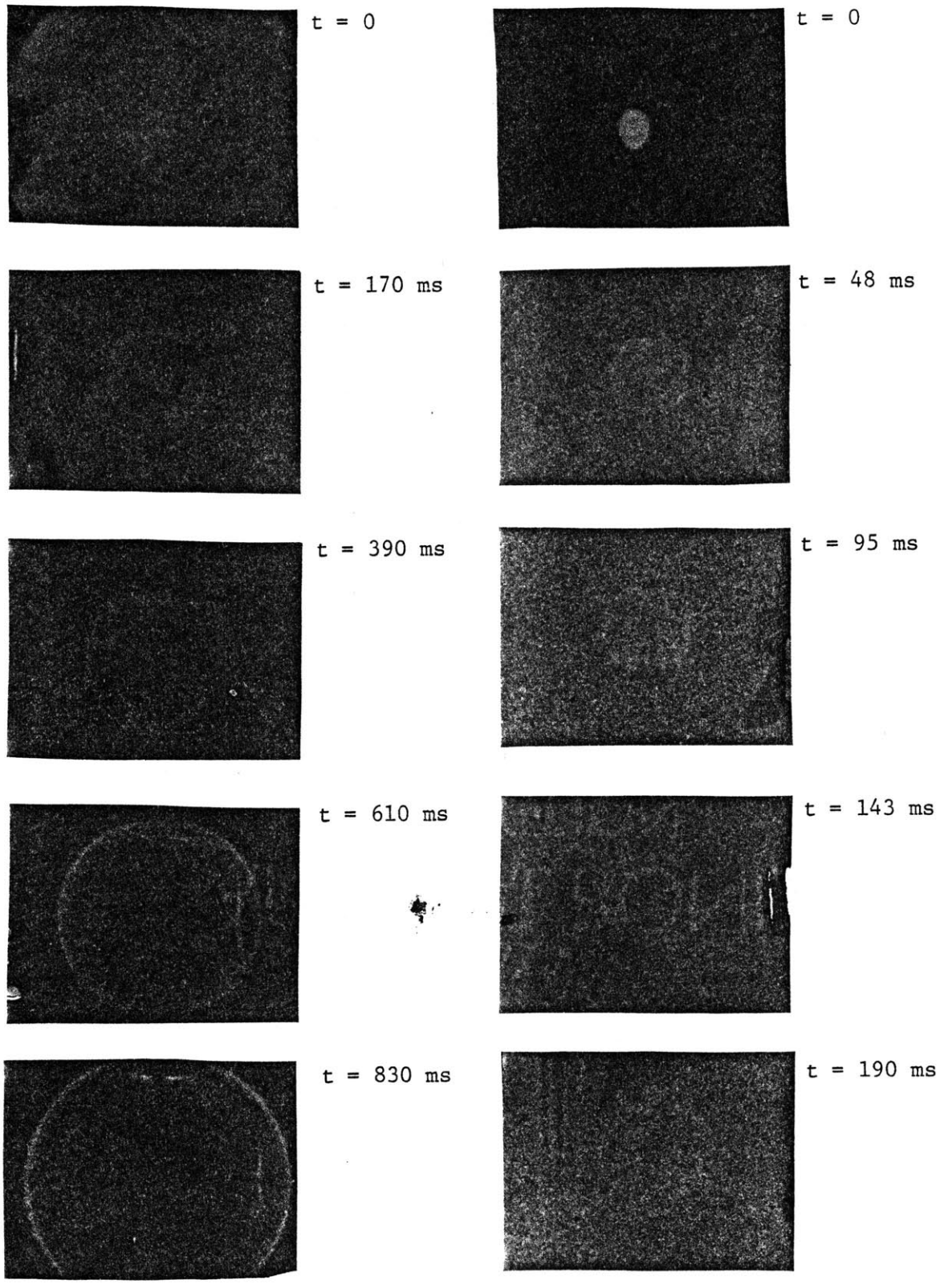

Figure 4-4. Sequential photographs of combustion of: a) 4.42%, b) 4.40% methane in air at 100 Torr total pressure. Spark energy about 4 joules in both cases.

there must be another mechanism to account for the propagation of disturbances in flames, at least in zero-g.

It is not clear why such disturbances and gross deformities should be more prevalent at high pressures. It is possible that due to the larger flame thickness at lower pressures, a larger combustion vessel is required in order to observe the same phenomena. This is unlikely, however, as the gross deformities were observed only 1500 Torr and not at all at 760 Torr or below. If we attempt to define a Reynolds number Re for a freely propagating flame based on the flame thickness, the result is

$$Re \equiv VD/\nu = S_u\delta/\nu = S_u(k/\rho_u C_p S_u)/\nu = 1/Pr,$$

where ν is the kinematic viscosity or momentum diffusivity, and Pr is the Prandtl number. Since Pr is almost independent of pressure for gases it is unlikely that pressure effects on viscous forces could account for the pressure effects on the propagation of disturbances. No plausible explanation for these pressure effects could be conceived. The pressure effects on the propagation of disturbances will be more evident based on the results presented in section 4.5

The presence of the spark electrodes and flame detectors did cause some disturbance in the flame fronts (Fig. 4-4a), but only for lean mixtures at low pressures, in which case the otherwise spherical zero-g flame fronts were concave with respect to the burned gases near these solid boundaries. This was almost certainly due to conductive heat loss to the solid boundaries, as conductive heat loss is most significant when the quenching distances are largest, which is at low pressures and for slow-burning mixtures. The heat loss acts to retard flame propagation, as is apparent from the indentations in the flame front under these conditions. The heat loss at the solid boundaries did not appear to have any effect on the overall flame propagation, as the

zero-g flame fronts were spherical except near the solid boundaries, and when SIFD behavior was observed, flame failure occurred simultaneously everywhere along the flame front (Fig. 4-4b). If the heat loss to the solid boundaries were important in determining flammability limits or burning velocities, flame failure would have occurred near the solid boundaries first. Since the mixtures which exhibited SIFD behavior were leaner and slower burning than any other mixtures investigated at these pressures, they would be more affected by conductive heat loss than any other mixtures at these pressures. The conclusion is that heat loss to the spark electrodes and flame detectors caused local disturbances in the flame fronts, but under no circumstances investigated had significant effect on the overall flame behavior.

4.2 Flammability limits

4.2.1 Method of determination

Three flammability limit definitions were employed in the current investigation. The one-g downward propagation limit was defined as the limiting mixture for flame propagation throughout the entire combustion vessel in one-g. For sublimit mixtures, the flame would not burn all the way to the bottom of the vessel, as reported in the previous section. The one-g upward propagation limit was defined as the limiting mixture for propagation all the way to the top of the vessel in one-g. Of course, upward limit mixtures only burn upward, and not outward or downward, as previously reported. The zero-g propagation limit was defined as the limiting mixture for steady flame propagation throughout the vessel in zero-g. For sublimit mixtures in zero-g, the SIFD or normal non-ignition behavior was observed.

The downward flammability limit definition is well-defined but somewhat arbitrary because a vessel of different size or shape almost certainly would have yielded a different limiting mixture. The upward flammability limit was not well-defined in addition to being arbitrary. The upward limit mixture was not well-defined because it was difficult to determine whether the flame propagated to the top of the vessel as a result of self-propagation or only due to the ignition energy imparted to gas and because sometimes near-limit flames would break up to smaller "flamelets", some of which would reach the top of the vessel and some of which would not. The upward flammability limit definition was arbitrary because a vessel of a different size would have resulted in a different limit mixture, since in a larger vessel a wider range of mixtures would have resulted in flames that would break up and extinguish before reaching the top of the vessel. The zero-g flammability limit definition was well-defined and nonarbitrary, as the limit mixture was practically independent of vessel size or spark energy, as explained in the following section. These observations on the definition and arbitrariness of flammability limits in one-g and zero-g are in agreement with the predictions of section 2.2.3.2.

In all cases, the maximum available spark energy, on the order of several joules, was used in the flammability limit determinations. The effect of this finite spark energy on the results is discussed in the following section.

4.2.2 Results

The measured flammability limits as a function of pressure for upward, downward, and zero-g propagation as previously defined are shown in Fig. 4-5. As expected, for any given total pressure, the zero-g flammability limit was between the upward and downward one-g limits and the limit concentration

decreased with decreasing pressure in all three cases. It is quite remarkable that all three limits appear to be nearly straight lines on a semilogarithmic plot except for the upward-only one-g limit at low pressures. Of course, this trend could not continue indefinitely, because extrapolation to much lower pressures leads to the absurd conclusion that at a sufficiently low pressure a flame could be produced with no fuel or a negative amount of fuel, and extrapolation to a sufficiently high pressure leads to the equally absurd conclusion that a flame could be produced with 100% methane or more. In the high pressure case, a more practical limit is that at some pressure the lean flammability limit would be a rich mixture (>9.5% methane), another absurd conclusion. Also, extrapolation in the lower pressure case leads to the conclusion that a low enough pressure, the downward flammability would be leaner than the upward flammability limit, with the zero-g limit being leaner than either of these, a totally implausible situation. It is clear that at some point both the high-pressure and low-pressure trends must level out to a constant mixture ratio or reverse direction.

The narrowing of the gap between the upward and downward flammability limits at lower pressures indicates the decreasing effects of buoyancy at lower pressures, as expected based on previous results (section 2.2.3.3). Also at lower pressures, the gap between the upward and zero-g flammability limits narrows, suggesting that in the low pressure limit, flame propagation in zero-g is similar to one-g upward flame propagation.

The fractional pressure drop $\Delta P/P$ in the vessel due to combustion (section 3.7.2) as a function of total pressure and methane concentration is shown in Fig. 4-6. Most graph points are an average of two or more individual datum. While the consistency of the data was obviously poor, a number of important conclusions can still be drawn. It is clear that at the upward

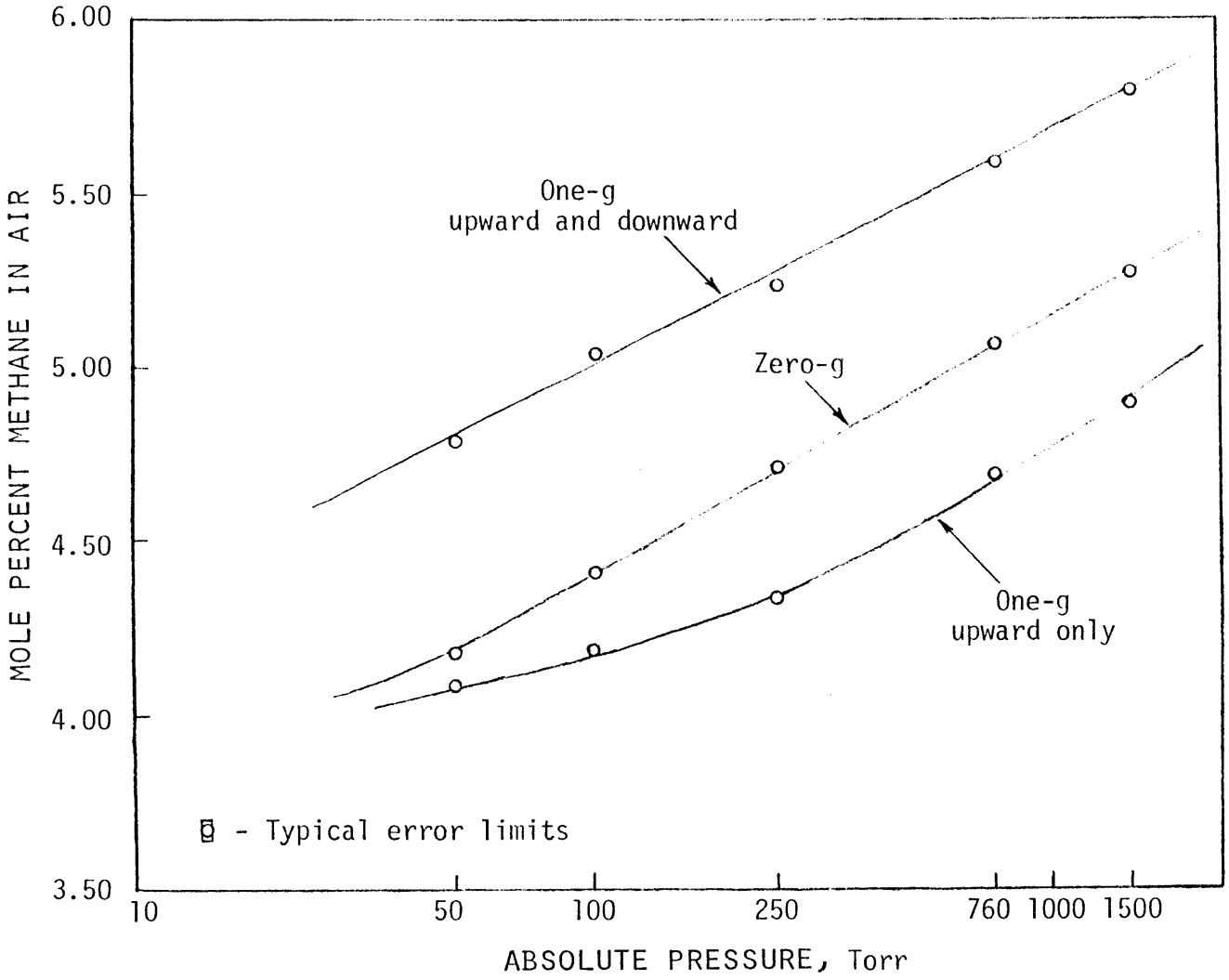

Figure 4-5. Lean flammability limits of methane and air as a function of pressure for various gravitational conditions

flammability limit only a very small fraction of the available fuel is consumed. This is also apparent from inspection of the film records (Figs. 4-1d, e, f). More significantly, since the pressure drop does not change rapidly as the one-g downward or zero-g flammability limit is approached from the "flammable" side, there is conclusive evidence that combustion was nearly complete, if not totally complete, at these limits. This indicates that any volume of gas that the flame front passes through is transformed completely from reactants to products and that the full energy release due to chemical reaction is realized. Thus, the one-g downward and zero-g flammability limits in the current investigation cannot be accounted for by a progressively decreasing ability of the flame to cause chemical reaction as the limit is approached. The degree of completion of combustion in SIFD behavior is discussed in section 4.5.1.

Fig. 4-6 shows that for a given stoichiometry, the fractional pressure drop due to combustion decreases with decreasing pressure. This is expected, since at lower pressures thermodynamic considerations dictate that more of the water will remain in the vapor phase. Also at lower pressures, the change in pressure drop between near-stoichiometric and near-limit flames is much less. This supports the suggestion (section 3.7.2) that at low pressures more water than expected condenses due to surface effects and not thermodynamic considerations, because at low pressures the amount of condensation is almost independent of the amount of water available for condensation.

Because the drop tower was not air conditioned, some zero-g tests were performed at ambient temperatures other than the nominal range of 23 ± 1°C. While these tests were not included in the results reported up to now, they can be of some use in determining the effect of temperature on the zero-g flammability limit. Over the range of 14°C to 30°C ambient temperature, it

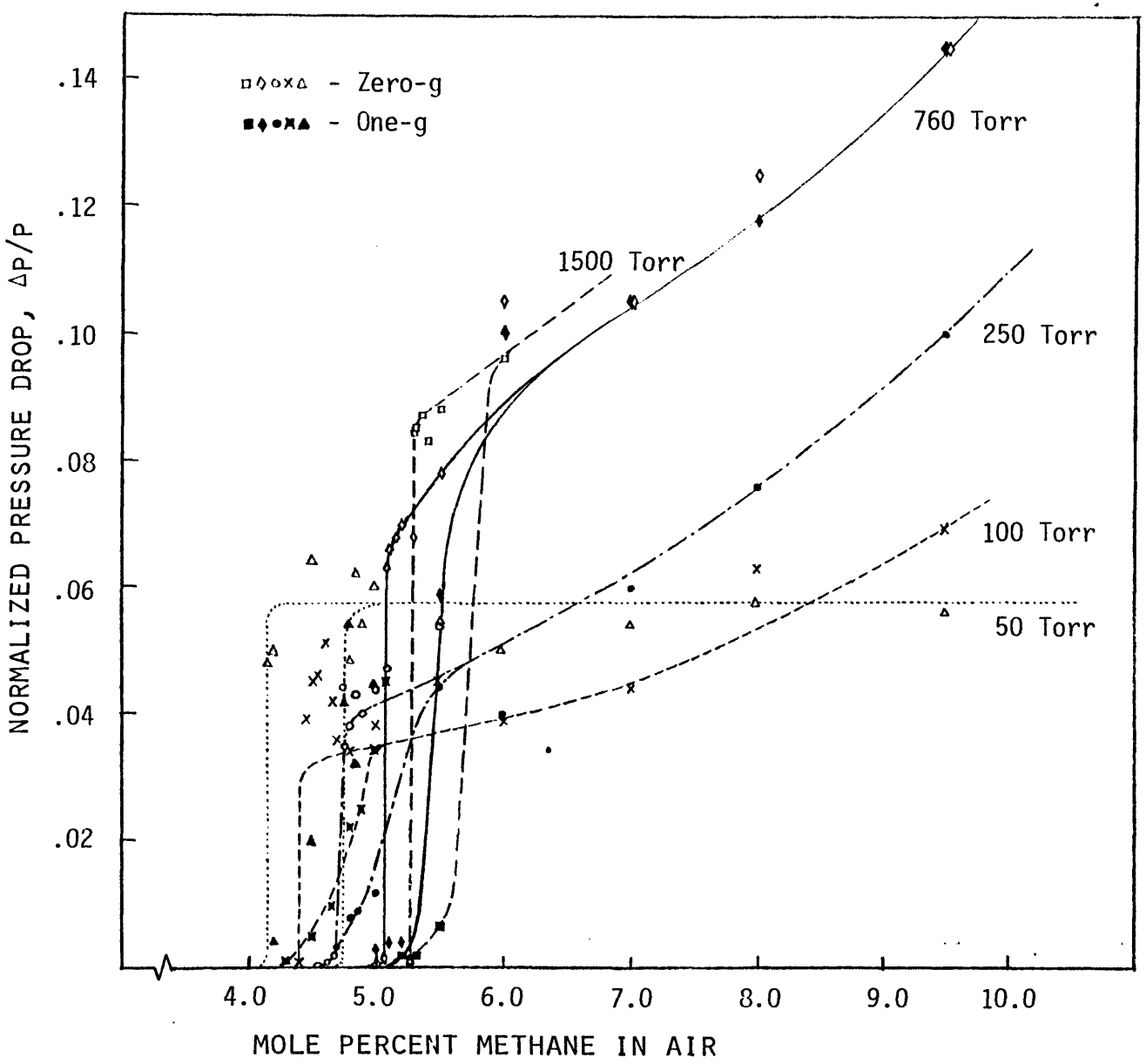

Figure 4-6. Equilibrium pressure drop in closed vessel due to combustion as a function of mixture and total pressure

appeared that the adiabatic flame temperature at the zero-g flammability limit was constant. In other words, the increase or decrease in ambient temperature was offset by a corresponding change in fuel concentration at the flammability limit. This is in agreement with previous results (section 2.2.3.3). This conclusion is only tentative, however, as the range of temperatures is too narrow and the results too sparse for firm conclusions to be drawn.

This constancy of adiabatic flame temperature, if valid, implies a nearly constant burning velocity at the zero-g flammability limit for a given total pressure (section 2.2.4.2), independent of ambient temperature. While it was clear how a constant burning velocity at the flammability limit could be a proper criterion for many types of flammability limit measurements in one-g (section 2.2.3.4), it is not apparent why this should be the case for an unconfined system in zero-g. This question is addressed in the following section.

A question arises as to the adequacy of the spark energy for the flammability limit tests, particularly for the upward and zero-g limits. If the spark energy was inadequate, an ignition limit rather than a flammability limit would have been determined. The results of section 4.4.1 show that the MIE is increasing extremely rapidly near the observed upward and zero-g limits, except possibly at 50 Torr, so even if the spark energy were increased drastically the change in the limit concentration would be very minimal, again with the possible exception of 50 Torr. In an attempt to determine the effect of spark orientation and type of discharge on the measured flammability limits, a few tests were performed in one-g where the polarity of the spark electrodes was reversed, and in one-g and zero-g where an AC spark discharge was used. In neither case was the limit concentration altered noticeably.

Another question arises as to the effects of finite vessel size on the observed flammability limits. The effects of finite vessel size on the one-g upward and downward flammability limits have already been discussed, and the conclusion was that any such limit is somewhat arbitrary because it depends on the vessel size and shape. It was shown that the zero-g limit was not arbitrary, but the effects of rising temperature and pressure due to flame kernel expansion during combustion may have been significant. It is not immediately obvious what the net effect would have been, because increasing pressure tends to make the mixture "less flammable", as the results (cf. Fig. 4-5) have shown, but increasing temperature makes the mixture "more flammable", as was just reported. Because the flame front was spherical, the flame front radius at which temperature and pressure effects became significant can be estimated from the dependence of these quantities on flame radius (appendix C) and the results already presented in this section.

Based on Fig. 4-5, it appears that the effect of pressure on the methane concentration at the zero-g flammability limit over the range of pressures investigated can be expressed as

$$c = .0507 + .0073 \log P$$

where c is the mole fraction of methane at the flammability limit and P is the total pressure in atmospheres. Because the adiabatic flame temperature at the zero-g flammability limit appears to be constant, the effect of unburned gas temperature on the methane concentration at the flammability limit can be expressed as

$$c = K(T_{b,fl} - T_u)$$

where K is a constant which is weakly dependent on the total pressure and $T_{b,fl}$ is the adiabatic flame temperature at the flammability limit at that

pressure. Starting with unburned gas at the zero-g flammability limit concentration c_o, temperature T_{uo} and pressure P_o, for the pressure effect,

$$c/c_o = (1 + a \log P)/(1 + a \log P_o)$$

and for the temperature effect

$$c/c_o = (T_b - T_u)/(T_b - T_{uo})$$

where c is understood to represent the flammability limit concentration at temperature T_u and pressure P. Using the adiabatic compression law

$$T_u/T_{uo} = (P/P_o)^{(\gamma-1)/\gamma}$$

and assuming that the temperature and pressure effects are independent so that the two expressions for c/c_o can be multiplied together, the final result is

$$\frac{c}{c_o} = \frac{(1 + a \log P)(1 - b(\frac{P}{P_o})^{\frac{\gamma-1}{\gamma}})}{(1 + a \log P_o)(1 - b)}$$

where $a = .0073/.0507 = 0.144$ and $b = T_{uo}/T_{b,f1}$, which is slightly dependent on P_o, and is shown in table 4-1. Values of $T_{b,f1}$ are computed by the flame temperature program in appendix B. If we let $P = P_o + \Delta P$ and assume $P_o >> \Delta P$ (this ΔP must not be confused with the pressure drop in the vessel due to combustion mentioned earlier in this section), then the result can be expressed in the form

$$c/c_o = 1 - d(\Delta P/P_o)$$

where d is a constant dependent on P_o as shown in table 4-1. On closer inspection of the nonlinearized equation, the linear approximation is valid up to about $\Delta P/P_o \simeq 0.1$, and for $\Delta P/P_o > 0.1$, d increases slowly.

The result of this analysis is very significant: as the combustion progresses, the net effect of the rising temperature and pressure is to make the remaining unburned mixture more readily flammable. This means that any flame failures (SIFD's) which occurred were not due to the finite vessel size,

but in fact may have failed slightly sooner in a completely unconfined, constant pressure system. The importance of this effect is shown in table 4-2 for typical values of P_o = 250 Torr and P_f/P_o = 6.7, a typical value near the lean flammability limit. The results for other initial pressures are very similar. The dependence of P/P_o on r_b/r_v is taken from appendix C. The vessel in the current investigation had a volume of 10.9 x 10^3 cm^3, and so the effective vessel radius r_v (see appendix C) is 13.7 cm. Table 4-2 shows that for a flame front radius r_b of 6 cm, the net change in the flammability limit of the remaining unburned gas is only 0.1%, and at r_b = 9 cm is only 0.5%, a very small change indeed. Since the largest extinction radius observed was 8.7 cm (section 4.5.1), the conclusion that the effect of rising temperature and pressure during combustion had a negligible effect on the observed zero-g flammability limits and extinction radii.

Another important point concerning the effect of finite vessel size on the observed zero-g flammability limits is the question of the flame radius at which steady-state propagation was reached in limit mixtures in relation to the vessel radius. The flame front radius at which steady-state propagation is first achieved in limit mixtures is about 4-5 cm, as can be seen in Figs. 4-15 a,b,d, and f. Surprisingly, this is more or less independent of the total pressure. Larger flame development times and flame development radii

---

P_o, Torr	b	d
1500	.192	7.94 x 10^{-3}
760	.197	7.60 x 10^{-3}
250	.207	7.41 x 10^{-3}
100	.217	7.56 x 10^{-3}
50	.225	7.58 x 10^{-3}

Table 4-1. Effect of pressure and temperature rise in a closed vessel on observed zero-g flammability limit

r_b/r_v	r_v, current investigation, cm	P/P_o	c/c_o
0.00	0.00	1.000	1.0000
0.10	1.37	1.001	1.0000
0.30	4.12	1.031	.9998
0.50	6.87	1.159	.9986
0.70	9.62	1.557	.9935

Table 4-2. Effect of flame front radius on zero-g flammability limit of remaining unburned mixture in a closed vessel (P_o = 250 Torr, P_f/P_o = 6.7)

---

would be expected at lower pressures (section 2.2.5.2), but this is apparently not so at the flammability limit. In any case, this 4-5 cm radius is much smaller than the flame radius at which the effects of finite vessel size become significant, as was just shown, and so even in limit mixture, steady-state propagation exists independent of the confines of the current system, except possibly for 50 Torr. Evidence presented in section 4.4.2 shows that the zero-g lean limit mixture of 4.20% may have actually been an SIFD victim but the vessel was too small to show this, so that the actual limit mixture may have been 4.25%.

The final conclusion of this analysis is simple: the finite size of the combustion vessel did not influence the observed zero-g flammability limits or extinguishment behavior, except possibly for a few tests at 50 Torr.

4.2.3 Interpretation and comparison with previous results.

It is difficult to make exact comparisons of the results presented here with the results of previous investigations because it appears none of the previous experiments have used exactly the same apparatus, procedures, and flammability limit definitions. Even if an exact comparison were available, it is not clear that the results would be identical, as this has not been so

in the past (section 2.2.3.3). Nevertheless, legitimate approximate comparisons can be made.

Considering first the results for one atmosphere total pressure, the upward flammability limit of 4.70% is somewhat leaner than most previous investigations report, but this is expected. Most investigations in unconfined systems have used larger combustion vessels, allowing more time and distance for self-destructive convection currents and turbulence to occur, leading to richer, faster burning limit mixtures. The limit mixtures determined this way are usually only 0.5% or less richer than in the current investigation (section 2.2.3.3), which is again expected because the burning velocity decreases very rapidly with decreasing fuel concentration near the upward flammability limit, as is shown later in this section. The conclusion is that the upward flammability limits determined in this work and in previous investigations using the same technique are consistent. For other types of apparatus (flat-flame burner, tube, etc.), other factors become important, as discussed in section 2.2.3.2.

For downward propagation, the lean flammability limit at one atmosphere is 5.55% methane. This is also slightly leaner than most measurements, but this again is expected. 5.55% methane does not actually burn downward upon ignition, but burns upward to the top of the vessel, then outward and downward, eventually consuming the entire contents of the vessel. A lean downward flammability limit definition which required the mixture to propagate downward initially would result in a richer, faster burning lean limit mixture. As with upward propagation, the resulting limit mixture is only 0.5% or less richer than the current result (section 2.2.3.3), so the results are still consistent.

Only one previous zero-g flammability limit determination for methane-air mixtures has been made. Reuss [16] investigated near-lean-limit mixtures in a SFLT and found that a 5.22% mixture at one atmosphere was almost certainly flammable, as it had developed a steady propagation velocity by the end of the 2.2 seconds of free-fall available, a 5.10% mixture mixture burned throughout the free-fall at a continually decreasing rate, and a 4.98% mixture extinguished before the end of the drop. He believed that the 5.10% mixture would have extinguished had more zero-g time been available. In the current investigation the zero-g flammability limit at one atmosphere was 5.07%. Thus, within the limitations and experimental accuracy of these two experiments, the results are in complete agreement. This is very significant, especially considering that in Reuss' experiment, flame propagation was quasi-one-dimensional, and in the current work, was fully three-dimensional and spherically symmetric. This is very strong evidence that the zero-g flammability limit is in some way fundamental in the sense that it is independent of the experimental apparatus, which is certainly not true in one-g. It is very unlikely that such a result could occur if the zero-g flammability limit were caused by geometrical factors such as "flame stretch" (section 2.2.3.4) because the geometries of the two systems are entirely different, and besides, there is no flame stretch in a spherically symmetric system of adequate size (section 2.2.3.4). Reuss himself felt that his flammability limit was not caused by flame stretch. Further evidence that the observed flammability limits could not have been caused by flame stretch is presented in section 4.4.2. It is also very unlikely that such a close agreement between the two experiments could occur if the limit were caused by heat losses, as a SFLT would have greater conductive heat loss than a large closed bomb because of the closer proximity of the solid boundaries to the

flame front, and a different quantity of radiant heat loss because of the different radiative path lengths in the two systems. Further comparisons of the two experiments are presented in section 4.3.3.

The effect of pressure on lean flammability limits in methane-air combustion does not appear to be well documented, particularly at pressures below atmospheric. The results (section 2.2.3.3) show that the flammable range expands as the total pressure is reduced. Jones and Kennedy [92] found that the lean upward flammability limit of natural gas (similar to methane) and air in a 5 cm tube was 0.5% leaner at 100 Torr than at 760 Torr total pressure. This is identical to the shift found in the current work (4.7% at 760 Torr vs. 4.2% at 100 Torr), although the results cannot be directly compared, as previously explained. While it appears that zero-g flammability limit may be independent of the experimental apparatus, so that direct comparisons could be made, no previous investigations on the pressure effects on zero-g flammability limits have been performed.

Based on these comparisons of the current work with previous investigations, it is concluded that the results of the current study are self-consistent and consistent with, although not identical to, previous one-g investigations. This is about all that can be expected, as explained in section 2.2.3.2. It is also concluded that zero-g flammability limits may be independent of the experimental apparatus under some conditions.

For upward propagation in one-g the flammability limit seems to correspond closely to the mixture where the burning velocity is nearly zero, as evidenced by extrapolation of the plots of burning velocity vs. fuel concentration to $S_u \simeq 0$ (section 4.3.2). The comparison is shown in table 4-3. At high pressures the measured flammability limit is slightly leaner than the methane concentration extrapolated to $S_u \simeq 0$ and at low pressures the

measured flammability limit is slightly richer than the methane concentration extrapolated to $S_u \simeq 0$, but in all cases the agreement is remarkably close. Because of the inverse relationship between burning velocity and MIE (section 2.2.5.3), when the burning velocity is nearly zero the MIE should be almost infinite, and indeed this was found to be the case for the one-g upward flammability limit (section 4.4.2). This is strong evidence that the observed one-g upward flammability limit in a large, unconfined system is not a fundamental limit but is merely due to the rapidly decreasing burning velocity and rapidly increasing MIE with decreasing fuel concentration, which makes ignition and propagation impractical below a certain fairly well-defined concentration. Especially significant is that the measured upward flammability limit at 760 Torr (4.7%) and the methane concentration extrapolated to $S_u \simeq 0$ (4.85%) are very similar to the methane concentration extrapolated to $S_u \simeq 0$ shown in Fig. 2-8 (4.8%) and the methane concentration (4.62%) corresponding to the minimum reaction zone temperature in a "Swiss roll" burner (section 2.2.3.3). The conclusion is that the upward flammability limit as measured in a large, unconfined system is a practical flame propagation limit, but not a fundamental limit.

The downward flammability limit is related to the ability of the flame to propagate downward against its own buoyancy. This is apparent based on previous investigations (section 2.2.3.3), the film records in the current work (Fig. 4-1c), and the plain fact that many sub-downward-limit mixtures could burn perfectly well upward and in zero-g. Based on the results of previous investigations, it would be expected that the crucial parameter would be the burning velocity at the flammability limit. Table 4-4 shows the burning velocity at the downward flammability limit as a function of total

Total Pressure, Torr	Upward Flammability Limit, % Methane	Methane Concentration at $S_u \simeq 0$ (extrapolated)
1500	4.90%	5.10%
760	4.70%	4.85%
250	4.35%	4.45%
100	4.20%	4.10%
50	4.10%	3.80%

Table 4-3. Comparison of upward flammability limits with methane concentration extrapolated to $S_u \simeq 0$ (cf. Fig. 4-10)

---

pressure. The values of S_u are obtained from the results presented in section 4.3.2. The equation which most reasonably fits the data is

$$S_{u,lim} = 4.63\ P^{-0.20}$$

with S_u in cm/sec and P in atmospheres. This relation is accurate to within ± 10% over the range of pressures investigated. This relationship does not agree with the prediction of Lovachev's theory (section 2.2.3.3) that $S_{u,lim} \sim P^{-1/3}$, however, even if it were certain that Lovachev's theory were correct, this discrepancy would not be surprising. The method used to calculate burning velocity in this work underestimates the true value to some extent, the underestimate being greater at low pressures (section 4.3.2), so the true relationship for this investigation is probably slightly closer to Lovachev's result than is apparent here. More fundamentally, combustion in a closed bomb creates complicated flow patterns which are not addressed by the models of Lovachev or Hertzberg, and so no such comparison is strictly valid. Since results were obtained only at one-g and zero-g in this investigation, it is not possible to check the dependence of $S_{u,lim}$ on gravitational conditions as predicted by these models.

It is difficult to suggest a zero-g flammability limit mechanism at this point. For sub-limit mixtures, the SIFD behavior is observed, but it is not

clear why normal flame propagation does not exist for these mixtures. SIFD behavior is characterized by a continually decreasing flame propagation velocity up to the point of extinguishment, as Figs. 4-15 and 4-16 show, which is in agreement with the observations reported in the two previous investigations (section 2.2.3.3) on flammability limits in zero-g. Since this phenomenon has not been investigated in detail before, a closer inspection is warranted. Observations on SIFD are reported in section 4.5.

The effect of pressure on the methane concentration, burning velocity, and adiabatic flame temperature at the zero-g flammability limit is shown in Fig. 4-7. Of course, such a composite plot for these parameters at the one-g downward flammability limit would be similar but is of less fundamental interest. The values of burning velocity are obtained from the results presented in section 4.3.2. The values for adiabatic flame temperature are obtained from the model presented in appendix B. The most striking feature of Fig. 4-7 is that as total pressure decreases, even though both the fuel concentration and the adiabatic flame temperature decrease, the burning velocity actually increases, showing that increasing pressure has a strongly negative effect on near-limit methane-air flame propagation. The equation which most reasonably fits the data is

$$S_{u,lim} = 1.45\ P^{-0.35}$$

Pressure, Torr	Downward flammability limit, % methane	Burning velocity, cm/s
1500	5.80	3.8
760	5.60	4.7
250	5.25	6.4
100	5.05	7.1
50	4.80	7.6

Table 4-4. Burning velocity vs. total pressure for downward flammability limit mixtures

with S_u in cm/sec and P in atmospheres. This relationship is accurate to within ±4% over the range of pressures investigated. While this relation appears to be in good agreement with both Lovachev's model and the model presented in section 2.2.5.3, such a comparison is invalid because these models attempt to predict something entirely different from the zero-g limit burning velocity. The limit burning velocity is in surprisingly good agreement with Spalding's flammability limit model based on radiant heat loss (section 2.2.3.4) at atmospheric pressure, but the pressure dependence in Spalding's model $S_{u,lim} \sim P^{-1/2}$ does not agree with the experimental result $S_{u,lim} \sim P^{-1/3}$, thus it does not appear likely that radiant heat loss can account for the observed zero-g flammability limits. Much more evidence of this is presented later in this chapter. The significance of the observed zero-g limit burning velocity and the effect of pressure on the limit burning velocity is not immediately obvious. Information on this important parameter for other fuels and other ambient temperatures is needed in order to draw firm conclusions.

In an attempt to determine if the concentration of radicals could have had some effect on the zero-g flammability limit, the equilibrium concentrations of the radicals H, OH, and O, and the CO molecule at the zero-g flammability limits for different pressures were compared. The concentrations of these species were calculated from the adiabatic flame temperature program (appendix B). The idea was that since dissociation, and therefore the concentration of these dissociation products, increases with increasing equilibrium temperature and decreasing pressure, and since equilibrium flame temperature at the zero-g flammability limit increases with increasing pressure (Fig. 4-6), the effects of temperature and pressure on dissociation would offset each other to some extent. This could possibly have led to a

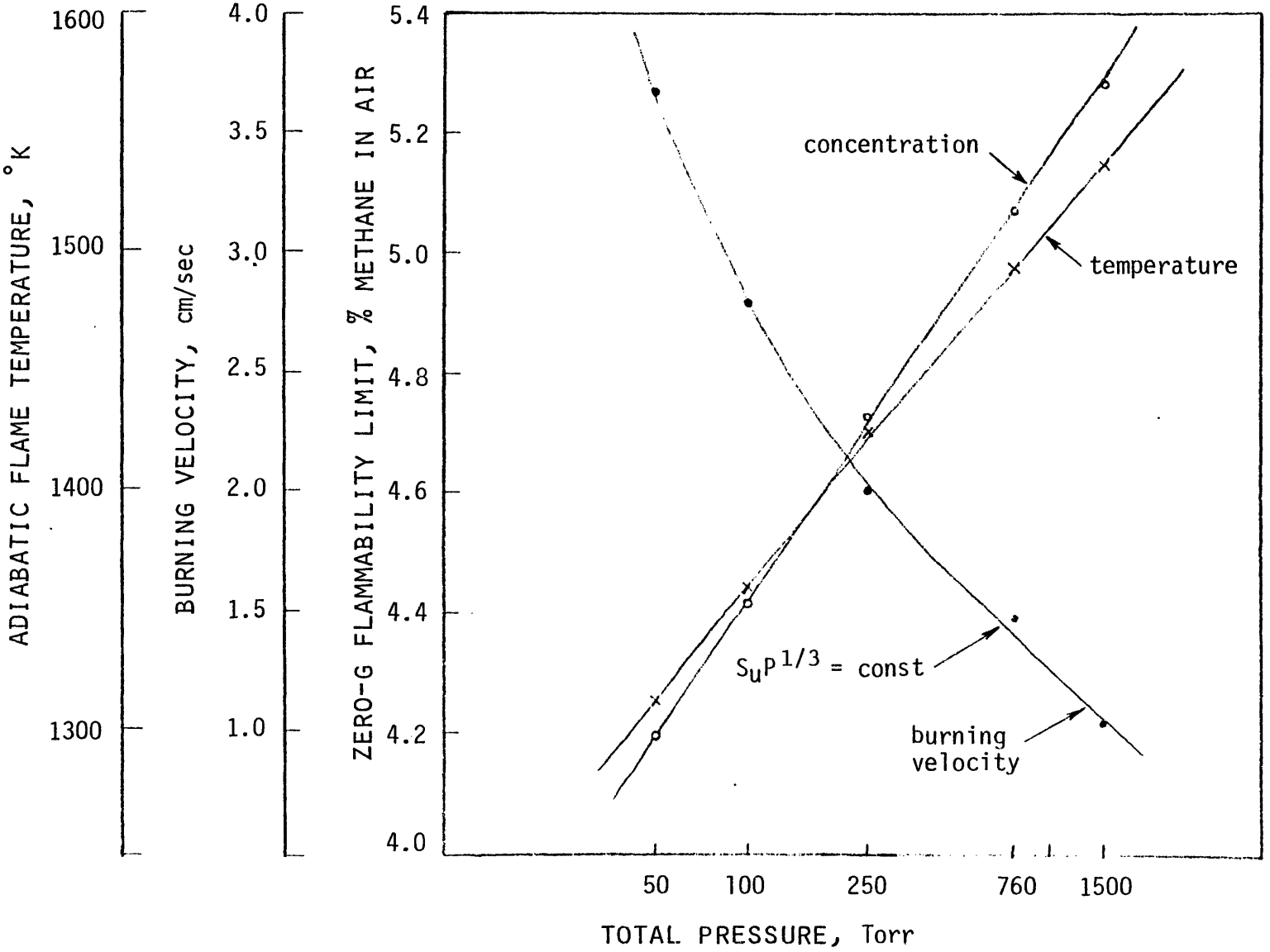

Figure 4-7. Effect of pressure on fuel concentration, burning velocity, and calculated adiabatic flame temperature at the zero-g flammability limit

constant equilibrium concentration of one or more of these species at the zero-g flammability limit. The results of the comparison are shown in table 4-5. It is clear that the temperature effects on dissociation outweigh the pressure effects, so none of the calculated equilibrium concentrations are constant at the flammability limit. The conclusion is that the zero-g flammability limit is not related to a requirement for a minimum equilibrium concentration of some radical or radicals. It is very difficult to know whether a constant radical concentration could exist somewhere within the flame reaction zone, as this would require solving the complete set of flame equations involving thermal conduction, molecular diffusion, and chemical reaction for all species involved, which is a formidable task which is beyond the scope of the current work. It would seem unlikely that such an effect could exist, however, because roughly the same trends with changing temperature and pressure would be expected for nonequilibrium and equilibrium concentrations of radicals.

While it was stated in section 2.1.1 that the pressure drop across the flame front and the kinetic energy change of the flowing gases were both negligible in LPGC, because of the unusual results obtained in this investigation it is worthwhile to determine exactly how negligible they are. The pressure drop ΔP across the flame can be calculated from conservation of momentum as [30]

$$\Delta P = \rho_u S_u^2 (\rho_u/\rho_b - 1),$$

and with the ideal gas law $P = \rho_u R T_u$, the fractional pressure drop $\Delta P/P$ can be written as

$$\Delta P/P = (S_u^2/RT_u)(\rho_u/\rho_b - 1).$$

Using typical values at the zero-g flammability limit at 760 Torr, namely $S_u = 1.49$ cm/s, $T_u = 295^{\circ}K$, and $\rho_u/\rho_b \simeq T_b/T_u = 1494/295 = 5.06$, the result is

Pressure, Torr	Zero-g lean flammability limit, % methane	Adiabatic flame temperature, °K	H x 10^9	OH x 10^5	O x 10^7	CO x 10^8
1500	5.28	1537	15.6	7.46	14.2	102
760	5.07	1494	12.3	6.11	11.6	72.0
250	4.73	1425	7.45	4.37	8.25	40.4
100	4.42	1361	3.20	2.70	4.61	17.5
50	4.20	1314	1.34	1.68	2.53	7.67

Table 4-5. Equilibrium mole fractions of radical species and CO at the zero-g lean flammability limits.

$\Delta P/P = 3.7 \times 10^{-7}$, a truly negligible change. Also, $\Delta P/P$ at the flammability limit is not constant with respect to pressure, hence $\Delta P/P$ does not represent a scaling factor for zero-g flammability limits. The kinetic energy change of the flowing gases can be written as

$$\Delta KE = \rho_b S_b^3 A_f/2 - \rho_u S_u^3 A_f/2,$$

and with the relation (section 2.2.4.1) $\rho_u S_u = \rho_b S_b$, and normalizing by the change in chemical energy $\Delta CE = \dot{m}\Delta h_c = \rho_u S_u A_f \Delta h_c$, the final result is

$$\Delta KE/\Delta CE = S_u^2[(\rho_u/\rho_b)^2 - 1]/2\Delta h_c,$$

where Δh_c is the net enthalpy change due to combustion. Again using typical values at the zero-g flammability limit at 760 Torr, with Δh_c = 211 kcal/mole CH_4 = 211 x .0507 = 10.7 kcal/mole mixture x (1 mole mixture/.029 kg mixture) = 369 kcal/kg mixture, the final result is $\Delta KE/\Delta CE = 1.8 \times 10^{-9}$, again a truly negligible amount that is not constant with respect to pressure. The conclusion is that neither the pressure drop across the flame front nor the kinetic energy change of the flowing gases due to combustion can account for the observed zero-g flammability limits.

4.3 Burning velocity

4.3.1 Method of determination

For mixtures which produced nearly spherical flame propagation in one-g, burning velocities measured in one-g and zero-g were identical within the limits of experimental error and so are reported interchangably. The limit of near-spherical propagation was only a few tenths of a percent richer than the lean downward flammability limit as defined in this report. For example, at 760 Torr the lean downward flammability limit was 5.55% methane and one-g flame propagation was nearly spherical, thus burning velocity measurements

were usable, down to 6.0% methane. Below this concentration, interpretation of one-g results to obtain burning velocities is difficult (section 2.2.4.1) and so measurements of burning velocity can only be obtained from zero-g flames, which are of course (almost) always spherically symmetric. Since reliable measurements of the burning velocities of these slow-burning, near-limit flames can be obtained only from zero-g tests, these measurements represent one of the major contributions of this investigation.

The spark energies used in the burning velocity tests were generally only slightly higher than the minimum ignition energies for these mixtures. It was found that increasing the spark energy above this value only affected the flame propagation velocity in the early stages of combustion, that is, when the flame radius was on the order of or less than the radius of a sphere of burned gas with an energy content equal to the spark energy input (section 2.2.5.2). The net effect is that the curves of flame radius r_b versus time t shift upward with increasing spark energy, as shown graphically in Figs. 4-14 d-f. This effect is undoubtedly due to the faster burning rate caused by the excess energy imparted to the gas by larger sparks. The effect is only noticeable at lower pressures because of the lower volumetric heat capacity of gases at lower pressures.

The flame propagation velocity S_b was determined from both the film records (section 3.6.3) and the flame detectors (section 3.5.3). The problem with the sensitivity adjustment on the flame detectors, particularly at low pressures, has already been mentioned. At higher pressures (250 Torr and above), the film record and flame detectors were in excellent agreement when both measurements were taken. At lower pressures (100 Torr and below) there was a delay between the passage of the luminous zone of the flame front by each flame detector and the triggering of that detector. This is probably

because the flame detector triggers on a part of the flame front closer to the hot boundary than the luminous zone which the film records. At reduced pressures the flame is thicker, and since the burning velocity is not greatly affected by pressure, the delay between the luminous zone and the detector trigger is greater. This would be a completely adequate explanation if the delay were the same for each flame detector, but unfortunately, this was not the case. At these low pressures, the detectors further from the spark electrodes had a greater delay, thus leading to an underestimate of the slope of the flame radius r_b vs. time t curve, which gives the flame propagation velocity S_b, thereby leading to an underestimate of the burning velocity S_u. Had the delay been constant, the determination of S_b would not have been affected. The reason for the variation in delay is not apparent, but it may be related to the three-dimensional effects associated with the spherically propagating "thick" flame front or the greater quenching effect at low pressures. Because of this problem, when a discrepancy existed between the film record and the flame detectors, which was only at low pressures, the film record was considered the more reliable source and the flame detector data was disregarded.

The propagation velocity S_b for each combustion test was calculated by plotting r_b vs. t as measured by the film record or flame detectors and graphically determining the slope of this curve. Examples of these plots for 760 Torr total pressure are shown in Fig. 4-8. The results at other pressures were very similar in nature. In general the plots for near-stoichiometric mixtures were straight lines passing through the origin, the plots for leaner mixtures were curved slightly to the right, indicating a lower S_b during the later stages of combustion, and the plots for near-limit mixtures were sharply bent initially but became straight at a flame radius well before the effects

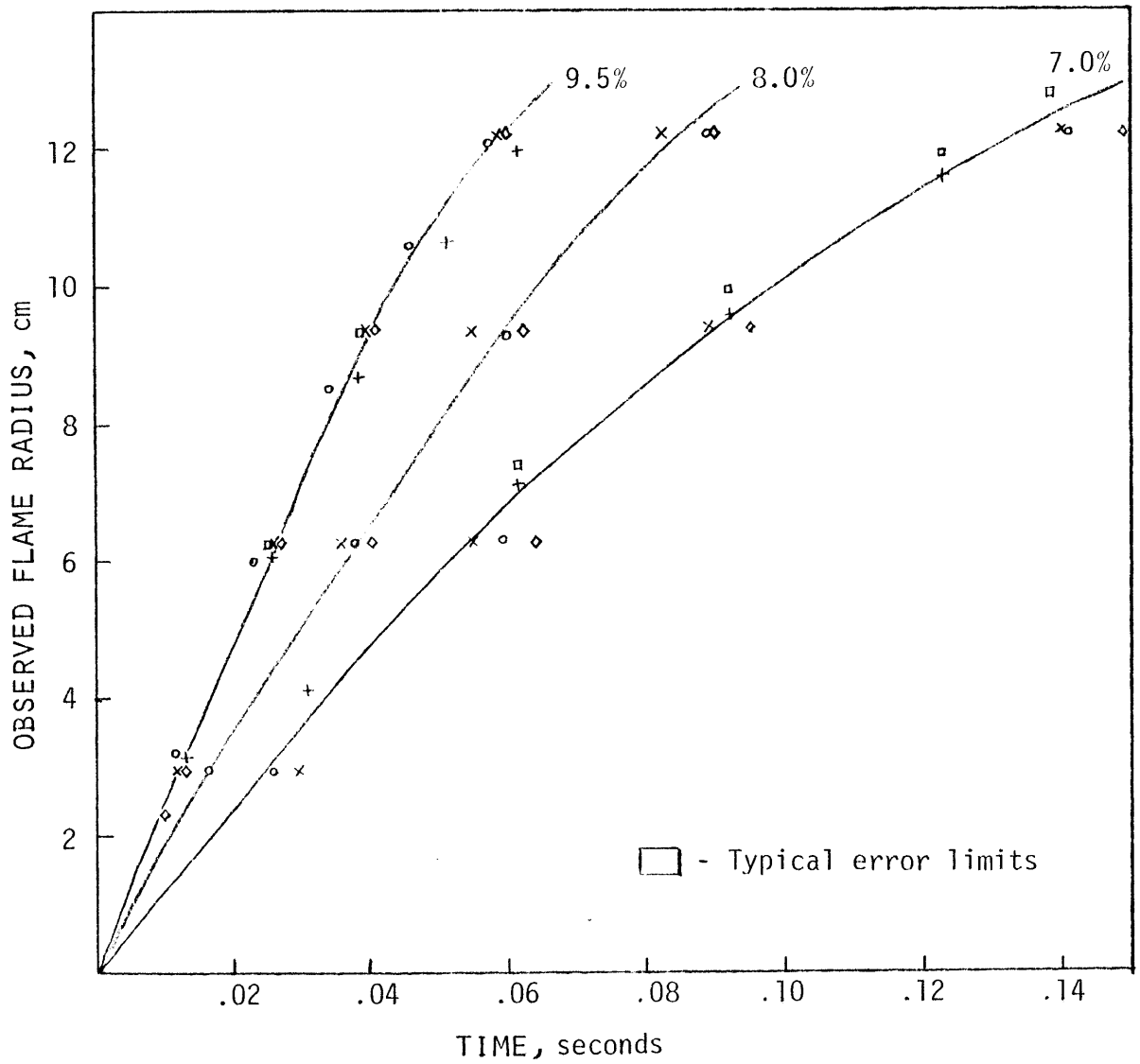

Figure 4-8a. Observed flame radius vs. time for near-stoichiometric mixtures at 760 Torr

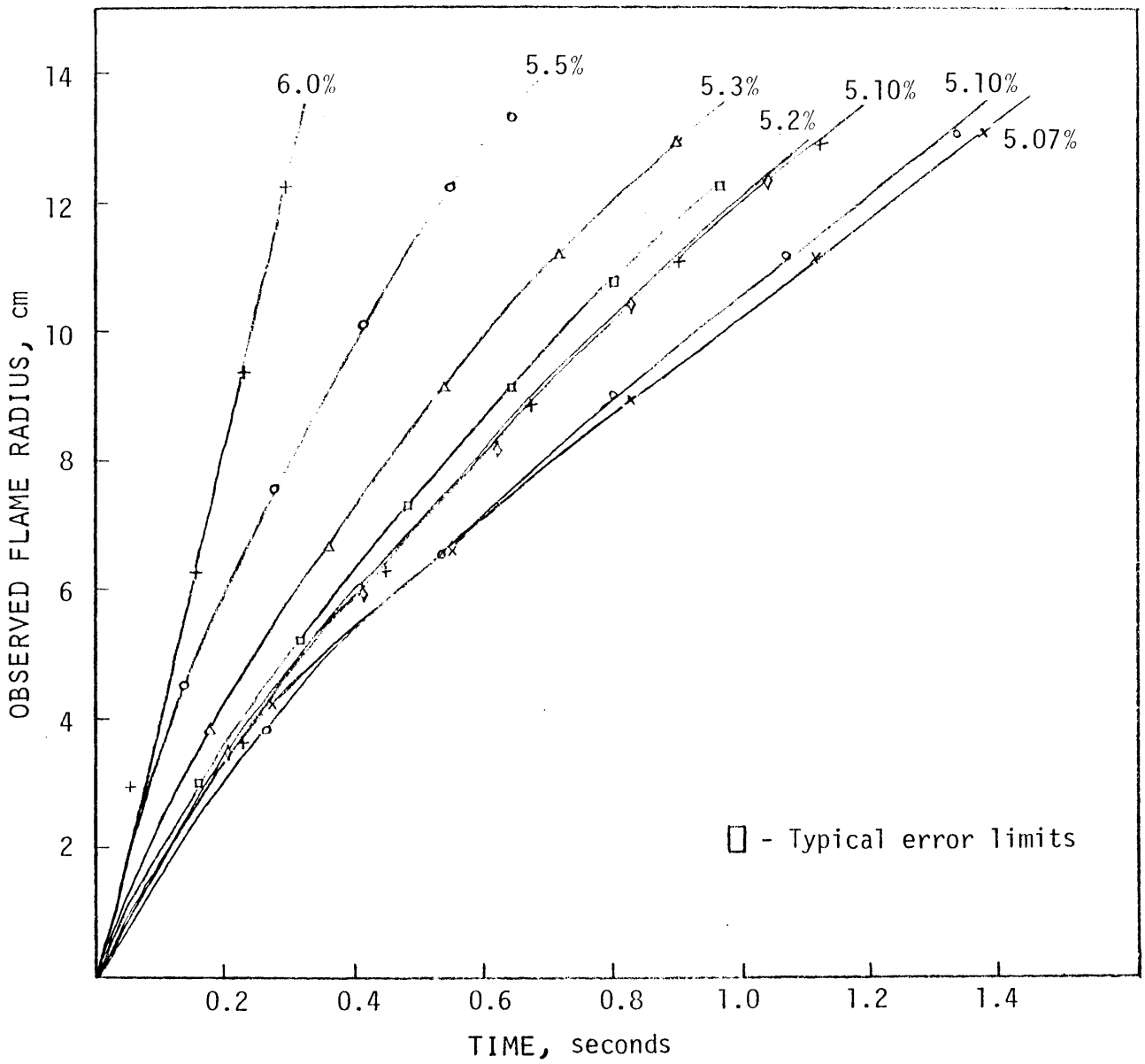

Figure 4-8b. Observed flame radius vs. time for near-limit mixtures at 760 Torr.

of rising temperature and pressure due to combustion became significant, as shown later in this section.

Theoretically one would expect these curves to be straight lines after the ignition process is complete. The ignition process is completed at a flame radius corresponding to a few flame thicknesses. This would explain the observed behavior of "thin" near-stoichiometric flames and "thick" near-limit flames, but the continuous curvature of the r_b vs. t plots for intermediate concentrations is somewhat of a mystery. The curvature appears well before the effects of rising pressure and temperature due to combustion become important. Since no reconcilliation of this problem could be found, an arbitrary criterion for determining S_b had to be used. A spherical flame most nearly approximates the ideal one-dimensional, constant pressure flame when the flame radius is as large as possible but still small enough relative to the vessel that the effects of rising pressure and temperature due to flame kernel expansion are negligible. This flame radius was determined to be about 7 cm in the current investigation. At this radius $P/P_o \simeq 1.17$ and $T_u/T_{uo} \simeq 1.05$ (appendix B). Using the approximate relation (section 2.2.4.2)

$$S_u \sim P^{(n-2)/2}\, T_u^{1/2} \exp[-E_a/2RT_b]$$

and typical values $n = 1.5$ and $E_a = 30$ kcal/mole (section 2.2.4.2), with $T_{uo} = 300^oK$ and $T_{bo} = 1800^oK$, the net effect is that at this slightly elevated temperature and pressure the burning velocity decreases by only 0.04%, a negligible amount. Thus, the pressure and temperature effects offset each other almost exactly in this typical case. The curvature of the r_b vs. t curves is such that the difference in S_b at $r_b = 7$ cm and S_b at the lowest value of r_b that S_b could reasonably be calculated at, about 3 cm, is only 15% or less, so this somewhat arbitrary method of measuring S_b at $r_b = 7$ cm does

not affect the value of S_u substantially. If anything, this method causes a slight underestimate of S_u .

With S_b determined, S_u was calculated as outlined in section 2.2.4.1.

4.3.2 Results

The burning velocities as a function of mixture ratio and total pressure are shown in Fig. 4-9. Most graph points shown are the average of two or more tests. Under some conditions, usually low pressures and lean mixtures, the variation in S_u between runs could be as much as 10% on either side of the average. Since the probable error in the measurements was quite low, a few percent at most, most of the variation was probably due to the nonrepeatability of the process itself, and this is manifested in the poor consistency of the data points for lean mixtures at low pressures. Under other conditions, burning velocities were much more repeatable.

The most striking feature of Fig. 4-9 is that, except for near-stoichiometric mixtures, the curves of S_u vs. fuel concentration for a given pressure are nearly straight, parallel lines. This was to some extent expected, based on previous experimental and theoretical results (Fig. 2-8).

As expected, the burning velocity decreased with decreasing fuel concentration below stoichiometric, and increased with decreasing pressure, the amount of increase in the latter case being greater for leaner, slower burning mixtures. For stoichiometric mixtures (9.5% methane), roughly $S_u \sim P^{-0.010}$ and for 6.0% methane, roughly $S_u \sim P^{-0.41}$.

As with flammability limits, the variation in ambient temperature in the drop tower had some effect on the measured values of burning velocity. While no attempt at a systematic study was made, the results seemed to show that the burning velocity increased slightly with increasing ambient temperature. This

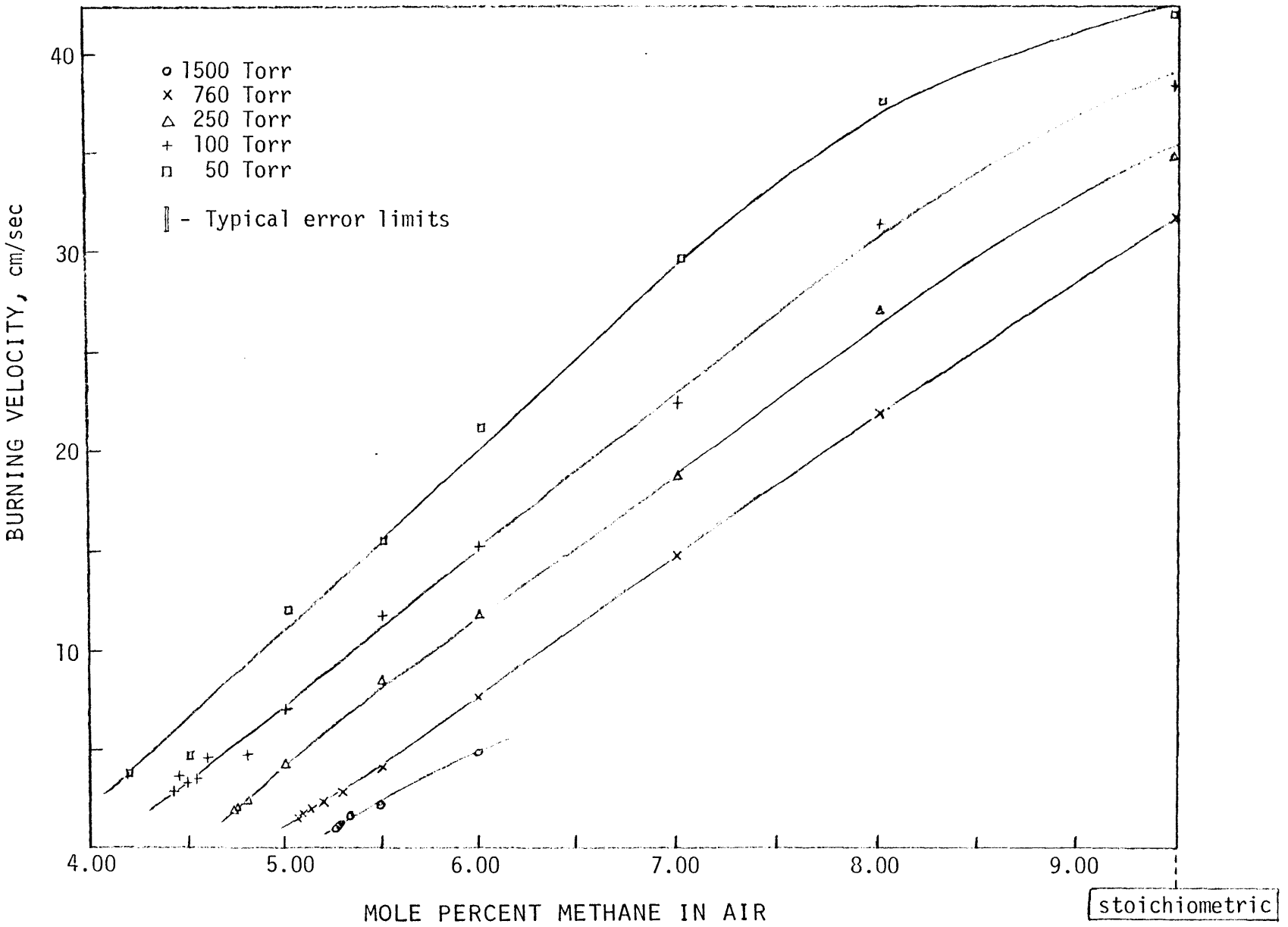

Figure 4-9. Burning velocities for methane-air mixtures as a function of absolute pressure and fuel concentration

was expected based on accepted theory and previous results (section 2.2.4.2), but the available data were too sporadic and obtained over too narrow a temperature range to draw any firm conclusions about the exact dependence of burning velocity on ambient temperature.

It is possible at this point to examine semiquantitatively the effect of nonzero flame thickness on the calculated values of burning velocity. Neglecting flame thickness leads to an underestimate of burning velocity, as explained in section 2.2.4.2. The first step is to estimate the preheat zone thickness δ from the equation (section 2.2.2)

$$\delta = k/\rho_u C_p S_u.$$

Estimates of δ for stoichiometric, lean limit, and 6.0% methane mixtures are shown in table 4-6. The values of k and C_p are taken at the mean flame temperature, $(T_b + T_u)/2$. As expected, the estimated preheat zone thickness increases with decreasing pressure and burning velocity. The significant result is that even the largest calculated preheat zone thickness is still fairly small in relation to the flame radius at which the propagation velocities were calculated, namely 7 cm. The calculated preheat zone thicknesses at 760 Torr of 0.018 cm, 0.039 cm, and 0.31 cm for stochiometric, 6.0% methane, and zero-g flammability limit mixtures, respectively, compare to experimental values [69] of 0.11 cm, 0.21 cm, and 0.45 cm, respectively, for the overall flame thicknesses of the same mixtures. This comparison is quite favorable because the overall flame thickness should be larger than the preheat zone thickness, and because for near-stoichiometric mixtures a smaller percentage of the overall flame thickness is in the preheat zone than in the case for near-limit mixtures, as explained below. This comparison suggests that the method used to calculate preheat zone thicknesses is at least reasonably accurate.

In order to determine the effect of finite flame thickness on the calculated burning velocity, it is necessary to know the temperature profile of the flame front from the visualized point in the flame front, in this case the luminous zone, to the burned gas boundary (section 2.2.4.1). Of course this cannot be determined from the arbitrarily defined preheat zone thickness, but previous reports [30, 32, 33, 37] show that for near-stoichiometric hydrocarbon-air flames, usually the preheat zone thickness is roughly comparable to the reaction zone thickness, and for lean hydrocarbon-air the reaction zone thickness accounts for a smaller proportion of the overall flame thickness. For the purposes of this crude analysis, it is reasonable to assume that the reaction zone begins near the point of inflection of the flame temperature profile, which is also the approximate position of the luminous zone (section 2.1.1). The conclusion is that the thickness of the flame from the luminous zone to near the hot boundary is probably always less than the preheat zone thickness calculated here.

By inspection of the definition of the burning velocity correction I to account for finite flame thickness (section 2.2.4.1), it is apparent that with the upper limit of integration at r = 7 cm and the thickness of the flame from the luminous zone to near the hot boundary always less than 1.8 cm, the correction factor will always be small. A very crude estimate of the maximum

---

Pressure, Torr	δ, stoichiometric mixture, cm	δ, 6.0% methane, cm	δ, lean limit mixture, cm
1500	--	.030	.23
760	.018	.030	.31
250	.051	.075	.71
100	.12	.25	1.4
50	.21	.35	1.8

Table 4-6. Estimated preheat zone thickness for stoichiometric, lean limit, and 6.0% methane-air mixtures

value of I under these conditions is about 1.35, and this is only at the lean limit at 50 Torr. For all other mixtures tested the correction would be closer to 1.00, in most cases much closer.

The final conclusion of this drastically oversimplified analysis is that the correction to the burning velocity to account for nonzero flame thickness was negligible except for near-limit mixtures at low pressures. No great faith should be put into this conclusion, however, as a number of assumptions were made based on very little hard data. Flame temperature profile measurements would allow an actual correction factor to be calculated, and so would be of great value in future experiments.

There was also some experimental evidence that the effects of nonzero flame thickness in the calculation of burning velocities were small. Fig. 4-9 shows that at reduced pressures, the burning velocity increased despite the underestimate caused by the neglect of the increasing flame thickness. Also, the plots of S_u vs. fuel concentration were practically straight lines, in agreement with theory and previous measurements from results obtained using other types of experimental apparatus which may be less affected by nonzero flame thickness. If the neglect of the flame thickness correction had caused a serious underestimate of burning velocity, the lines would have curved downward at an increasing slope for progressively leaner mixtures, since they have progressively larger flame thicknesses. This would have been especially so at 50 Torr, the lowest pressure investigated. While this experimental evidence is by no means conclusive, it helps to support the results of the analysis presented above.

In addition to nonzero flame thickness, heat losses also cause an underestimate of burning velocity (section 2.2.4.1). Some evidence has already been presented to suggested that heat losses were small in the current

experiments, and much more evidence is presented in the following pages. Thus, it is very unlikely that the values of burning velocity reported here were seriously underestimated by the neglect of heat loss.

4.3.3 Interpretation and comparison with previous results

The measured burning velocities at 760 Torr are somewhat lower than those shown in Fig. 2-8, for example 32 cm/s vs. about 40 cm/s for stoichiometric mixtures, but are in very good agreement with other investigations using the same method [38, 93]. The basic shape of the burning velocity vs. methane concentration curves is almost precisely the same as the shape of the curves in Fig. 2-8. The effect of pressure on burning velocity for stoichiometric mixtures is similar to the results presented in section 2.2.4.2, but with a slightly lower pressure exponent, about 0.10 in this work as compared to 0.12 previously reported. The effect of pressure on burning velocity for other mixture ratios does not appear to be documented in the literature, so no comparison can be made. While the results of the current work may not agree exactly with previous investigations, the trends are certainly correct and the data in the current work are self-consistent, which is certainly more important for the purposes of this investigation.

The previously cited work of Reuss [16] contains the only information reported to date (other than in the current investigation) on burning velocities for near-limit mixtures in zero-g. Since methane-air mixtures at atmospheric pressure and room temperature in a SFLT were tested in Reuss' work, a comparison can be made between his work and this report. Reuss did not report burning velocities per se except at 5.87% methane, but instead reported only flame propagation velocities. He shows a picture of a 5.33%

methane flame burning in zero-g, for which the flame front appears to be nearly hemispherical. From the relation (section 2.2.4.1)

$$S_u = A_t/A_f(S_b - S_g)$$

for a flame propagating in a long tube, with $S_g = 0$ in Reuss' experiment because the tube was closed at the non-ignition end, and $A_t/A_f = \Pi r_t^2/[(1/2)4\Pi r_t^2] = 1/2$ for a hemispherical flame front, the result is simply $S_u = S_b/2$. By assuming all flames burning in mixtures less than 5.87% methane had hemispherical flame fronts, a rough calculation of burning velocity can be made. This calculation based on his results, along with interpolated results from the current investigation and the one-g flat-flame burner of Badami and Egerton [47] are shown in table 4-7. The agreement between Reuss' data and the findings of this work is very good, in fact it is remarkable considering the differences in experimental apparatus and calculation methods. The agreement with Badami and Egerton's results is not nearly as good, suggesting a gravitational influence in their experiment. This finding is very significant; it reinforces the suggestion presented in section 4.2.3 that in zero-g, near-limit flame behavior is to a large extent independent of the experimental apparatus. This is certainly not true in one-g, as has been stressed throughout this report. This finding also reinforces the conclusion that near-limit phenomenon observed in Reuss' experiment and this work were not affected by heat loss, as the two experiments had different heat loss characteristics (section 4.2.3) but the near-limit burning velocities are nearly identical.

Still more evidence of the similarity of near-limit flame behavior for different experimental apparatus in zero-g can be found by a comparison of flame development times in Reuss' experiment and the current work. Reuss reported that 0.46-0.54 seconds were required for the development of steady

Methane concentration, %	S_u, this work, zero-g	S_u, Reuss [16], zero-g	S_u, Badami and Egerton [47], one-g
5.87	6.8 cm/s	6.4 cm/s	9.1 cm/s
5.63	5.0	4.9	7.1
5.45	3.8	4.0	5.6
5.33	3.0	3.7	3.4
5.22	2.4	2.2	-
5.10	1.7	1.7	-

Table 4-7. Comparison of burning velocities for near-limit methane-air mixtures at atmospheric pressure and room temperature.

---

near-limit flame propagation in zero-g in a SFLT, as compared with 0.3-0.4 seconds in the current investigation under the same conditions. These times are closer than might be expected considering the differences in geometry and ignition conditions for the two experiments.

Since the plots of burning velocity vs. fuel concentration are nearly straight lines, the data invite extrapolation to $S_u \simeq 0$. This is shown in Fig. 4-10, which is merely a blown-up version of Fig. 4-9. The results of these extrapolations are shown in table 4-3. It appears that the fuel concentration corresponding to $S_u \simeq 0$ is closely related to the one-g upward flammability limit. The significance of this result is discussed in section 4.2.3.

The shape of the plots of burning velocity vs. fuel concentration near the flammability limits are of great interest in assessing the degree to which the observed flammability limits may be due to heat losses, as discussed in section 2.2.3.4. Inspection of Figs. 4-9 and 4-10 show that, within the limits of experimental error and repeatability, the curves of burning velocity vs. fuel concentration are almost straight lines right down to the zero-g flammability limit. If anything, the curves are leveling off slightly toward the horizontal as the limit is approached. It appears as if the burning

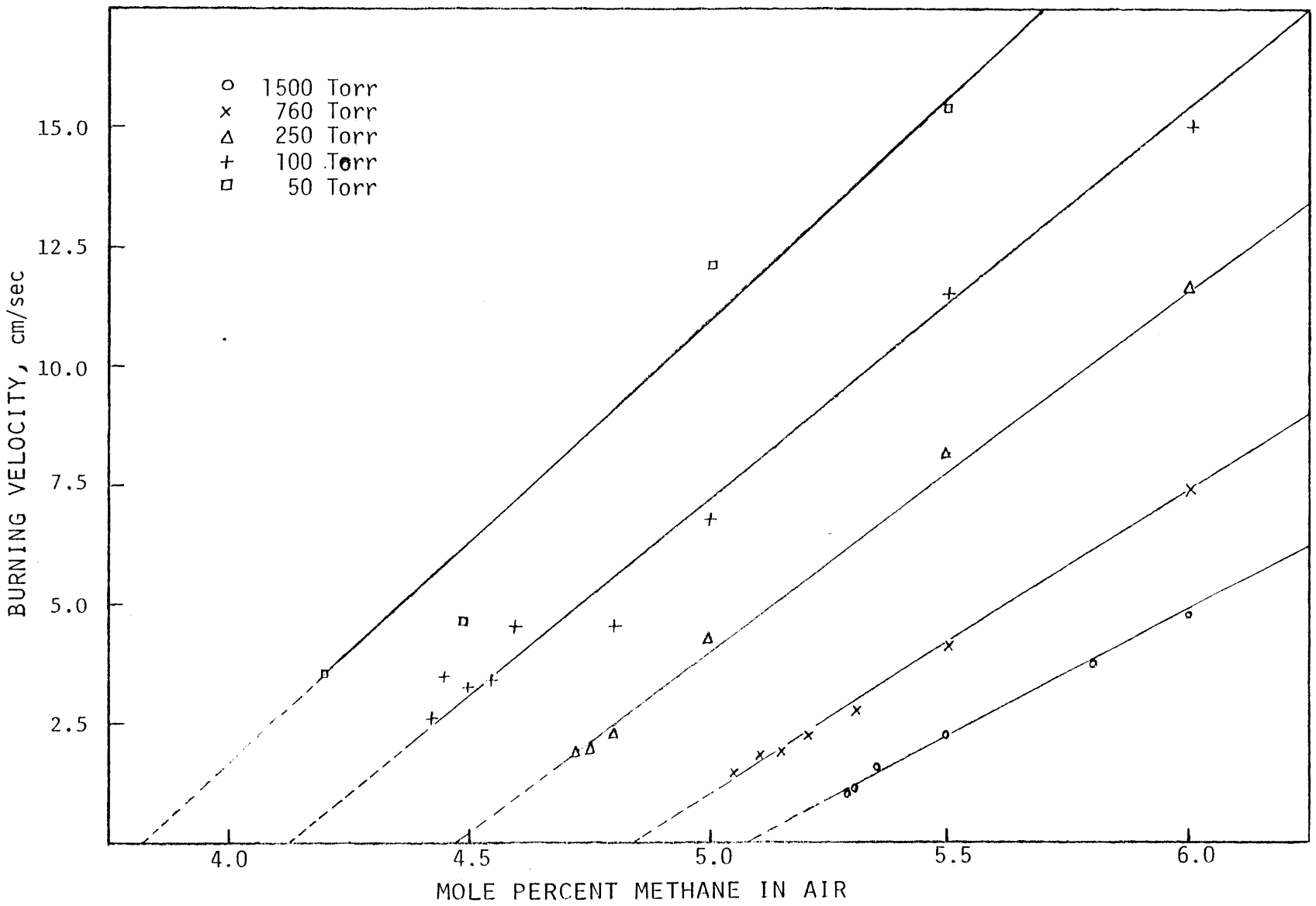

Figure 4-10. Burning velocities extrapolated to $S_u \simeq 0$ (near-limit detail of Fig. 4-9)

velocity curve is abruptly truncated at the zero-g flammability limit, suggesting that the mechanism of flame propagation does not change as the flammability limit is approached, but rather another factor comes into effect at the flammability limit which is not significant for near-limit mixtures. Certainly it is not the case that dS_u/dT_b approaches infinity or that the burning velocity drops to half of its "adiabatic" value at the zero-g flammability limit, which experimental results (section 2.2.3.3) and theories (section 2.2.3.4) show would occur at a flammability limit caused by heat loss. This would be most likely to occur at the lowest pressures, where the theory predicts that for a given size vessel conductive and radiant heat losses would be greatest, but the results show that even at 50 Torr no evidence for significant heat loss exists. The shape of the burning velocity vs. fuel concentration curves is extremely strong evidence that the observed zero-g flammability limits are not caused by heat loss, perhaps the most persuasive single clue found in this investigation.

Further evidence that heat losses did not have a significant effect on the results of this experiment can be seen from a comparison of Fig. 4-9 and corresponding curve for 760 Torr from "complete" models of methane-air combustion [36, 37], one of which is shown in Fig. 2-8. The agreement is extremely good despite the fact that the models are adiabatic but the experiment is not. This again suggests that heat losses in the current investigation were negligible.

An interesting feature of Figs. 4-8 a and b is that there appears to be a "no man's land" for normal zero-g flame propagation in r_b - t space. The same effect was found at pressures other than 760 Torr as well. The boundaries of this "no man's land" are the r_b vs. t plot for a zero-g lean-limit mixture and the t-axis. The r_b vs. t plots for richer mixtures seem forced to bend around

this region. Leaner mixtures, which must have slower burning velocities and so would have to "invade" the "no man's land", do not exhibit normal flame propagation at all in zero-g but instead show SIFD behavior (section 4.5). Apparently a minimum propagation rate is required for normal flame propagation in zero-g, and in mixtures which cannot meet the minimum requirement, normal flame propagation is unstable. In one-g no such effect was found for unconfined propagation in a large vessel. These findings suggest that gravitational forces add stability to near-limit flame propagation. Further evidence to support this idea is presented in sections 4.4.2 and 4.5.1.

4.4 Minimum ignition energies

4.4.1 Results

The procedure used in this investigation for determining minimum ignition energies was outlined in section 3.7. In accordance with the one-g upward flammability limit definition, ignition was defined as occuring if the spark produced flame propagation to the top of the vessel. The same considerations of arbitrariness of this definition for flammability limits applies to minimum ignition energies as well. Only a few near-limit mixtures at low pressures could have been affected by the arbitrariness of this definition. The results for one-g are shown in Fig. 4-11. The curves of MIE vs. mixture ratio are all of the same shape. The minimum value of MIE occurs for a mixture slightly leaner than stoichiometric, as previous results (section 2.2.4.2) have shown is the case for methane-air mixtures, and the MIE increases rapidly as the one-g upward flammability limit is approached. The effect of decreasing pressure is to shift the MIE curve upward and slightly to the left, i.e. toward higher minimum ignition energies and slightly leaner mixtures. Minimum

ignition energies were the same in one-g and zero-g except for mixtures extremely near the zero-g flammability limit and leaner, as Figs. 4-12 a-d show. No corresponding figure is shown for 50 Torr because only sparse data was taken at this pressure, but the data showed the same trends. Near the zero-g flammability limit, the MIE increased dramatically in zero-g but remained virtually unchanged in one-g. For example, at 1500 Torr total pressure the zero-g MIE was 6 millijoules at 5.30% methane, 8 mj at 5.29%, 115 mj at 5.28%, and greater than 3 joules at 5.27%. This amounts to a virtual "brick wall" of ignition energy, and extrapolation to 5.20% methane leads to the conclusion that an atomic bomb (10^{15} joule) would be required for ignition of this mixture. The one-g MIE varied from 4.5 mj at 5.30% to 6 mj at 5.20%. There can be no doubt of the drastic effect of gravity on minimum ignition energies under certain conditions.

In one-g, extinguishment of flame kernels resulting from sparks of insufficient energy for ignition was always very fast, faster than could be photographed successfully with the apparatus used. This was true even for very lean mixtures at low pressures, where the size of the minimal flame kernels was largest and the flame development times were longest (section 2.2.5.3). This was also the case in zero-g for mixtures significantly richer than the zero-g lean flammability limit, but for near-limit and sub-limit mixtures the clearly visible SIFD behavior was observed under some circumstances, while normal non-ignition behavior, which was only visible for very lean mixtures at low pressures, was observed in other cases. These phenomena are discussed further in section 4.5.

At 50 Torr the zero-g MIE was about 1.5 J at 4.30% methane, 2.5 J at 4.25% methane, and 5 J at both 4.20% and 4.15%. Based on this information, it is possible that the flames at 4.20% as well as 4.15% were SIFDs that were too

large to extinguish within the confines of the vessel. Unfortunately a couple of key film records were lost due to bad processing by a film laboratory in Cleveland. [The interested reader is advised to avoid using FilmLab Service Inc. in Cleveland.] Thus, it is possible that the zero-g flammability limit at 50 Torr is closer to 4.25% or 4.15% than to the stated limit of 4.20%.

As with flammability limits and burning velocities, variations in ambient temperature in the drop tower had some effect on the observed values of zero-g minimim ignition energies. Because the variation in temperature was small, again no firm conclusions can be drawn. It appeared that the effect of ambient temperature was negligible except near the zero-g flammability limit, where the "brick wall" in MIE occured. The net effect was that at increased temperature, the MIE curve shifted slightly to the left, causing a slightly leaner zero-g flammability limit, as discussed in section 4.2.2. Of course, the opposite effect was found for reduced ambient temperature.

The repeatability of the minimum ignition energies measured in this investigation was reasonably good but not outstanding. A nonrepeatability of ±10% was found under many conditions. This was somewhat expected based on previous results (section 2.2.5.2). As with burning velocities, this non-repeatability was greater than the uncertainty of the measurements, and so constitutes the major cause of inconsistency in the experimental results.

At this point a few questions concerning the effects of the spark discharge characteristics on the observed results should be addressed. The characteristics in question are the type of discharge (AC vs. DC), spark gap, spark duration, and spark orientation with respect to the gravity vector.

An early version of RASCAL (section 3.5.3) which was discarded for a variety of reasons was capable of producing AC as well as pulsed DC sparks. Early MIE tests performed using this version of RASCAL were in very good

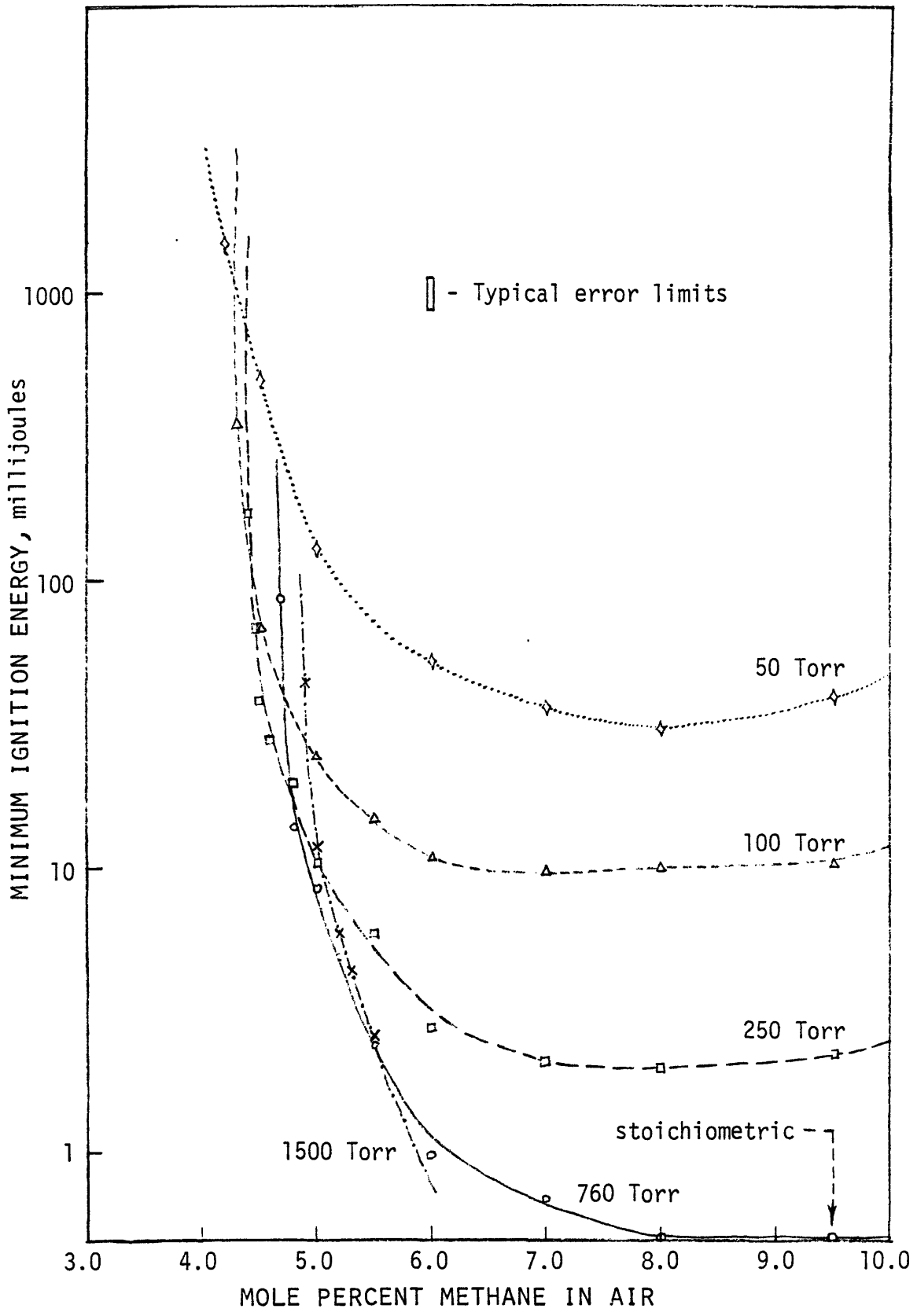

Figure 4-11. One-g minimum ignition energies as a function of mixture ratio for various total pressures

agreement with later results obtained using the final version of RASCAL which produced a steady DC spark. The discrepancies observed could be accounted for by the stochastic nature of the spark ignition process and the resulting inconsistency discussed above. Thus, the type of spark discharge did not have a significant effect on the minimum ignition energies determined in this experiment.

In order to assess the effect of spark gap on the minimum ignition energies determined in this investigation, a few tests were performed in which the minimum ignition energies for different spark gaps were determined for fixed values of total pressure and mixture ratio. The results are shown in table 4-8. The results show that the MIE increases very little with a spark gap longer than the optimum determined by the method outlined in section 3.7.1. This was expected based on previous results such as Fig. 2-12. For spark gaps shorter than optimum the increase in MIE is greater, but still not particularly important. The conclusion is that the method used for estimating the proper value of spark gap for use in the current investigation was adequate and the results would not have been affected significantly by using slightly different spark gaps.

In order to assess the effect of spark duration on the minimum ignition energies determined in this investigation, a few tests were performed in which the minimum ignition energies for different spark durations were determined for fixed values of total pressure and mixture ratio. The results are shown in table 4-9. The results show that the MIE increases little for spark durations longer than optimum determined by the method outlined in section 3.7.1, but increases more for spark durations shorter than optimum. This was not expected based on previous results (section 2.2.5.2), but since the study of optimum spark durations was not one of the objectives of this

Mixture	Short gap	Normal gap	Long gap
4.5%	1.0 cm	2.0 cm	2.5 cm
100 Torr	150 mj	70 mj	85 mj
4.8%	0.5 cm	1.0 cm	--
760 Torr	13 mj	13 mj	
9.5%	0.5 cm	1.0 cm	1.5 cm
100 Torr	17 mj	10 mj	10 mj
6.0%	0.5 cm	1.0 cm	1.5 cm
250 Torr	3.5 mj	2.5 mj	2.7 mj

Table 4-8. Effect of spark gap on minimum ignition energy for selected combustible mixtures.

Mixture	Short duration	Normal duration	Long duration
4.5%	170 μs	240 μs	1000 μs
100 Torr	95 mj	70 mj	150 mj
4.8%	45 μs	130 μs	--
760 Torr	25 mj	13 mj	
9.5%	45 μs	130 μs	300 μs
100 Torr	22 mj	10 mj	16 mj
6.0%	5 μs	13 μs	120 μs
250 Torr	3.4 mj	2.5 mj	2.8 mj

Table 4-9. Effect of spark duration on minimum ignition energy for selected combustible mixtures

---

investigation, it was not a serious concern. What was important was that the results showed that the method used for estimating optimum spark duration was adequate.

In order to determine if the orientation of the spark with respect to the gravity vector had any effect on the measured one-g minimum ignition energies, a few tests were performed in which the polarity of the spark electrodes was

reversed (positive on top, negative on the bottom). No noticeable change in minimum ignition energies was found, and the flame propagation for near-limit mixtures was still upward from the ignition source, with no tendency for initially downward propagation. The conclusion is that the spark orientation had no effect on the measured results, even for near-limit mixtures.

4.4.2 Interpretation and comparison with previous results

The minimum ignition energies for near-stoichiometric mixtures determined in this experiment (Fig. 4-11) are in good agreement with previous results, where available (section 2.2.5.2), over the entire range of pressures investigated. There appears to be little hard data available in the literature on minimum ignition energies for near-limit mixtures, so a direct comparison is not possible, but the trend of rapidly increasing MIE for progressively leaner near-limit mixtures is certainly correct. As there have been no previous experimental investigations on the effect of gravity on minimum ignition energies, no comparisons can be made. The only conclusion that can be drawn is that the results are consistent with previous experimental results to the extent that comparisons are valid.

On the analytical side, there have been no models of the ignition process presented that are detailed enough to make accurate predictions of the minimum ignition energies of methane-air mixtures. The simple model proposed in section 2.2.5.3 predicted that the critical burning velocity for significant gravitational effects on MIE at one-g is given by $S_{u,crit} \simeq 2.1\ P^{-1/3}$, whereas the burning velocity at the zero-g flammability limit is given by (section 4.2.3) $S_{u,lim} \simeq 1.5\ P^{-1/3}$. Since significant gravitational effects on MIE occur only extremely near the zero-g flammability limit, the correlation between the model and experiment is quite good, especially considering the

crudeness of this model. On the other hand, it will be shown that the one-g minimum ignition energies are probably the more fundamental values, so that the zero-g values are, in a sense, the ones being affected by gravity. The simple model proposed here yields a critical burning velocity for significant gravitational effects at zero-g of zero, thus it does not appear that this simple model has predicted anything of value. The only detailed model available of the effect of gravity on minimum ignition energies (section 2.2.5.3) predicts a slight decrease in MIE at reduced gravity, which is clearly contrary to the findings of this investigation. On the other hand, the decrease predicted is too small to be detected in this experiment, and the model was only applied to a carbon monoxide-oxygen mixture, so it is not clear that agreement between the model and the results of this work can be expected.

The relation $E \sim P^{-2}$ (section 2.2.5.3) appears to be valid for near-stoichiometric mixtures but less valid for mixtures nearer the flammability limit. As the MIE curves cross for sufficiently lean mixtures, obviously the relation cannot be expected to hold under these conditions. This discrepancy is undoubtedly related to the greater effect of pressure on burning velocity for lean mixtures which results in lower than expected values of MIE for lean mixtures at low pressures. The relation $E \sim S_u^{-3}$ (section 2.2.5.3) does not appear to hold at all. A closer approximation appears to be $E \sim S_u^{-1}$. The reason for this discrepancy is not at all evident. It suggests that the simple model of ignition does not provide an adequate description of the phenomena under some conditions.

Of special interest is the relationship between MIE and S_u near the zero-g flammability limit. At all pressures, the results show that as the zero-g limit is approached the MIE increases dramatically in a totally incongruous manner, but the burning velocity decreases only very slowly in

exact accordance with the expected trend. The burning velocity does not decrease drastically as an inverse relationship between the zero-g MIE and burning velocity would imply. Instead, the burning velocity decreases only slightly as an inverse relationship between the one-g MIE and burning velocity would imply. This is very strong evidence that the one-g MIE, and not the zero-g MIE, is the more "fundamental" value. This fact suggests that for near-limit mixtures in zero-g, some factor that allows normal flame propagation in one-g is missing. It appears that gravitational forces lend a stabilizing influence to near-limit flame propagation, as suggested in section 4.3.3.

The separate one-g and zero-g MIE curves (Figs. 4-12 a-d) also strongly suggest that the zero-g flammability limit could not have been a "flame stretch" limit. Lewis and von Elbe [30] have shown that the normal MIE threshold can be considered a flame stretch limit where sparks of subcritical energy input are "stretched" into too large a volume and lose too much heat to the surrounding gases before the developing flame kernel reaches a critical size. It has been shown that the fundamental MIEs are probably the one-g values, so the one-g MIE curve probably represents the flame stretch limit in the current investigation. Thus, the zero-g limit represents a different type of limit, so it is unlikely that the zero-g flammabiliy limit, which is defined by the zero-g MIE curve, could be considered a flame stretch limit.

For a given pressure, the one-g MIE increases very rapidly below a certain well-defined mixture, as Fig. 4-11 shows. Closer inspection reveals that this mixture is the one-g upward flammability limit, which is also closely related to the mixture for which $S_u \simeq 0$ (section 4.3.3). Because of the inverse relationship between E and S_u described above, this result is expected, and again it suggests that the one-g upward flammability limit is a

practical limit beyond which the MIE is too high and the burning velocity too low for normal flame propagation to be observed, but that it does not provide a fundamental barrier to flame propagation.

4.5 Sudden Infant Flame Death

4.5.1 Description and catalog of phenomena

In this investigation a new type of combustion phenomenon has been discovered and analyzed. This phenomenon, called Sudden Infant Flame Death, or SIFD, was first described in section 4.1. SIFD represents an intermediate range of combustion phenomena between the limits of normal flame propagation and normal non-ignition. SIFD is characterized by propagation well beyond the limit of influence of the normal ignition process at a continually decreasing rate and sudden extinction. Apparently SIFD only occurs for near-limit mixtures and only in zero-g. SIFD propagation was always spherically symmetric except for a few exceptional cases discussed later.

The basic phenomenon is cataloged in Figs. 4-12 a-d. No corresponding figure for the results at 50 Torr is presented because only sparse data was taken at that pressure. Each figure shows the one-g near-limit detail of one of the curves from Fig. 4-11 along with the zero-g results for the same pressure. The lower solid curve is the one-g MIE curve, the upper solid curve is the zero-g MIE curve, and the dashed curves are curves of constant zero-g SIFD extinguishment radius. These dashed curves were obtained by drawing a map of extinguishment radii measured from the film records for various combinations of spark energy and mixture ratio and drawing approximate best fit curves through the data. The moderate inconsistency of the data causes the exact location of the dashed curves to be somewhat questionable, but the

trends are unmistakable. For reference, the approximate sensible energy E_s residing in flame kernels with radii equal to the various SIFD extinction radii (section 2.2.5.2) is shown for each dashed curve.

The most startling aspect of Figs. 4-12 a-d is the ratio of sensible energy E_s (which is equal to the energy liberated by chemical reaction plus the initial spark energy) to the initial spark energy input E for some SIFDs. The most extreme example is 5.29% methane at 1500 Torr total pressure (Fig. 4-12a). A 4 mj spark produces no observable ignition, a 7 mj spark produces a 5.9 cm SIFD for which $E_s \simeq 490J$, and a 10 mj spark produces normal flame propagation. The ratio of sensible energy to spark energy E_s/E in the 5.9 cm SIFD is 70,000, almost 4 orders of magnitude higher than found in normal non-ignitions (section 2.2.5.2). Other SIFDs show a lower energy ratio, but still much higher than normal non-ignitions. The crucial question is: "How does the developing flame kernel "know" after liberating 490J of energy (in the case of 5.29% methane at 1500 Torr) whether its initial spark energy was 7 mj, in which case it extinguishes, or 10 mj, in which case it propagates to the limits of the vessel?" The same question applies to large vs. small SIFDs caused by initial sparks of varying energy content. This unusual behavior was found at all pressures but was more pronounced at high pressures, as Figs. 4-12 a-d show.

It appears that all of the curves of constant SIFD extinguishment radius asymtotically approach the one-g MIE curve, so it is likely that the one-g MIE curve corresponds to an SIFD extinguishment radius of zero. This means that the MIE for SIFD behavior is the same as for one-g flame propagation. If this is the case, the one-g MIE curve determined here would be the same for other nonzero gravitational conditions. Why normal flame propagation is observed in one-g (and possibly other nonzero gravitational conditions) above this MIE,

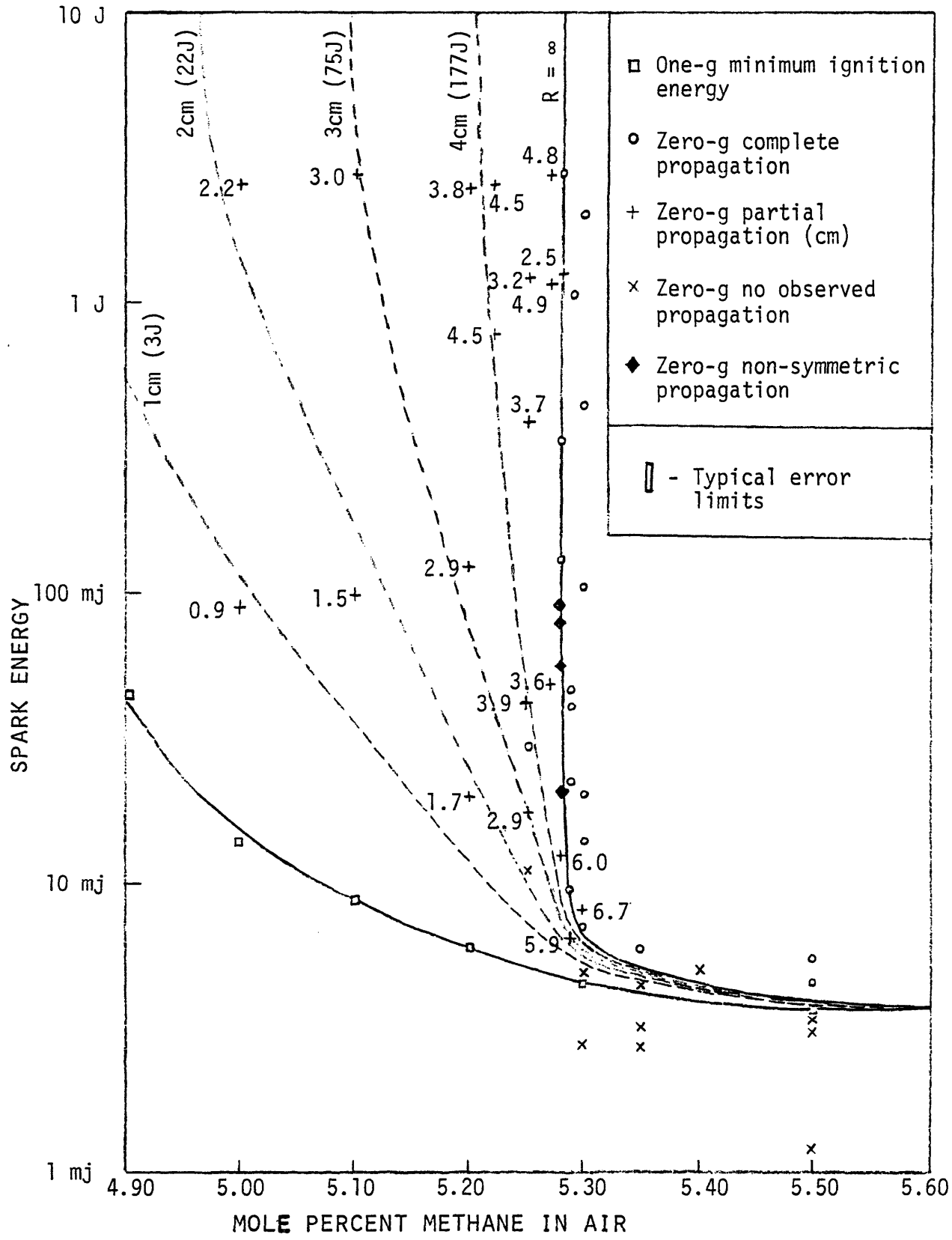

Figure 4-12a. Near-limit propagation and extinction behavior at 1500 Torr total pressure

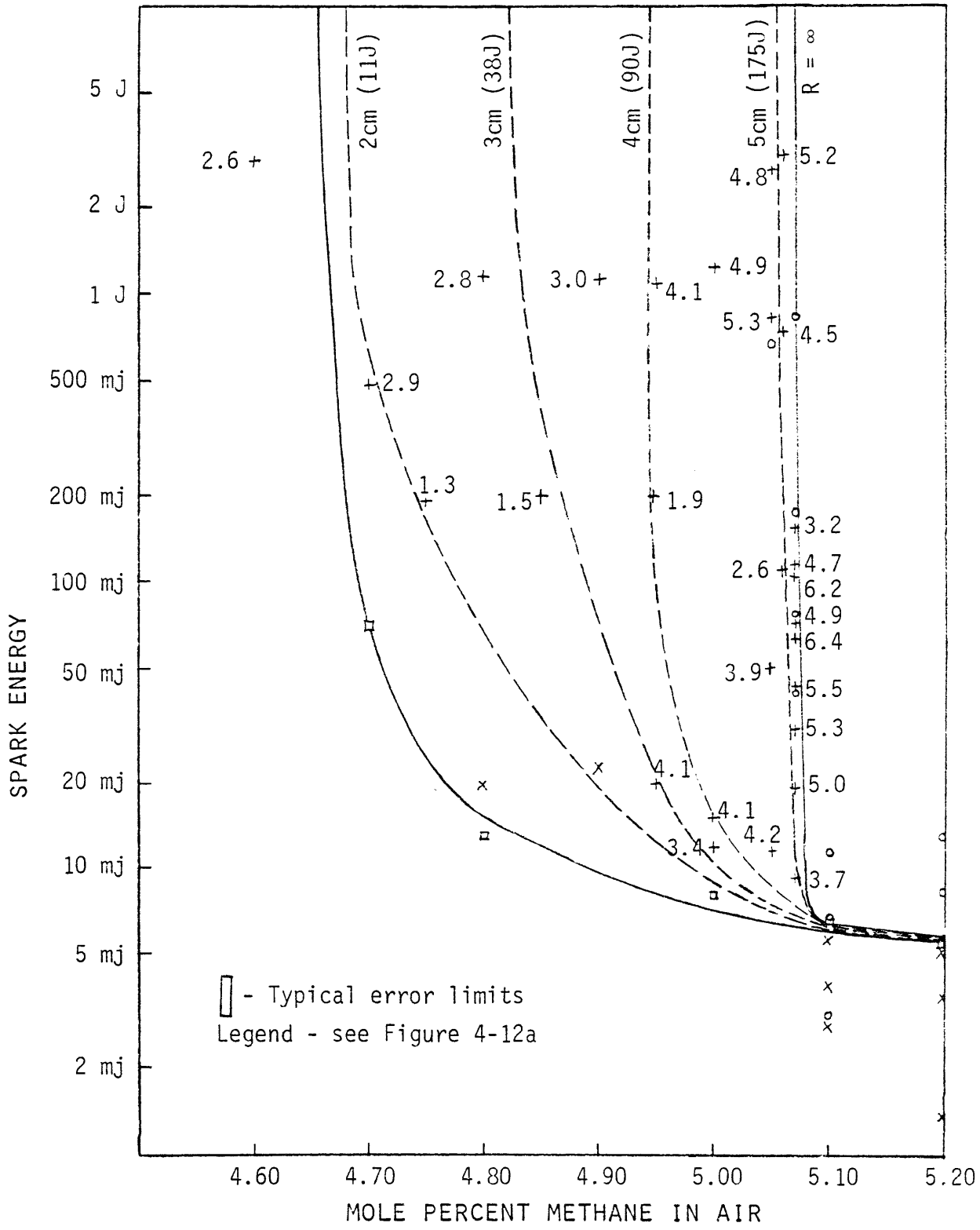

Figure 4-12b. Near-limit propagation and extinction behavior at 760 Torr total pressure

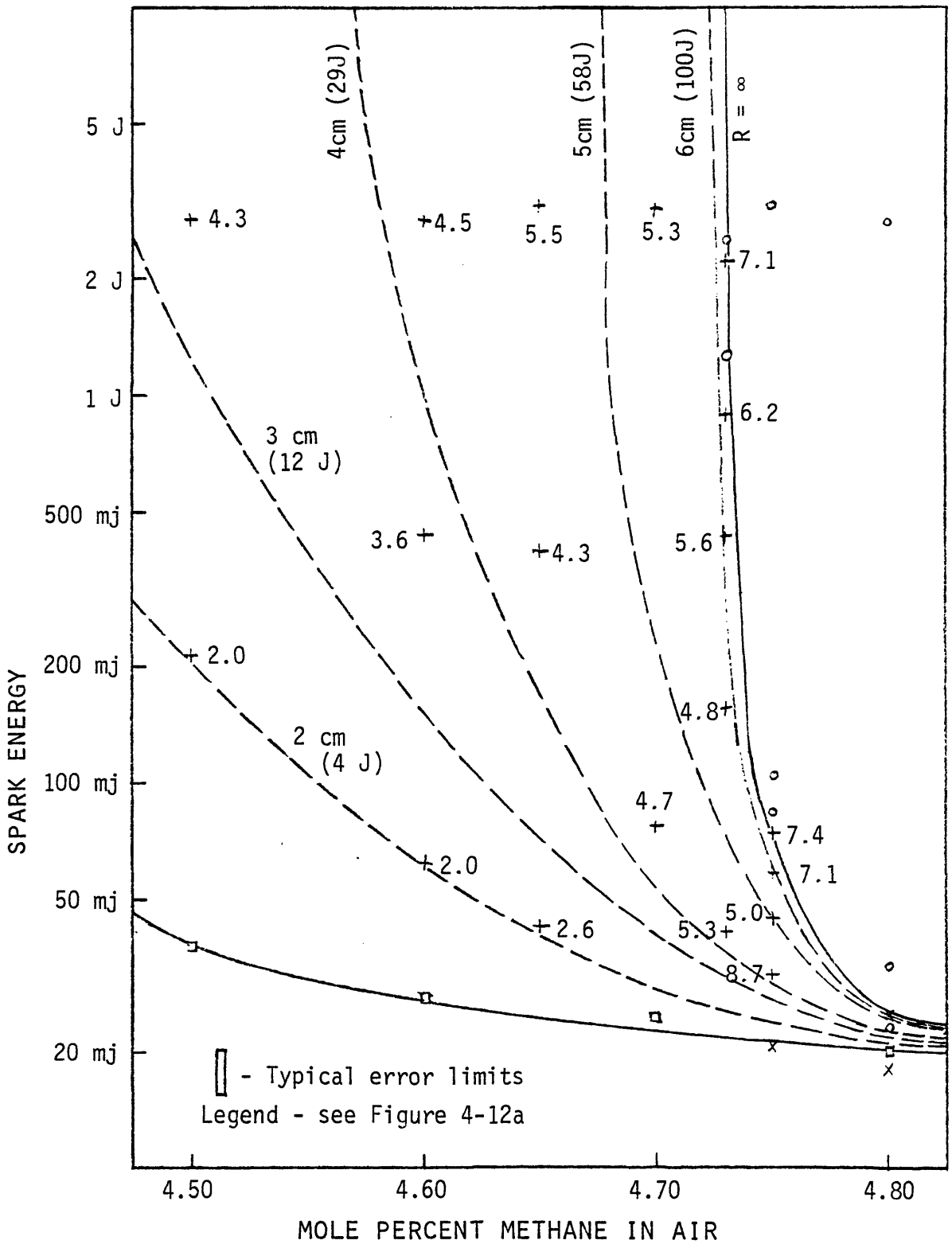

Figure 4-12c. Near-limit propagation and extinction behavior at 250 Torr total pressure

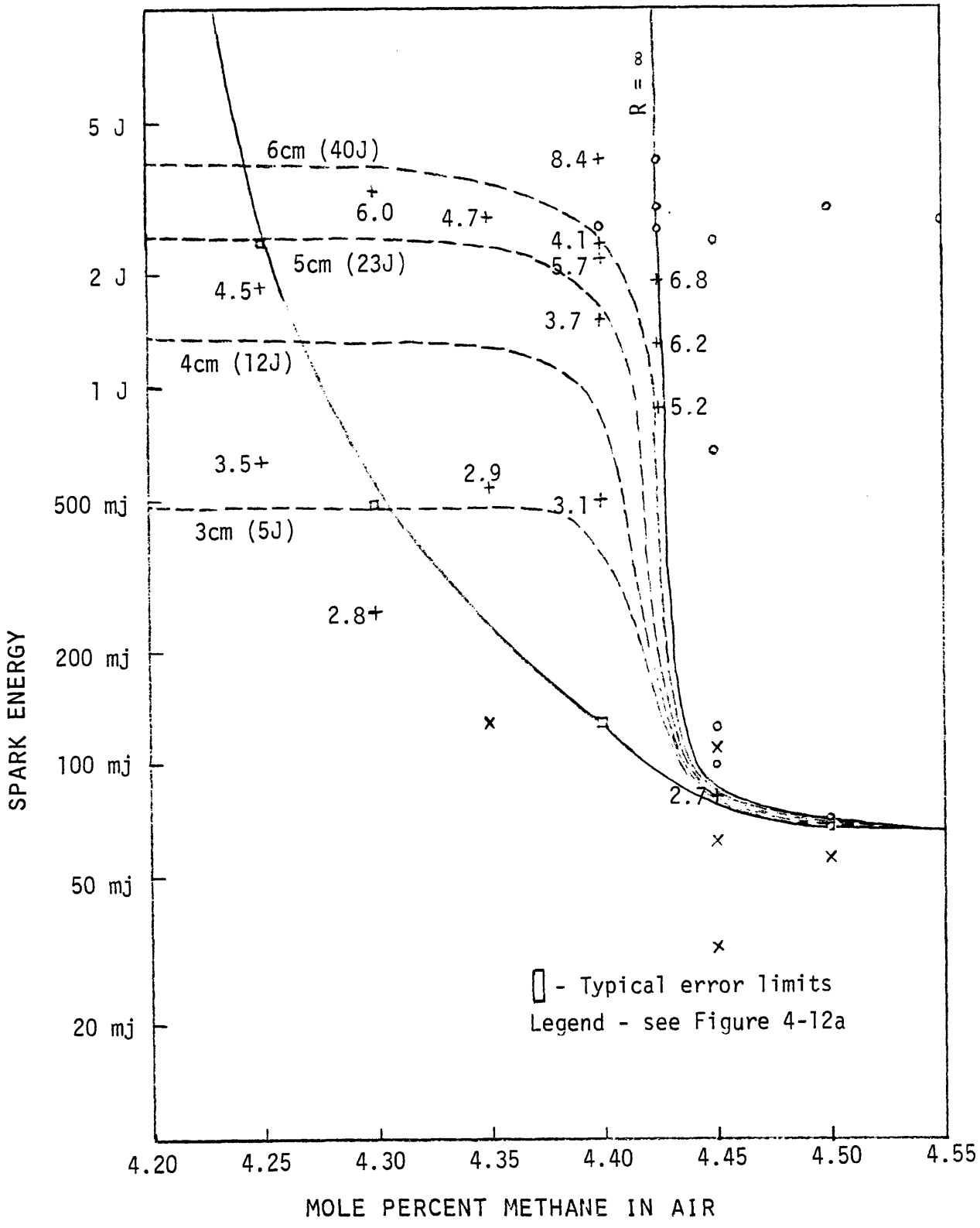

Figure 4-12d. Near-limit propagation and extinction behavior at 100 Torr total pressure

whereas in zero-g only SIFD behavior is observed below the well-defined zero-g flammability limit, is a mystery. It suggests that gravitational forces add a certain stabilizing influence to flame propagation, as previously suggested.

It is clear that the observed one-g propagation for near-limit mixtures is normal flame propagation because it follows a smooth transition from the flame behavior for richer mixtures. On the other hand, SIFD propagation is a separate mode because it does not follow from extrapolation of richer mixtures, in fact the results show that both SIFD and normal flame propagation can exist for some mixtures. This shows that SIFD behavior cannot be considered to be a zero-g analog to the observed one-g flame propagation for the same mixture, and so constitutes a separate, less stable mode of flame propagation. This reinforces the idea that gravity adds a stabilizing influence to flame propagation for near-limit mixtures, and that SIFD represents a stability-limited mode of flame propagation in zero-g.

Based on Figs. 4-12 a-d, it appears that the mixtures to the right of the zero-g MIE curves are indeed true steady state flames and not simply SIFDs that are too large to reach the extinguishment point within the confines of the vessel. This is so because as the zero-g MIE curve is approached horizontally from the SIFD side, the curves of constant SIFD extinguishment radius become closer together and appear to approach an infinite extinguishment radius at the zero-g MIE. This will be much clearer based on the flame radius vs. time records presented later in this section.

At low pressures (Fig. 4-12d) the SIFD curves fold over to the left for sufficiently lean mixtures and sufficiently high spark energies. At first this result seems surprising but closer inspection shows that this "fold-over" portion of the curve has an energy ratio E_s/E of about 10, which is about that of normal non-ignition. Apparently for mixtures which exhibit "fold-over"

normal non-ignition produces more observed flame propagation than SIFD, and so becomes the dominant mode. This "fold-over" effect was not seen at higher pressures because the spark energy available from RASCAL was inadequate under these conditions. For a fixed flame radius, E_s is directly proportional to pressure (section 2.2.5.2), so at higher pressures a larger spark energy is required to reach the "fold-over" portion of the SIFD curve. The result is that for a flame radius of greater than about 3 cm, the spark energy required to reach the "fold-over" portion of the SIFD curve was beyond the capability of the current system except at a pressure of 100 Torr and below.

There is practically a bifurcation point where the one-g MIE, zero-g MIE, and multiple SIFD curves meet, thus repeatable results cannot be expected near this point. In accordance with other experimental results, the bifurcation point moves to richer mixtures and lower spark energies at higher ambient pressures.

The current investigation has shown that in addition to the normal regions of ignition and non-ignition on an ignition energy vs. mixture ratio plot as seen in one-g (Fig. 4-13a), in zero-g a third region exists where SIFD behavior is observed, as shown schematically in Fig. 4-13b. The SIFD region is actually split into two sections, one where SIFD is actually seen and the other where "fold-over" is observed because the SIFD extinguishment radius is so small that non-ignition is observed instead. While normal flame propagation and normal non-ignition occupy an infinite area in ignition energy-mixture ratio space, observable SIFD propagation occupies only two banana-shaped regions, one on the lean side of the stoichiometric mixture, and (presumably) another on the rich side.

There is substantial evidence that combustion was nearly complete in most SIFD propgation. The fraction of fuel burned in SIFDs, estimated by the

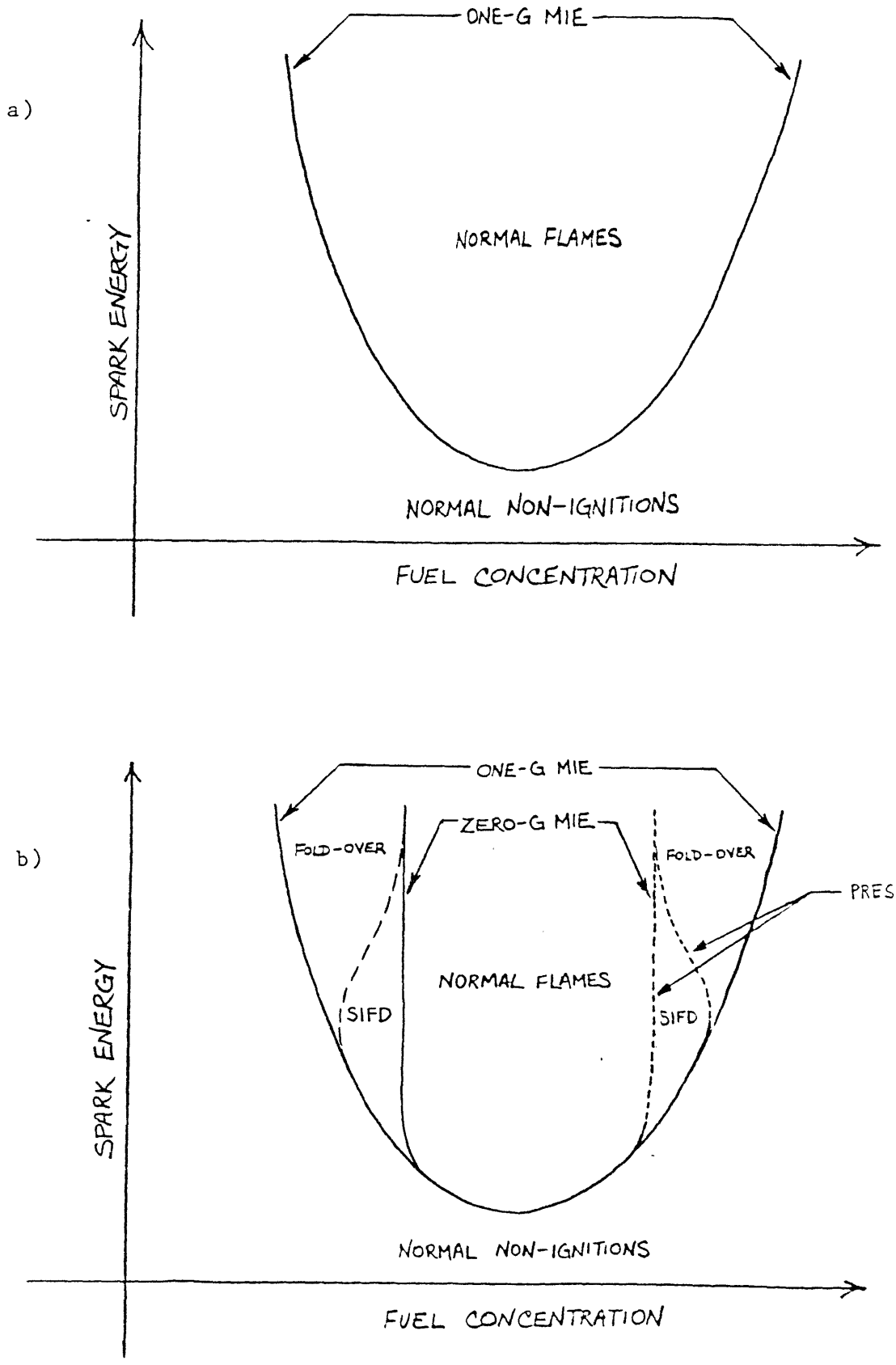

Figure 4-13. Schematic diagram showing regions of flame ignition and extinction behavior; a) one-g, b) zero-g

volume of flame produced, appeared to be about the same as the fraction of the normal pressure drop due to combustion (sections 3.7.2 and 4.2.2) found in SIFDs, although most SIFDs burned too little fuel to make accurate measurements. The possibility of incomplete carbon combustion (section 3.7.2) also clouds the issue somewhat. Until near the point of extinction, the luminosity of SIFDs, with a few exceptions at 1500 Torr, was comparable to that of normal, steadily propagating flames at the same pressure. This suggests that normal chemical reaction took place in SIFDs. The very fact that a luminous zone was observed is strong evidence that the temperature of SIFDs is at least 800-1000°K (section 2.1.1), close to the adiabatic flame temperature of normal zero-g lean limit flames (1300-1550°K). Because of a fault in the apparatus, in a few drop tests a second spark fired just before impact of the drop assembly in the deceleration container. In no case did this cause reignition of extinguished SIFDs. This shows that enough chemical reaction occurred in SIFDs, at least near the spark source, that the process of SIFD could not be repeated. In two very unusual cases at 1500 Torr described below, the flame front failed on one side in zero-g, in a very SIFD-like manner, but the pressure drop in the vessel showed that combustion was eventually completed. Again this suggests that SIFD flame propagation consumes most of the available fuel. By no means is any of this evidence definitive, but all of these bits of information point to the same conclusion.

SIFD flame propagation is apparently unable to ignite normal steady flame propagation. This situation was never observed in zero-g. Impact of the drop assembly in the deceleration container never caused reignition of extinguished SIFDs, even those occurring in mixtures which exhibited substantial flame propagation in one-g. Also, impact of the drop assembly caused immediate extinction of SIFDs which had not extinguished during the drop, apparently

without any additional flame propagation. This last finding is particularly unusual considering that normal flames which burned slowly enough that they did not consume all of the available fuel during the drop continued burning upon impact, consuming all of the available fuel. For both SIFDs and normal flames, the impact promptly restored natural convective effects, indicating that the density of the "burned" gas in SIFDs is low, and therefore the temperature high, in relation to the unburned gases, just as is the case with normal flames.

The preceding two paragraphs suggest contradictory findings. On one hand normal flame propagation and SIFD propagation seem almost identical, but on the other hand they are very different in their ability to spread their influence. It appears that the difference between the two is more related to their relative abilities to propagate and less to their relative abilities to cause chemical reaction in the gases which they propagate through.

The most bizarre finding of this investigation was the appearance of non-spherically-symmetric flame propagation in zero-g. This was found only for 5.28% methane at 1500 Torr, which is the zero-g flammability limit at that pressure, and only for spark energies above that required required to cause normal SIFD propagation with extinguishment at about 6 cm (about 15 mj) and below that required for normal flame propagation (about 120 mj). No normal flames or normal SIFDs were observed under these conditions. These very unusual flames seem to correspond to modes of flame propagation between normal SIFD behavior and normal steady flames. The results are shown in Figs. 4-14 a-d. Unfortunately, some of the film records were too dim to reproduce properly. This was not because these flames were dimmer than the others, but because of poor processing by a film laboratory in Cleveland (see comment about film processing in section 4.4.1). For these film records, approximate

sketches of the position of the leading edge of the flame front are shown instead. These were the only four cases of non-symmetric SIFDs found except for another flame very similar to Fig. 4-14d. All of these started out as normal SIFDs, as the flame radius versus time records presented later in this section will show. In Fig. 4-14a, the SIFD started out spherically symmetric and failed in the middle but continued to propagate on the "top" and "bottom" (such distinctions are of course meaningless in zero-g), forming a peanut-shaped flame which propagated until the impact of the drop assembly. In Fig. 4-14b, a 3-lobe structure is visible in the early stages of propagation and this structure continues throughout the free-fall, although one of these lobes failed almost completely. The entire lobe structure was also rotating at a rate of about 20 degrees per second. In Fig. 4-14c, the SIFD started out normally and failed in all but one direction, and continued to propagate at a nearly steady rate throughout the drop. In Fig. 4-14d, the opposite of Fig. 4-14c occurred. The flame failed in only one direction, the other directions continuing to propagate at a rate close to that of normal flames. It appeared that the flame would have reignited in the direction that failed had more zero-g time been available.

It should be remembered that film records provide a two-dimensional projection of a three-dimensional image, therefore it cannot be determined precisely what the true three-dimensional shapes of these flames were with only one camera angle.

As with normal flames and normal SIFDs, the pressure drop in the vessel due to combustion suggested that combustion was nearly complete in the volume of gas consumed by these non-symmetric SIFDs. This can be said with more certainty than was possible with normal SIFDs, because the non-symmetric SIFDs

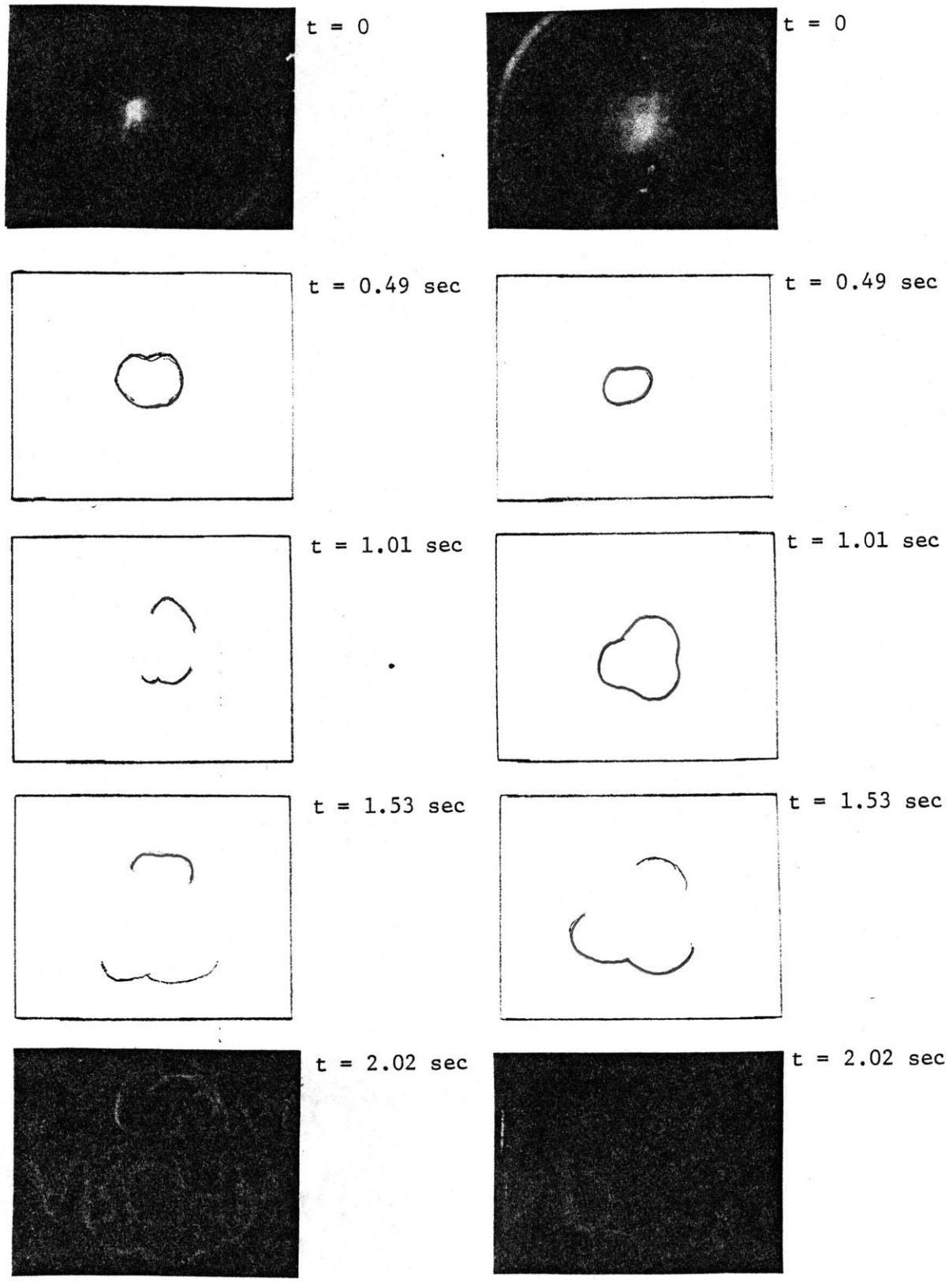

Figure 4-14 a,b. Sequential photographs of combustion of 5.30% methane in air at 1500 Torr total pressure; spark energy a) 20.7 mj, b) 56.9 mj

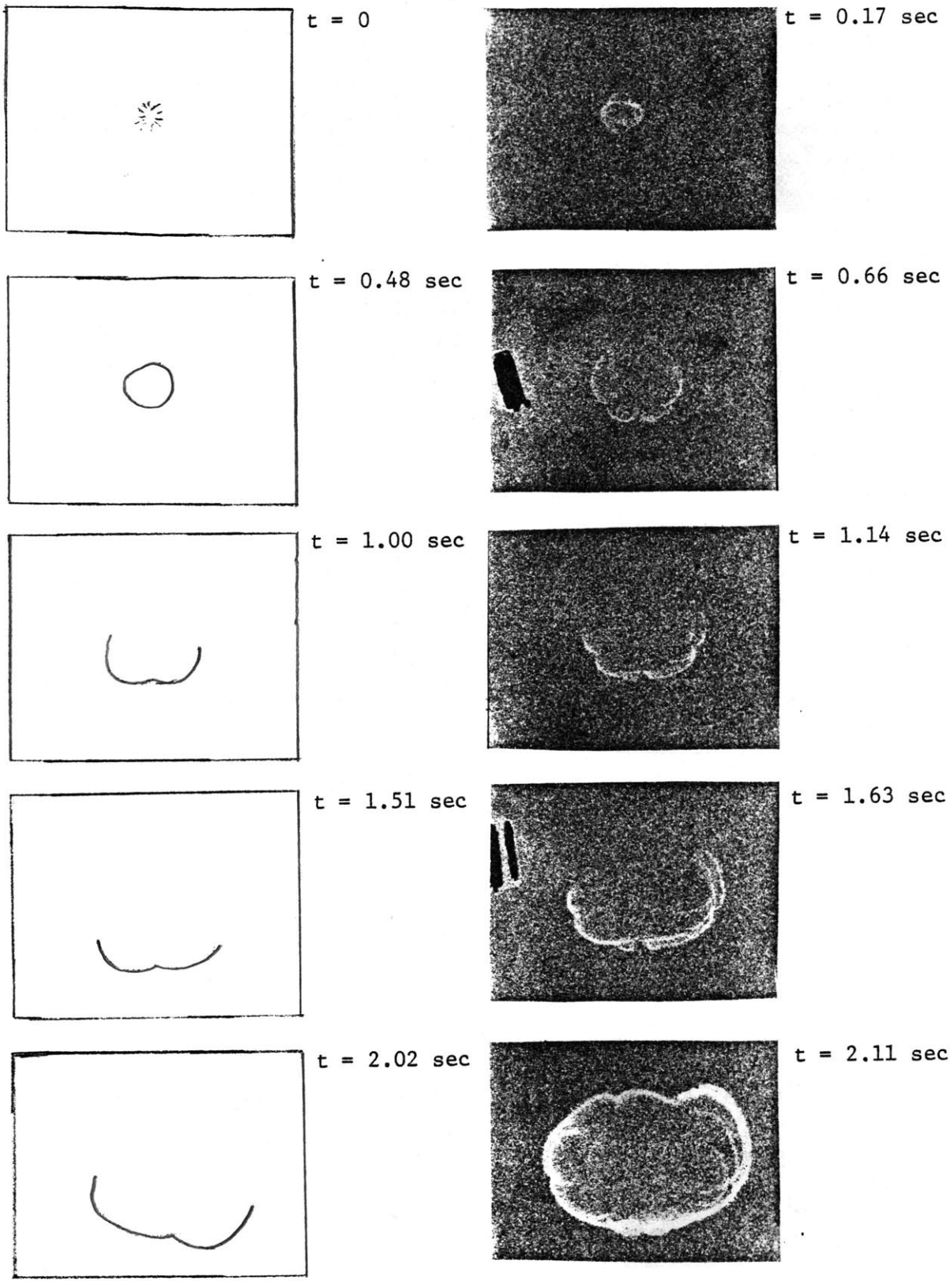

Figure 4-14 c,d. Sequential photographs of combustion of 5.30% methane in air at 1500 Torr total pressure; spark energy a) 77.9 mj, b) 93.2 mj

consumed a larger volume of gas than normal SIFDs, resulting in a larger, more accurately measurable pressure drop.

It is unclear whether the various non-symmetric flames were distinct, separate modes of propagation or were merely random perturbations. Figure 4-15a shows, as expected, that these flames were clearly an intermediate range of phenomena between normal flames and normal SIFDs in terms of propagation rate as well as extinguishment radius. Since there was no consistent failure location, it is unlikely that the observed behavior could be accounted for by the presence of solid objects (i.e. spark electrodes, flame detectors) in the path of the flame front. Random perturbations could be caused by pseudo-random factors such as the aerodynamics generated by the spark discharges, and since the results have already shown that disturbances in near-limit or sub-limit flames can propagate over some distance, random factors caused by the ignition process could account for the observed results. The fact that the non-symmetric propagation was apparently still symmetric with respect to the spark electrodes supports this idea, but is certainly not conclusive. In either case it is certainly likely that other non-symmetric modes could be found, particularly at still higher pressures.

It is also unclear why this non-symmetric propagation was observed only at 1500 Torr and only for 5.28% methane. SIFD behavior was most pronounced at higher pressures and mixtures at or extremely near the zero-g flammability limit, so this mixture is the most likely to exhibit extreme SIFD behavior, but this does not explain why no traces of non-symmetric zero-g propagation were found at, for example, 5.07% methane at 760 Torr.

The zero-g flame radius r_b versus time histories as a function of spark energy for most of the mixtures which exhibited both normal and SIFD propagation are shown in Figs. 4-15 a-f. Only data taken at ambient

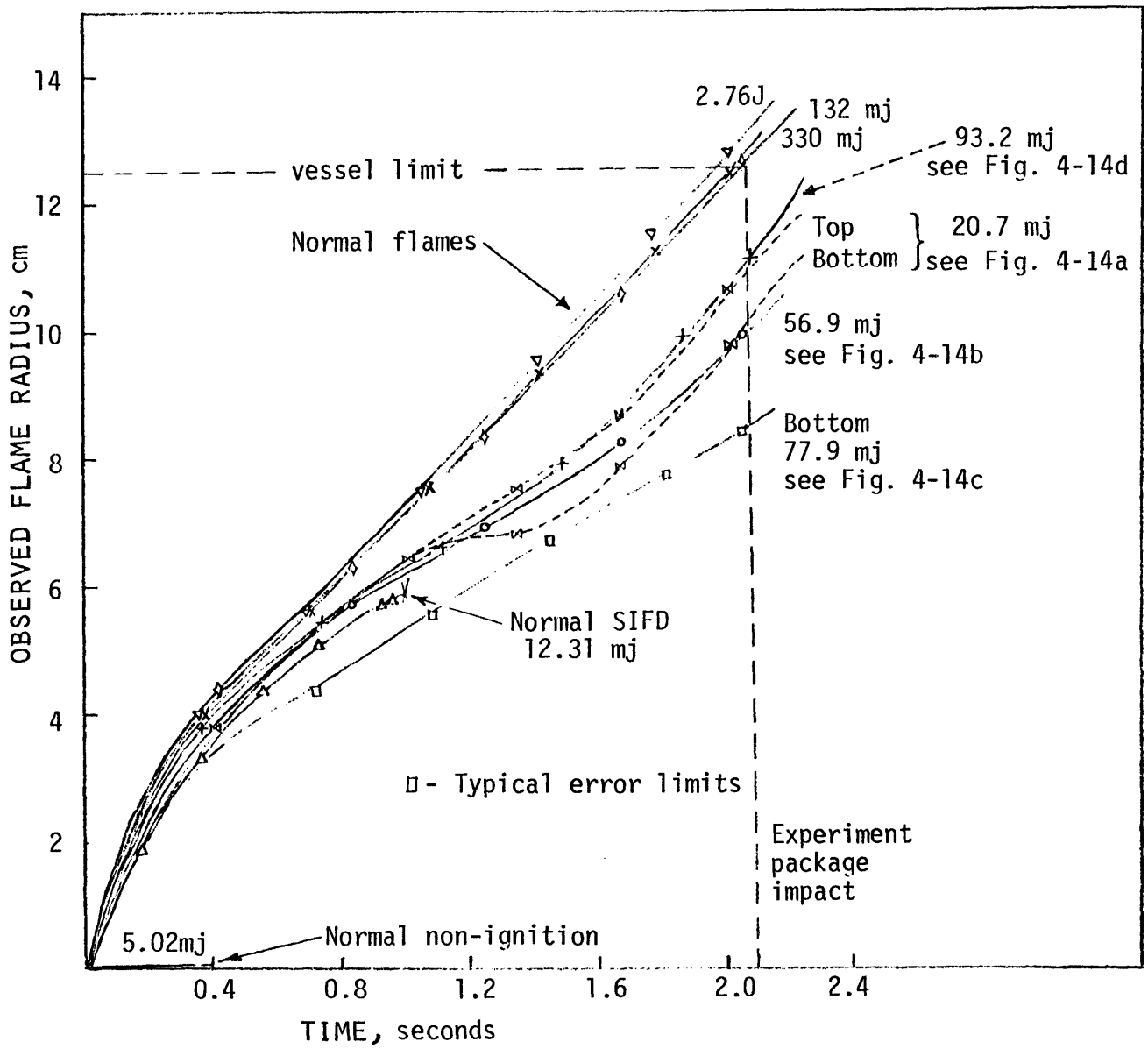

Figure 4-15a. Observed flame radius vs. time for various spark energy inputs
Mixture: 5.28% methane in air at 1500 Torr total pressure

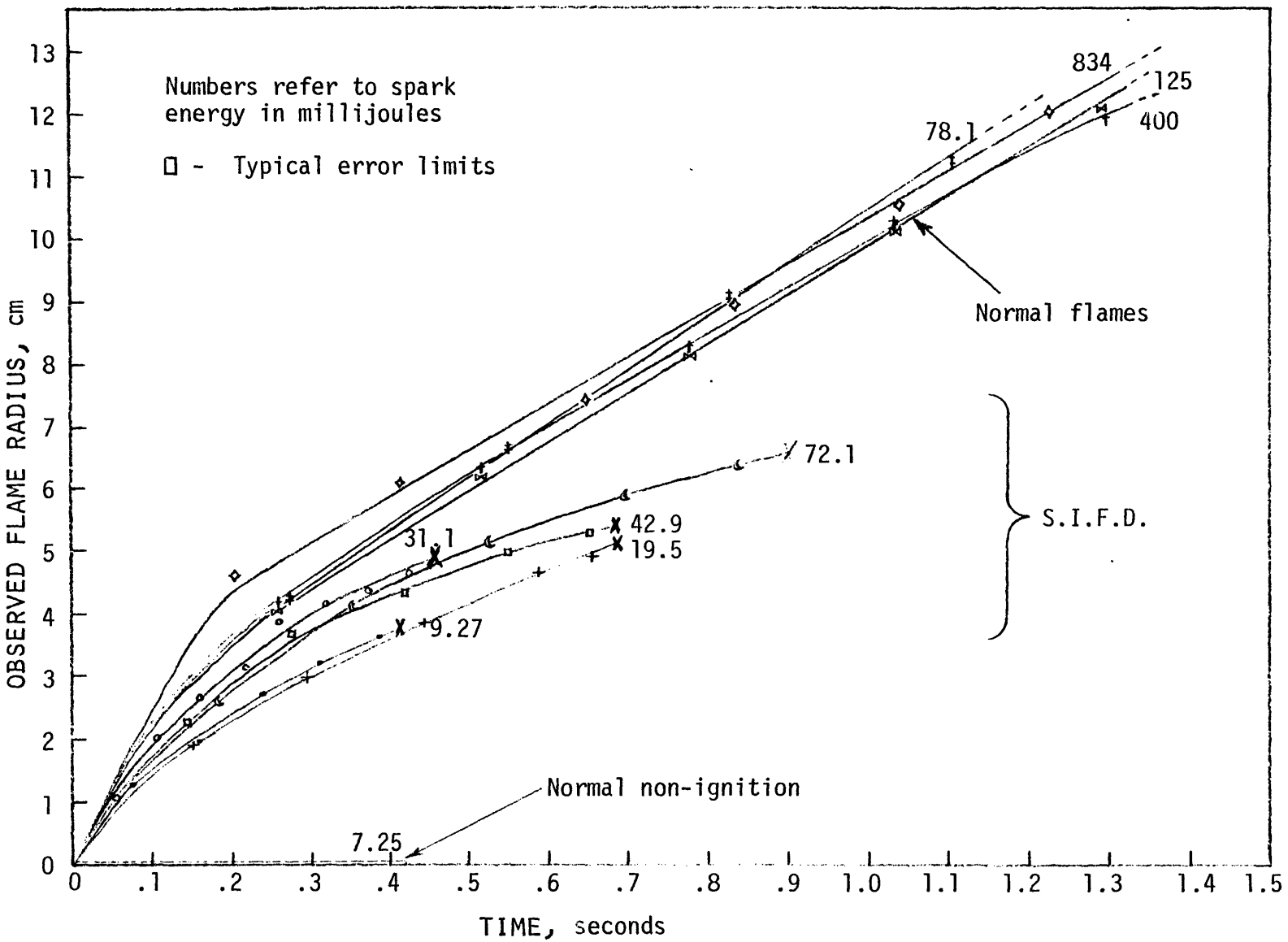

Figure 4-15b. Observed flame radius vs. time for various spark energy inputs
Mixture: 5.07% methane in air at 760 Torr total pressure

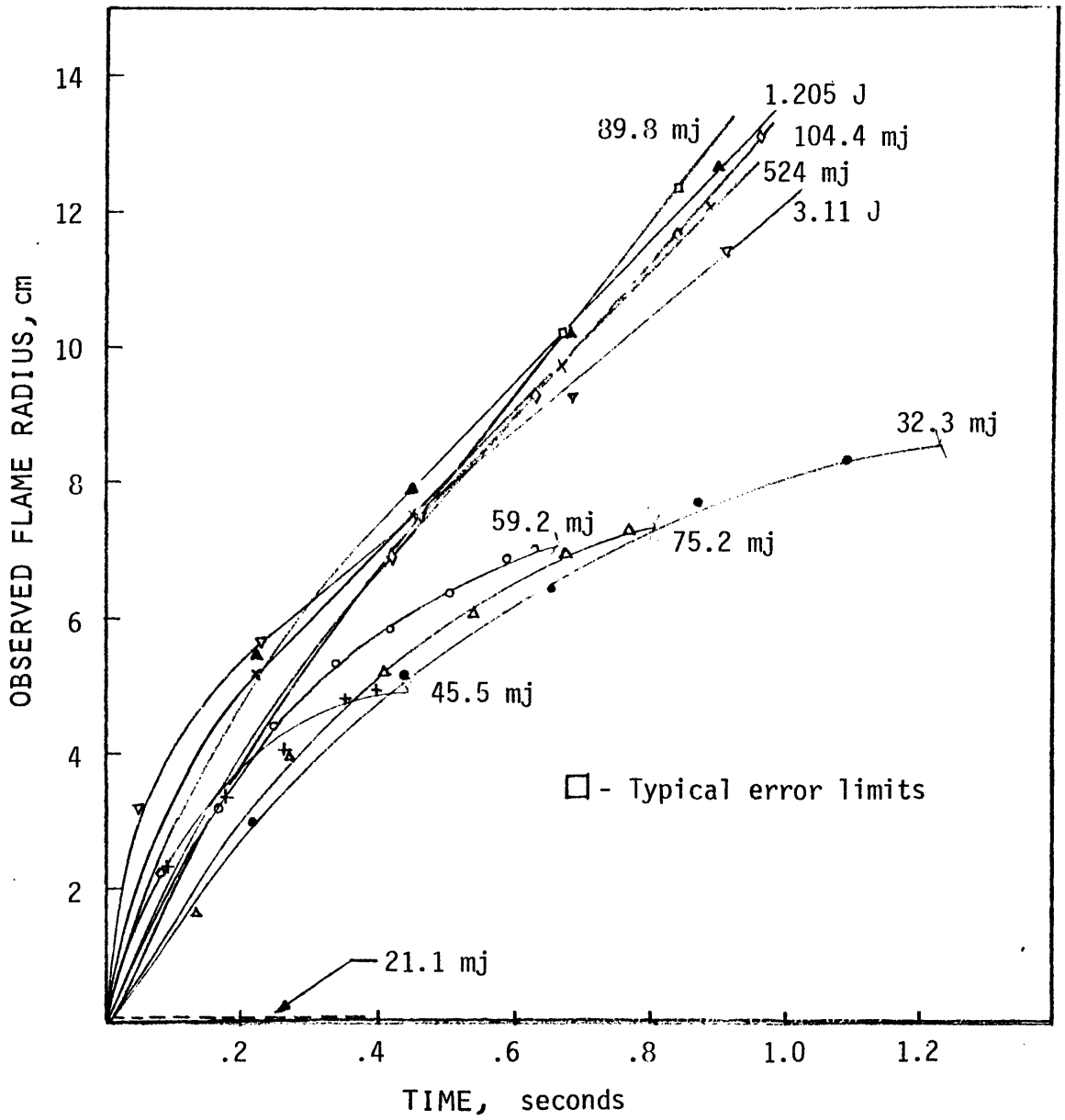

Figure 4-15c. Observed flame radius vs. time for various spark energy inputs
Mixture: 4.75 % methane in air at 250 Torr total pressure

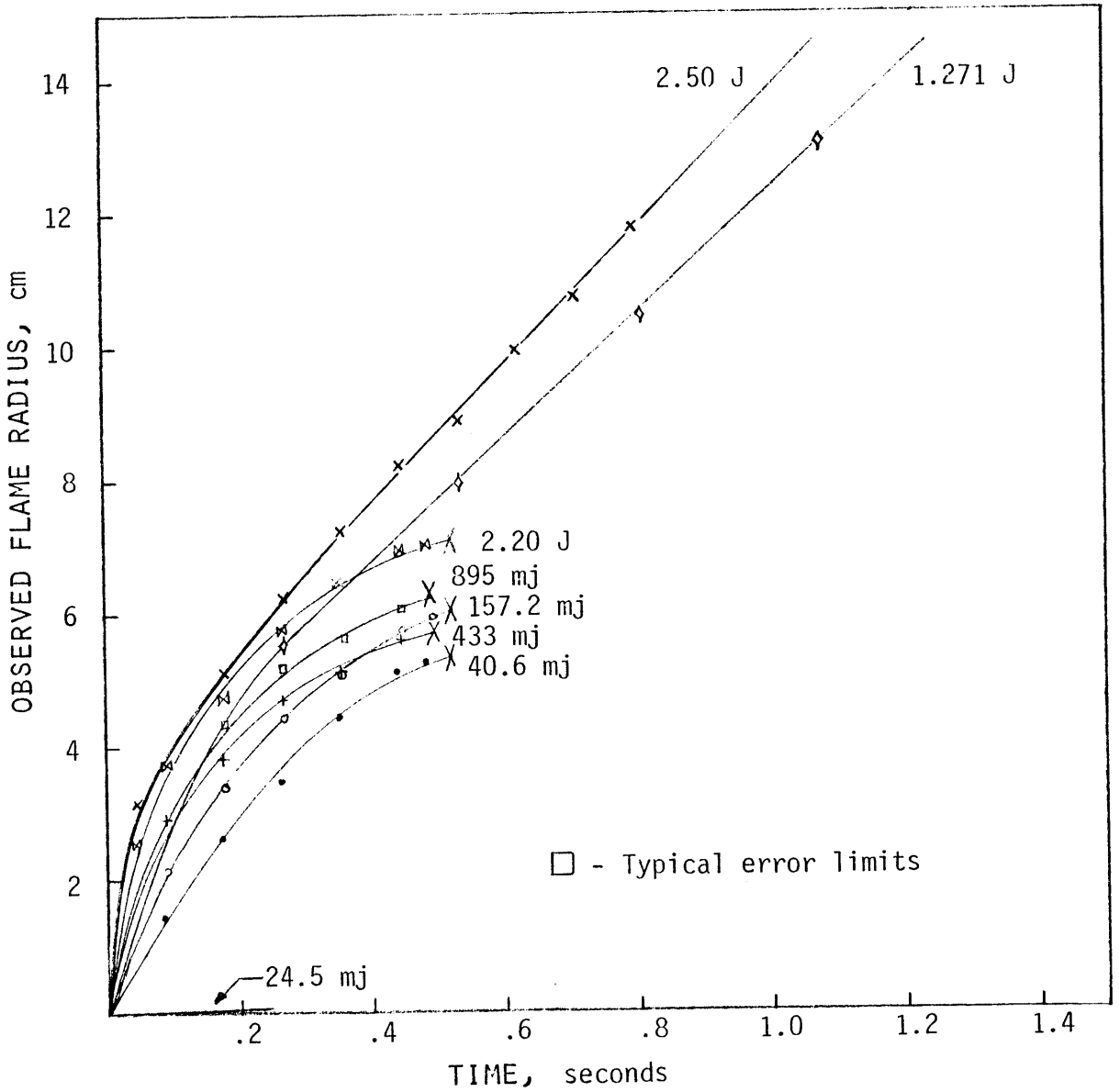

Figure 4-15d. Observed flame radius vs. time for various spark energy inputs
Mixture: 4.73% methane in air at 250 Torr total pressure

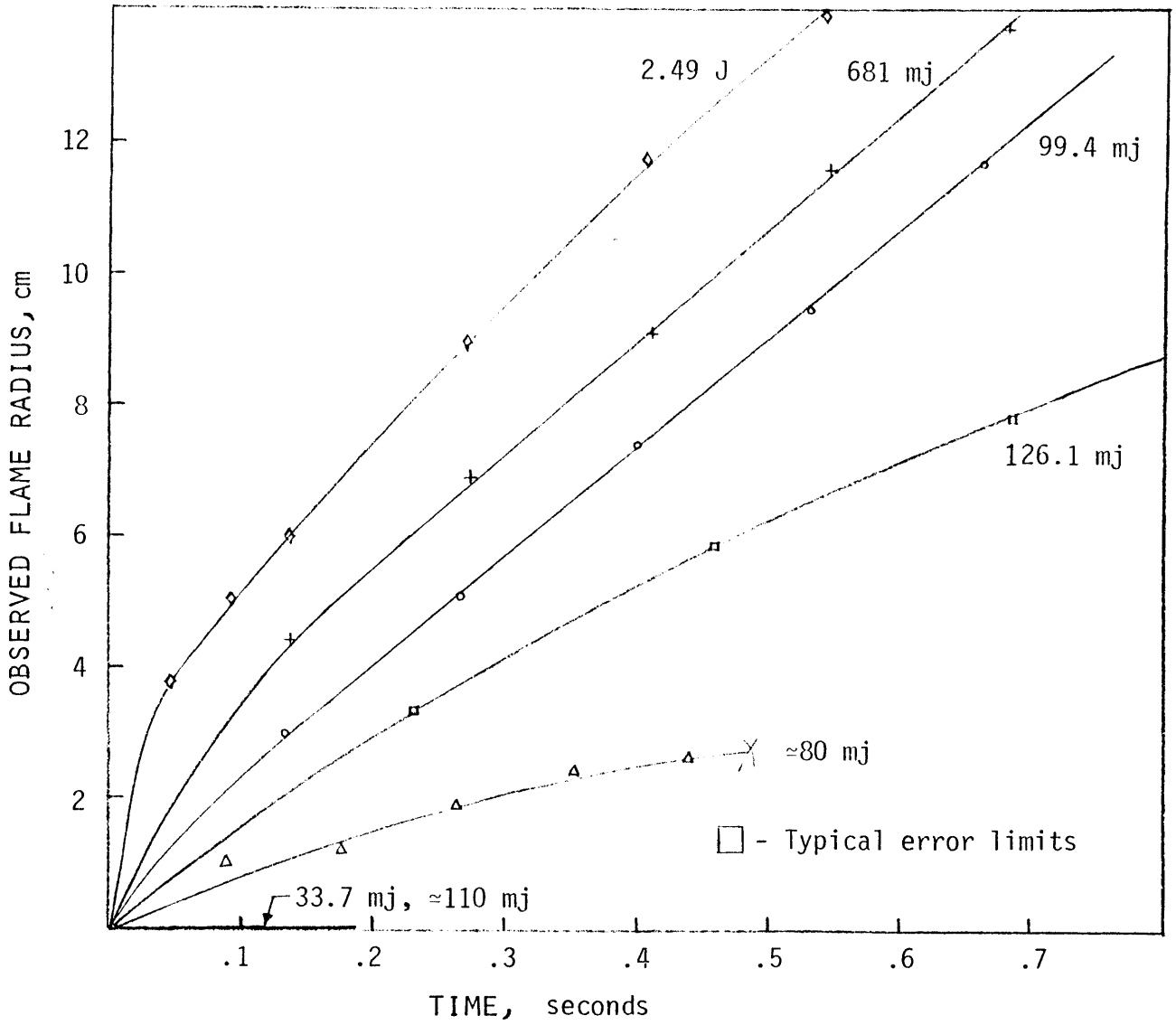

Figure 4-15e. Observed flame radius vs. time for various spark energy inputs
Mixture: 4.45% methane in air at 100 Torr total pressure

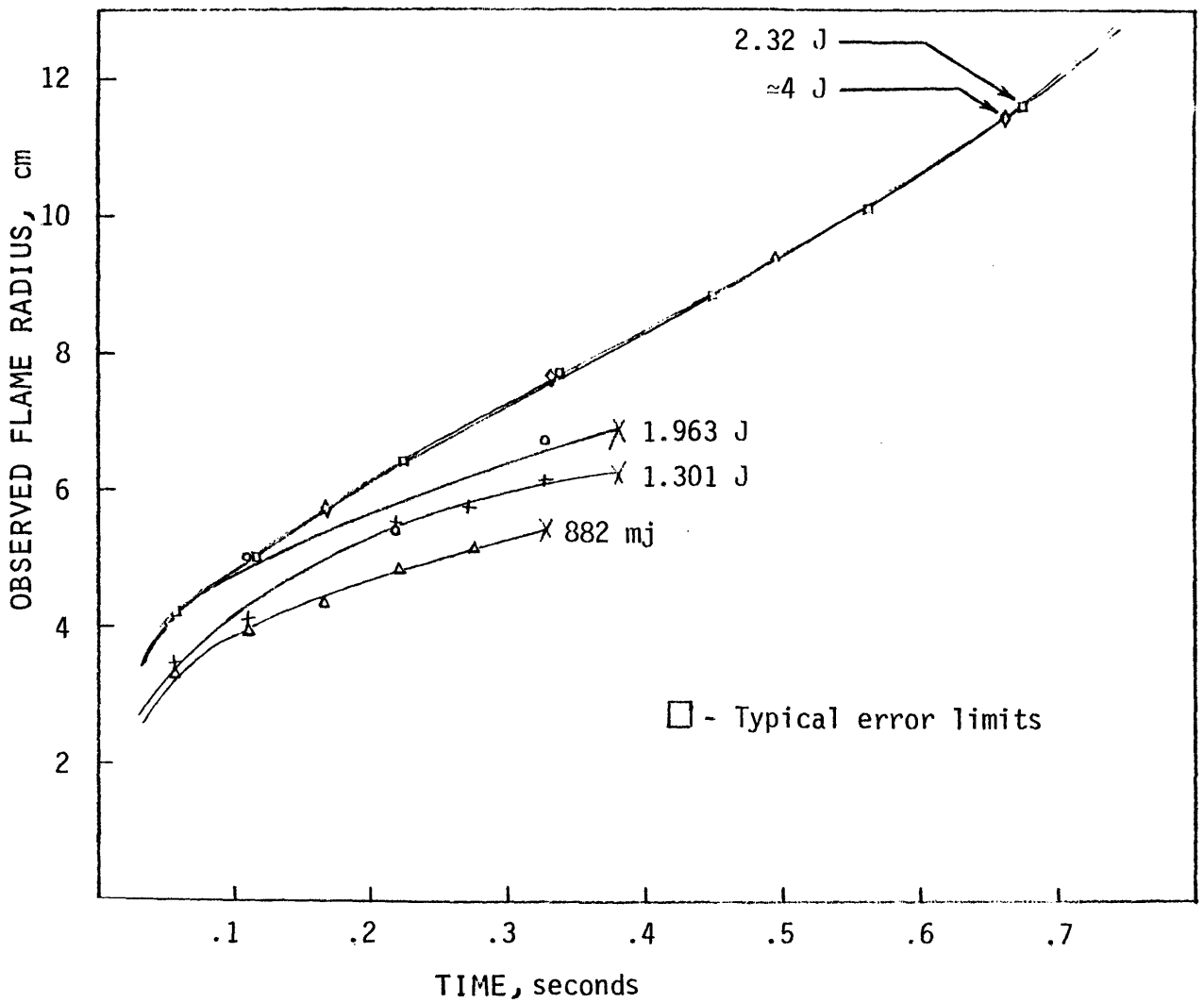

Figure 4-15f. Observed flame radius vs. time for various spark energy inputs
Mixture: 4.42% methane in air at 100 Torr total pressure

temperatures of 23 ± 1°C are presented because the zero-g near-limit flame behavior was very sensitive to the ambient temperature (section 4.2.2). It is clear from these plots that a definite distinction exists between normal flame propagation and SIFD behavior, and to within the limits of accuracy and repeatability of the experiment, all SIFDs for a given mixture follow the same r_b vs. t path and extinguish suddenly at a radius dependent on the initial spark energy. Apparently the flame "knows" shortly after ignition whether it is a normal flame or an SIFD. If it is an SIFD, the effect of the initial spark energy becomes diluted as the flame kernel expands, eventually leading to extinction. Thus, it is clear that SIFD is a completely seperate, distinct, and unique mode of flame propagation. In general, the distinction between normal flame propagation and SIFD behavior becomes noticeable well before extinction. Normal non-ignition for these mixtures extinguished too quickly and in too little distance to be seen on the film record. It appears from the plots that the time dependence of flame radius can be expressed by an equation of the form $r_b = At^{1/2}$, where A is a constant dependent on the combustible mixture. As with normal flame propagation (section 4.3.1), at lower pressures increasing the spark energy resulted in an upward shift in the r_b vs. t plots (Figs. 4-15 e-g) without changing their shape, and so at lower pressures the equation is of the form $r_b = At^{1/2} + B$ except at small times, where B is another constant. At higher pressures this shift was negligible.

The characteristics of SIFDs for other mixtures are shown in Figs. 4-16 a-d. A large number of data points are shown but curves are specified for only a few sets of data points in order to prevent the plots from becoming hopelessly crowded. The reason that some SIFD extinguishment radii are incongruous with those shown in Figs. 4-12 a-d is that data for a variety of ambient temperatures are shown in Figs. 4-16 a-d but not in Figs. 4-12 a-d.

The important point to note about these plots is that for mixtures only slightly leaner than the zero-g flammability limit, the plots of r_b vs. t are very similar to the corresponding curves at the flammability limit. This is further evidence that SIFD is a mode of flame propagation completely seperate from normal flames. Another important point is that for still leaner mixtures an increase in curvature is apparent, eventually coinciding with the r_b vs. t curvature for normal non-ignitions. Which flames are SIFDs and which are normal non-ignitions can be determined from Figs. 4-12 a-d. It can be seen that the r_b vs. t plots are sharply curved for non-ignitions, similar to the logarithmic time dependence that would be expected based on previous results (section 2.2.5.2). Again increasing spark energy causes a net upward shift in the r_b vs. t curves without changing the curvature except in the early stages of propagation.

An interesting feature of Figs. 4-16 a-d is that there is a "no man's land" in r_b - t space for SIFDs and non-ignitions where practically no data points appear, as occurred with normal flame propagation (section 4.3.3). This implies that a certain minimum propagation rate required for any flame propagation, whether it be normal flames, normal non-ignitions, or SIFDs. The boundaries of the "no man's land" are the t-axis and the SIFD r_b vs. t plot for the richest mixture that would produce SIFD behavior. Leaner mixtures exhibit greater curvature in the r_b vs. t plots but do not cross over the boundary because of smaller extinguishment radii for a given spark energy and the upward shift in the r_b vs. t plots for increased spark energy. Apparently stability considerations similar to those that were applicable to normal zero-g flame propagation vs. SIFDs also apply to SIFDs and non-ignitions vs. no propagation at all.

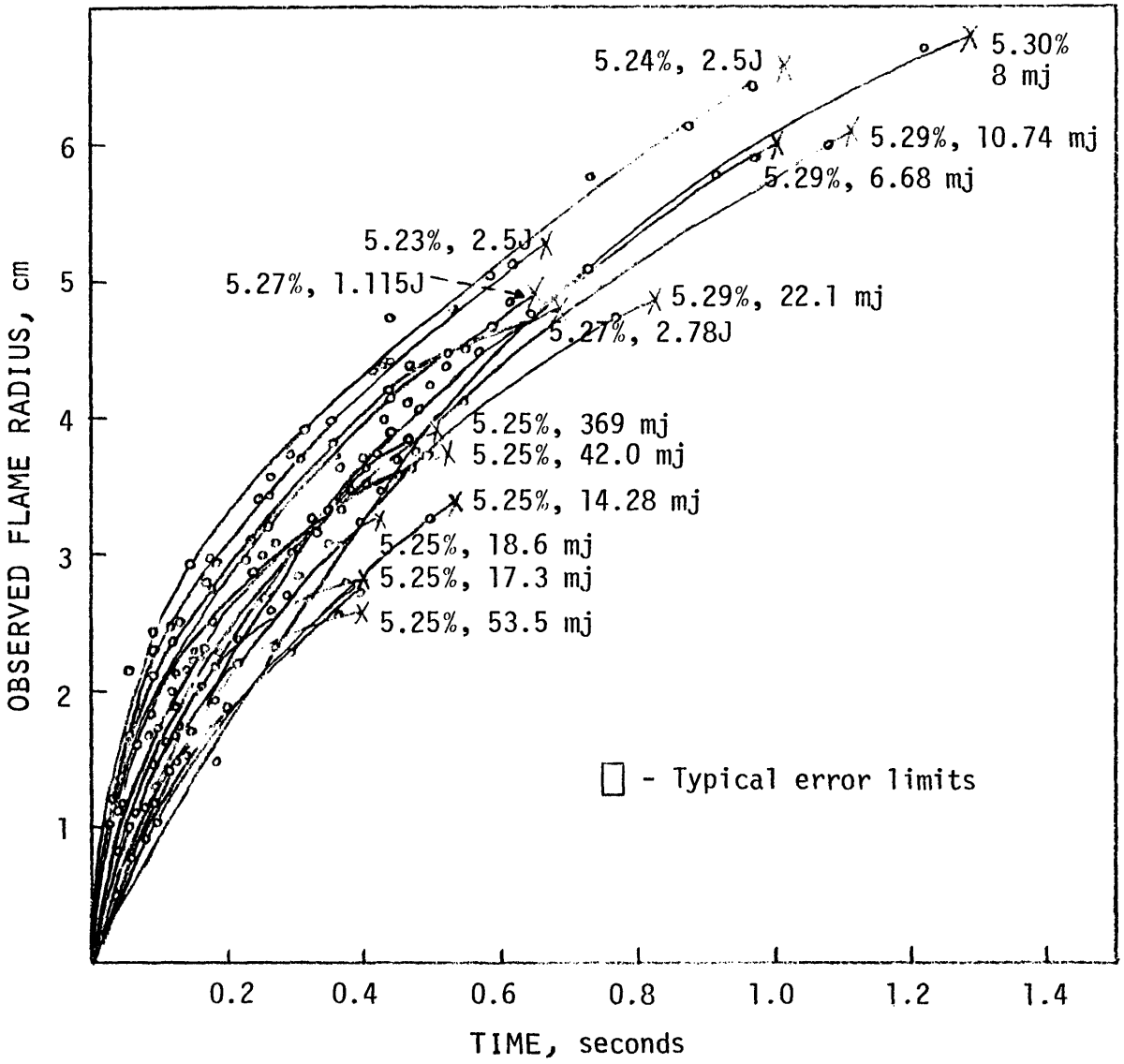

Figure 4-16a. Observed flame radius vs. time for various SIFDs at 1500 Torr total pressure

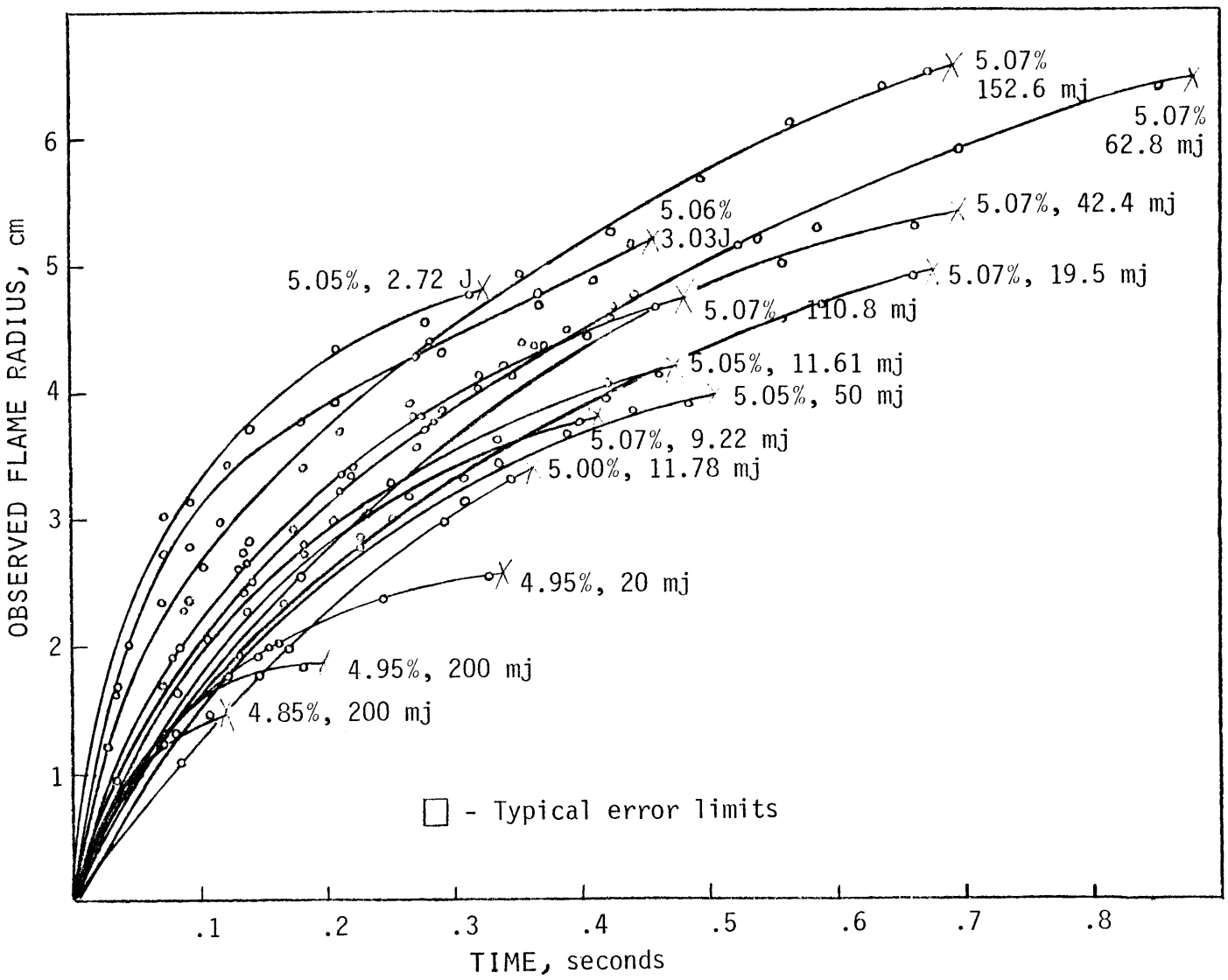

Figure 4-16b. Observed flame radius vs. time for various SIFDs at 760 Torr total pressure

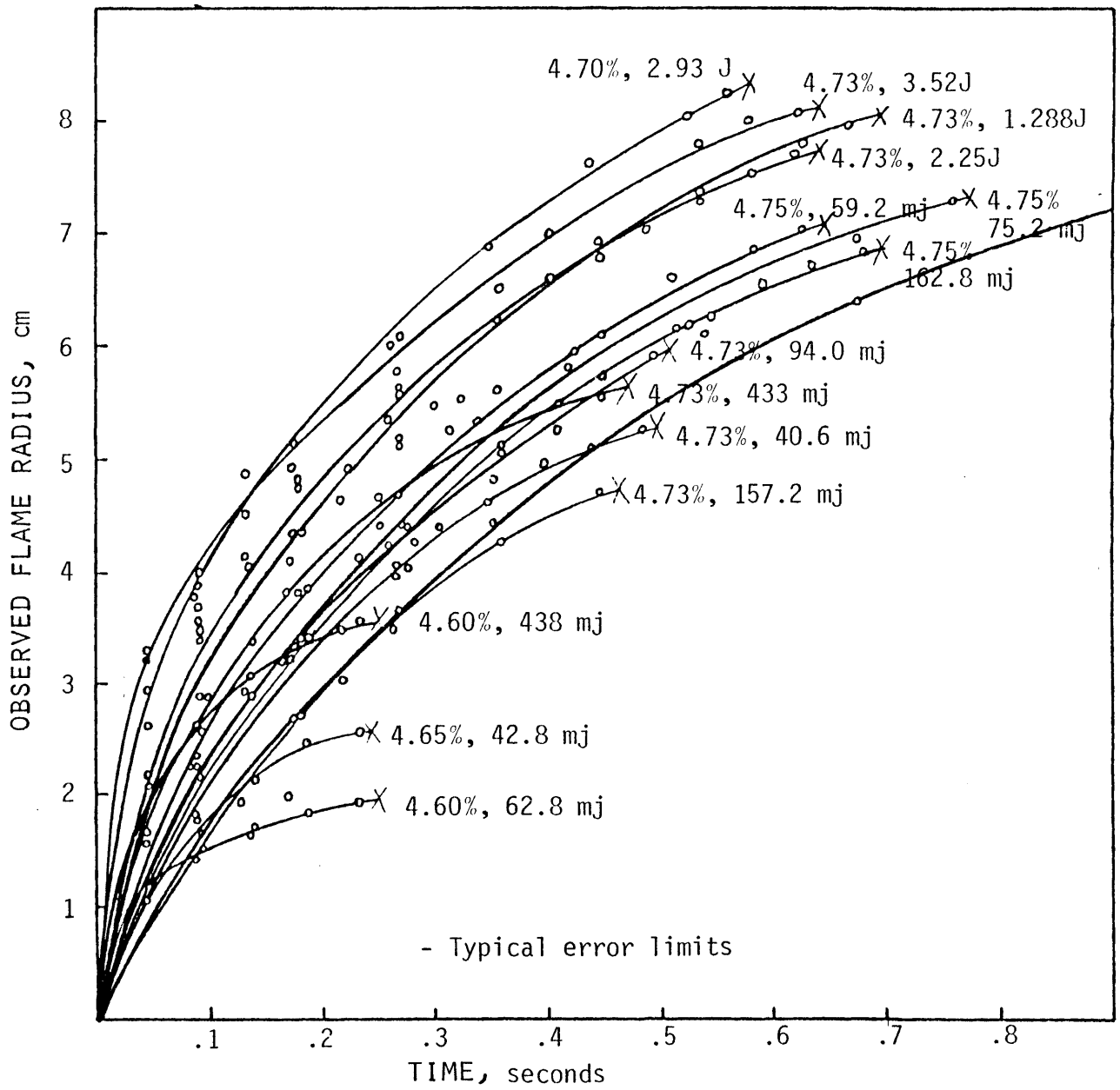

Figure 4-16c. Observed flame radius vs. time for various SIFDs at 250 Torr total pressure

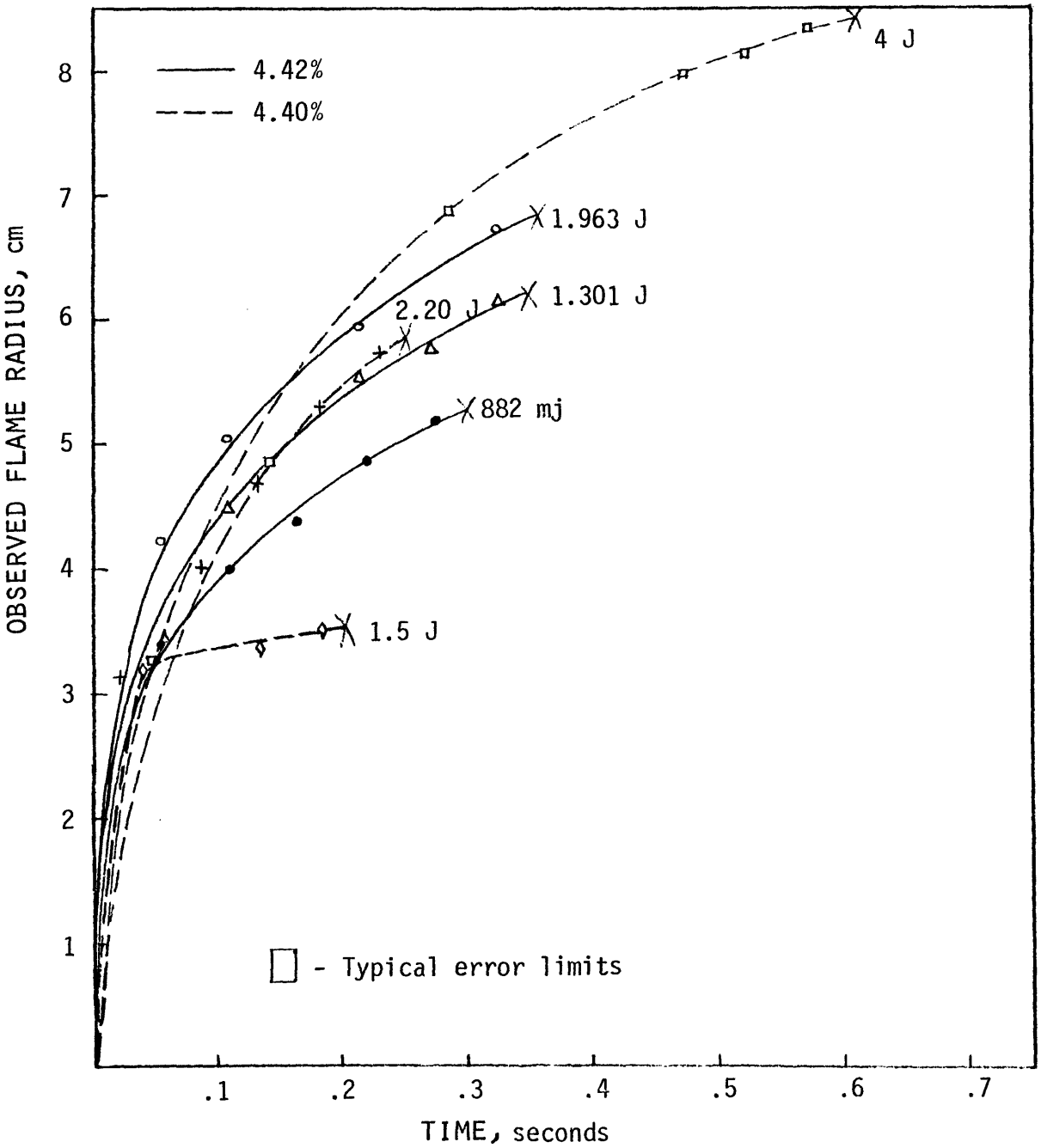

Figure 4-16d Observed flame radius vs. time for various SIFDs at 100 Torr total pressure

4.5.2 Interpretation of results

It is difficult to make comparisons of SIFD behavior observed here with previous investigations because it is not clear that such behavior has been seen before. Apparently no similar mode of flame extinction exists in one-g (section 2.2.3.3). As in the current investigation, Krivulin et al. [15] and Reuss [16] observed continually decreasing propagation rates until the extinction point for sub-limit mixtures in their respective zero-g flammability limit experiments. Krivulin et al. found an extinction radius of 6.5 cm after 1.4 seconds in an 8.8% propane-air mixture with an initial spark of 17 joules burning in a closed bomb at atmospheric pressure. This flame may have been a normal non-ignition and not an SIFD, as shown in table 2-1. In any case, this compares with an extinction time of 0.9 second found in this work for a 6.5 cm SIFD in a lean methane-air mixture at atmospheric pressure (Fig. 4-15c). The propagation rate in the experiment of Krivulin et al. was decreasing roughly linearly with time, as compared to inverse square-root relationship found in the current investigation. Reuss [16] found that extinction of a 5.10% methane-air mixture burning in a SFLT in zero-g required more time than the duration of free-fall (2.2 seconds), but that extinguishment of 4.98% to 4.77% mixtures took place after 8-10 cm of flame travel. It is difficult to estimate the effective ignition energy for Reuss' experiment but the fact that the extinction lengths (as opposed to extinction radii in the current investigation) are so similar for these different mixtures suggests that the effective ignition energy was adquate to put the resulting combustion into a regime corresponding to the "fold-over" regime (section 4.4.1) in the current investigation. On the other hand, the 5.10% mixture almost certainly would have been exhibiting behavior corresponding to the SIFD behavior in this work had the flame extinguished as Reuss expected it

to if more zero-g time had been available. He did not state the temporal dependence of flame propagation velocity other than to say that the velocity was decreasing with time. As with flammability limits and burning velocities, these results for extinguishment of non-flammable mixtures in Reuss' experiment are in complete agreement with the results of the current investigation to the extent that comparisons are valid, within the limits of experimental error. Also, this shows that SIFDs can be ignited by a normal flame, the ignition source in Reuss' experiment, and not just a spark, as was the case in this work.

All of the above comparisons point to the conclusion that SIFD behavior can exist for different experimental apparatus, fuels, and ignition sources, but the evidence is by no means decisive. It certainly lends further credibility to the notion that in zero-g, combustion properties are mostly independent of the experimental apparatus, even for near-limit and sub-limit mixtures, and that the zero-g flammability limit is a more "fundamental" limit than any limit determined in one-g.

It should be noted that all of the observed results were thermally consistent in the sense that increasing spark energy, fuel concentration, or ambient temperature for these lean mixtures resulted in an increase in the amount and/or rate of the resulting propagation. This was true for flammability limits, burning velocities, and minimum ignition energies as well as SIFDs. While the degree of change varied in some unusual ways under certain conditions, the trends were monotonic and in the expected directions. This suggests that there are no phenomena present that run completely contrary to conventional combustion wisdom.

The possibility exists that extinction of SIFDs is followed by a non-luminous chemical reaction which continues for some distance past the

point of extinction. This is possible because the film can only detect luminous (light-emitting) chemical reactions. While a non-luminous reaction does not satisfy the classical defintion of a flame, it could still produce some effects similar to normal flames. Temperature measurements in extinguishing SIFDs would be necessary to determine if post-extinguishment behavior included some chemical reaction or only normal thermal conduction. Because the beginning of the reaction zone corresponds closely to the luminous zone in hydrocarbon-air flames (section 2.1.1), significant non-luminous chemical reaction is unlikely.

It appears that for SIFD propagation $r_b \sim t^{1/2}$, or $r_b/t^{1/2}$ = constant, which is of the same form as the similarity parameter for thermal conduction, $r_b/(\alpha t)^{1/2}$ = constant, where $\alpha = k/\rho c_p$, the thermal diffusivity. This invites exploration to see if a thermal conduction similarity parameter for SIFD propagation can be found. The results are shown in table 4-10. The values of α are taken at the average of the burned and unburned gas temperatures at the zero-g flammability limits, and the values of r_b^2/t are taken from Figs. 4-15 a-f. Table 4-10 shows that the thermal conduction similarity parameter is not constant for SIFDs, but decreases slowly with decreasing pressure. While this analysis is certainly too simplistic, it suggests that factors other than thermal conduction are important, such as molecular diffusion and chemical reaction. The former is closely related to thermal conduction since the Lewis number, which is the ratio of thermal to molecular diffusivities, is about unity for many flames [31, 33, 68]. Because of this, it is more likely that the pressure effects on chemical reaction rates account for the dissimilarities of SIFDs at varying pressures.

Another interesting feature of Figs. 4-15 a-f is that for mixtures close to the zero-g flammability limit the ratio of the distance required for

Pressure, Torr	α, cm²/sec	r_b^2/t, cm²/sec	$r_b/(\alpha t)^{1/2}$
1500	.743	36.0	6.96
760	1.41	50.6	5.98
250	4.05	71.6	4.20
100	9.57	98.0	3.20

Table 4-10. Thermal conduction similarity parameter for SIFD behavior as a function of pressure.

---

steady-state flame development to the estimated flame thickness (section 4.3.2) is about 20 at 1500 Torr, 15 at 760 Torr, 6 at 250 Torr, and 3 at 100 Torr. Such large ratios at high pressures are contrary to conventional combustion wisdom (section 2.2.5.2) which says that this ratio should be a small number and relatively constant with respect to the state of the unburned gas. Apparently at high pressure a change in the mechanism of flame development occurs as the zero-g flammability limit is approached. This occurs even for mixtures richer than the point where the zero-g MIE increases suddenly and dramatically (section 4.4.1).

In summary, the following sequence of zero-g flame phenomena occurs with decreasing methane concentration as the zero-g flammability limit is approached from the "flammable" side: The first sign of dramatic change occurs when the distance required for steady-state flame development from the ignition source increases rapidly with only a small decrease in methane concentration, despite the fact that the burning velocity has decreased only slightly and the MIE has increased only slightly. This seems to occur because the flame radius vs. time profile must pass around a "forbidden" zone. For 760 Torr total pressure this occurs at about 5.30% methane. The next stage is where the MIE increases drastically despite the fact that the burning velocity has decreased only slightly. For 760 Torr total pressure this occurs at about

5.10% methane. The next stage is where steady-state propagation cannot be achieved, at least with reasonable spark energies, and instead SIFD, an unstable mode of flame propagation, occurs. For 760 Torr total pressure this occurs at about 5.06% methane. For still leaner mixtures the SIFD extinguishment radius decreases, eventually coinciding with that of normal non-ignition. For 760 Torr total pressure this occurs at about 4.7% methane. For still leaner mixtures only normal non-ignition phenomena is observed.

While it is not possible at this point to determine the cause of SIFD behavior, it is possible to infer some effects that are not responsible for SIFD. SIFD behavior almost certainly could not be cause by heat loss because of the sensitivity of SIFDs to initial spark energy. For example, it is inconceivable that the difference between 7 and 10 millijoule sparks could cause the difference between an SIFD with a 490J energy release and normal flame propagation because of heat losses. The extra 3 millijoules of spark energy would be vastly outweighed by the change in heat loss due to any number of random factors such as slight variations in fuel concentration or ambient pressure and temperature, yet the extra 3 millijoules were consistently needed to obtain normal flame propagation. The same argument also applies to the effect of spark energy on SIFDs of varying extinguishment radius. Also, SIFD failure was spherically symmetric (except for the few cases previously mentioned), which would not be the case if SIFD failure was caused by conductive heat loss to the spark electrodes or flame detectors. In this case, flame failure would occur near the heat sink first and spread outward. In addition, the SIFD propagation rate was always decreasing with time, well beyond the time and distance where the initial spark could have had a direct effect, despite the fact that the surface area to volume ratio of the flame kernel was decreasing. For almost any conceivable heat loss mechanism the

rate of heat loss would be dependent mostly on the flame surface area, and the total heat capacity of the burned gas is proportional to its volume. Thus, with a decreasing surface area to volume ratio, the effect of heat loss should be decreasing as the flame radius increases. Still, the SIFD propagation rate decreased with increasing flame radius, an unlikely situation if SIFDs could be attributed to heat loss. All of this evidence further reinforces the belief that the zero-g flammability limits, SIFDs, and near-limit flame behavior are not caused by heat losses.

It is clear that SIFD behavior is not related to the pressure and temperature rise in the vessel during combustion. The SIFD extinguishment radius is extremely sensitive to spark energy and fuel concentration, which would not be the case if extinguishment were caused by the pressure and temperature rise. SIFD failure almost always occurred before the effects of rising pressure and temperature became significant, as was shown in section 4.2.2, and analysis showed that flame failure should have been less likely to occur, not more likely, as the combustion progressed. Still more significantly, the difference between SIFD and normal flame propagation appears well before the extinction of SIFDs, which is long before the effects of finite vessel size can be "felt" by the flame, as was shown in the previous section. All of these facts show that there is simply no reason to believe that any of the observed flammability limits, SIFDs, or near-limit flame behavior can be attributed to the pressure and temperature rise in the vessel during combustion.

It is apparent that factors such as "flame stretch" or natural convection cannot account for the existence of SIFD, as outlined in sections 4.2.3 and 4.4.2. Because the r_b vs. t paths jump suddenly from one distinct curve to another at the critical values of mixture ratio and spark energy with no

intermediate curve or set of curves, and because of the "brick wall" of ignition energy at the zero-g flammability limit (Figs. 4-12 a-d), it is unlikely that any simple, continuous phenomenon such as those mentioned above could explain the observed propagation and extinction behavior. Indeed, it is quite remarkable that such sharply discontinuous flame phenomena can occur as a result of the supposedly continuous thermodynamic and chemical processes occurring in laminar premixed gas flames. Of all the possible causes of flammability limits described in section 2.2.3.4, the only one not eliminated thus far is flame front stability considerations. This appears to be the only effect mentioned in this report which cannot be ruled out as a cause for the flammability limit and SIFD behavior observed in this investigation, and within the limits of the author's imagination offers the only possible explanation for these phenomena.

Evidence was presented in sections 4.3.3, 4.4.2, and 4.5.1 to show that gravity appears to provide a stabilizing force to flame propagation. This implies that in the absence of gravity, a certain stabilizing force is absent and so a combustion-related instability can exist. Still more evidence for such an instability can be seen in Figs. 4-12 a-d. If the zero-g MIE curves are taken as the limits of stability in spark energy-fuel concentration space, combinations of spark energy and fuel concentration outside the stable region can be considered perturbations near a stability limit. The results show that the amount of unstable propagation (i.e. the SIFD extinguishment radius) is closely related to how near the perturbation is to the stability limit, with more unstable propagation for perturbations closer to the limit. The one-g MIE curves represent a completely different type of stability limit which has been observed countless times and is much better understood.

Exactly what the supposed instability is and what causes it is a mystery. Based on the experimental evidence, it appears that the instability is related to thermodynamic considerations such as heat transfer and chemical reaction and not mechanical considerations such as fluid flow. Solid obstructions (flame detectors, spark electrodes) did not cause any SIFD failures, even local ones, but extinguishment was very sensitive to spark energy and the state of the unburned gas, particularly the ambient temperature. Also, the stability limit seemed to be identical for spherically symmetric three-dimensional propagation and quasi-one-dimensional propagation (section 4.2.3). Beyond this it is difficult to say much about the instability despite all the clues, such as burning velocity at the stability limit ($S_{u,lim} \sim P^{-1/3}$), the temporal dependence of flame radius ($r_b \sim t^{1/2}$), the effects of varying spark energy input, and the "no man's land" for SIFD and normal non-ignition. Perhaps the most reasonable "intelligent" guess for a cause of this instability would be a previously unseen and unpredicted interaction between the thermal conduction and chemical reaction processes occurring in these flames, but this is only conjecture and without more details does not provide an explanation for the various characteristics of the instability as mentioned above.

It is also difficult to say what the stabilizing factor is in one-g propagation. Natural convection forces the burned gases into the fresh, unburned mixture and deforms the developing flame kernel into what is probably a more stable shape. Whether the additional stability in one-g is due to the resulting increase in heat transfer, molecular species exchange, turbulence, or some other unknown factor is unclear. Additional information on the zero-g extinguishment phenomena is needed in order to determine what missing factor

accounts for the limit of zero-g flame stability, and thus the additional one-g stability.

While there is at least one theory [62] which predicts stability limits for laminar premixed gas flames, generally favored are those theories which show that all steadily propagating laminar flames are stable (section 2.2.5.4), and the author finds these theories more believable despite experimental evidence to the contrary. As explained in section 2.2.5.4, the theory which does predict stability limits for laminar premixed gas flames appears to predict that virtually all hydrocarbon-air flames with the unburned gas at room temperature are unstable, and so does not provide a valid model for comparison with the experimental data. The author did not provide enough information on transient conditions to determine whether SIFD or similar behavior could be predicted.

In order to find out more about SIFDs, the most useful continuation of this work would be to make temperature measurements in developing and extinguishing normal flames and SIFDs. The experimental results have shown that a flame somehow "knows" even in the early stages of its development (cf. Figs. 4-15 a-f) whether it is a normal flame or an SIFD, and if it is an SIFD, what its extinguishment radius will be. If one believes in a deterministic universe, there must be some difference in the state of the system after ignition for SIFDs and normal flames. The best way to derive some information about the state of the system is to make temperature profile measurements at various times in the development of the normal flame or SIFD. The flame temperature at any given point is a good indication of the degree of completion of chemical reaction at that point [30, 31, 33]. Temperature gradients also indicate the direction and magnitude of conductive heat transfer. It would be of great value to know how the temperature profiles in

SIFDs compare with those in developing normal flames in the same mixture, whether the temperature profiles are smooth or discontinuous, and whether or not the temperature near the spark origin decreases after the passage of the luminous zone. It is almost certain that at least some portion of the SIFD profiles are at a lower temperature than the corresponding points in normal flames, otherwise it is difficult to imagine how SIFDs could propagate slower than normal flames. A sudden break in the temperature SIFD profile could indicate the failure of a certain chemical reaction or set of reactions. A decrease in temperature near the spark origin over time indicates a heat loss, although this is very unlikely based on the experimental evidence.

Chemical species concentration measurements would provide much of the same information as temperature measurements along with some new information, but are much more difficult to implement experimentally. Analysis of the combustion products after the drop and comparison with the volume of SIFD combustion measured from the film record would determine how complete combustion was overall in SIFDs, but would yield no information on the temporal or spatial variation of the degree of reaction completion. If such measurements were still considered useful, it would probably be best to measure the product (CO_2 and H_2O) concentrations in the final mixture because the reactant (CH_4 and O_2) concentrations would change only slightly for small SIFDs, thus making accurate measurements difficult. Of course this would mean that the initial CO_2 and H_2O content of the mixture would have to be monitored carefully. Because the H_2O had a tendency to condense on the combustion vessel walls, probably the CO_2 content would be the simplest and most reliable gauge of the degree of completion of reaction. Combustion vessel pressure measurements during combustion in free-fall would be useful because, with good approximation, at any time during combustion the fraction of the total

pressure rise due to combustion is equal to the fraction of fuel consumed [30]. On the other hand, this information can probably be deduced from flame temperature measurements and so is not as important.

Another interesting addition to the current investigation would be to extend the tests to higher ambient pressures. Because SIFD behavior was most pronounced at higher pressures and non-symmetric SIFDs were found only at the highest pressure investigated, it is possible that even larger and more unusual SIFDs could be found at still higher pressures.

It is easy to see why SIFD behavior has not been observed before, at least not in detail. At least three experimental conditions are required to observe SIFD behavior: 1) zero-gravity, 2) a carefully controllable, measurable source of ignition energy, and 3) one must look very near the zero-g flammability limit using a very accurate, repeatable gas measuring and mixing system. Rarely have even two of these three requirements been met in a single experiment, and never before have all three come together in an investigation.

Chapter 5. Summary and conclusions

5.1 Flammability limits

The flammability limits determined in this experiment were in good agreement with previous investigations to the extent that such comparisons were valid. Particularly significant was that the observed zero-g flammability limit at atmospheric pressure was in excellent agreement with a previous zero-g experiment using a completely different apparatus. It is clear that gravitational effects on combustion, particularly on flammability limits, were less significant at reduced pressures, and that at reduced pressures all mixtures were more "flammable" by almost any reasonable criteria.

The one-g upward flammability limit in an unconfined system is not a fundamental limit but rather a practical limit where the burning velocity is so low and the minimum ignition energy so high that normal propagation is difficult to initiate and gravity-induced self-destructive convection currents usually lead to extinction of the developing flame. While this limit is not well-defined, in practice both the burning velocity and minimum ignition energy change very rapidly near a critical concentration, at least for methane-air mixtures, and so different interpretations of the limit mixture in an unconfined system will vary only slightly, e.g. 4.6% methane to 4.8% methane in air at atmospheric pressure.

The one-g downward flammability limit is caused by the inability of the flame to propagate downward against the buoyancy of its burned gases when the burning velocity drops below a critical value. The downward flammability

limit is a function of the arbitrarily chosen limit criteria but is always closer to the stoichiometric concentration than the one-g upward flammability limit. In the current investigation the limit burning velocity was only slightly affected by ambient pressure, but other apparatus may yield different results. For downward flammability limit studies other methods with simpler fluid flow patterns should be used, such as the flat flame burner or Standard Flammability Limit Tube.

Based on the findings of this and other investigations on one-g upward flammability limits, it appeared that very lean, slow burning flames could be expected in zero-g. This was not found to be the case; instead, a well-defined, nonarbitrary flammability limit was found in zero-g. Two previous investigations had reported such a result but did not study the phenomena in detail. The zero-g limit was always between the one-g upward and downward limits at the same pressure. The zero-g flammability limit is the only limit that can be construed as non-aerodynamic, that is, where there is no fluid motion generated by external factors such as gravitational forces or solid boundaries. That such a limit exists at all shows the inadequacy of some flammability limit models which attempt to predict limit based solely on gravity-induced natural convection. Based on a comparison with one of the previous zero-g flammability limit investigations, it appeared that the limit mixture and limit burning velocity were independent of the experimental apparatus, which is rarely true in one-g. The limit burning velocity for lean methane-air mixtures between 50 and 1500 Torr ambient pressure is given by the equation $S_{u,lim} \simeq 1.45\ P^{-0.35}$, or approximately $S_{u,lim} \sim P^{-1/3}$. The significance of this limit burning velocity could not be explained. For sub-limit mixtures some flame propagation was observed but was unstable and extinguished after some period of time. This phenomenon was named "sudden

infant flame death", or SIFD, and was found only in zero-g. SIFD ha been hinted at in the two previous zero-g flammability limit investigations but again had not been carefully studied nor had its significance been appreciated.

In this investigation zero-g flammability limits and SIFD behavior were studied carefully for the first time and so represent the major contribution of this work.

A number of effects thought to cause flammability limits in some systems were ruled out as potential causes of the zero-g flammability limits observed here. The foremost amongst these is heat losses. While superficially heat losses might seem to provide a simple, neat answer, the experimental evidence overwhelmingly showed that this was not the case. There was simply no convincing evidence that the observed zero-g flammability limits could be attributed to any conceivable form of heat loss, and there was a great deal of evidence to support the contrary notion. This could be inferred from the experimental data alone, plus there was little or no agreement between the data and previous analytical and experimental models of flammability limits caused by heat losses. It was also shown that the zero-g limits could not be attributed to the rising pressure and temperature in the closed vessel during combustion, to geometrical factors (i.e. "flame stretch"), to effects associated with the pressure drop across the flame front, or to the kinetic energy change of the flowing gases due to combustion. The zero-g flammability limit also could not be related to a requirement for a constant equilibrium concentration of some molecular species or group of species at the limit.

The only imaginable cause for a zero-g flammability limit that could not be eliminated based on the experimental data was a flame instability. While there does not appear to be a flame instability model available in the

literature that is even marginally satisfactory in explaining the observed results, all the evidence suggested that zero-g flames were limited by stability and that gravitational forces aided stability, allowing a wider range of mixtures to propagate in a gravitational environment. The ramification of this stability limit was SIFD, an unstable mode of flame propagation.

5.2 Burning velocities

The burning velocities measured in this investigation were in general slightly lower than those determined by the most widely accepted methods, but in very good agreement with other results using the same method as used here. Particularly significant was that the zero-g near-limit burning velocities at atmospheric pressure were in excellent agreement with a previous zero-g experiment using an entirely different experimental apparatus. Apparently near-limit flame propagation in zero-g is mostly independent of the experimental apparatus, which is rarely true in one-g. Agreement with one-dimensional adiabatic models of methane-air burning velocities was also good. For fast-burning mixtures both one-g and zero-g flame propagation was spherically symmetric and the one-g and zero-g burning velocities measured in this experiment were identical. For slow-burning mixtures interpretation of one-g observations to obtain burning velocities is difficult because of severe distortions of the flame front caused by natural convection, so only zero-g observations can be used to obtain burning velocity data for these mixtures. These data constitute a major contribution of this work. The burning velocities for these slow-burning mixtures down to the zero-g flammability limit were exactly as expected based on the aforementioned models and

extrapolations of previous one-g data, which indicates that the current understanding of the phenomenon is substantially valid down to near the zero-g flammability limit. At the zero-g flammability limit the burning velocity versus fuel concentration curve is abruptly truncated, again suggesting a stability-related limit.

Analysis showed that the effect of nonzero flame thickness on the values of burning velocity calculated here was probably negligible except for near-limit mixtures at the lowest ambient pressure investigated. Other analyses showed that neither the effects of rising pressure and temperature during combustion in the closed vessel nor heat losses had any significant effect on the measured burning velocities.

It appeared that if the burning velocity for a given mixture were too low, the flame radius r_b versus time t from ignition plot would pass into a "no man's land" in r_b - t space where steady flame propagation was not allowed. Mixtures which could not "avoid" the "no man's land" exhibited the unstable SIFD propagation instead. The exact cause of the "no man's land" remains a mystery.

5.3 Minimum ignition energy

Agreement between the minimum ignition energies measured in this work and in previous investigations was satisfactory to the extent that such comparisons were considered valid. Agreement with elementary ignition theory was poor and no detailed theory for methane-air ignition is available. One-g and zero-g minimum ignition energies were identical except extremely near the zero-g flammability limit, where the zero-g minimum ignition energy suddenly increased dramatically. It cannot be stated positively whether the zero-g

flammability limit was truly a flame propagation limit or an ignition limit, but the increase in minimum ignition energy near the limit was so drastic that for all practical purposes it was a flame propagation limit. It is very interesting that the zero-g burning velocity did not decrease drastically near the zero-g flammability limit as might be expected for these mixtures because their minimum ignition energies increased drastically; in fact, the effect of fuel concentration on the zero-g burning velocities was in much better accordance with the effect of fuel concentration on the one-g rather than the zero-g minimum ignition energies. In zero-g, for spark energies between the one-g and zero-g minimum ignition energies, SIFD propagation was observed. The minimum ignition energy for SIFD propagation, even for mixtures which did not exhibit steady flame propagation under any circumstances, was the same as the one-g minimum ignition energy.

The above set of facts suggested that the one-g minimum ignition energy was the more "fundamental" value and added further credence to the conclusion that gravitational forces are a stabilizing factor in the ignition and propagation of slow-burning mixtures.

Agreement between an existing model of the effect of gravity on minimum ignition energies and the results of this investigation was nonexistent, although it was not certain that the model was directly applicable.

5.4 Sudden Infant Flame Death (SIFD)

In this investigation a new type of combustion phenomena, SIFD, which can only be seen in zero-g has been discovered and analyzed. SIFD represents an intermediate range of unstable combustion phenomena between the limits of normal flame propagation and normal non-ignition. One-g propagation under the

same conditions, or any conditions, was definitely not SIFD. The results of two previous zero-g experiments suggested that SIFD exists for other fuels and other experimental apparatus, but the data were much too sketchy to draw firm conclusions. In SIFD propagation the flame radius increases in proportion to the square root of the time interval from ignition, unlike the linear dependence in normal flames and the logarithmic dependence in normal non-ignition. The distinction between SIFDs and normal flames appears well before SIFD extinction. Extinction is quite sudden and fairly predictable. Unlike normal non-ignition, the chemical energy released before extinction of SIFDs is orders of magnitude greater than the spark energy input in many cases. The zero-g minimum ignition energy versus fuel concentration curve can be considered a stability limit and the amount of SIFD propagation decreases with increasing distance from this stability limit. For a given mixture, all SIFDs follow the same flame radius vs. time curve and for this mixture the extinguishment radius increases with increasing spark energy input. The curvature of the flame radius vs. time curves increases slightly and the SIFD extinction radius decreases drastically with decreasing fuel concentration in lean mixtures. As a result, a "no man's land" in r_b - t space, similar to that found for normal flames (section 5.2) was found for SIFD and normal non-ignition as well. Again the reason for the existence of the "no man's land" is not clear.

SIFD was seen at all pressures investigated but was much more pronounced at higher pressures, at least in the sense of the ratio of energy liberated by chemical reaction before extinction to the initial spark energy (E_s/E). All SIFDs were spherically symmetric except for a few unusual cases at the highest pressure studied. How non-symmetric propagation could occur in zero-g was not evident. Either these non-symmetric flames were higher modes of SIFD

propagation or were merely caused by random disturbances in the ignition process, but there was little evidence favoring one idea over the other.

Because SIFD is the ramification of the observed zero-g flammability limits, none of the possible effects listed in section 5.1 that were ruled out as causes of the zero-g flammability limits could be construed as causes of SIFD propagation and extinction. Again only a flame front instability seems capable of explaining the observed behavior, and gravity seems to add a certain stability which allowed normal flame propagation to be observed for a wider range of mixtures in one-g, since SIFD propagation was not observed in one-g. The results suggested that combustion in SIFDs was nearly normal and complete; that the failure of SIFDs was more related to an inability of the flame to propagate into the unburned gases than an inability to cause chemical reaction in the gases it consumed; and that the instability was more thermal than mechanical or geometrical in nature. A conjecture was made that the instability was due to a previously unseen and unpredicted interaction between the thermal conduction and chemical reaction processes occurring in laminar premixed gas flames. More information, particularly on the temperature profiles in developing flames and SIFDs, is required to confirm or discredit these notions. The inability to explain why a limit of stable flame propagation exists in zero-g and why the resulting instability (i.e. SIFD) has the characteristics as described here is the major shortcoming of this work.

It is not clear what the stabilizing factor is in one-g propagation. Probably it is related to the increase in heat transfer, molecular species exchange, turbulence, or some other transport property between the burned and unburned gases. More information on the causes of the zero-g instability is needed to clarify this matter.

It seems intuitively unlikely that any model based only on the normal continuous flame processes of thermal conduction, molecular diffusion, and chemical reaction would be capable of predicting and explaining the highly discontinuous flame behavior and flame instabilities observed in this investigation. It would appear that a new element is required, but what that element should be is not obvious.

A question arises as to the importance of studying and analyzing SIFD propagation when it occurs only for a very narrow range of conditions (Figs. 4-12 a-d and 4-13). The zero-g flammablilty limits discovered in this investigation represent a significant phenomenon which affects all mixtures outside well-defined concentration limits and apparently cannot be explained by any conventional combustion wisdom. Since the SIFD phenomenon is responsible for the existence of (or perhaps is the result of) these limits, detailed study of SIFD is necessary if one hopes to understand these limits.

5.5 Fire safety in spacecraft

The results have shown that one-g flammability tests for quiescent premixed gases are an acceptable, although somewhat conservative, measure of the zero-g flammability hazards of these mixtures except for a narrow range of fuel concentrations. In the case of lean methane-air mixtures at atmospheric pressure (cf. Figs. 4-5 and 4-12b) the flammability hazards are virtually identical down to 5.6% methane. For mixtures between 5.6% and 5.07% methane the flammability hazards are greater in zero-g than in one-g. For mixtures leaner than 5.07% methane the flammability hazards are greater in one-g, although they are virtually nil below 4.7% methane in both one-g and zero-g.

In practice combustible premixed gases per se are rarely found in orbiting spacecraft, except perhaps in propulsion systems, so these results are generally not directly applicable. More common in spacecraft are flammable solid materials. With the completion of this study, the effects of gravity on all of the burning processes for many solid materials, namely heating, vaporization, mixing, ignition, and combustion, are known. The effects of gravity on the latter two processes were not previously known. It is probably now possible to form a model for the effects of gravity on the burning of solid materials by piecing together the effects of gravity on all of the individual processes. This would be of significant value to the spacecraft designer.

Since the actual combustion of solid materials generally takes place in the gaseous phase and most fire extinguishment systems use a gaseous flame retardant, a study of the effects of gravity on the effectiveness of flame retardants in premixed gases would have direct applications to the assessment of spacecraft flame retardant effectiveness. The U.S. Space Shuttle has such a fire extinguishment system but apparently its effectiveness in zero-g has not been tested. Of course the system has been tested in one-g and the results of the current investigation show that this is probably an adequate test for zero-g as well, but some zero-g testing would still be useful for verification.

5.6 Recommendations for future work

Despite a large collection of data available on near-limit flame behavior in one-g, several key experiments have not been performed. It appears that most one-g flammability limits can be related to a minimum burning velocity

requirement, yet few experiments have actually measured these limit burning velocities. A few measurements of limit and near-limit burning velocities as a function of pressure in tubes or on flat-flame burners could add significant new insight into the causes of one-g flammability limits. Similar measurements for varying tube radius, ambient temperature, and different fuels would also be useful.

The next crucial task for drop testing is to make temperature measurements in developing normal flames and SIFDs. This information would go a long way towards explaining the cause and nature of SIFD propagation, allow computation of correction factors for burning velocity calculations, and detect the presence of any non-luminous chemical reactions. Measurement of chemical species concentrations in the flame fronts would be equally or more useful but much more difficult to implement, and pressure or final combustion product concentration measurements would be easier to implement but would not yield nearly as much information as temperature measurements. It would also be interesting to investigate flame propagation at higher pressures in order to look for other non-symmetric SIFDs. While all indications are that the same zero-g combustion phenomena would be observed with fuels other than methane, it is still important to verify this. It would also be useful to perform more zero-g tests in other experimental apparatus in order to verify the conclusion that near-limit zero-g propagation and extinction phenomena are mostly independent of the experimental apparatus. Some tests should be made with fuels similar in chemical nature to methane but with different diffusivities in air, such as ethane and propane, and some tests should be made with fuels that have reaction mechanisms very different from methane, such as hydrogen and carbon monoxide. Finally, the effect of various flame retardants on the

zero-g combustion phenomena observed in this study should be investigated in detail.

A larger combustion vessel and more zero-g time are needed to study non-symmetric SIFDs, to search for larger symmetric and non-symmetric SIFDs, and to extend the results to lower ambient pressures, but this is not possible in the NASA-Lewis 2.2 Second Zero-Gravity Facility. Aircraft flying zero-g trajectories can provide up to 30 seconds of zero-g time, which is probably adequate, but the opportunity for real-time control of the experiment by the operator, a crucial requirement for this type of study, is limited. A Spacelab or Space Shuttle mid-deck flight experiment provides the ideal laboratory because of the unlimited zero-g time available (for the purposes of this experiment) and the opportunity for investigator observation and interaction with an experiment in progress.

The current investigation has shown that the study of laminar premixed gas combustion in zero-g can yield substantial new information and in some cases better understanding of this process. It is therefore quite likely that the study in zero-g of other forms of combustion that are not well understood, for example the surface combustion of coal or similar fuels, would also be productive. The near-term accessilibity of zero-gravity laboratories (e.g. Spacelab, the Space Operations Center, etc.) should facilitate these investigations. The author anxiously awaits such developments in the field.

Appendix A. List of commonly used symbols and acronyms

Symbols

A_f	flame front area
A_t	tube cross-sectional area
c	fuel concentration
C_p	gas specific heat capacity at constant pressure
d	quenching distance
D	tube diameter
E	spark energy
E_a	chemical reaction activation energy
E_{min}	minimum ignition energy
E_s	sensible energy residing in gas volume
g	gravitational acceleration
g_o	earth gravity (980 cm/s)
I	correction factor in burning velocity calculation
k	thermal conductivity
K	dimensionless heat loss parameter
$\dot{m}$	mass flow rate
n	moles of burned gas per mole of unburned gas
n	order of reaction
P	pressure
P_f	final equilibrium pressure in closed vessel
P_o	initial pressure
r_b	flame front radius
r_t	tube radius
r_v	combustion vessel radius
R	ideal gas constant
S_b	velocity of burned gases relative to flame front
S_c	convective gas rise velocity
S_g	velocity of unburned gas in laboratory frame
S_u	velocity of unburned gas relative to flame front
$S_{u,lim}$	burning velocity at the flammability limit
t	time
T	temperature
T_b	burned gas temperature
T_u	unburned gas temperature
T_{uo}	initial unburned gas temperature
$\dot{w}$	chemical reaction rate per unit volume
α	thermal diffusivity
γ	specific heat ratio
δ	flame preheat zone thickness
ΔP	pressure drop across flame front (section 4.2.3)
ΔP	equilibrium pressure drop due to combustion (section 4.2.2)
ΔP	pressure rise due to expanding flame kernel (section 4.2.2)
λ	dimensionless burning velocity parameter
ρ_b	burned gas density
ρ_u	unburned gas density

Acronyms

GRIEF	Gravity's Role on Ignition Energy and Flammability
LPGC	Laminar Premixed Gas Combustion
MAMMAL	Methane-Air Measuring, Mixing, And Loading System
MIE	Minimum Ignition Energy
OTIS	Onboard Timer and Ignition Sequencer
RASCAL	Remote Automatic Spark Controller And Limiter
SFLT	Standard Flammability Limit Tube
SIFD	Sudden Infant Flame Death
SSL	Space Systems Laboratory
VARMINT	Voltage-Amperage Resolver, Multiplier, and INTegrator

Appendix B. Adiabatic flame temperature program

A computer program for calculating adiabatic constant-pressure equilibrium flame temperatures was written based on the algorithm given by Gaydon and Wolfhard [68] and using thermochemical data for equilibrium constants, gas enthalpies, and heats of formation from the JANAF tables [94]. This information is important for calculation of burning velocities and estimation of heat loss effects in the current investigation. In general, the adiabatic flame temperature of any combustible gas mixture is a tradeoff between the heat of reaction between the fuel(s) and oxidizer(s) in the mixture and the heat capacities of the product gases. The complication is that as the temperature of the gas rises, the effects of dissociation of the product gases in equilibrium may become important, and because energy is absorbed in the dissociation process, the final flame temperature is lower than it would be without dissociation. Without considering all the details of the algorithm here, it can be said that the problem becomes one of finding a final temperature that will satisfy two sets of equations, one set of which involves the equilibrium constants of the chemical species involved (which are strong functions of temperature) and the conservation of atoms, and the other set of which involves the heats of reaction and the heat capacities of all the molecular species. In the current program 10 product species were considered: H_2O, O_2, O, H_2, H, OH, CO, CO_2 , N_2 , and NO.

The data in the JANAF tables for equilibrium constants and gas enthalpies were fit to functions of temperature using a least-square-fit routine. The functional form of the equations which produced the best fit of the data was found by trial and error. The equilibrium constants were all of the form

$$\log K_i = a_{i1} + a_{i2}T + a_{i3}T^{-1} + a_{i4}T^{1/2} + a_{i5}T^2 + a_{i6}T \ln(T)$$

where K_i is the equilibrium constant for reaction i, T is the temperature, and a_{i1} to a_{i6} are the least-square-fit coefficients for reaction i. The gas enthalpies are all of the form

$$H_j = h_{j0} + h_{j1}T + h_{j2}T^{-1.5} + h_{j3}T^{-1} + h_{j4}T^{1/2}$$

where H_j is the specific enthalpy of species j and h_{j0} to h_{j4} are the least-square-fit coefficients for species j. The equations for the equilibrium constants fit the data from the JANAF tables to within ±0.5% over the temperature range of 400°K to 3100°K, and the enthalpy equations fit the data to within ±0.2% over the same temperature range.

Without considering the details, the overall scheme of the program is as follows:

1. Guess T_b
2. Guess partial pressure of H_2O
3. Guess the CO_2:CO partial pressure ratio
4. Compute partial pressures of all species
5. If the oxygen to hydrogen atom ratio is incorrect, go to step 3
6. If the sum of the partial pressures of all the gases does not equal the specified total pressure, go to step 2
7. If the change in total enthalpy of the product gases mixture does not equal total heat of formation for all reactions, go to step 1
8. Calculate product to reactant mole ratio and print results

Basically this routine is a triple iteration to solve a large set of equations which can be reduced to three highly nonlinear inseparable algebraic equations in the three unknowns T_b, P_{H_2O}, and P_{CO_2}/P_{CO}. The BASIC computer program, called AUTOTF, is shown in Figure B-1.

In addition to the adiabatic flame temperature determined by Gaydon and Wolfhard's algorithm, it is necessary to find the ratio of total moles of product gas to total moles of reactant gas in order to calculate burning velocities (section 2.2.4.1). This mole ratio is given by

$$n = \frac{M_u}{M_b} = \frac{(\sum_u M_i P_i)/P_u}{(\sum_b M_j P_j)/P_b} = \frac{\sum_u M_i P_i}{\sum_b M_j P_j}$$

where M is the molecular weight, P is the partial or total pressure, the subscripts u and b refer to the overall properties of the unburned and burned gases, respectively, and the subscripts i and j refer to the properties of the individual component gases in the unburned and burned gases, respectively.

The calculated values of T_b and n are shown in table B-1. Execution time on a TRS-80 computer was about 10 minutes per mixture.

```
10 REM  *-----------------------------------------------*
        *         AUTOMATIC CALCULATION OF FLAME        *
        *        TEMPERATURES IN CONSTANT PRESSURE      *
        *          COMBUSTION OF METHANE AND AIR        *
20 REM  *-----------------------------------------------*
30 REM  *      ---CONCEIVED BY DOCTORAL CANDIDATE,      *
        *      PAUL RONNEY, HEAD OF THE G.R.I.E.F.      *
        *      GROUP OF THE MIT SPACE SYSTEMS LAB       *
        *      ---WRITTEN BY STEPHEN ADKINS, CLASS      *
40 REM  *      OF 1984 THANKS TO THE SUPPORT OF THE     *
        *      MIT UNDERGRADUATE RESEARCH OPPORTUNITIES *
        *      PROGRAM (UROP).                          *
        *      ---COMPLETED 1/21/83 FOR THE TRS-80      *
50 REM  *-----------------------------------------------*

60 REM              ---*** INITIALIZATION ***---
70 DEFSNG A,R,B,F,H,K,M,N,P,T,X,Y:DEFINT I,J,L
80 CLS:DIM A(6,6),K(6),P(11),MOLES(11),HC(11),HF(11),HP(10,4
),RESULTS(50,3)

90 REM    ---*** DATA FOR POLYNOMIAL COEFFICIENTS ***---
100 REM               FOR EQUILIBRIUM CONSTANTS
110 DATA2.79677164554596,-.01238345220917836,-14707.66680622
101,.1770747569389641,-7.096712195675536D-08,2.8482231136877
09D-03
120 DATA.4475892558693886,-3.678911074530333D-3,-12486.60614
967346,.1153698796406388,1.934736459929809D-8,6.628998671658
337D-4
130 DATA.6793251186609268,-9.826400200836361D-3,-14529.79030
847549,.189539578743279,-3.274767035321702D-8,2.135704533429
816D-3
140 DATA2.100934565067,1.987804600503296D-3,-11338.731481790
54,7.148131262511015D-3,2.901352225137543D-8,-5.503140273503
959D-4
150 DATA1.101146653294563,-.01005940145114437,-12893.8932805
0613,.1654825881123543,-5.904101696430075D-8,2.2905389778316
02D-3
160 DATA.5492009967565 5,-8.455672359559685D-4,-4711.15878057
4799,.01050539361312985,-1.127686255486537D-8,2.081016136799
008D-4
170 REM   ---*** READ THE COEFFICIENTS INTO AN ARRAY ***---
180 REM                    FOR FUTURE USE
190 PRINT:PRINT"                         PLEASE STAND BY"
200 RESTORE:FORI=1TO6:PRINT"       INITIALIZING COEFFICIENTS
FOR CALCULATING  K(";I;")":FORJ=1TO6:READA(I,J):NEXTJ,I

210 REM    ---*** DATA FOR POLYNOMIAL COEFFICIENTS ***---
220 REM                  FOR HEAT CONTENTS
230 DATA 10.26541242917301 , .01958979817776907 , 14022.5183
2509041 , -2021.271711103618 , -.698065301792667
240 DATA 2.292867619267781,.01165870834882199,9422.785672783
852, -990.0098160281777 , -.247550862857679
250 DATA -1.455813268423151 , 4.994665068202236D-3 , 0 , 0 ,
 0
```

Figure B-1. Adiabatic flame temperature program

```
260 DATA 8.915374226911809 , .0128836727222017 , 27331.71320
766211 , -2986.322863705456 , -.4660384592425544
270 DATA -1.481141049184866 , 4.968088057493165D-3 , 0 , 0 ,
 0
280 DATA 5.1092960130336 , .01179965821692264 , 12041.811729
13313 , -1515.97848688066 , -.3406941802218171
290 DATA -2.290391651113168 , 9.838423746245439D-3 , -11341.
72284811735 , 944.8384609669447 , -.09329720800678842
300 DATA -5.081501490058145 , .01641984276873387 , -21002.54
573190212 , 2040.994345277548 , -.1495682548138575
310 DATA -1.641671096876962 , .0100129021550508 , -10173.667
83219576 , 792.1907442137599 , -.117394284355214
320 DATA -2.992097005408141 , 9.62120880462436D-3 , -11993.4
7695100307 , 1055.13052611798 , -.06296272591089292

330 REM  ---*** READ THE COEFFICIENTS INTO AN ARRAY ***---
340 REM                  FOR FUTURE CALCULATION
350 FOR I=1TO10:PRINT"        INITIALIZING COEFFICIENTS FOR C
ALCULATING  H(";I;")":FORJ=0TO4:READ HF(I,J):NEXTJ,I

360 REM ---*** DATA ON HEATS OF FORMATION ***---
370 DATA 17.895 , -57.798 , 0 , 59.559 , 0 , 52.100 , 9.432
,  -26.417 , -94.054 , 0 , 21.580
380 FOR I=0TO10:READ HF(I):NEXT I

390 REM  ---*** TRIPLETS OF DATA TO BE ANALYZED ***---
400 REM                  OF THE FORM...
410 REM   'MIXTURE(%)','PRESSURE(TORR)','RESULT INDEX'
420 DATA 4.15,50,1, 4.2,50,2, 4.25,50,3, 4.3,50,4, 4.5,50,5,
 5,50,6, 5.2,50,7, 5.5,50,8, 6,50,9, 7,50,10, 8,50,11, 9.5,5
0,12, 4.42,100,13, 4.45,100,14, 4.5,100,15, 4.55,100,16
430 DATA 4.6,100,17, 4.8,100,18, 5,100,19, 5.5,100,20, 6,100
,21, 7,100,22, 8,100,23, 9.5,100,24, 4.75,250,25,4.8,250,26
440 DATA 5,250,27, 5.5,250,28, 6,250,29, 7,250,30, 8,250,31,
9.5,250,32, 5.07,760,33, 5.1,760,34, 5.15,760,35, 5.2,760,36
, 5.3,760,37, 5.5,760,38, 6,760,39, 7,760,40
450 DATA 8,760,41, 9.5,760,42, 5.28,1500,43, 5.29,1500,44, 5
.3,1500,45, 5.35,1500,46, 5.5,1500,47, 6,1500,48, 7,1500,49,
8,1500,50, 9.5,1500,51, 9.5,76,52


460 REM ---*** INITIALIZE TEMPERATURE VARIABLES TO ***---
470 REM              BE USED FOR INTERPOLATION
480 T=1200:DATA 3.1416
490 T1=0:T2=0

500 REM---** READ NEXT TRIPLET OF DATA TO BE ANALYZED **---
510 READ MIX:IF MIX=3.1416 THEN 1360
520 READ P:P=P/760:READ IR:PRINT"FOR  MIX =";MIX;" &  P =";P
*760;",        T =";

530 REM    ---*** EQUILIBRIUM CONSTANT CALCULATION ***---
540 FORI=1TO6:K(I)=10[(A(I,1)+A(I,2)*T+A(I,3)*T[-1+A(I,4)*T[
.5+A(I,5)*T[2+A(I,6)*T*LOG(T)/LOG(10)):NEXTI
```

Figure B-1. (continued)

```
550 REM   ---*** CALCULATE OX/HYD MOLE RATIO ***---
560 NER=2E*.21E*(100-MIX)/(4E*MIX):GOTO 660


570 REM ---------------S U B R O U T I N E----------------
580 REM       ---*** PARTIAL PRESSURE CALCULATION ***---
590 P(1) = PH2O:
    P(2) = (K(1) * PCOPC)[2:
    P(3) = K(5) * SQR(P(2)):
    P(4) = K(2) * P(1)/SQR(P(2)):
    P(5) = K(4) * SQR(P(4)):
    P(6) = K(3) * P(1)/SQR(P(4))
600       NH = 2 * P(4) + P(5) + P(6) + 2 * P(1):
          NC = NH/4:
          NN = NH * .395E * (100-MIX)/MIX
610 P(7) = NC/(1 + PCOPC):
    P(8) = NC - P(7)
620 P(10) = K(6) * SQR(P(2)*NN/2):
    P(10) = P(10) * (-P(10)/2/NN + SQR((P(10)/2/NN)[2+1D)):
    P(9) = (NN - P(10))/2:
          NO = P(1) + 2*P(2) + P(3) + P(6)+P(7)+2*P(8)+P(10)
630      NR = NO/NH:
    P(0)=P(1)+P(2)+P(3)+P(4)+P(5)+P(6)+P(7)+P(8)+P(9)+P(10)
640 RETURN
650 REM ------------------------------------------------


660 REM         ---*** CONVERGENCE ROUTINE ***---
670 REM------------E X P L A N A T I O N-----------------
680 REM       THE PARTIAL PRESSURES FOR ANY GIVEN TEMPERATURE
        ARE GIVEN BY THE EQUATIONS IN THE SUBROUTINE ABOVE.
        USING THE METHOD IN "GAYDON AND WOLFHARD", THEY CAN
        ALL BE FOUND IF THE RATIO OF PARTIAL PRESSURES,
690 REM P(CO2)/P(CO) (DENOTED BY PCOPC), AND THE PARTIAL
        PRESSURE, P(H2O) (DENOTED BY PH2O), ARE KNOWN.  WE
        CAN FIND THESE BY TRIAL AND ERROR, AND INTERPOLATION
        SINCE WE KNOW THAT THE CALCULATED AND ACTUAL TOTAL
700 REM PRESSURES MUST BE EQUAL (P(0)=P) AND THE CALCULATED
        AND ACTUAL OXYGEN-HYDROGEN MOLE RATIOS MUST BE EQUAL
        (NR=NER).  THIS CONVERGENCE ROUTINE IS THE TRIAL AND
        ERROR AND INTERPOLATION PROCESS SO THAT WHAT EMERGES
710 REM IS THE CORRECT PARTIAL PRESSURES FOR THE GIVEN TRIAL
        TEMPERATURE.

720 REM KEY TO PRESSURE INDICES:        0:TOTAL     1:H2O
        2:O2        3:O         4:H2        5:H         6:OH
        7:CO        8:CO2       9:N2        10:NO

730 REM SCHEMATIC OF CONVERGENCE ROUTINE:
        ( A )       MAKE INITIAL GUESSES
        ( B )       MODIFY PCOPC GUESS UNTIL NR=NER (APPROX)
        ( C )       IF P(0)=P (APPROX) THEN (F)
740 REM ( D )       MODIFY PH2O GUESS UNTIL P(0)=P (APPROX)
        ( E )       IF NR=NER (APPROX) THEN (F) ELSE (B)
        ( F )       EXIT -- MISSION ACCOMPLISHED
```

Figure B-1. (continued)

```
750 REM EXPLANATION OF VARIABLES, A,B,X, & Y:
        (DURING PHASE (B)):
             Y0=Y1=Y2=BEST CURRENT GUESS OF PH2O
             X0=GUESS OF PCOPC YIELDING (NR < NER)
760 REM      X1=GUESS OF PCOPC YIELDING (NR > NER)
             X2=NEW GUESS OF PCOPC BY INTERPOLATION
             (A0,B0)=(NR,P(0)) USING (X0,Y2)
             (A1,B1)=(NR,P(0)) USING (X1,Y2)
770 REM      (A2,B2)=(NR,P(0)) USING (X2,Y2)
        (DURING PHASE (D)):
             X0=X1=X2=BEST CURRENT GUESS OF PCOPC
             Y0=GUESS OR PH2O YIELDING (P(0) < P)
780 REM      Y1=GUESS OF PH2O YIELDING (P(0) > P)
             Y2=NEW GUESS OF PH2O BY INTERPOLATION
             (A0,B0)=(NR,P(0)) USING (X2,Y0)
             (A1,B1)=(NR,P(0)) USING (X2,Y1)
790 REM      (A2,B2)=(NR,P(0)) USING (X2,Y2)
         - - - - - - - - - - - - - - - - - - - - - - - - - -

800 REM PHASE ( A ):  INITIAL GUESSES
810 Y2=.01E:X2=1E

820 REM PHASE ( B ):  MODIFY PCOPC UNTIL NR=NER
830 Y1=Y2:Y0=Y2
840 PCOPC=X2:PH2O=Y2:GOSUB 580:A2=NR:B2=P(0)
850 IF A2>NER THEN X2=X2/10:GOTO 840
860 X0=X2:X2=10*X0:A0=A2:B0=B2
870 PCOPC=X2:PH2O=Y2:GOSUB 580:A2=NR:B2=P(0)
880 IFA2<NER THEN 860
890 X1=X2:A1=A2:B1=B2
900 IF ABS(1-A0/A1)<.4 THEN X2=(NER-A0)/(A1-A0)*(X1-X0)+X0:
GOTO 920
910 X2=(X1+X0)/2
920 PCOPC=X2:PH2O=Y2:GOSUB 580:A2=NR:B2=P(0)
930 IF ABS(A2-NER)<.0001 THEN 970
940 IF A2>NER THEN X1=X2:A1=A2:B1=B2:GOTO 900
950 A0=A2:X0=X2:B0=B2:GOTO 900

960 REM PHASE ( C ):  IF P(0)=P STILL THEN EXIT
970 IF ABS(B2-P)<.0001 THEN 1150

980 REM PHASE ( D ):  MODIFY PH2O UNTIL P(0)=P
990 X1=X2:X0=X2
1000 PCOPC=X2:PH2O=Y2:GOSUB 580:A2=NR:B2=P(0)
1010 IFB2>PTHEN Y2=Y2/2:GOTO 1000
1020 Y0=Y2:A0=A2:B0=B2:Y2=Y0*2
1030 PCOPC=X2:PH2O=Y2:GOSUB 580:A2=NR:B2=P(0)
1040 IF B2<P THEN 1020
1050 Y1=Y2:A1=A2:B1=B2
1060 IFABS(1-B0/B1)<.4THENY2=(P-B0)/(B1-B0)*(Y1-Y0)+Y0:
GOTO1080
1070 Y2=(Y1+Y0)/2
1080 PCOPC=X2:PH2O=Y2:GOSUB 580:A2=NR:B2=P(0)
1090 IF ABS(B2-P)<.0001 THEN 1130
```

Figure B-1. (continued)

```
1100 IF B2>P THEN Y1=Y2:A1=A2:B1=B2:GOTO 1060
1110 Y0=Y2:A0=A2:B0=B2:GOTO 1060

1120 REM PHASE ( E ):  IF NR=NER STILL THEN EXIT ELSE (B)
1130 IF ABS(A2-NER)>.0001 THEN 830

1140 REM PHASE ( F ):  EXIT
1150 X1=X2:X0=X2:Y1=Y2:Y0=Y2:A1=A2:A0=A2:B1=B2:B0=B2

1160 REM      ---*** MOLES OF EACH GAS CALCULATED ***---
1170 MOLES(0)=P(0)/NC:FORI=1TO10:MOLES(I)=MOLES(0)*P(I)/P(0)
:NEXTI

1180 REM     ---*** HEAT CONTENTS CALCULATED ***---
1190 FOR I=1TO10:HC(I)=HP(I,0)+HP(I,1)*T+HP(I,2)*T[(-1.5)+HP
(I,3)*T[(-1)+HP(I,4)*T[.5:NEXT I

1200 REM        ---*** HEAT BALANCE ***---
1210 HR=0:FORI=1TO10:HR=HR+MOLES(I)*HC(I):NEXT I
1220 HA=HF(0):FORI=1TO10:HA=HA+MOLES(I)*HF(I):NEXTI:HA=-HA
1230 IF ABS(HA-HR)>.01 THEN 1290 ELSE RESULTS(IR,0)=MIX
1240 RESULTS(IR,1)=P:RESULTS(IR,2)=T:RESULTS(IR,3)=P(0)*(MIX
*16/100+(1-MIX/100)*.79*28+(1-MIX/100)*.21*32)/(18*P(1)+32*P
(2)+16*P(3)+2*P(4)+P(5)+17*P(6)+28*P(7)+44*P(8)+28*P(9)+30*P
(10))
1250 PRINT T:PRINT"      MOLE RATIO =";RESULTS(IR,3):GOTO360

1260 REM       ---*** TEMPERATURE INTERPOLATION ***---
1270 REM     (T1=GUESS FOR TEMPERATURE LESS THAN ACTUAL)
1280 REM     (T2=GUESS FOR TEMPERATURE GREATER THAN ACTUAL)
1290 IF T1=0 THEN T1=T:D1=HA-HR:T=2800:GOTO 530
1300 IF T2=0 THEN T2=T:D2=HA-HR:GOTO 1330
1310 IF HA-HR>0 THEN T1=T:D1=HA-HR:GOTO 1330
1320 T2=T:D2=HA-HR
1330 IF ABS(T2-T1)>200 THEN T=(T2+T1)/2:GOTO 530
1340 T=D1/(D1-D2)*(T2-T1)+T1:GOTO 530

1350 '       ---*** FINISH INFORMATION ***---
1360 PRINT:PRINT"FINISHED CALCULATING ALL FLAME TEMPERATURES
 AND MOLE RATIOS":PRINT"RESULTS ARE STORED IN THE ARRAY RE(6
0,3)":PRINT"     RE(N,0) = THE MIXTURE (%)"
1370 PRINT"     RE(N,1) = THE PRESSURE (ATM)":PRINT"     RE(N,
2) = THE TEMPERATURE (DEG K)"
1380 PRINT"     RE(N,3) = THE RATIO OF MOLES OF GAS AFTER TO
BEFORE":STOP

1390 REM NOTICE ON POLYNOMIAL-FITTED TABULAR DATA:
         EQUILIBRIUM CONSTANTS WERE CALCULATED BY...
                                   -1      .5      2
         LOG(K)=A1 + A2 T + A3 T  + A4 T  + A5 T  + A6 T LN(T)

1400 REM HEAT CONTENTS WERE CALCULATED BY...
                                   -1.5       -1         .5
         HC = HP0 + HP1 T + HP2 T    + HP3 T    + HP4 T
```

Figure B-1. (conclusion)

Pressure, Torr	Mixture, % methane in air	T_b, °K	n
50	4.20	1314	1.000
	4.50	1377	1.000
	5.00	1480	1.000
	5.50	1580	1.000
	6.00	1676	1.000
	7.00	1857	1.001
	8.00	2012	1.003
	9.50	2151	1.013
100	4.42	1361	1.000
	4.45	1367	1.000
	4.50	1377	1.000
	4.55	1388	1.000
	4.60	1398	1.000
	4.80	1439	1.000
	5.00	1480	1.000
	5.50	1580	1.000
	6.00	1677	1.000
	7.00	1860	1.001
	8.00	2021	1.002
	9.50	2172	1.011
250	4.73	1425	1.000
	4.75	1429	1.000
	4.80	1439	1.000
	5.00	1480	1.000
	5.50	1580	1.000
	6.00	1677	1.000
	7.00	1862	1.000
	8.00	2030	1.002
	9.50	2198	1.010
760	5.07	1494	1.000
	5.10	1500	1.000
	5.15	1510	1.000
	5.20	1520	1.000
	5.30	1540	1.000
	5.50	1580	1.000
	6.00	1678	1.000
	7.00	1865	1.000
	8.00	2037	1.001
	9.50	2226	1.007
1500	5.28	1537	1.000
	5.29	1539	1.000
	5.30	1541	1.000
	5.35	1551	1.000
	5.50	1580	1.000
	6.00	1678	1.000

Table B-1. Values of T_b and n as calculated by the adiabatic flame temperature program.

Appendix C. Effect of flame kernel expansion on unburned gas pressure and temperature in a closed vessel

Lewis and von Elbe [30] predict the pressure dependence on observed flame radius in an adiabatic spherical vessel from the equation

$$\frac{r_b}{r_v} = \left[1 - \left(\frac{P}{P_o}\right)^{-1/\gamma} \frac{P_f - P}{P_f - P_o}\right]^{-1/3}$$

where r_b and r_v are the instantaneous flame radius and vessel radius, respectively, P, P_o, and P_f are the instantaneous, initial, and final pressure, respectively, and γ is the specific heat ratio of the gases. The temperature of the unburned gas can be calculated from the adiabatic compression law

$$T_u/T_{uo} = (P/P_o)^{(\gamma-1)/\gamma}$$

where T_u and T_{uo} are the instantaneous and initial unburned gas temperature, respectively. For nonspherical vessels, the effective vessel radius can be estimated as the radius of a sphere that would have the same volume as the vessel. These equations assume zero flame thickness and constant gas thermodynamic properties, which of course is not true in practice, but the equations should still be adequate for estimates. Calculated values of P/P_o and T_u/T_{uo} as a function of r_b/r_v for $P_f/P_o = 10$ and $P_f/P_o = 6.7$ with $\gamma = 1.4$ are shown in table C-1. These values of P_f/P_o are representative of stoichiometric and near-limit hydrocarbon-air mixtures, respectively, in closed bombs (see below). From the results, it is clear that the pressure rise in the vessel becomes significant at about $r_b/r_v = 0.4$. The temperature rise becomes significant at about $r_b/r_v = 0.6$.

	P_f/P_o = 6.7		P_f/P_o = 10.0	
r_b/r_v	P/P_o	T_u/T_{uo}	P/P_o	T_u/T_{uo}
0.000	1.000	1.000	1.000	1.000
0.100	1.001	1.000	1.001	1.000
0.300	1.031	1.009	1.034	1.010
0.500	1.159	1.043	1.173	1.047
0.700	1.557	1.135	1.627	1.149
0.900	3.175	1.391	3.741	1.458
1.000	6.700	1.722	10.000	1.931

Table C-1. Effect of observed flame radius on pressure and temperature of unburned gases (γ = 1.4) in a closed spherical vessel.

The final equilibrium pressure P_f can be estimated from the normal adiabatic flame temperature at constant pressure, T_b, assuming equal heats of combustion for constant pressure and constant volume combustion, from the equation

$$\Delta h_c = C_p(T_b - T_u) = C_v(T_v - T_u)$$

where Δh_c is the net heat of combustion, C_v is the gas specific heat at constant volume, and T_v is the equilibrium flame temperature for constant volume combustion. Assuming constant molecular weight throughout, which is reasonable for hydrocarbon-air combustion, the ideal gas law yields

$$T_v/T_u = P_f/P_o$$

and with the definition $\gamma = C_p/C_v$, the final result is

$$P_f/P_o = \gamma(T_b/T_u - 1 + 1/\gamma).$$

For typical values of T_b = 2200°K for stoichiometric and T_b = 1500°K for near-limit hydrocarbon-air combustion with T_u = 295°K (see appendix B), the results are P_f/P_o = 10.0 and P_f/P_o = 6.7, as indicated above.

Appendix D. Spalding's theory of flammability limits due to heat loss

Spalding [59] predicts the dependence of burning velocity on heat loss from the equation

$$\lambda = (n + 1)(n + 2)/2\tau_1^{n+2} ,$$

where λ is a dimensionless burning velocity parameter, n is the exponent in the approximate reaction rate expression $\dot{w} \sim T^n$, and τ_1 is the ratio of the maximum flame front temperature in the presence of heat losses to the adiabatic flame temperature T_b. Spalding recommends using n = 11 for hydrocarbon-air mixtures, thus $\lambda \sim \tau_1^{-13}$. λ is given by the expression

$$\lambda = \Delta h_c \dot{w}^* k_b/(T_b - T_u)C_p^2 \rho_u^2 S_u^2 ,$$

where Δh_c is the net heat of combustion, $\dot{w}^*$ is the reaction rate at $T = T_b$, and k_b is the thermal conductivity at T_b. Since approximately $\Delta h_c = C_p(T_b - T_u)$, $\dot{w}^* \sim T_b^{11}$, $k_b \sim T_b$, and C_p is mostly independent of T, the above expression can be written as $\lambda \sim T_b^{12}/S_u^2$. Combining this with $\lambda \sim \tau_1^{-13}$, the result is

$$S_u \sim T_b^6 \tau_1^7 .$$

Spalding gives the relation between heat loss and τ_1 as

$$K = [2\tau_1^{n+2-m}/(n + 1)(n + 2)](1 - \tau_1),$$

where K is a dimensionless heat loss parameter and m is the exponent in the approximate expression for the rate of heat loss $L \sim T^m$. Spalding recommends using m = 4 for radiant heat loss, thus $K \sim \tau_1^9(1 - \tau_1)$. K is given by the expression

$$K = L^*/\dot{w}^* \Delta h_c ,$$

where L^* is the heat loss rate at $T = T_b$. Since approximately $L^* \sim T_b^4$, $\dot{w}^* \sim T_b^{11}$, and $\Delta h_c = C_p(T_b - T_u)$, the above expression can be written as

$$K \sim 1/T_b^7(T_b - T_u) \simeq T_b^{-8} ,$$

since $T_b >> T_u$. Combining the two expressions for K yields

$$*** \quad T_b \sim [\tau_1^9(1 - \tau_1)]^{-1/8} \quad ***$$

and from the relation $S_u \sim T_b^6 \tau_1^7$,

$$*** \quad S_u \sim [\tau_1^9(1 - \tau_1)]^{-3/4} \tau_1^7 \quad ***$$

From these two relations the dependence of burning velocity S_u on adiabatic flame temperature T_b can be determined. This dependence is shown in table D-1 and Fig. 2-6b. As Spalding showed, for T_b less than a critical value, no real values of S_u exist. At the "nose" of the curve, $\tau_1 \simeq 0.90$, which indicates that only a 10% drop in flame temperature below the adiabatic value is required to cause extinction of the flame in this example. For adiabatic combustion, $\tau_1 = 1$ so that $S_u \sim T_b^6$, which is shown also in table D-1 and Fig. 2-6b.

τ_1	T_b	S_u	S_u(adiabatic)
1.000	∞	∞	∞
.995	1.95	53.1	55.0
.990	1.80	31.5	33.8
.980	1.67	18.7	21.6
.950	1.54	9.34	13.4
.920	1.51	6.51	11.7
.900	1.50	5.48	11.5
.870	1.51	4.46	11.8
.800	1.57	3.16	15.1
.700	1.74	2.26	27.4
.600	1.99	1.75	62.5

Table D-1. Burning velocity vs. adiabatic flame temperature according to Spalding's [59] theory of flammability limits due to heat loss with n = 11, m = 4. (τ_1 is dimensionless, T_b and S_u in arbitrary units).

Appendix E. Combustion vessel detail drawings

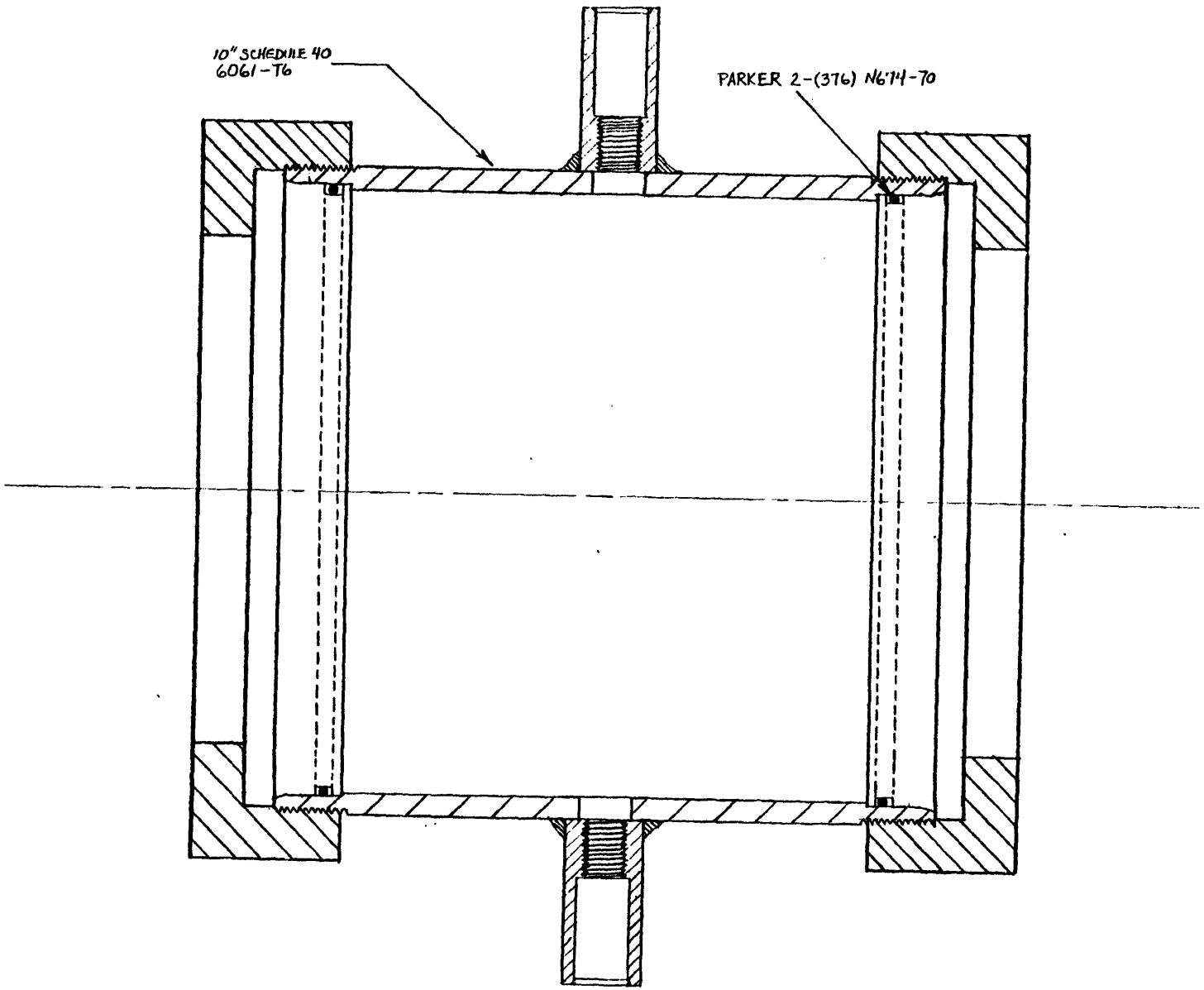

Figure E-1. Assembly drawing

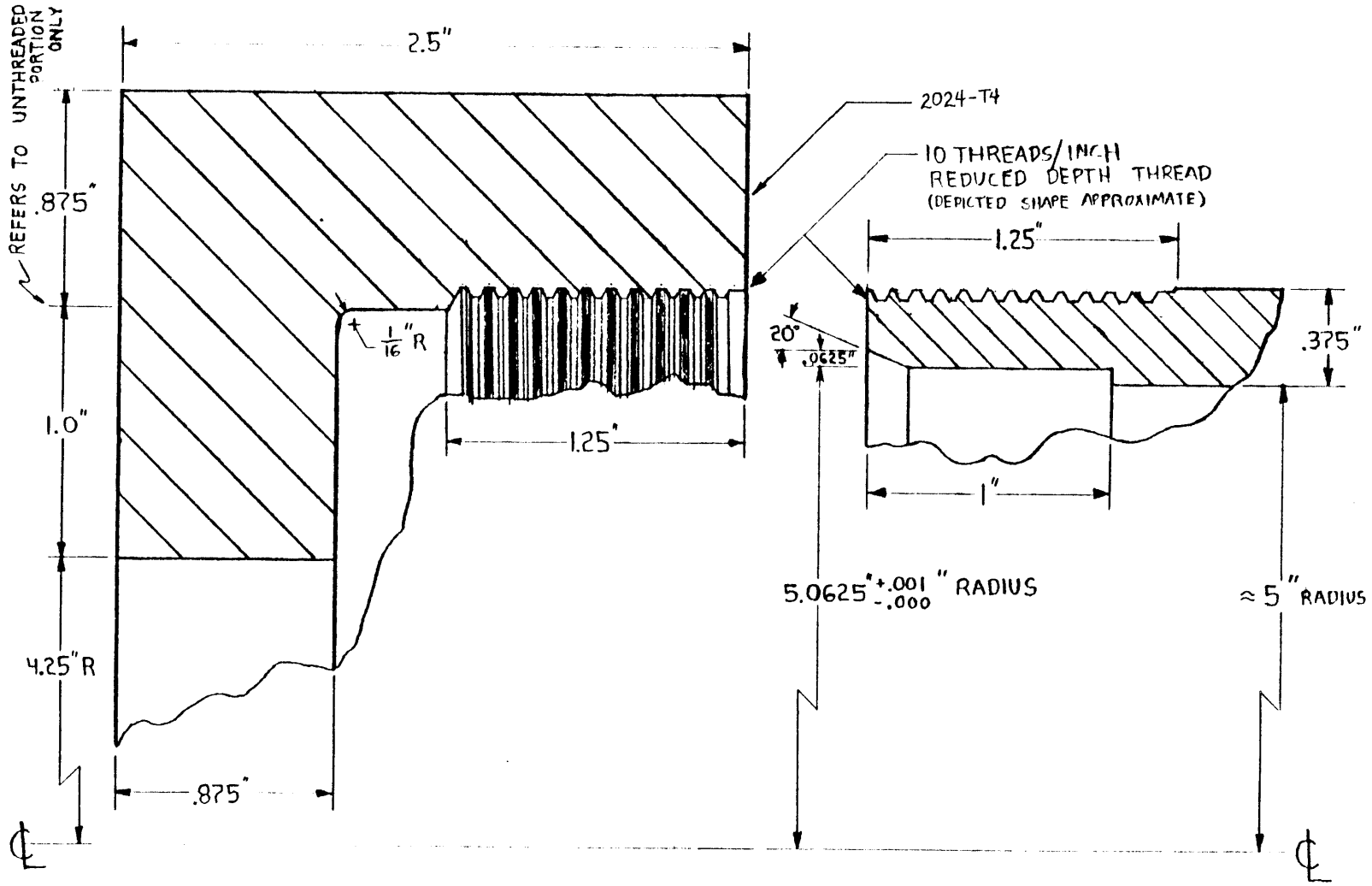

Figure E-2. Sectioned detail: vessel joint

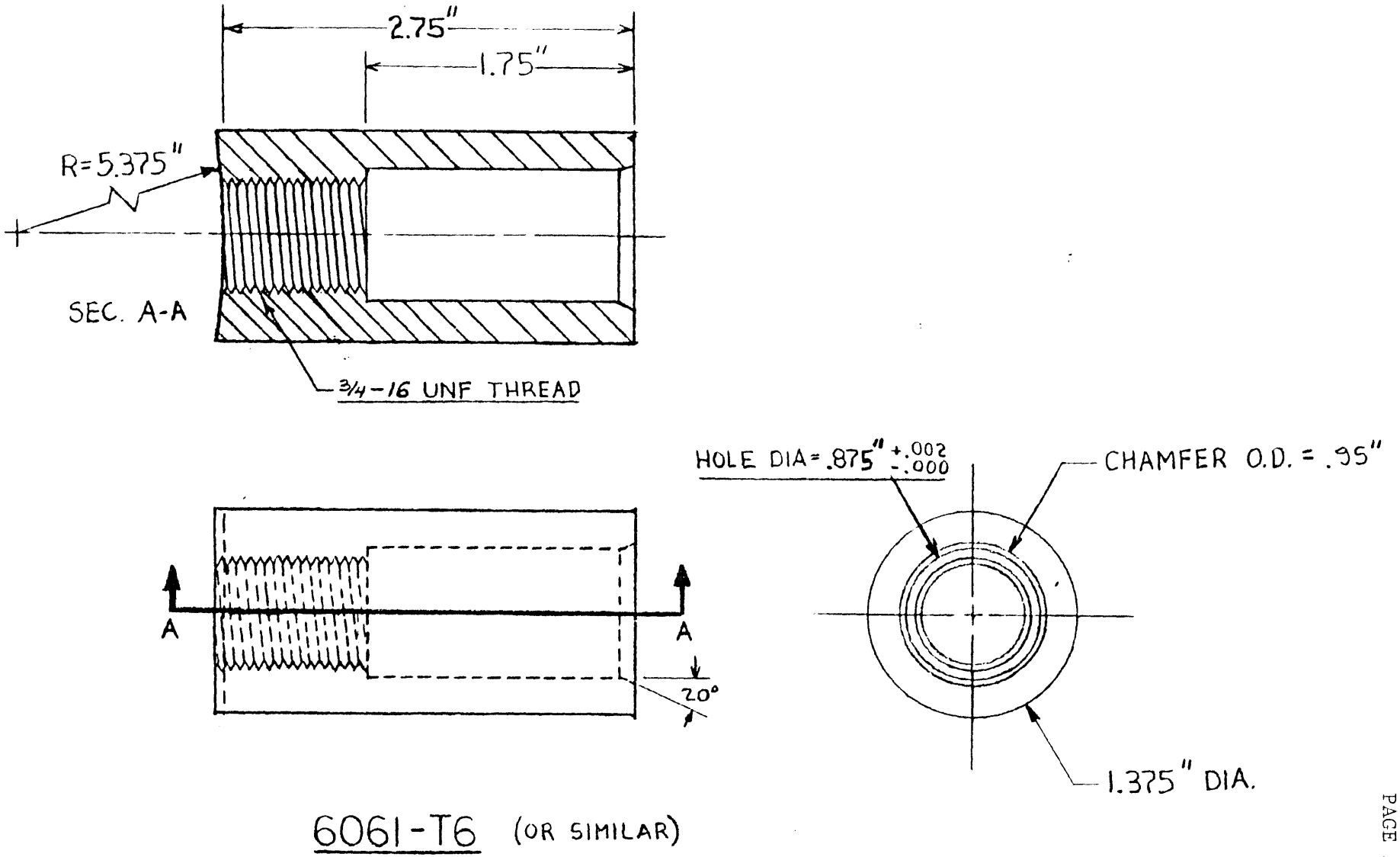

Figure E-3. Spark electrode holder detail

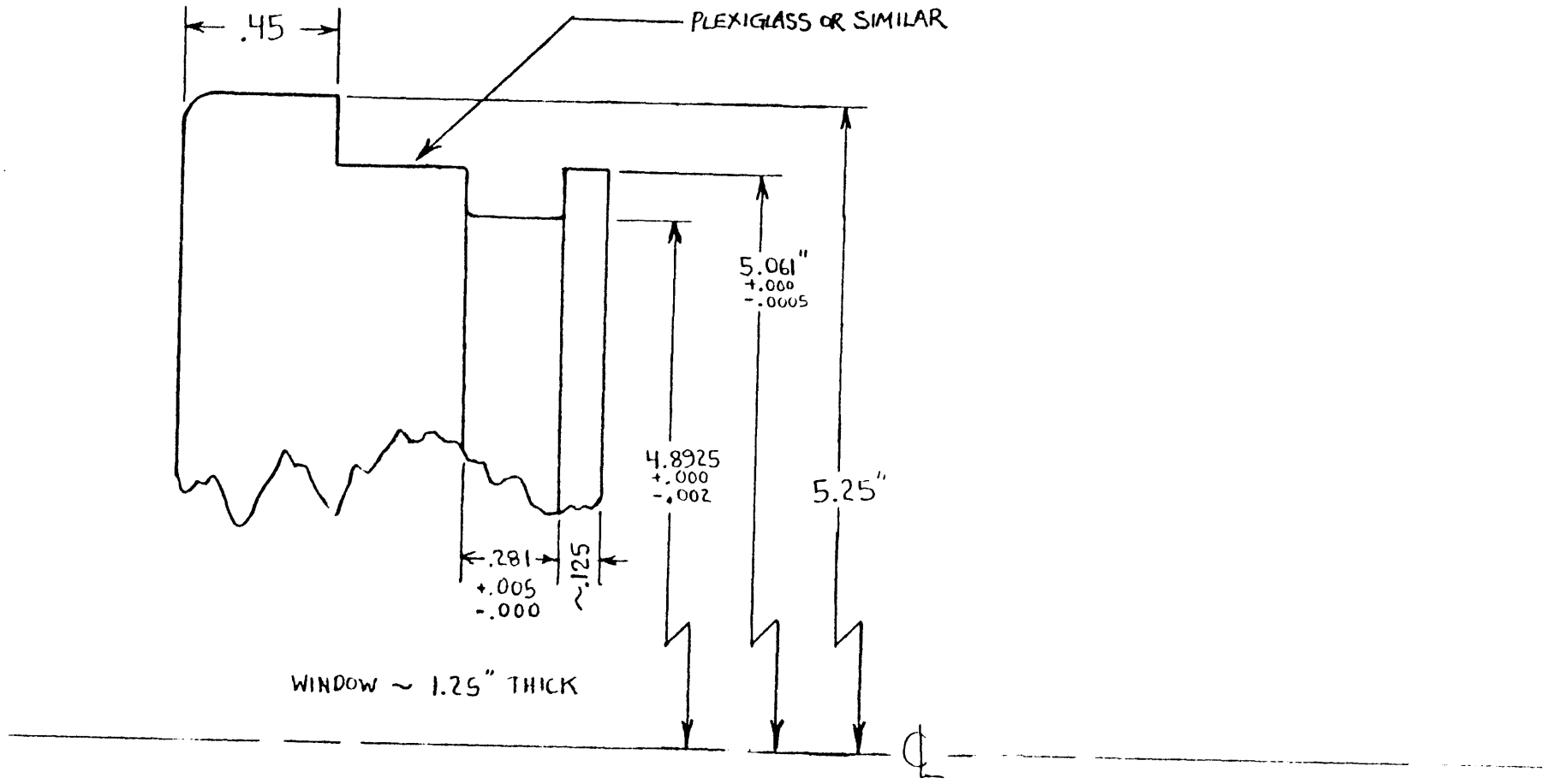

Figure E-4. End cap detail

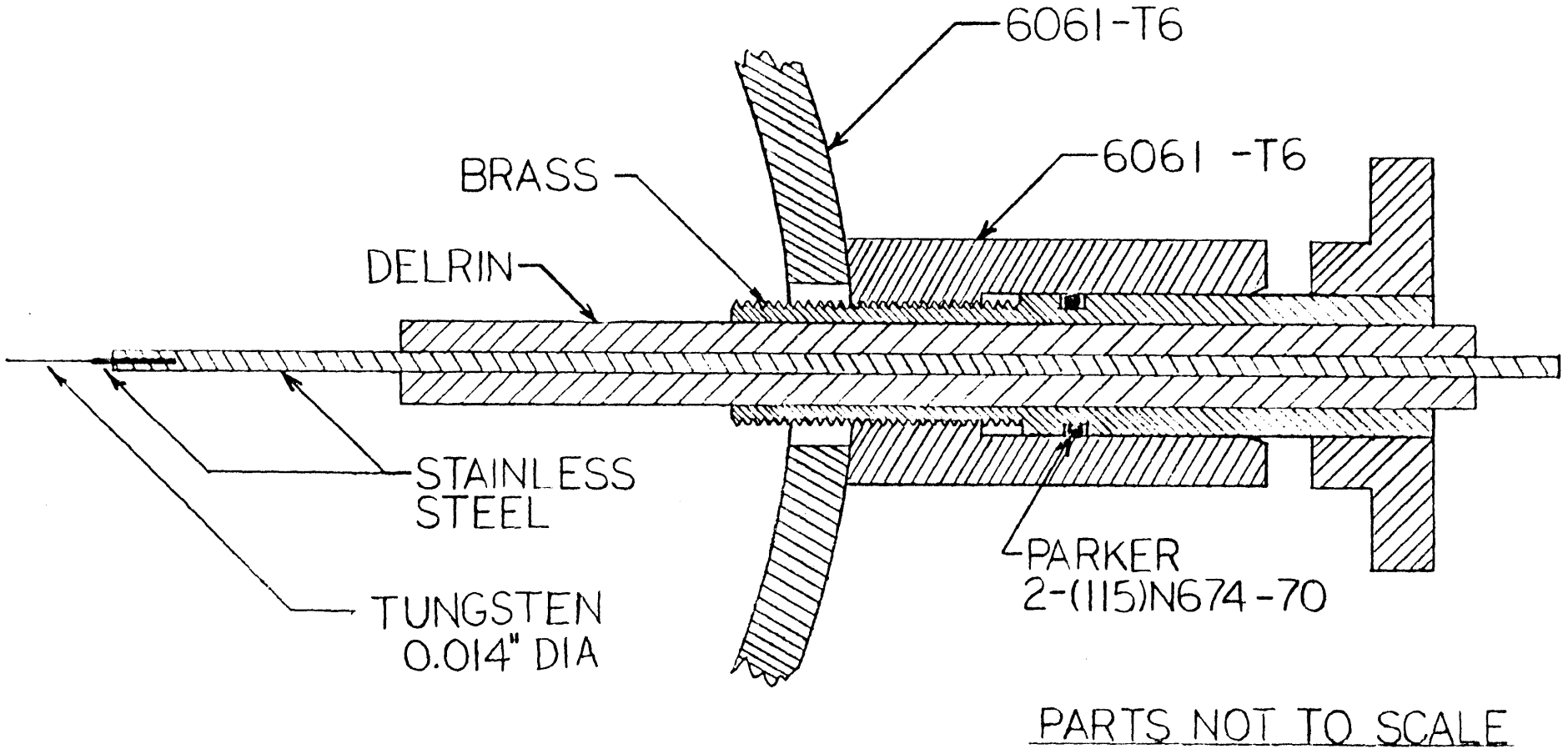

Figure E-5. Spark electrode assembly

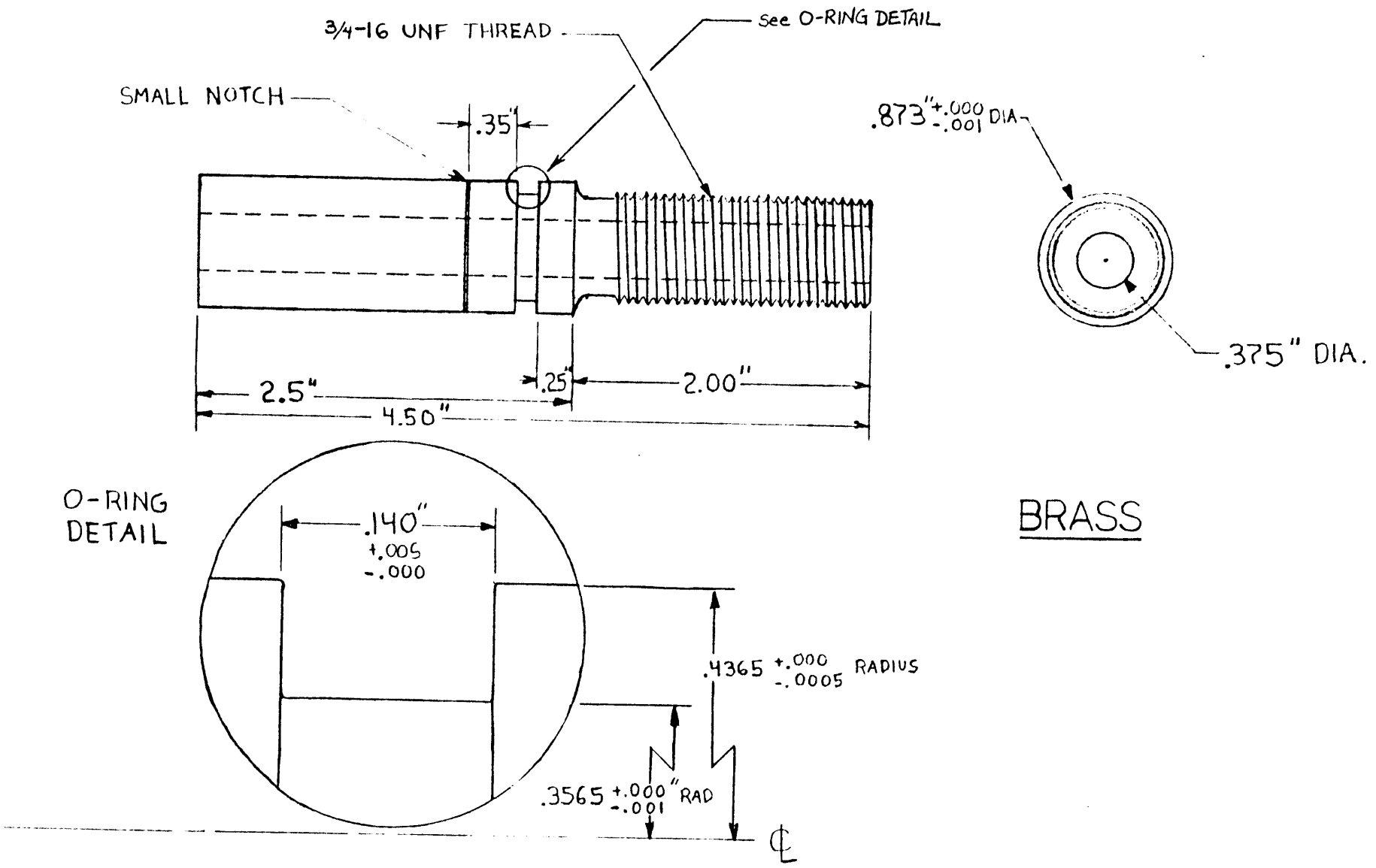

Figure E-6. Spark electrode sleeve detail

Appendix F. Electrical schematics

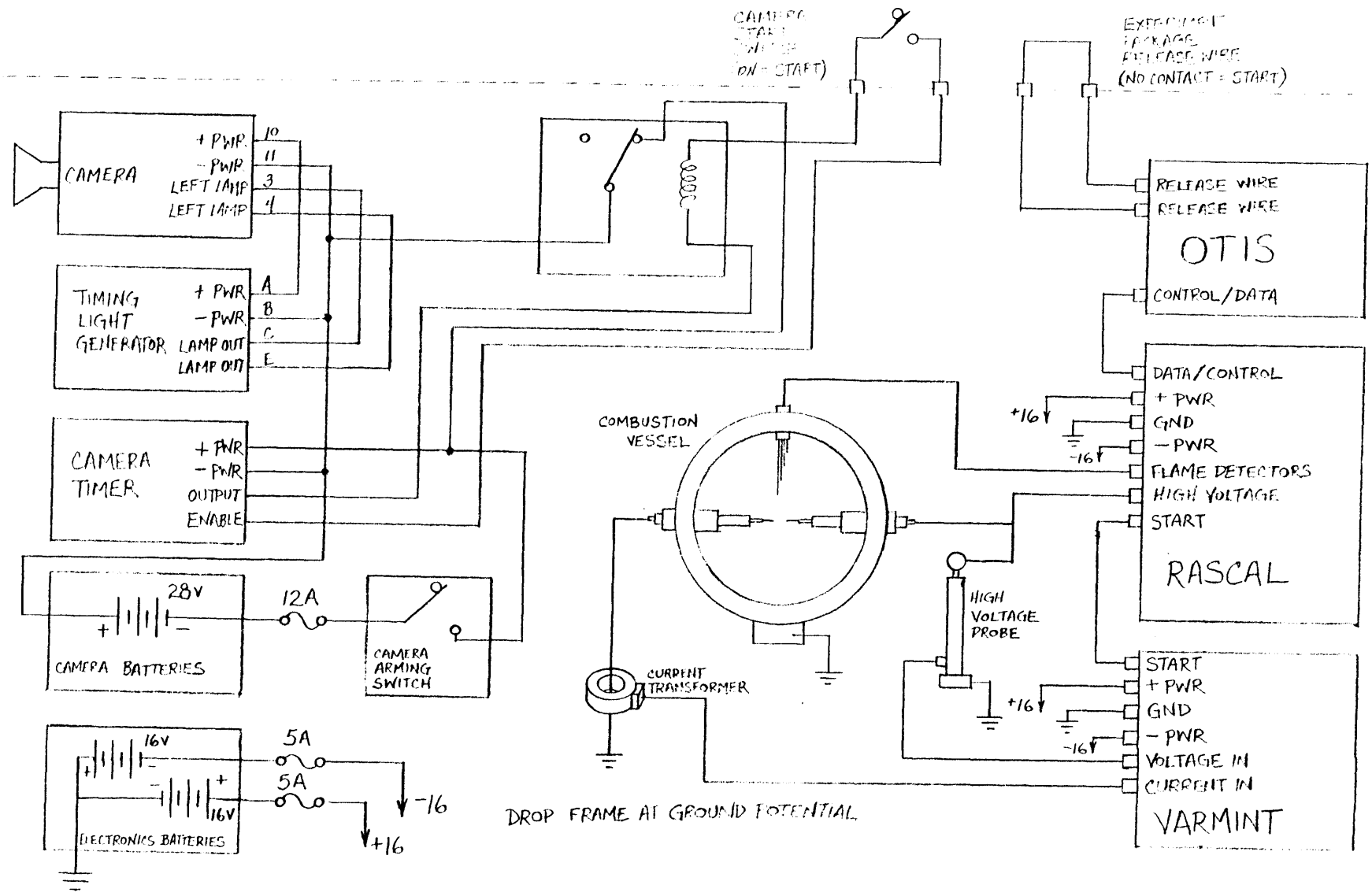

Figure F-1. Overall electrical system schematic

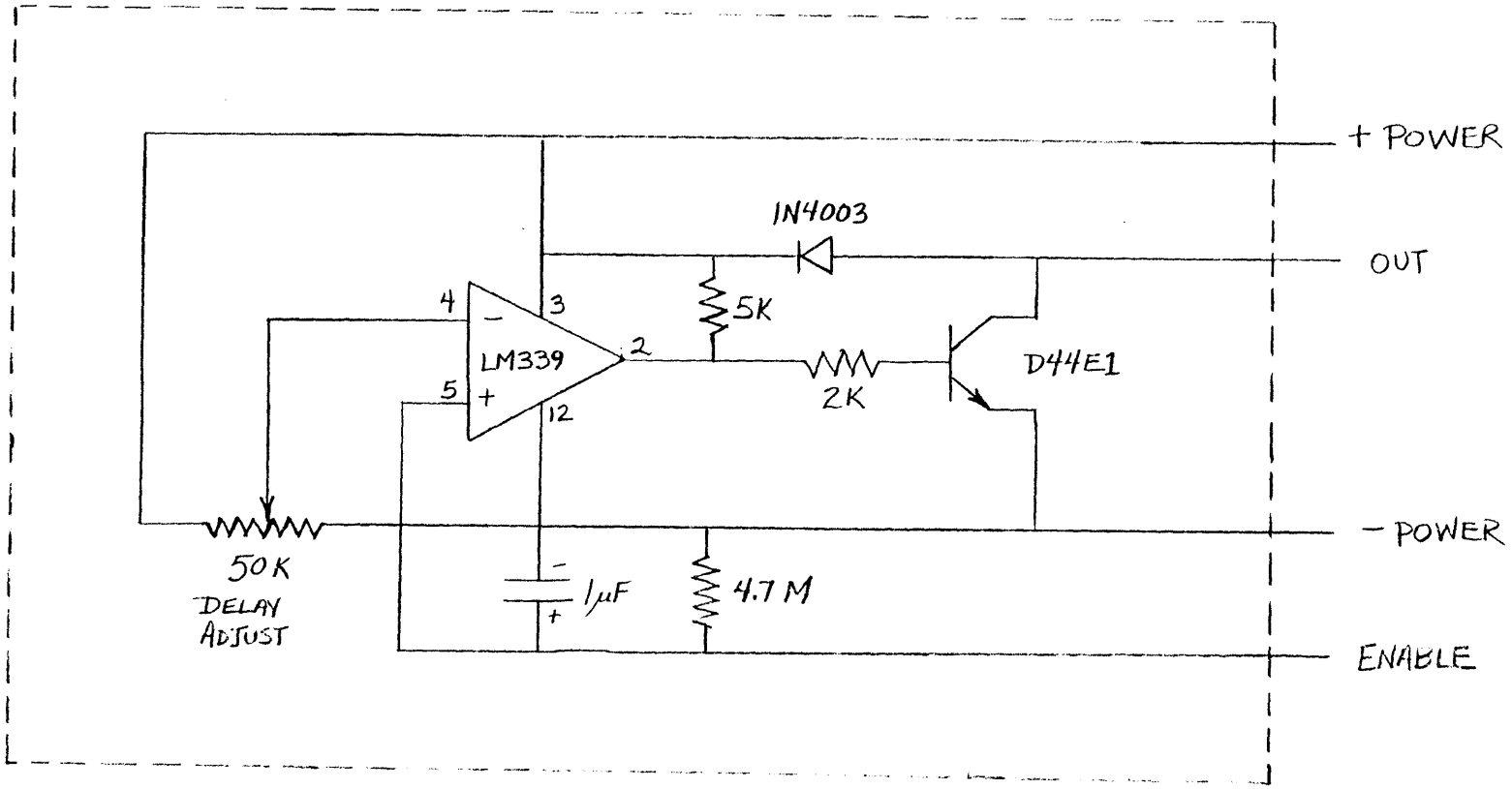

Figure F-2. Camera timer

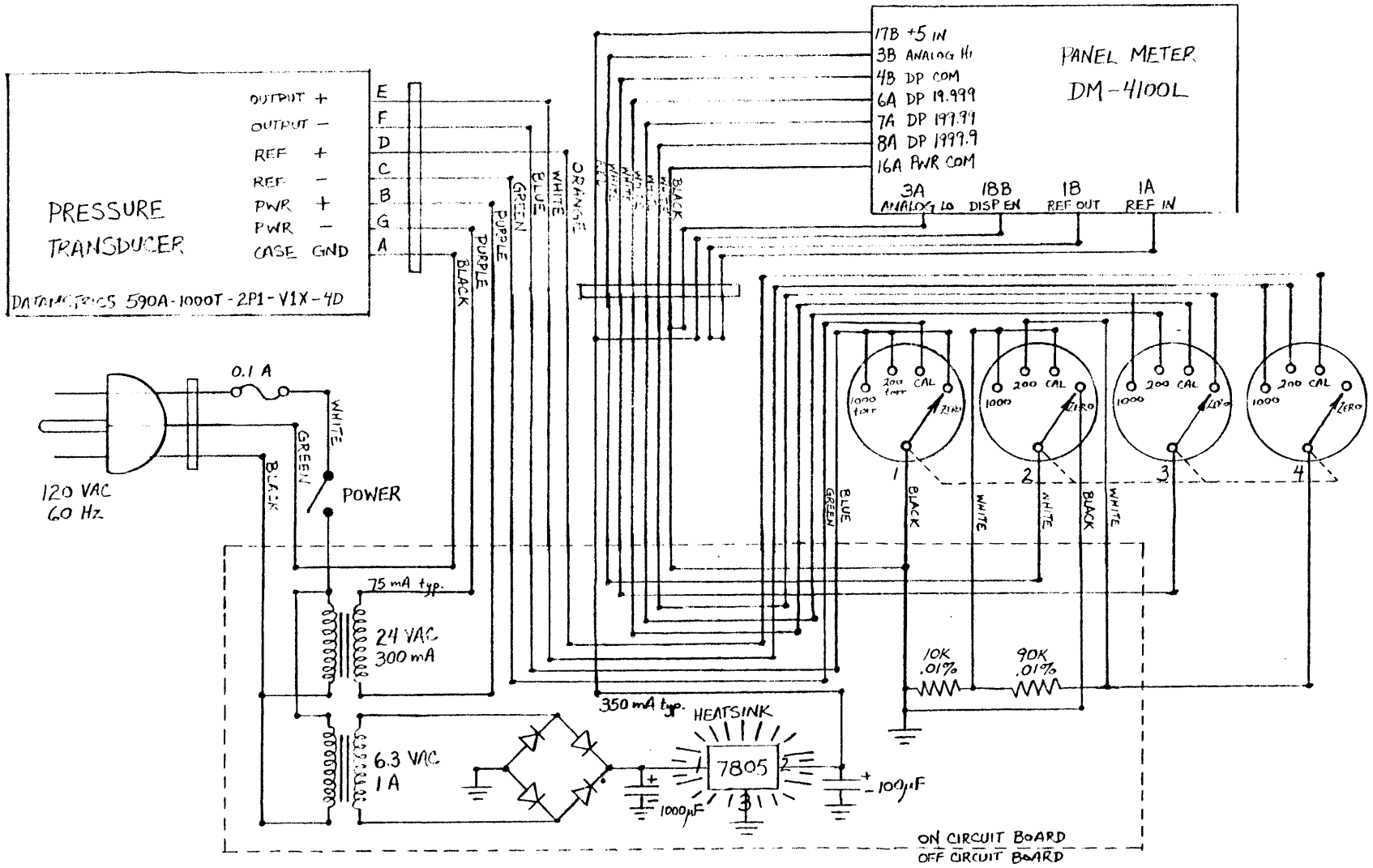

Figure F-3. MAMMAL

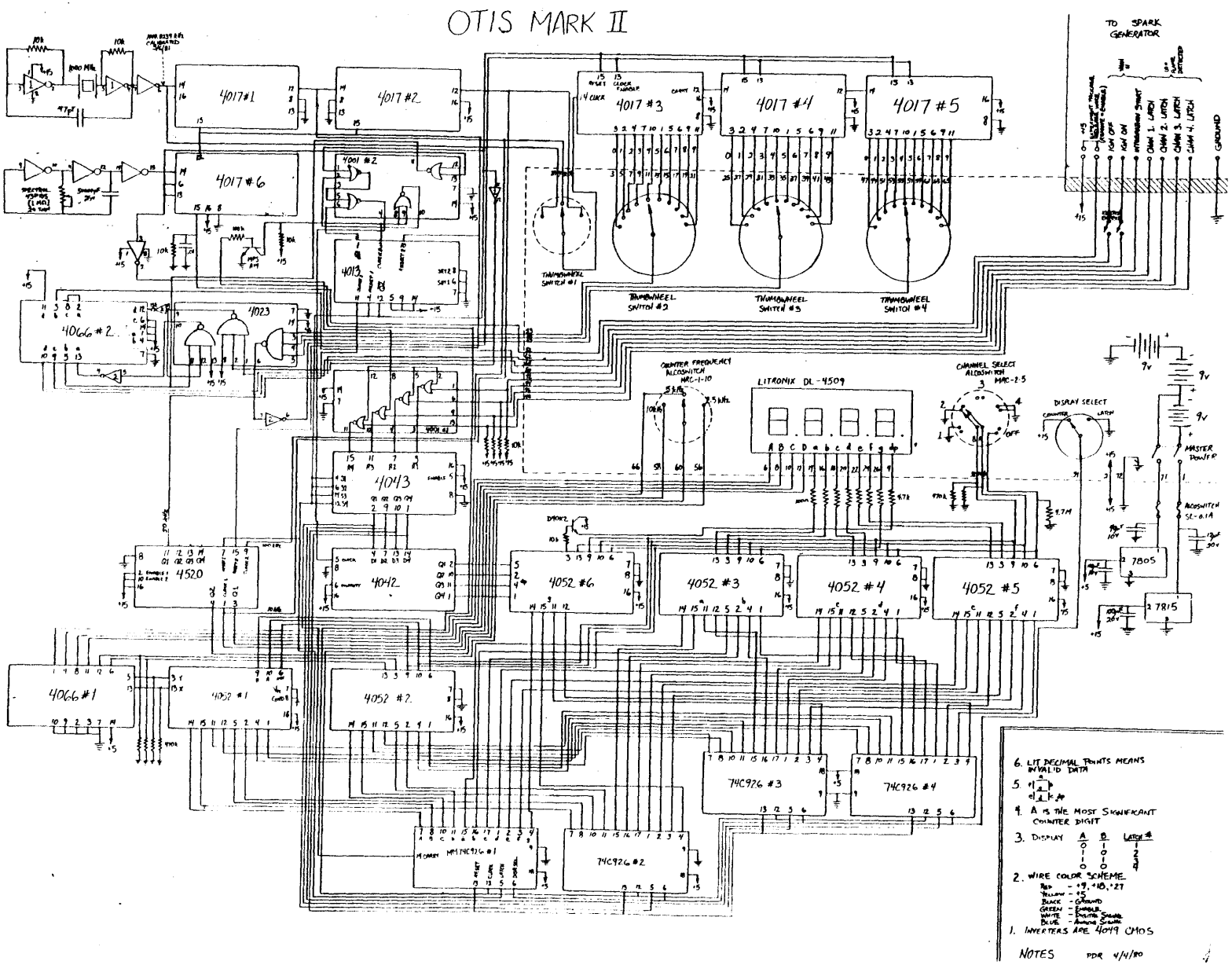

Figure F-4. OTIS detail schematic

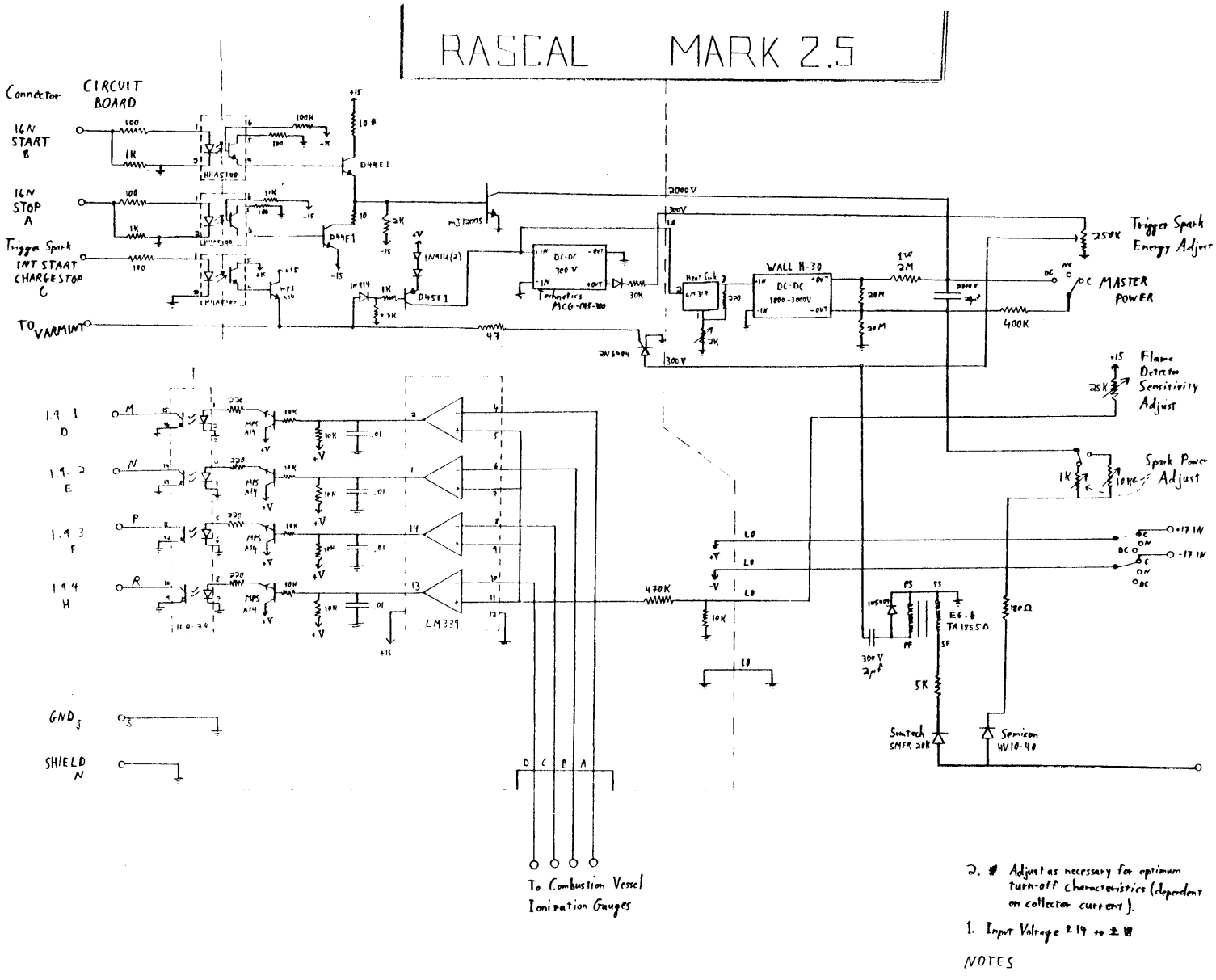

Figure F-5. RASCAL detail schematic

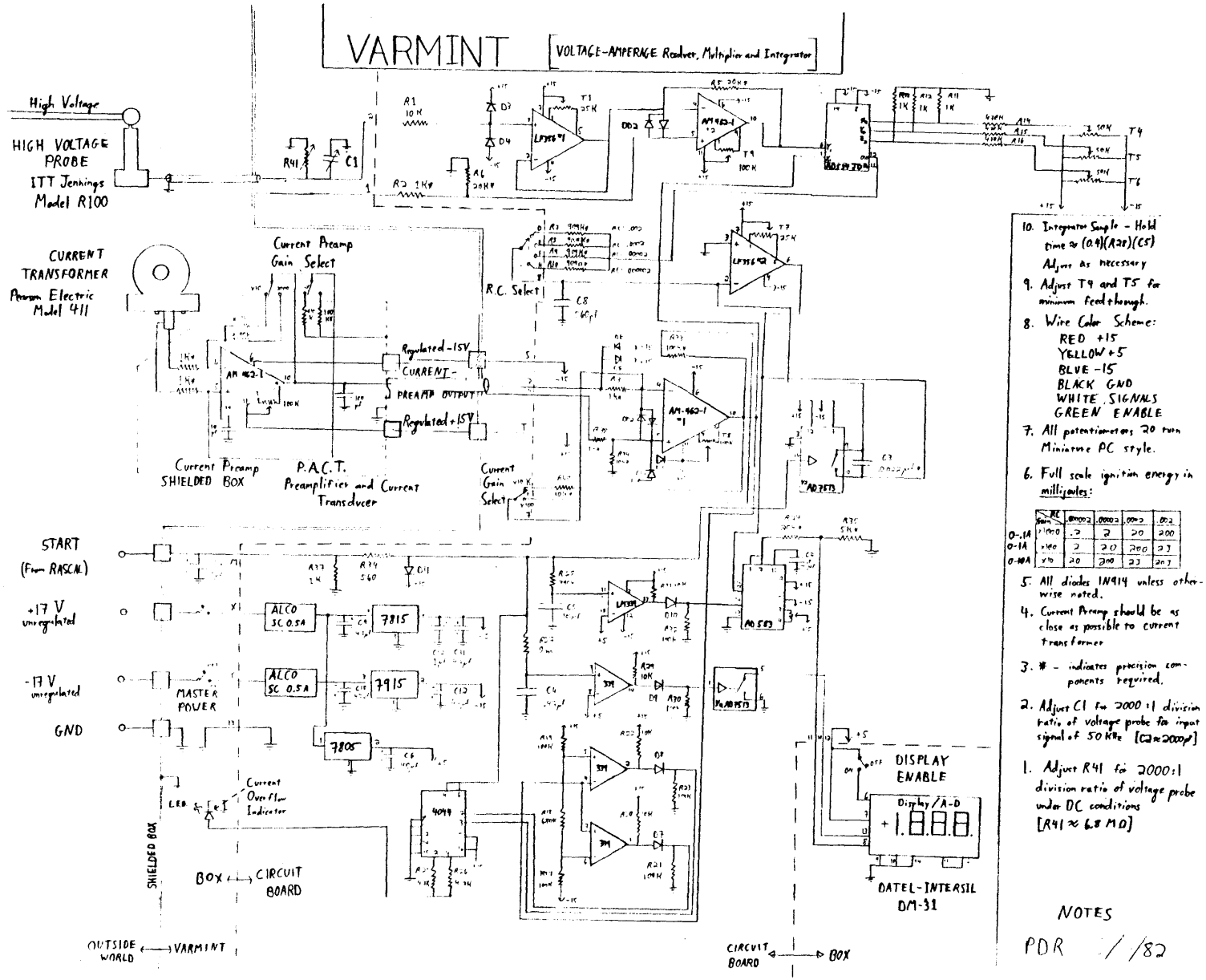

	R[C]	.00002	.0002	.002	.02
0-.1A	1000	.2	2	20	200
0-1A	100	2	20	200	23
0-10A	10	20	200	23	207

Figure F-6. VARMINT detail schematic

References

1. Wardell, A.W., in: NASA SP-5096, 1971

2. Cochran, T.H., Masica, W.J., Thirteenth Symposium (International) on Combustion, Combustion Institute, Pittsburgh (1971), p. 821

3. Haggard, J.B., Jr., Cochran, T.H., Comb. Sci. Tech. 5, 291 (1972)

4. Haggard, J.B., Jr., Cochran, T.H., NASA TN-D-7165, 1973

5. Isoda, M., Kumagai, S., Seventh Symposium (International) on Combustion, Butterworths, London (1959), p. 532

6. Okajima, S., Kumagai, S., Fifteenth Symposium (International) on Combustion, Combustion Institute, Pittsburgh, (1975), p. 401

7. Williams, F.A., NASA CR-159531, 1979

8 Knight, B., Williams, F.A., Combust. Flame 38, 111 (1980)

9. Kimsey, J.M., Down, W.R., Eldred, C.M., Noriss, C.W., NASA TR-R-256, 1966

10. Andracchio, C.R., Aydelott, J.C., NASA TM-X-1992, 1970

11. Cochran, T.H., Petrash, D.S., Andracchio, C.R., Sotos, R.G., NASA TM-X-2174, 1971

12. Kimsey, J.M., NASA TM-X-70252, 1970, p. 115

13. Berlad, A.L., Kilroy, J., NASA CR-3197, 1979

14. Parfenov, L.K., Comb. Expl. and Shock Waves 14, 412 (1978)

15. Krivulin, V.N., et al., Dokl. Acad. Nauk SSSR 247, 1184 (1979)

16. Reuss, D.L., Ph.D. Thesis, Univ. of Ill. at Urbana-Champaign, 1979

17. Strehlow, R.A., Reuss, D.L., NASA CR-3259, 1980

18. Edelman, R.B., et al., Fourteenth Symposium (International) on Combustion, Combustion Institute, Pittsburgh (1973), p. 399

19. Elghobashi, S., et al., NASA CR-135077, 1974

20. Lovachev, L.A., Combust. Flame 17, 275, 1971

21. Hertzberg, M., U.S. Bur. Mines Rept. Invest. 8127, (1976)

22. Shtessel, E.A., Comb. Expl. and Shock Waves 15, 294, 1979

23. Berlad, A.L., et al., NASA CR-134744, 1974

24. Committee on Scientific and Technological Aspects of Materials Processing in Space of the Space Applications Board, Assembly of Engineering, National Research Council, Materials Processing in Space, National Academy of Sciences, Washington, D.C. (1978)

25. Cochran, T.H., Combustion Experiments in a Zero-Gravity Laboratory, Progress in Aeronautics and Astronautics, Volume 73, American Institute of Aeronautics and Astronautics, New York (1981)

26. ANON: Rept. No. TIR-738699316A, The Apollo Dept., General Electric Co., 1969

27. ANON: Rept. No. DAC-62431, McDonnell Douglas Astronautics Co., 1968

28. Krivulin, V.N., Lovachev, L.A., Baratov, A.N., Makeev, V.I., in: Gorenie i Vzryv, Nauka, Moscow (1972), p. 296

29. Krivulin, V.N., et al., Comb. Expl. and Shock Waves 17, 37 (1981)

30. Lewis, B., von Elbe, G., Combustion, Flames and Explosions of Gases, 2nd ed., Academic Press, New York (1961)

31. Williams, F.A., Combustion Theory, Addison-Wesley, Reading, Mass. (1965)

32. Strehlow, R.A., Fundamentals of Combustion, International Textbook, Scranton, Penn. (1968)

33. Fristrom, R.M., Westenberg, A.A., Flame Structure, McGraw-Hill, New York (1965)

34. Westbrook, C.K., Dryer, F.L., Combust. Flame 37, 171 (1980)

35. Stephenson, P.L., Taylor, R.G., Combust. Flame 20, 231 (1973)

36. Smoot, L.D., Hecker, W.C., Williams, G.A., Combust. Flame 26, 323 (1976)

37. Tsatsaronis, G., Combust. Flame 33, 217 (1978)

38. Andrews, G.E., Bradley, D., Combust. Flame 18, 133 (1972)

39. Schlichting, H., Boundary Layer Theory, 6th ed., McGraw-Hill, New York (1968)

40. Linnett, J.W., Simpson, C.J.S.M., Sixth Symposium (International) on Combustion, Reinhold, New York (1957), p.20

41. Andrews, G.E., Bradley, D., Fourteenth Symposium (International) on Combustion, Combustion Institute, Pittsburgh (1972), p. 1119

42. Lovachev, L.A., et al., Combust. Flame 20, 259 (1973)

43. Lovachev, L.A., Comb. Sci. Tech. 20, 209 (1979)

44. Coward, H.F., Jones, G.W., U.S. Bur. Mines Bull. 503, (1952)

45. Berl, E., Werner, G., Z. Angew. Chemie 40, 245 (1927)

46. Bone, W.A., Newitt, D.M., Smith, C.M., Proc. Roy. Soc. (London) A117, 553 (1928)

47. Badami, G.N., Egerton, A.C., Proc. Roy. Soc. (London) A228 , 297 (1955)

48. Levy, A., Proc. Roy. Soc. (London) A282, 134 (1965)

49. Bregeon, B., Gordon, A.S., Williams, F.A., Combust. Flame 32, 33 (1978)

50. Lewis, B., in AGARD, Selected Combustion Problems, Butterworths, London (1954), p. 177

51. Clusius, K., Kolsch, W., Waldmann, L., Z. Physik. Chem. (Leipzig) A189, 131 (1941)

52. Lloyd, S.A., Weinberg, F.J., Nature 257, 357 (1975)

53. Jones, A.R., Lloyd, S.A., Weinberg, F.J., Proc. Roy. Soc. (London) A360, 97 (1978)

54. Kaskan, W.E., Sixth Symposium (International) on Combustion, Reinhold, New York (1957) p. 134

55. Yumlu, V.S., Combust. Flame 10, 147 (1966)

56. Pritchard, R., Edmondson, H., Heap, M.P., Combust. Flame 18, 13 (1972)

57. Dixon-Lewis, G., Isles, G.L., Seventh Symposium (International) on Combustion, Butterworths, London (1959), p. 475

58. Kydd, P.H., Foss, W.I., Combust. Flame 8, 267 (1964)

59. Spalding, D.B., Proc. Roy. Soc. (London) A240, 83 (1957)

60. Mayer, E., Combust. Flame 1, 438 (1957)

61. Egerton, A.C., Powling, J., Proc. Roy. Soc. (London) A193, 172 (1948)

62. Rosen, J.B., J. Chem. Phys. 22, 733 (1954)

63. Higgin, R.M.R., Williams, A., Twelfth Symposium (International) on Combustion, Combustion Institute, Pittsburgh (1969), p. 579

64. Layzer, D., J. Chem. Phys. 22, 222 (1954)

65. Richardson, J.M., Fourth Symposium (International) on Combustion, Williams and Wilkins, Baltimore (1953), p. 182

66. Karlovitz. B., Denniston, D.W., Knapschaefer, D.M., Wells, F.E., Fourth Symposium (International) on Combustion, Williams and Wilkins, Baltimore (1953), p. 613

67. Strehlow, R.A., Savage, L.D., Combust. Flame 31, 209 (1978)

68. Gaydon, A.G., Wolfhard, H.G., Flames: Their Structure, Radiation and Temperature, Fourth Edition, Chapman and Hall, London (1979)

69. Andrews, G.E., Bradley, D., Combust. Flame 19, 275 (1972)

70. Gunther, R., Janisch, G., Combust. Flame 19, 49 (1972)

71. Lewis, B., in: AGARD, Selected Combustion Problems, Butterworths, London (1954), p. 177

72. Guest, P.G., U.S. Bur. Mines Rept. Invest. 3753, (1944)

73. Blanc, M.V., Guest, P.G., von Elbe, G., Lewis, B., Third Symposium on Combustion, Flame and Explosion Phenomena, Williams and Wilkins, Baltimore (1949), p. 363

74. Swett, C.C., NACA Rept. No. 1287, 1956

75. Kravachenko, V.S., Erygin, A.T., Yakalev, V.A., Comb. Expl. and Shock Waves 9, 523 (1973)

76. Ballal, D.R., Lefebvre, A.H., Combust. Flame 24, 99 (1975)

77. Kono, M., Kumagai, S., Sakai, T., Sixteenth Symposium (International) on Combustion, Combustion Institute, Pittsburgh (1976), p. 757

78. Kono, M., Kumagai, S., Sakai, T., Combust. Flame 27, 85 (1976)

79. Lintin, D.R., Wooding, E.R., Brit. J. App. Phys. 10, 159 (1959)

80. Litchfield, E.L., Combust. Flame 5, 235 (1961)

81. Rose, H.E., Priede, T., Seventh Symposium (International) on Combustion, Butterworths, London (1959), p. 436

82. Litchfield, E.L., Hay, M.H., Kubala, T.A., Monroe, J.S., U.S. Bur. Mines Rept. Invest. 7009, (1967)

83. Avery, W.H., Olsen, H.L., in: AGARD, Selected Combustion Problems II, Butterworths, London (1956), p. 147

84. Yang, C.H., Combust. Flame 6, 215 (1962)

85. Vilyunov, V.N., Nekrasov, E.A., Baushev, V.S., Timokin, A.M., Comb. Expl. and Shock Waves 12, 32 (1976)

86. Kailasanath, K., Oran, E., Boris, J., Combust. Flame 47, 173 (1982)

87. Overley, J.R., Knowles, K.A., Reddien, G.W., Combust. Flame 36, 69 (1978)

88. Jones., W.W., Am. Chem. Soc. Symposium on Supercomputers and Chemistry, Wiley, New York (1981)

89. Jahn, G., Der Zundvorgang in Gasgemischen, Oldenbourg, Berlin (1934)

90. Baumeister, T., ed., Standard Handbook for Mechanical Engineers, 7th ed., McGraw-Hill, New York (1967)

91. Ouseph, C.V., Loth, J.L., Combust. Flame 19, 309 (1972)

92. Jones, G.W., Kennedy, R.E., U.S. Bur. Mines Rept. Invest. 3798, (1945)

93. Sharma, G.P., Agrawal, D.D., Gupta, C.P. Eighteenth Symposium (International) on Combustion, Combustion Institute, Pittsburgh (1981), p. 493

94. Stull, D.R., Prophet, M., eds., JANAF Thermochemical Tables, 2nd ed., U.S. Nat. Bur. Stand., Washington, D.C. (1971)

Biographical Note

PAUL DAVID RONNEY

Birthdate: May 1, 1957

Birthplace: Los Angeles, California

Permanent residence: Newport Beach, California

Education: Massachusetts Institute of Technology September 1979-February 1983
Sc.D. in Aeronautics and Astronautics, May 1983
Honors: Dupont Fellowship, Upham Fellowship

California Institute of Technology September 1978-June 1979
M.S. in Aeronautics, June 1979
Honors: Guggenheim Fellowship

University of California, Berkeley September 1977-June 1978
B.S. in Mechanical Engineering, June 1979
Honors: Tau Beta Pi, Pi Tau Sigma, Phi Beta Kappa; Union Oil Scholarship; Dean's List

University of California, Irvine September 1974-June 1977
Mechanical Engineering Major
Honors: ASME Mechanical Engineering Student of the Year, 1976-1977; Dean's List

Professional Experience:

Massachusetts Institute of Technology, Cambridge, Mass.
Research Assistant, September 1979 - November 1982

Ford Aerospace and Communications Corp., Newport Beach, Calif.
Systems Integration Engineer, August 1978 - September 1979

Member of the American Institute of Aeronautics and Astronautics

Interests: Mountain climbing, backpacking, whitewater rafting and kayaking, cross-country and downhill skiing, flying, skydiving, amateur radio, music composition, guitar playing, and ice hockey.